D.2.1.1 Structural Framework

Based on the observation that all Pliocene and Quaternary basaltic volcanoes in the YMR are located in the Amargosa trough, this feature provides the framework for the location of potential future volcanic events (Figure D.2-2). The Amargosa trough is a major tectonic feature that has influenced the location of Miocene silicic volcanic activity in the region and has localized basaltic volcanic activity in the YMR for the past 5 Ma.

Figure D.2-3 shows modified boundaries of the Amargosa trough, which include fault boundaries (green lines) from the geologic map of Slate et al. (1999) and orange, red, and blue lines that adjust and extend the trough boundaries used for this elicitation model. My modifications, shown on Figure D.2-3, include the following:

1. The western and eastern boundaries are extended south to the approximate eastern extension of the southern Death Valley fault zone (orange lines; the southern boundaries extend beyond the lower map boundary).

2. North of Bare Mountain, the western trough boundary is inferred to follow the edge of a gravity gradient and the southwestern part of the Timber Mountain-Oasis Valley caldera complex (orange line north of western green line).

3. In the vicinity of the Sleeping Butte, the western trough boundary is inferred to follow either of two equally probable traces: (1) the approximate western boundary of the Black Mountain caldera (orange line) or (2) the Thirsty Canyon lineament (red line).

4. The north-northeast extension of the eastern boundary is inferred to extend across Jackass Flats, follow a gravity gradient across Shoshone Mountain, and extend along the approximate trace of the Belted Range thrust, taking a minor diversion along the inferred eastern margin of the Red Rock Valley caldera (orange line north of eastern green line). This boundary coincides approximately with the eastern boundary of the volcanic domain as drawn on the isostatic residual gravity map of Grauch et al. (1999).

5. The northern limit of the Amargosa trough is not well constrained. It is defined somewhat arbitrarily by the northernmost extent of the basalt of Silent Canyon (blue line on Figure D.2-3).

The boundaries of the Amargosa trough are reasonably well defined by gravity gradients east and west of Yucca Mountain, but become increasingly uncertain at the northern and southern limits of the structure.

A critical assumption of my conceptual model for the PVHA-U is that future basaltic volcanic activity will occur preferentially within the Amargosa trough. This assumption establishes a boundary condition that requires a probability gradient at the western and eastern boundaries of the trough (Figure D.2-3), with a higher probability of future volcanic activity within than outside the trough. Yucca Mountain is located *in* the Amargosa trough.

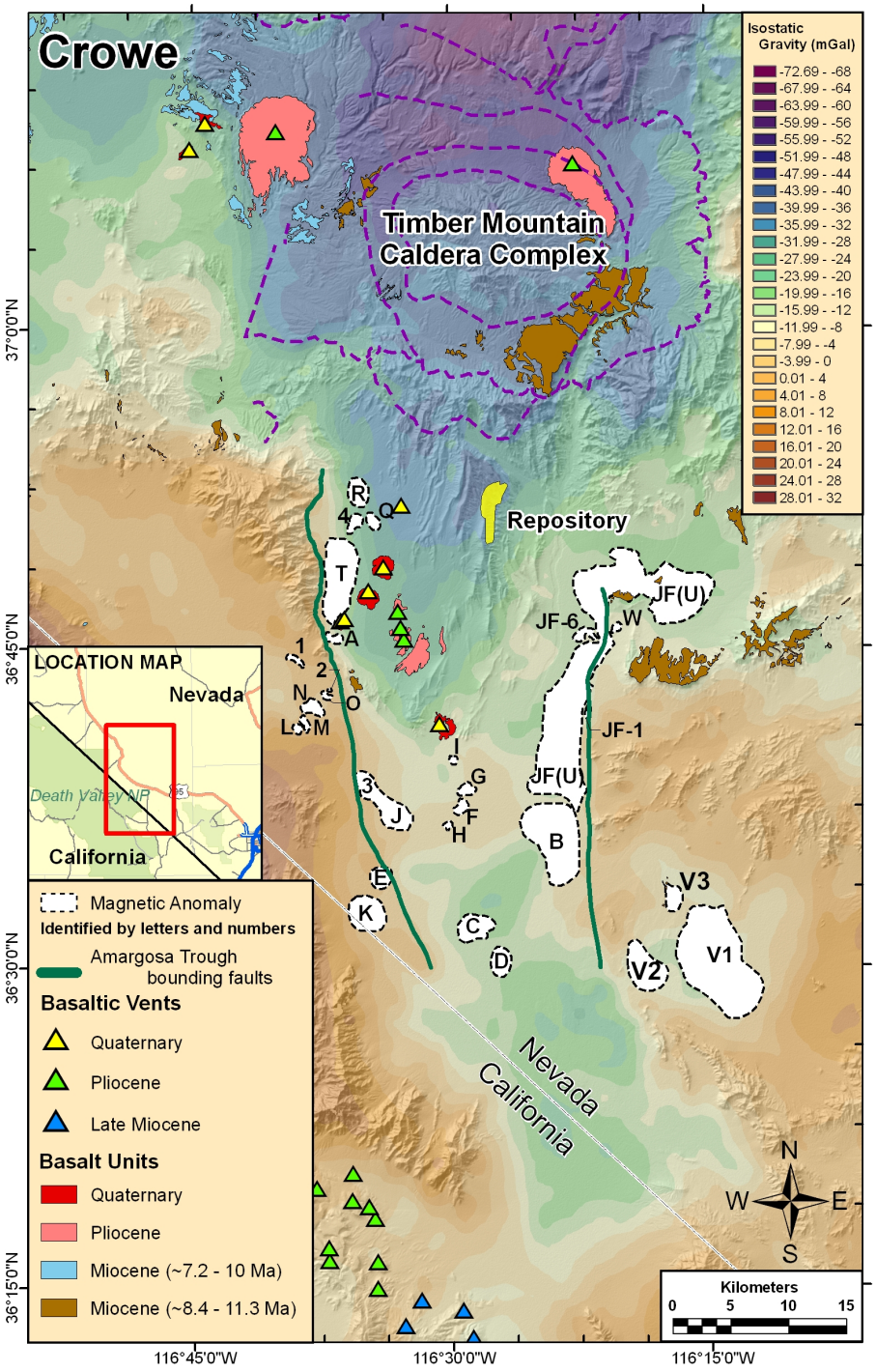

NOTE: Surface volcanic units from Slate et al., 1999; boundaries of Amargosa trough based on fault locations from Slate et al., 1999.

Figure D.2-2. Generalized Geologic Setting and Local Boundaries (green lines) of the Amargosa Trough

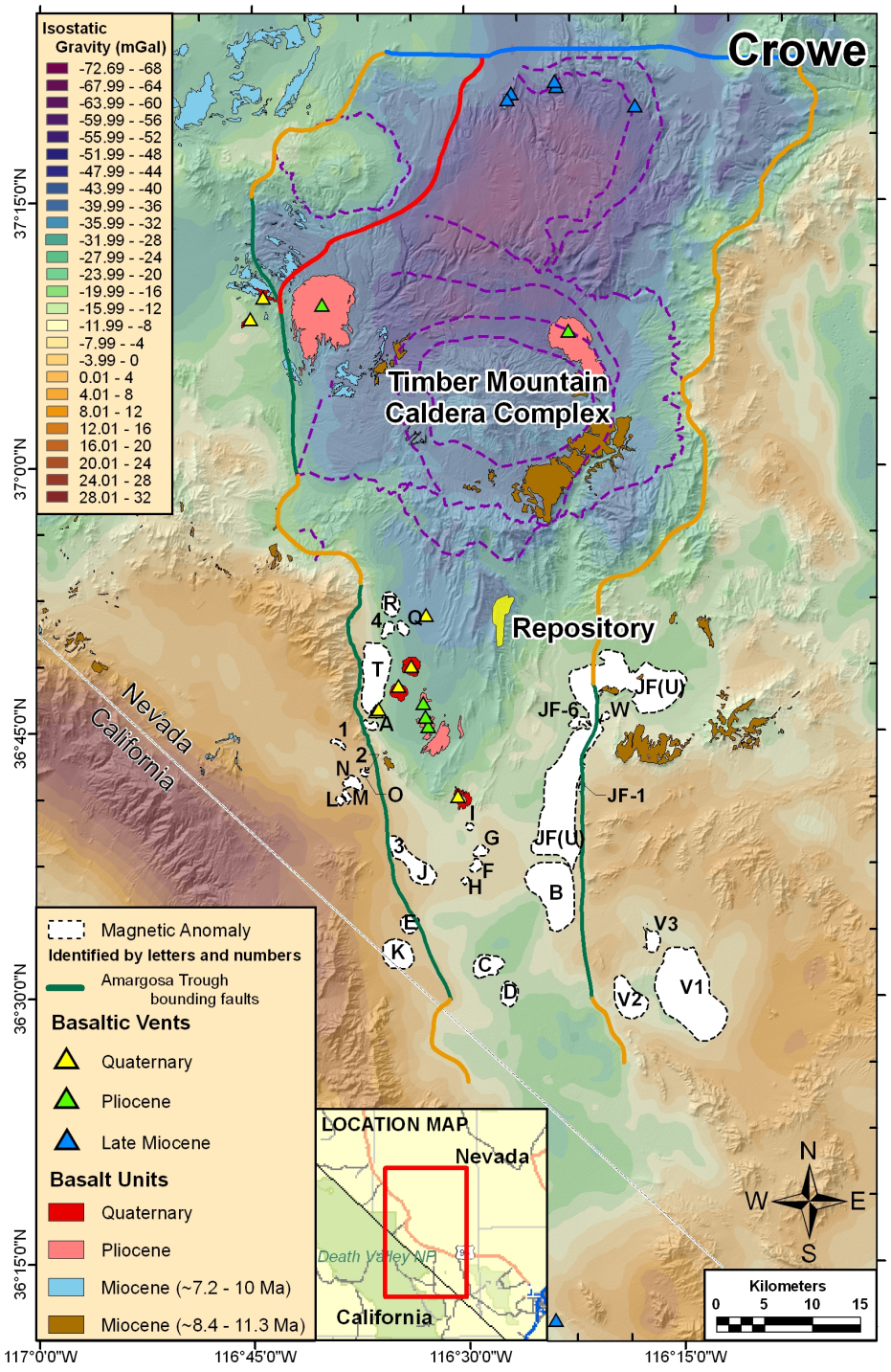

NOTE: See text section for description of alternative trough boundaries.

Figure D.2-3. Boundaries of the Amargosa Trough from Figure D.2-2 (green lines) Modified for Use in This Elicitation Model (by orange, blue, and red lines)

D.2.1.2 Volcanic Cycles and Alternative Rate Models

The concept of volcanic cycles is used to predict patterns of future volcanic activity. Past patterns are recorded in the history of episodic basaltic volcanism in the region. Four volcanic cycles are identified in the post-11.5-Ma volcanic record of the YMR, including the following [see Crowe (2007), Excel Worksheet titled *Cycle Patterns*].

1. Bimodal basalt-rhyolite volcanism associated with the waning phase of the Timber Mountain caldera (11.5 to 9.5 Ma)

2. The Frenchman Flat/Yucca Flat volcanic cycle (8.6 to 7.3 Ma)

3. The Pliocene volcanic cycle of the Crater Flat and Amargosa Valley basins of the southern Amargosa trough (~4.9 or 4.6 Ma to 3.0 Ma)

4. The Quaternary volcanic cycle of Crater Flat (1.1 Ma to recent; this cycle may be continuing at present).

I consider the fourth, most recent cycle of the Quaternary basaltic volcanism (1.1 Ma to recent), in the Crater Flat basin to be the most relevant cycle for predicting future patterns of volcanic activity. Additional insights are derived from the record of post-caldera small-volume (<3 km^3) basaltic volcanism (the second and third cycles). The Miocene cycle of larger-volume (>3 km^3) basaltic volcanism is part of a fundamentally different tectonic and volcanic regime and differs from the younger, small-volume basaltic volcanic cycles (cycles two through four). Data from Miocene basalt-rhyolite cycle provide perspectives on basaltic volcanic processes but are not used in the detailed components of the elicitation model.

My elicitation model assumes that the past patterns of cycles of small-volume basaltic volcanic activity separated by intervals of inactivity are continuing now and will continue into the future. Predictions of the recurrence rate at any point in the future depend on subjective interpretations of whether that future point is within or between volcanic cycles.

I use alternative interpretations of volcanic cycles and recurrence rate models to define various future volcanic states. The multiple alternative models of future volcanic states are:

1. Within the present Quaternary volcanic cycle of Crater Flat
2. Within the time gap between volcanic cycles
3. Within a new or future volcanic cycle.

Alternative recurrence rate models are:

1. Steady-state rate model
2. Increasing rate model
3. Background rate model
4. New volcanic cycle.

As described below, my assessment of the detailed characteristics of future events differs under each different rate model, and the weighting of the rate models differs for the 10,000-year and 1-My compliance periods. The overall logic of the alternative future volcanic cycles and rate models is illustrated and described in Figure D.2-4.

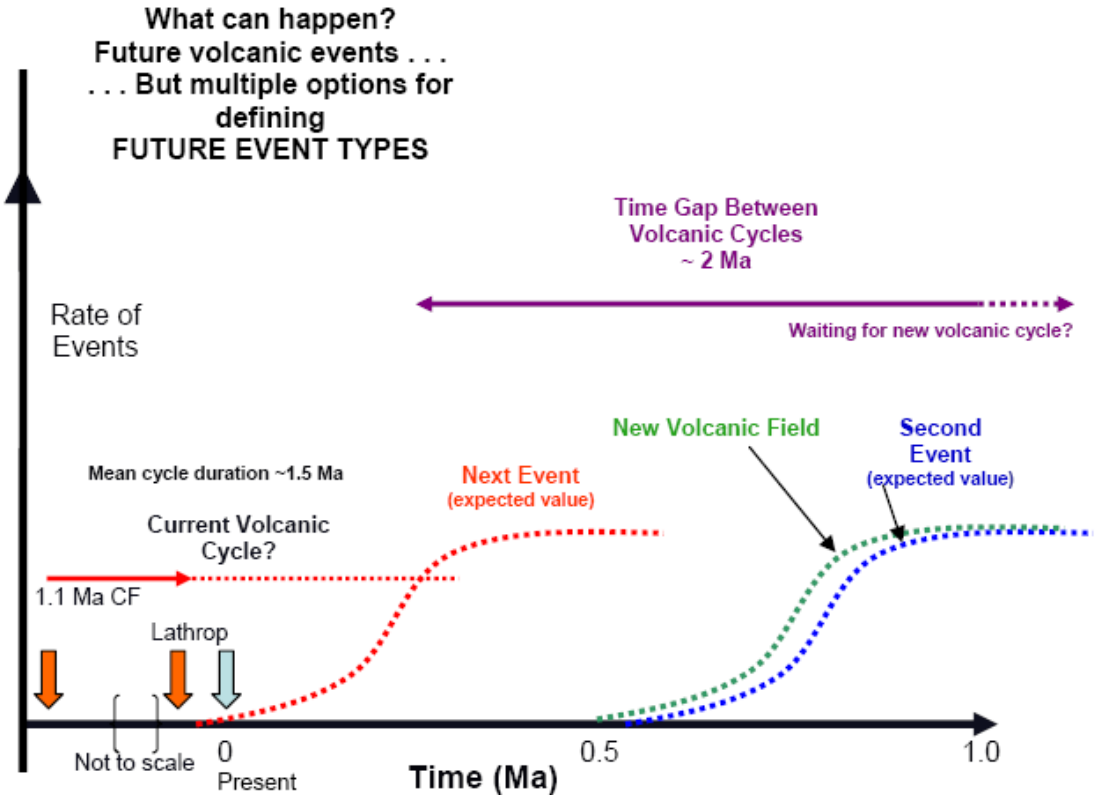

NOTE: The x-axis is time in millions of years (approximate scale with a time gap in the volcanic record shown by the brackets). The y-axis (not to scale) represents rates of events increasing upward. The left vertical red arrow marks the start of the current volcanic cycle at 1.1 Ma, initiating after a 1.8-Ma gap since the end of the Pliocene volcanic cycle (dated by the basalt of Buckboard Mesa at 2.87 Ma). The horizontal red arrow above the label, "1.1-Ma CF," represents the duration of the current volcanic cycle, which could end with the Lathrop Wells event (second vertical red arrow) or continue (the vertical blue arrow marks today). For a 10,000-year compliance period, the YMR could be within the Quaternary volcanic cycle. Given this volcanic state, the most likely future event is another small-volume (~0.1 km^3) event somewhere in the Crater Flat volcanic field. The cumulative distribution function (CDF) for this event is represented by the dashed red curve. Alternatively, the YMR could be *between* volcanic cycles and experiencing background recurrence rates. For the 1-My compliance period, the YMR could still be within the Quaternary volcanic cycle. For this alternative, the red CDF again represents the next event, and the blue CDF represents a possible second event during the longer 1 My compliance period. Alternatively, the YMR could be between volcanic cycles and background recurrence rates would apply. A third alternative is that the 1-My compliance period could include a new volcanic cycle formed at an unknown location with volcanic events of larger magma volumes (~0.1 km^3). This alternative (and only this alternative) includes the possibility of large-footprint volcanic events.

Figure D.2-4. Schematic of Possible Future Volcanic States for the Yucca Mountain Region (YMR)

D.2.2 DEFINITION OF VOLCANIC EVENT

The definition of a volcanic event evolved from the definition used in the 1996 PVHA, supplemented by concepts developed during discussions at the PVHA-U workshops. I define a volcanic event as the eruptive products and inferred subsurface feeder systems formed during a synchronous pulse of basaltic volcanic activity. Pulses of activity are assumed to be associated with the ascent and eruption of a temporally and spatially discrete batch of basaltic magma. The patterns recorded in multiple volcanic cycles in the YMR show variability in the dimensions and patterns of volcanic events and these properties are used to predict the nature and variability of future volcanic events.

Events are identified and described through a two-step process that includes (1) identifying synchronous pulses of volcanic activity using geochronology data for the YMR, then (2) assessing the record of variability in the attributes of identified volcanic events. Insights gained from upgraded geochronology data obtained since the 1996 PVHA study aid the identification of volcanic events. These data, along with new information from drilling of aeromagnetic anomalies, increase confidence in the ages and spatial distributions of Pliocene and Quaternary volcanic events in the YMR. These new data also support the recognition of less common, spatially dispersed volcanic events, which are referred to as large-footprint events (event length >28 km; multiple spatially dispersed clusters of cones, vents, and lavas).

Identified volcanic events or pulses can range from single to multiple scoria cones (four cones maximum) and associated lava flows to large-footprint volcanic events. This natural variability in volcanic events is an irreducible component of event uncertainty, a part of statistical uncertainty. Natural variability is represented in my elicitation model by defining volcanic events that represent the characteristics and frequencies of observed patterns of events in the three volcanic cycles.

The two-step process described above is used to classify volcanic events into four types depending on the number of primary cones or coalesced cones identified for a synchronous pulse of magma. The four types are:

1. Single-cone events
2. Two-cone events
3. Three-cone, or cluster events
4. Four-cone, or cluster events.

Figure D.2-5 shows satellite images of basaltic volcanoes in the YMR that illustrate the event types in the four-fold classification. The three- and four-cone events include large-footprint events. The time gap required between separate events is not well defined, but varies with the age of the event and the reproducibility of the geochronology data. A gap of 25,000 to 100,000 years is required to discriminate pulses of volcanic activity.

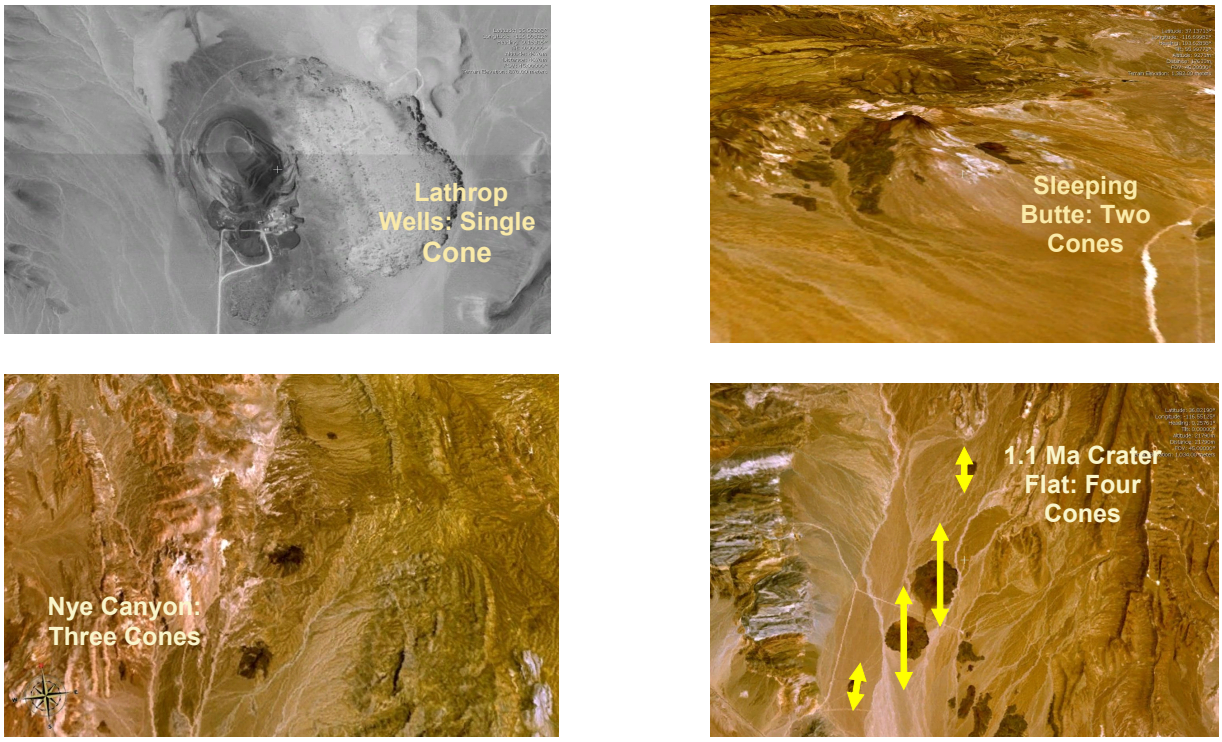

Figure D.2-5. Satellite Photographs Showing Typical Examples of the Four Types of Volcanic Events Associated with Basaltic Volcanic Cycles of the Yucca Mountain Region

Cones, which consist of thick accumulations of scoria and spatter, represent the deposits of maintained Strombolian eruption columns. In contrast, *vents* are secondary or satellite eruption sites having smaller volumes of vent-facies deposits. These deposits are consistent with formation from less energetic fissure fountaining, spatter, and minor Strombolian activity. They are not formed from maintained column eruptions. Hidden or undetected events are not included in the event definition because of the low probability of an event ascending to repository depth and not erupting at the surface. *Sills* can form beneath basaltic volcanoes (for example, Paiute Ridge; possible interpretation of Anomaly A). Sills are unlikely to form in the competent rock of the densely welded Topapah Springs member of the Paintbrush Tuff (host rock for the repository) within the interior of a mountain range. Thus sills are not included in my elicitation model.

Table D.2-1 shows how I categorized each of the past events in the YMR as a one-, two-, three-, or four-cone or cluster event. For the events that can be interpreted in alternative ways, all possible interpretations are listed. For example, because of uncertainty in the age of Little Cones, the 1.1-Ma Crater Flat event is defined both as a four-cone event (with Little Cones) and as a three-cone event (without Little Cones). The 3.8-Ma large-footprint Crater Flat/Amargosa Valley event is defined both as a three-cluster and four-cluster event because of the lack of characterization data for aeromagnetic Anomalies C and D.

Table D.2-1. Events within the Region of Interest

Event	Age (Ma)	Cycle	Event Type					
			Single Cone	Two Cones	Three Cones	Four Cones	Three Clusters	Four Clusters
Lathrop Wells	0.77	Quaternary	x					
Little Cones	0.7 (0.5) 1.1 (0.5)	Quaternary	x	x				
Red Cone	1.1	Quaternary	x					
Black Cone	1.1	Quaternary	x					
Makani Cone	1.1	Quaternary	x					
Anomaly C	4.8	Pliocene	x					
Anomaly D	4.8	Pliocene	x					
Anomalies C and D	4.8	Pliocene		x				
Buckboard Mesa	2.87	Pliocene	x					
Thirsty Mountain	4.6	Pliocene	x					
Anomaly B	3.9	Pliocene	x	x				
Sleeping Butte	0.35	Quaternary		x				
1.1-Ma Crater Flat not including Little Cones	1.1	Quaternary			x			
3.8-Ma Crater Flat	3.8	Pliocene			x			

Table D.2-1. Events within the Region of Interest (Continued)

Event	Age (Ma)	Cycle	Event Type					
			Single Cone	Two Cones	Three Cones	Four Cones	Three Clusters	Four Clusters
Anomalies F, G, and H	3.95	Pliocene			x			
Nye Canyon	7.3	Miocene			x			
Paiute Ridge/Scarp	8.6	Miocene					x	
3.8-Ma large-footprint Crater Flat/Amargosa Valley event not including Anomalies C and D	3.8	Pliocene						
1.1-Ma Crater Flat including Little Cones	1.1	Quaternary				x		
3.8-Ma large-footprint Crater Flat/Amargosa Valley event including Anomalies C and D	3.8	Pliocene						x

D.2.2.1 Characterization of Volcanic Events

A fundamental assumption of my characterization of potential future volcanic events is that past patterns and attributes of events in volcanic cycles of the YMR provide the primary basis for predicting the characteristics of future events. Future volcanic events are assumed to be variable, and this variability is captured in the event tables developed from the volcanic record [Tables D.2-2 through D.2-5; see also Crowe (2007) Excel Worksheet titled *All Event Summary*].

Events are characterized by the following attributes.

- Number and spacing of cones
- Event length, width, and orientation
- Number of vents and dikes
- Orientation of feeder dikes
- Conduit, vent, and dike dimensions
- Location of dikes and vents relative to cones.

For the 10,000-year and 1-My compliance periods, my assessment of the frequency of each event type is:

- Single-cone events: 46%
- Two-cone events: 18%
- Three-cone or three-cluster events: 27%
- Four-cone or four-cluster events: 9%.

The formation of a new volcanic cycle is a possible future state of volcanic activity in the YMR for the 1-My compliance period. Based on the information from past volcanic cycles, the estimated frequency of future large-footprint events is 20%. Applying this frequency to the 1-My compliance period and a future involving formation of a new volcanic cycle, 20% of the 27% frequency at which three-cone or three-cluster events occur (5.2 % frequency) represents large-footprint events. Similarly, 20% of the 9% frequency at which four-cone or four-cluster events occur would represent large-footprint cluster events (2.6% frequency).

Tables D.2-2 through D.2-5 summarize the vent counts and variability in vent counts, event length, width, and orientation, and the cone spacing for the four event types. Data shown on the tables are derived from the volcanic record [see also Crowe (2007) Excel Worksheet titled *All Event Summary*]. Tables D.2-2b through D.2-5b include assessments of the characteristics of future events and a combination of probability distributions and regression models are used to represent the attributes of future volcanic events specific to the four event types. Attributes and distributions for the large-footprint events are presented in Table D.2-11, described below under "Large Footprint Events." The measurement methods used to develop the event tables are described in a following section.

Table D.2-2a. Attributes of Single-Cone Events

Single-Cone Events (46% of events are of this type)											
	Number of Vents			Event Length	Event Width	Event Orientation	Cone Spacing	Dike Length (km)			Number of Dikes
Event	Min.	Best Estimate	Max.	(km)	(km)	(degrees)	(km)	Min.	Best Estimate	Max.	(most likely)
Lathrop Wells	1	2	3	4.3	0.6	N10W	na	0.8	3.5	5.0	2
Little Cones	1	2	2	2.7	0.3	N30E	na	0.6	2.5	3.0	1
Red Cone	1	1	2	3.7	0.3	N5E	na	0.7	3.3	4.5	1
Black Cone	1	1	1	3.7	0.3	NS	na	0.7	3.3	4.5	1
Makani Cone	1	2	2	2.8	0.3	NS	na	0.6	2.8	3.3	1
Anomaly C	1	1	1	6.1	1.5	N15E	na	1.0	4.0	6.5	1
Anomaly D	1	1	1	6.1	1.5	N15E	na	1.0	4.0	6.5	1
Buckboard Mesa	1	2	3	5.4	1.3	N25W	na	1.5	5.0	7.3	2
Thirsty Mesa Mountain	1	2	4	10.2	1.5	N5W	na	1.3	6.0	10.0	1
Anomaly B	1	2	3	12.5	2.6	N10W	na	1.2	6.0	10.0	1
Quaternary Cycle, Mean	1.0	1.6	2.0	3.4	0.3			0.7	3.1	4.1	1.2
Pliocene Cycle, Mean	1.0	1.6	2.4	8.1	1.7			1.2	5.0	8.1	1.3
Both Cycles, Mean	1.0	1.6	2.2	5.8	1.0			0.9	4.0	6.1	1.2

Table D.2-2b. Attributes of Future Single-cone Events: Distributions Developed from Data in Table D.2-2a

	Steady-State/Increasing Rate Models				Background Rate Model				New Volcanic Field Model			
	Distribution	**Min.**	**Mode**	**Max.**	**Distribution**	**Min.**	**Mode**	**Max**	**Distribution**	**Min.**	**Mode**	**Max**
Event Length (km)	Triangular	2.7	3.4	5	Triangular	4.0	5.8	9.0	Triangular	5.0	8.1	13.0
Event Width (km)	Triangular	0.2	0.3	0.7	Triangular	0.3	1.0	1.7	Triangular	1.3	1.7	3
Dike Length (km)	Triangular	0.6	3.1	5	Triangular	0.9	4.0	6.1	Triangular	1	5	11
Other event attributes apply to all four rate models												

Number of cones = event type = 1		**Cone Spacing (km) = 0.38*Event Length –0.54[a]**		
	Distribution	**Min.**	**Mode**	**Max.**
Number of Dikes	Uniform	1		2
Number of Vents	Uniform	1		3
Dike Spacing (km)	Triangular	0.1	0.4	1

Table D.2-3a. Attributes of Two-Cone Events

Two-Cone Events (18% of events are of this type)											
	Number of Vents			Length	Width	Orient-ation	Cone Spacing	Dike Length (km)			Number of Dikes
Event	Min.	Best Estimate	Max.	(km)	(km)	(degrees)	(km)	Min.	Best Estimate	Max.	(most likely)
Sleeping Butte	2	2	3	6.0	0.5	N15E	2.5	0.7	2.8	3.3	2
Little Cones	1	2	2	2.7	0.3	N30E	0.4	0.7	2.5	3.0	2
Anomalies C and D	2	2	3	7.0	2.4	N20W	3.5	1.0	4.0	7.5	2
Anomaly B	1	2	3	12.5	2.6	N10W	2.6	1.2	6.0	10.0	1
Quaternary Cycle, Mean	1.5	2.0	2.5	4.4	0.4		1.5	0.7	2.7	3.2	2.0
Pliocene Cycle, Mean	1.5	2.0	3.0	9.8	2.5		3.1	1.1	5.0	8.8	2.0
Both Cycles, Mean	1.5	2.0	2.8	7.1	1.4		2.3	0.9	3.8	6.0	1.8

Table D.2-3b. Attributes of Future Two-cone Events: Distributions Developed from Data in Table D.2-3a

	Steady-State/Increasing Rate Models				Background Rate Model				New Volcanic Field Model			
	Distribution	Min.	Mode	Max.	Distribution	Min.	Mode	Max.	Distribution	Min.	Mode	Max.
Event Length (km)	Uniform	2.7		6.5	Uniform	5.5		9	Uniform	6.5		13.0
Event Width (km)	Uniform	0.2		0.6	Uniform	0.5		2.5	Uniform	2.3		2.7
Dike Length (km)	Uniform	0.7	2.7	3.3	Uniform	0.7		5	Uniform	1.0		9.0

Other event attributes apply to all four rate models

Number of cones = event type = 2		Cone Spacing (km) = 0.38*Event Length –0.54[a]		
	Distribution	Min.	Mode	Max.
Number of Dikes	Uniform	2		3
Number of Vents	Uniform	2		3
Dike Spacing (km)	Triangular	0.1	0.4	1

[a] Based on regression of cone spacing against event length for all events.

Table D.2-4a. Attributes of Three-Cone or Three-Cluster Events

Three-Cone or Three-Cluster Events (27% of events are of this type)											
	Number of Vents			Length	Width	Orientation	Cone Spacing	Dike Length (km)			Number of Dikes
Event	Min.	Best Estimate	Max.	(km)	(km)	(degrees)	(km)	Min.	Best Estimate	Max.	(most likely)
1.1-Ma Crater Flat (without Little Cones)	3	4	5	10.9	1.3	N20E	5.4	0.7	3.3	7.3	3
3.8-Ma Crater Flat	3	5	7	7.9	1.4	N5W	1.2	1.0	4.5	8.5	3
Anomalies F, G, and H	3	4	5	8.3	1.6	N10E	1.8	0.8	4.0	8.0	3
Nye Canyon	3	4	4	11.45	2.35	N25 E	6.23	0.5	3.5	8.0	5
Paiute Ridge/Scarp	5	7	10	33.1	3.5	N5W	25.2	0.5	4.0	9.0	7
3.8-Ma Crater Flat/Amargosa Valley (without Anomalies C and D)	7	11	17	28	12.6	N20W	16.6	0.4	4.0	8.3	12
Quaternary Cycle, Mean	3	4.0	5.0	10.9	1.3		5.4	0.7	3.3	7.3	3
Pliocene Cycle <15 km, Mean	3	4.3	5.3	9.2	1.8		3.1	0.8	4.0	8.2	4
Pliocene Cycle >30 km, Mean	6	9.0	13.5	30.6	8.1		20.9	0.5	4.0	8.7	10

Table D.2-4b. Characteristics of Future Three-cone Events: Distributions Developed from Data in Table D.2-4a

	Steady-State/Increasing Rate Models				Background Rate Model				New Volcanic Field Model			
	Distribution	**Min.**	**Mode**	**Max.**	**Distribution**	**Min.**	**Mode**	**Max.**	**Distribution**	**Min.**	**Mode**	**Max.**
Event Length (km)	Uniform	6.5		12.0	Uniform	8.0		12.0	Uniform	8.0		13.0
Event Width (km)	Uniform	1.0		1.5	Uniform	1.5		2.5	Uniform	1.5		2.5
Dike Length (km)	Triangular	0.7	3.3	5.0	Triangular	0.7	3.8	7.8	Triangular	0.7	4.0	9.0
Other event attributes apply to all four rate models												

Number of cones = event type = 3		**Cone Spacing (km) = 0.38*Event Length –0.54[a]**		
	Distribution	**Min.**	**Mode**	**Max.**
Number of Dikes	Uniform	3		4
Number of Vents	Uniform	3		6
Dike Spacing (km)	Triangular	0.1	0.4	1

[a] Based on regression of cone spacing against event length for all events.

NOTE: See Table D.2-11 for the characteristics used to define large-footprint events.

Table D.2-5a. Event Attributes for Four-Cone or Four-Cluster Events

Four-Cone or Four-Cluster Events (9% of events are of this type)											
	Number of Vents			Length	Width	Orient-ation	Cone Spacing	Dike Length (km)			Number of Dikes
Event	Min.	Best Estimate	Max.	(km)	(km)	(degrees)	(km)	Min.	Best Estimate	Max.	(most likely)
1.1-Ma Crater Flat, including Little Cones	4	5	6	14.3	1.3	N20E	6.18	0.5	3.1	6.8	4
3.8-Ma Crater Flat/Amargosa Valley, including Anomalies C and D	9	14	21	43.6	12.6	N10W	20.15	1.0	4.5	8.5	7

Table D.2-5b. Characteristics of Future Four-cone Events: Distributions Developed from Data in Table D.2-5a

	Steady State/Increasing Rate Models				Background Rate Model				New Volcanic Field Model			
	Distribution	Min.	Mode	Max.	Distribution	Min.	Mode	Max.	Distribution	Min.	Mode	Max.
Event Length (km)	Uniform	10		15	Uniform	10		15.0	Uniform	10		15
Event Width (km)	Uniform	1		1.5	Uniform	1		2.5	Uniform	1		2.5
Dike Length (km)	Triangular	0.5	3.1	5	Triangular	0.5	3.5	7.5	Triangular	1	4.5	8.5

Other event attributes apply to all four rate models

Number of cones = event type = 4	Cone Spacing (km) = 0.38*Event Length -0.54[a]		
	Distribution	Min	Mode	Max
Number of Dikes	Uniform	4		5
Number of Vents	Uniform	4		6
Dike Spacing (km)	Triangular	0.1	0.4	1

[a] Based on regression of cone spacing against event length for all events.

NOTE: See Table D.2-11 for the characteristics used to define large-footprint events.

D.2.2.2 Measurements and Assessments of Event Features

Features of surface volcanic events are measured from Google Earth imagery using the ruler tool, then cross-checked with the *YMR Dike and Fissure Lengths, Vent Spacing* table provided to the expert panel (developed from Los Alamos National Laboratory (LANL) analog studies and subsequently published as Keating et al., 2008). Deviations from the referenced table are based on my alternative interpretations of the field data. Data for the aeromagnetic anomalies are measured from the LANL GIS map provided to the expert panel (Map #m201425, Rev. 1). All measurements were repeated three times for verification.

My measurement method for event lengths at repository depth uses the following steps:

1. Locate the upper and lower edges of the primary cone vent/crater structure on the satellite photograph.

2. Extend those edges ½ dike length north and south (directions differ depending on event orientation) to account for approximate dike lengths at repository depth. The ½ dike length is determined from the expected dike length for individual event types.

3. Adjust the dike ends slightly if their termination is near a local structure.

4. Measure the event length from the upper to the lower end of the ½ dike length projections.

The measurement procedures change for multi-cone/cluster events in that the points of dike extension are located at the uppermost and lowermost volcanic events within the cluster (northernmost and southernmost cones for volcanic events oriented north-south).

Event widths, which are measured perpendicular to event length, are based on either the width of the primary cone (for single-cone events) or the distance between cones (for multiple-cone events). The width is expanded beyond the primary cone to account for the following two observations.

1. The local presence of satellite vents that require feeder dikes separate from the primary cones/clusters.

2. Field studies of dissected basaltic volcanoes in the YMR, which show dike/feeder structures extending away from the axis of event lengths. This observation is consistent with presentations on dike structures by Chuck Connor at PVHA-U Workshop 3.

The measurement of event widths is less precise and more subjective than is measurement of event lengths. The measurement of width depends on interpretations of the at-depth distribution of dikes associated with cones and vents.

The uncertainty in identifying volcanic vents is represented by stipulating minimum, best estimate, and maximum vent estimates (Tables D.2-2 through D.2-5). Observations at active basaltic volcanic eruptions, primarily at Kilauea volcano, reveal that secondary or satellite vents

commonly form along or near fissure systems and are often covered by subsequent eruption deposits. Examining only surface deposits of basaltic volcanoes can lead to underestimating satellite vents. Accordingly, my maximum vent counts attempt to compensate for bias toward lower vent counts by allowing for the possibility of buried or "hidden" vents associated with an event. For my event definitions, all cones are vents, so the number of vents cannot be less than the number of cones. Similarly, all dikes are associated with at least one vent, so the number of vents cannot be less than the number of dikes.

Distributions for dike length are derived from materials on analog studies conducted by LANL and provided as a preprint of Keating et al. (2008) to expert panel members at several PVHA-U workshops. The distributions apply the conceptual model of decreasing source footprints and dike lengths correlated with decreasing volumes described in Valentine and Perry (2006). Distributions of dike length differ for the various alternative models of the current and future volcanic setting of the Yucca Mountain site (see Tables D.2-2 through D.2-5*)*.

My assigned dike orientations are influenced by the distributions of cones and vents and by new, high-precision aeromagnetic data that show that dike orientations can deviate from event orientations (Table D.2-6). Because dike orientations do not appear to differ by event type, my assessment is based on the orientation of dikes for all past events in the Amargosa trough (data for Frenchman/Yucca Flats cycle are excluded).

Table D.2-6. Observed Dike Orientations and Assessment of Future Orientations

Dike Orientation (Degrees)	N25W to N15W	N15 to N5W	N5W to N5E	N5E to N15E	N15E to N30E
Number of Dikes Having This Orientation	1	6	42	12	5
Likelihood of a Future Dike Having This Orientation	2%	9%	64%	18%	8%

The orientations of specific dikes associated with various past events are included in Crowe (2007), Excel Worksheet titled *Event and dike orient*.

Event orientations were determined from the Google Earth imagery and the referenced GIS map for aeromagnetic anomalies. I assigned orientations in approximate 5- to 10-degree bin segments. Event orientation, like dike orientation, does not appear to differ for the four basic event types (Table D.2-7). My assessment of the orientation of any future event is based on the orientation of all past events.

Table D.2-7. Observed Event Orientations and Assessment of Future Orientations

Event Orientation (Degrees)	N25W to N15W	N15 to N5W	N5W to N5E	N5E to N15E	N15E to N30E
Number of Past Events in Orientation Category	3	4	5	5	5
Assessment: Likelihood of Future Event Having this Orientation	14%	18%	23%	23%	23%

Specific event orientations are included in Crowe (2007), Excel Worksheet titled *Event and dike orient*.

Cone spacing was measured from cone center to cone center (usually summit craters) on Google Earth imagery. These measurements are subjective for the aeromagnetic anomalies. Because cone spacing correlates strongly with event length, my assessment of cone spacing is a function of event length. The function was defined by developing a linear regression model with event length as the independent variable and cone spacing as the dependent variable. The data set used to develop the regression model and the regression results are shown in Table D.2-8. Detailed regression results are included in Crowe (2007), Excel Worksheet titled *Cone Space Regression*.

Table D.2-8. Event Lengths and Cone Spacing

Event	Cone Spacing (km)	Event Length (km)	Comments
Sleeping Butte	2.5	6.0	1/2 length added from the base of the main edifice of the NE and SW cones
Little Cones	0.4	2.7	1/2 dike length added from the base of the NE and SW cones
Anomalies C and D	3.5	7.0	Measured from GIS base map #m201425, Rev. 1
Anomaly B	4.4	12.5	
1.1-Ma Crater Flat without Little Cones	2.7	10.9	
1.1-Ma Crater Flat without Little Cones	5.2	10.9	
3.8-Ma Crater Flat	1.2	7.9	
3.8-Ma Crater Flat	1.2	7.9	
Anomalies F, G, and H	2.0	8.3	
Anomalies F, G, and H	2.2	8.3	
Nye Canyon	5.7	11.5	
Nye Canyon	3.8	11.5	
Nye Canyon	6.2	11.5	
Paiute Ridge	0.9	5.6	
Paiute Ridge	1.1	5.6	
1.1-Ma Crater Flat including Little Cones	2.7	14.3	
1.1-Ma Crater Flat including Little Cones	5.2	14.3	
1.1-Ma Crater Flat including Little Cones	3.8	14.3	

The number of dikes for each volcanic event is inferred from the following relationships:

1. The minimum number of dikes is equal to the number of cones (but there can be more dikes than cones).

2. Every dike has at least one vent, and may have more.

3. Dikes are estimated from assessments of the geometry and spatial distribution of vents.

4. Observations at eroded centers generally show more dikes or more complicated dike geometries than expected from the distribution of surface cones. Examples include the basalt of Paiute Ridge, the basalt of Nye Canyon, and the 3.7-Ma basalt of Crater Flat.

Dikes and vents are associated spatially with cones (i.e., are more likely to occur near than between cones). Dike spacing is measured adjacent to cones and perpendicular to event orientation; vent spacing is measured along dikes adjacent to cones. The spacing of vents and dikes can change along strike if dike orientations are non-parallel to cone orientations. My assessment of dike spacing (perpendicular to event orientation) is a triangular distribution having a minimum of 0.1 km, a maximum of 1 km, and a most likely value of 0.4 km. This assessment is based on the measurements summarized in Table D.2-9.

Table D.2-9. Measured Dike Spacing for Past Events

Event	Dike spacing[a] (km)	Comments
Lathrop Wells	0.30	3 dikes with 2 dikes probable and a 3rd possible but less likely.
Sleeping Butte	0.23	NW flank vent of Little Black Peak is inferred to be formed from a separate dike
Little Cones	0.30	Single primary cone (SW cone) and single vent (NE vent), each fed by a N-S-trending dike
Anomalies C and D	0.90	Two-cone model with a satellite vent on the NW cone; both cones are fed by a N-S dike
3.8-Ma Crater Flat	0.35	
3.8-Ma Crater Flat	0.20	
3.8-Ma Crater Flat	0.10	
3.8-Ma Crater Flat	0.10	
3.8-Ma Crater Flat	0.10	
Anomalies F, G, and H	0.40	Anomaly shapes permissive with satellite vents on the north and center cones
Anomalies F, G, and H	0.40	Anomaly shapes permissive with satellite vents on the north and center cones
Nye Canyon	0.40	
Paiute Ridge	0.75	From Paiute Ridge map assuming 5 feeder dikes
Paiute Ridge	0.25	From Paiute Ridge map assuming 5 feeder dikes
Paiute Ridge	0.60	From Paiute Ridge map assuming 5 feeder dikes
Paiute Ridge	1.00	From Paiute Ridge map assuming 5 feeder dikes
Mean	*0.40*	
Min.	*0.10*	
Max.	*1.00*	

[a] Dike spacing is measured as the distance between the primary cone and satellite vents or dikes.

To estimate vent spacing, I measured the distance between each vent and the nearest cone (see earlier discussion of the differences between cones and vents) for all past volcanic events. These vent spacings are shown in Table D.2-10. I used the measured vent spacings of Quaternary events as the basis for assessing vent spacing under the steady-state and increasing rate models.

The vent spacing follows a normal distribution with a mean and standard deviation shown in Table D.2-10, truncated at a minimum of 0.1 km and a maximum of 1 km. I used the measured vent spacings of Pliocene vents as the basis for the estimated spacing for a new volcanic cycle. Vent spacing follows a normal distribution with a mean and standard deviation shown in Table D.2-10, truncated at a minimum of 0.1 km and a maximum of 3 km. For the background rate model, I used the measured vent spacings of all events (Quaternary, Pliocene, and Miocene). Vent spacing follows a normal distribution with a mean and standard deviation shown in Table D.2-10, truncated at a minimum of 0.1 km and a maximum of 3 km.

Table D.2-10. Measured Vent Spacings of Past Events

Event	Vent Spacing (km)		Event	Vent Spacing (km)
Lathrop Wells	0.6		Sleeping Butte[e]	0.3
Lathrop Wells	0.4		Little Cones	0.5
Lathrop Wells	0.2		Anomalies C and D	0.8
Little Cones	0.5		Anomaly B	2.8
Red Cone[a]	0.7		3.8-Ma Crater Flat	0.3
Makani Cone	0.4		3.8-Ma Crater Flat	0.6
Buckboard Mesa[b]	0.4		3.8-Ma Crater Flat	0.7
Buckboard Mesa[b]	1.1		3.8-Ma Crater Flat	0.4
Thirsty Mountain[c]	2.0		3.8-Ma Crater Flat	0.3
Thirsty Mountain[c]	1.2		3.8-Ma Crater Flat	0.5
Thirsty Mountain[c]	0.6		3.8-Ma Crater Flat	0.3
Thirsty Mountain[c]	1.7		3.8-Ma Crater Flat	0.1
Thirsty Mountain[c]	2.3		3.8-Ma Crater Flat	1.6
Anomaly B[d]	2.6		Anomalies F, G, and H	2.0
Anomaly B[d]	5.1		Nye Canyon	0.5
Event Distributions				
For Quaternary Cycle			*For all events*	
Mean	0.4		Mean	1.0
Standard Deviation	0.2		Standard Deviation	1.1
For Pliocene Cycle				
Mean	1.3			
Standard Deviation	1.2			

[a] For Red Cone, assume a single vent on south flank of volcano.
[b] For basalt of Buckboard Mesa, distance is from primary cone to a zone of thick spatter along NW-trending fissure.
[c] For basalt of Thirsty Mesa, topography is used as an indicator of the distribution of spatter vents along strike of NE-trending fissure; primary cone identified where a series of N-S coalesced cones intersects the NE-trending fissure.
[d] For Anomaly B, speculative possible vents are identified from the shape of the aeromagnetic anomaly.
[e] For Sleeping Butte, a secondary vent is assumed for an inferred parallel dike that fed a lava breakout at the NW flank of Little Black Peak cone.

Conduit widths/diameters at repository depth are difficult to estimate for many reasons, including the following:

1. There are few sites where combined topography and erosion fully expose basalt conduits and enable reliable estimates of width/diameters and intrusion depths.

2. Conduit plugs are competent rock and resistant to erosion. Most exposures of conduits are not centered directly on the plug masses. Field measurements of many conduit widths/diameters are judged to be less than the maximum values.

3. Field observations at the Cima and Reveille volcanic fields (high-volume basaltic volcanic fields) reveal much larger conduits at repository depths and increase the uncertainty in assigning conduit width/diameters.

Distributions of conduit widths are provided for the multiple alternative models of potential future volcanic activity in the YMR. The models for steady-state and increased recurrence rates assume that the YMR is at the end of the Quaternary volcanic cycle with predicted event volumes less than or equal to ~0.1 km^3. Smaller conduit widths are assigned for the smaller-volume volcanic events. The model of a new volcanic cycle allows for the potential of larger-volume events (~1 km^3) having larger conduit dimensions.

Because there are so few observations in the YMR, the observed conduit widths based on regional analogs, which were presented in a summary table developed by LANL and provided to the expert panel (published as Keating et al., 2008) are assumed to represent expected values that provide limited information on minimum and maximum widths (upper tail of the probability density functions for conduit widths). I increased the uncertainty in my assessment of conduit diameters to compensate for the limited data and to reflect the assumption that measured values are expected widths. This approach is consistent with the approach used for estimating recurrence rates.

The following are my assessments of conduit widths for alternative recurrence rate models:

1. For steady-state and increasing recurrence rates: a triangular distribution having minimum = 10 m, most likely = 35 m, and maximum = 80 m

2. For a new volcanic cycle: a triangular distribution having minimum = 10 m, most likely = 70 m, and maximum = 140 m

3. For background recurrence rate: given the limited data for estimating conduit diameter, I weight the above two distributions equally.

Vents are smaller than conduits. My assessment of vent width is given below:

1. For steady-state and increasing recurrence rates: a triangular distribution having minimum = dike width, most likely = 10 m, and maximum = 20 m

2. For a new volcanic cycle: a triangular distribution having minimum = dike width, most likely = 15 m, and maximum = 30 m

3. For background recurrence rate: given the limited data, I weight the above two distributions equally.

Dike width follows a triangular distribution having a minimum of 1.5 m, a most likely value of 3 m, and a maximum of 6.5 m.

Large-Footprint Events

As discussed above, the volcanic record in the YMR shows that some events may occur as dispersed "cluster events" having a significantly larger footprint than the one-, two-, three-, or four-cone events described above. As noted previously, large-footprint events occur rarely and are relevant only to the model of a new volcanic cycle (which in turn is relevant only for the 1-My compliance period). Large-footprint volcanic events are modeled as having two to four (uniform distribution) clusters. The event orientation is uniform between N20°W and N5°W. Each cluster is located between 6.5 and 20 km (uniform distribution) from the event center in a direction parallel to the event azimuth, and between 1 and 9 km (uniform distribution) in a direction perpendicular to the event azimuth. At least one cluster must be located north and at least one south of the event center. Each cluster should be modeled as three cones spaced 1.2 to 5.5 km apart (uniform distribution), three to six dikes, and four to eight vents. Dike, conduit, and vent dimensions are as specified for three-cone events under the model of a new volcanic cycle. These assessments are based on the measurements of large-footprint events summarized in Table D.2-11. Figure D.2-6 illustrates the placement of clusters within a large-footprint event.

Table D.2-11. Measurements of Large-Footprint (>28 km) Volcanic Events

Event	Cluster Spacing[a] (km)		Event Length (km)	Event Width (km)	Notes
	Parallel	Perpendicular			
Paiute Ridge	13.1	na	33.1	3.5	Paiute Ridge data taken from analog table (Keating et al., 2008) modified slightly based on personal mapping.
Scarp Canyon	15.7	na	33.1	3.5	Scarp Canyon is known from surface outcrops (plugs) and inferences from buried basalt encountered in multiple drillholes in Frenchman Flat. Parallel spacing measured from the centroids of cone clusters.
3.8-Ma Crater Flat (without Anomalies C and D)	11.5	1.4	28	12.6	
Anomaly B	11.6	4.3	28	12.6	
Anomalies F, G, and H	6.5	8.9	28	12.6	
3.8-Ma Crater Flat and Anomalies C and D	15.4	1.1	43.6	12.6	
Anomalies B, C, and D	8.3	4.4	43.6	12.6	
Anomalies F, G, H, C, and D	6.7	7.8	43.6	12.6	
Anomalies C and D	19.6	2.1	43.6	12.6	

[a] Cluster spacing is defined as the distance from the midpoint of the event rectangle to the center of the cluster. Separate measurements are provided for the distance parallel and the distance perpendicular to the event orientation. See Figure D.2-6.

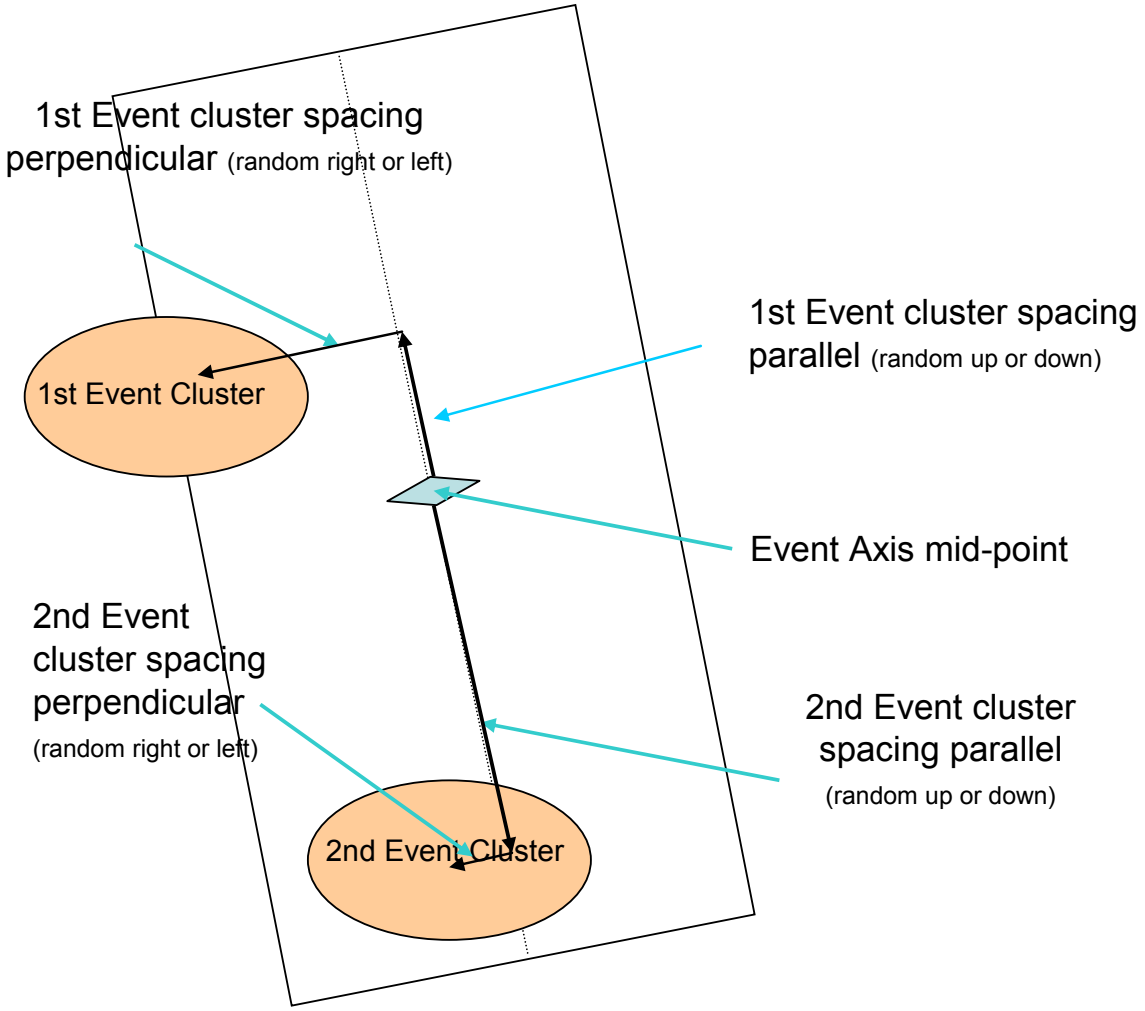

NOTE: The placement sequence should vary with each sampling of large-footprint events in disruption simulations.

Figure D.2-6. An Example of the Procedure for Placement of Clusters within a Large-Footprint Event

D.2.3 SPATIAL MODELS

The spatial distribution of potential future events in the YMR are established by first identifying regions of interest for the assessment, then evaluating the distribution of events (event frequency zones) within those regions.

D.2.3.1 Regions of Interest

Region(s) of interest (ROIs) form the structural framework for my PVHA-U models. I defined three alternative ROIs based on post-caldera basaltic volcanic cycles <9.5 Ma in the Amargosa trough, with the exception of an 8.6- to 7.3-Ma cycle of volcanic activity in the Yucca Flat and Frenchman Flat basins. All post-Miocene (<~4.9 Ma) basaltic volcanic activity in the YMR occurred in the Amargosa trough. These past patterns provide the basis for assuming that future volcanic activity would occur in the Amargosa trough and most likely within the Crater Flat part of the trough (based on the Quaternary record).

The three alternative ROIs, shown in Figure D.2-7, are described as follows:

1. The Crater Flat volcanic field (ROI 1) extends from the southeast edge of Bare Mountain, across Crater Flat and Yucca Mountain, and into Jackass Flats.

2. The Crater Flat-Amargosa Valley volcanic field (ROI 2) encompasses the Crater Flat volcanic field and areas that extend slightly north of Yucca Mountain to the Claim Canyon caldera segment and south of Crater Flat into the Amargosa Valley. ROI 2 includes identified aeromagnetic anomalies. Note that the boundaries of ROI 2 could change depending on the ages of uncharacterized aeromagnetic Anomalies C and D.

3. ROI 3 extends for nearly the full length of the Amargosa trough. It includes the Crater Flat and Crater Flat-Amargosa volcanic fields (ROI 1 and ROI 2), plus an expanded area to the north that encompasses the basalts of Buckboard Mesa, Sleeping Butte, and Thirsty Mesa. The approximate northern boundary of ROI 3 is drawn along the north ring-fracture zone of the Timber Mountain caldera.

The three ROIs, areas of occurrence of past Pliocene and Quaternary volcanism, are expected to be areas where potential future volcanic events would occur. By virtue of being the area of most recent volcanic activity, the Crater Flat volcanic field (ROI 1) is judged to be the most relevant area for potential volcanic events in the near future. ROI 2, which includes areas of Pliocene volcanism in the Amargosa Valley, is weighted lower than ROI 1 because the Amargosa Valley lacks Quaternary volcanism. ROI 3, which extends to include both Pliocene and Quaternary volcanic activity north and outside of Crater Flat, is weighted higher than is ROI 2 because of Quaternary volcanism in the Sleeping Butte area. The ROIs are weighted differently for the 10,000-year and the 1-My compliance periods. The length of the 1-My compliance period decreases the likelihood of remaining in the current volcanic cycle, increases the likelihood of starting a new cycle, and increases uncertainty in the spatial location of volcanic activity in the new cycle (resulting in near equal weightings of the ROIs).

Table D.2-12 shows the relative weights assigned to each ROI for the two compliance periods.

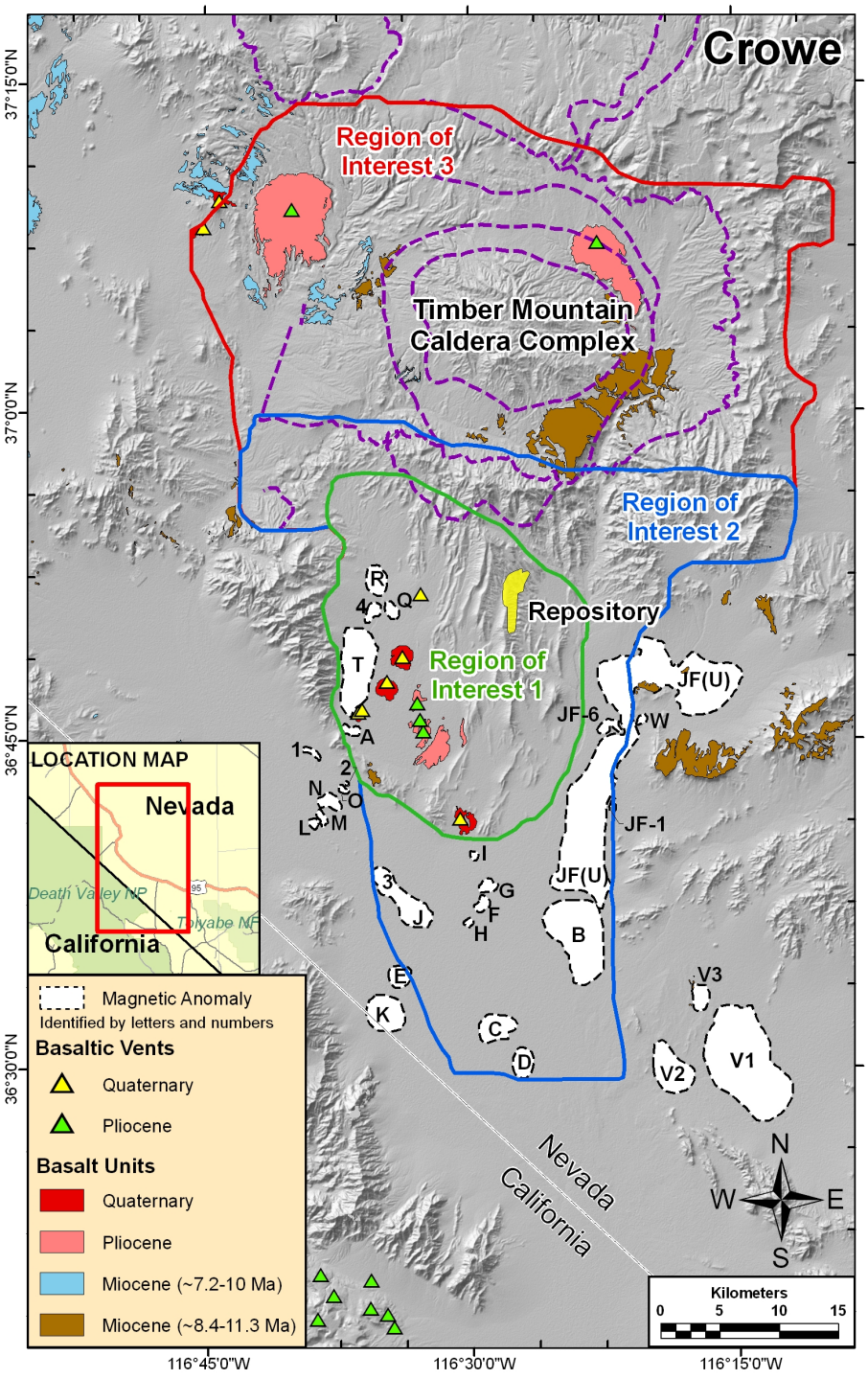

NOTE: Base figure was requested and supplied by the PVHA-U Methodology Development Team. ROI 2 includes ROI 1 plus the area to the north and south. ROI 3 includes ROI 2 plus the full length of the Amargosa trough.

Figure D.2-7. Identified Regions of Interest in the Amargosa Trough

Table D.2-12. Weighting of Regions of Interest Based on Compliance Period

	10,000-Year Compliance Period	1-My Compliance Period
ROI 1	60%	40%
ROI 2	15%	30%
ROI 3	25%	30%

D.2.3.2 Event Frequency Zones

I utilize the spatial setting of Pliocene and Quaternary basaltic volcanoes in the YMR to assess the spatial distribution of future events within each ROI. The data for the assignments are the observed frequency of events in three settings (or zones): (1) alluvial basins; (2) at or near range-front margins at the edges of alluvial basins; and (3) the interiors of mountain ranges.

A fourth zone is defined as an approximate topographic elevation (lithostatic pressure) within range interiors where future volcanic events are not expected (based on no observed events in the post-Miocene record of basaltic volcanism). The elevation of this zone is above the elevation of the topographically highest post-Miocene volcanic centers in the Amargosa trough (basalt of Buckboard Mesa, Little Black Peak Cone, and Thirsty Mountain).

Lithostatic pressure maps developed by George Thompson (see Parsons et al., 2006) and provided to expert panel members were selected in developing a preferred approach to describing the frequency of occurrence of volcanic events in the three settings (see Section D.2.3.3)

Uncertainty in the relative frequency of future events in the three spatial settings is quantified by assembling three sets of event frequencies, each based on a different assignment perspective.

1. Valley bias, which assumes events are focused primarily in alluvial basins

2. Expected case, which assumes events tend to occur in alluvial basins but can also occur in range interiors

3. Range bias, which assumes the valley bias is weak, and events can occur readily in range interiors.

Table D.2-13 shows assigned frequencies of past events for the three settings based on the three alternative perspectives. The expected case represents my best assessment of the observed volcanic record.

Table D.2-13. Past Events Assigned to Spatial Zones Using Alternative Perspectives

	Zone[a]				Zone		
Minimum No. Events	**1**	**2**	**3**	**Maximum No. Events**	**1**	**2**	**3**
Valley Bias							
Anomalies C and D	1			Anomaly C	1		
Thirsty Mountain		1		Anomaly D	1		
3.8-Ma Crater Flat	1			Thirsty Mountain		1	
Buckboard Mesa	1			3.8-Ma Crater Flat	1		
1.1-Ma Crater Flat (without Little Cones)	1			3.8-Ma Amargosa Valley	1		
Little Cones	1			Anomaly B	1		
Sleeping Butte		1		Buckboard Mesa	1		
Lathrop Wells	1			1.1-Ma Crater Flat (without Little Cones)	1		
Number of events	*6*	*2*		Little Cones	1		
Percentage of events	*75*	*25*	*0*	Sleeping Butte		1	
				Lathrop Wells	1		
				Number of events	*9*	*2*	*0*
				Percentage of events	*81.8*	*18.2*	*0*
Expected Case							
Anomalies C and D	1			Anomaly C	1		
Thirsty Mountain		1		Anomaly D	1		
3.8-Ma Crater Flat	1			Thirsty Mountain		1	
Buckboard Mesa		1		3.8-Ma Crater Flat	1		
1.1-Ma Crater Flat (without Little Cones)	1			3.8-Ma Amargosa Valley	1		
Little Cones	1			Anomaly B	1		
Sleeping Butte			1	Buckboard Mesa		1	
Lathrop Wells	1			1.1-Ma Crater Flat (without Little Cones)	1		
Number of events	*5*	*2*	*1*	Little Cones	1		
Percentage of events	*62.5*	*25*	*12.5*	Sleeping Butte		1	
				Lathrop Wells	1	1	
				Number of events	*8*	*4*	*0*
				Percentage of events	*66.7*	*33.3*	*0*

Table D.2-13. Past Events Assigned to Spatial Zones Using Alternative Perspectives (Continued)

	Zone[a]				Zone		
Minimum No. Events	**1**	**2**	**3**	**Maximum No. Events**	**1**	**2**	**3**
Range Interior Bias							
Anomalies C and D	1			Anomaly C	1		
Thirsty Mountain		1		Anomaly D	1		
3.8-Ma Crater Flat		1		Thirsty Mountain		1	
Buckboard Mesa		1		3.8-Ma Crater Flat	1		
1.1-Ma Crater Flat (without Little Cones)	1			3.8-Ma Amargosa Valley	1		
Little Cones	1			Anomaly B	1		
Sleeping Butte			1	Buckboard Mesa		1	
Lathrop Wells		1		1.1-Ma Crater Flat (without Little Cones)	1		
Number of events	*3*	*4*	*1*	Little Cones	1		
Percentage of events	*37.5*	*50*	*12.5*	Sleeping Butte			1
				Lathrop Wells	1	1	
				Number of events	*8*	*3*	*1*
				Percentage of events	*66.7*	*25.0*	*8.3*

[a] No events occurred in Zone 4, so only Zones 1 through 3 are shown.

Based on this characterization of past events, I developed the following assessment for the relative frequency of potential future events by zone (Table D.2-14).

Table D.2-14. Relative Frequency of Future Events Based on Alternative Event Perspectives

	Alternative		
Zone[a]	**Valley Bias**	**Expected Case**	**Range Interior Bias**
Zone 1	0.8	0.625	0.5
Zone 2	0.2	0.25	0.38
Zone 3		0.125	0.12

I assign a weight of 50% to the expected case, and 25% to each of the other cases.

D.2.3.3 Alternative Approaches to Modeling Spatial Distribution

I compared multiple alternative approaches against observed data on the spatial setting of basaltic volcanoes in the ROIs in order to select alternative spatial models that best fit the observed data.

I first tried mapping boundaries of alluvial valleys versus ranges within ROIs. This approach was abandoned because of arbitrary and gradational transitions from basin edges to ranges, no discrimination of deep versus shallow alluvial basins, and no discrimination of zones within ranges.

I examined but did not use the extensional model of Fridrich et al. (1999), because the model accounts for extension in only the Crater Flat basin and cannot be applied to other areas of the Amargosa trough. Additionally, there is limited stratigraphic control on the timing of extension, much of which occurred before the Pliocene and Quaternary volcanic cycles in the Amargosa trough.

I examined but did not use the cluster model of Connor (discussed in Workshop #2A). Cluster analysis is primarily a method that utilizes multivariate data reduction to identify patterns within large data sets. The event definition used in this elicitation model results in a small data set for event locations. Additionally, clusters of Pliocene and Quaternary volcanic activity occur across areas of complex and varying structural and geologic settings.

I examined but did not use the teleseismic tomography data for assigning frequency zones because of low resolution, coarse grid size, and ambiguous interpretations.

As noted above, spatial patterns of lithostatic pressure maps were compared against distribution data for the three cycles. I performed trial-and-error iterations using hand-contoured subdivisions of the pressure field. For verification, the contoured zones were compared iteratively with the assigned frequency data for basaltic centers in the alternative ROIs. Best-fit hand-contoured maps of lithostatic pressure zones were submitted to the LANL GIS support team, who developed lithostatic pressure divisions to match the maps. These maps (Figure D.2-8) define the three spatial zones of my elicitation model. The primary benefit of the lithostatic pressure maps over topographic data is that the pressure subdivisions are less arbitrary to define and can be applied more consistently to designate basin edges and identify gradations in the thickness of fill deposits in alluvial basins. Additionally, the pressure subdivisions, including the ranges, are combined with conceptual models of dike propagation toward higher topography to define lithostatic pressure zones in range interiors. Finally, the lithostatic pressure maps can be applied consistently to all three ROIs.

The PVHA-U methodology development team will estimate the probability of disruption of the repository using simulation modeling and sampling of parameters from data provided in my elicitation model. This team will decide upon the procedures for performing the simulations; however, a suggested simulation sequence is provided in Supplement B.

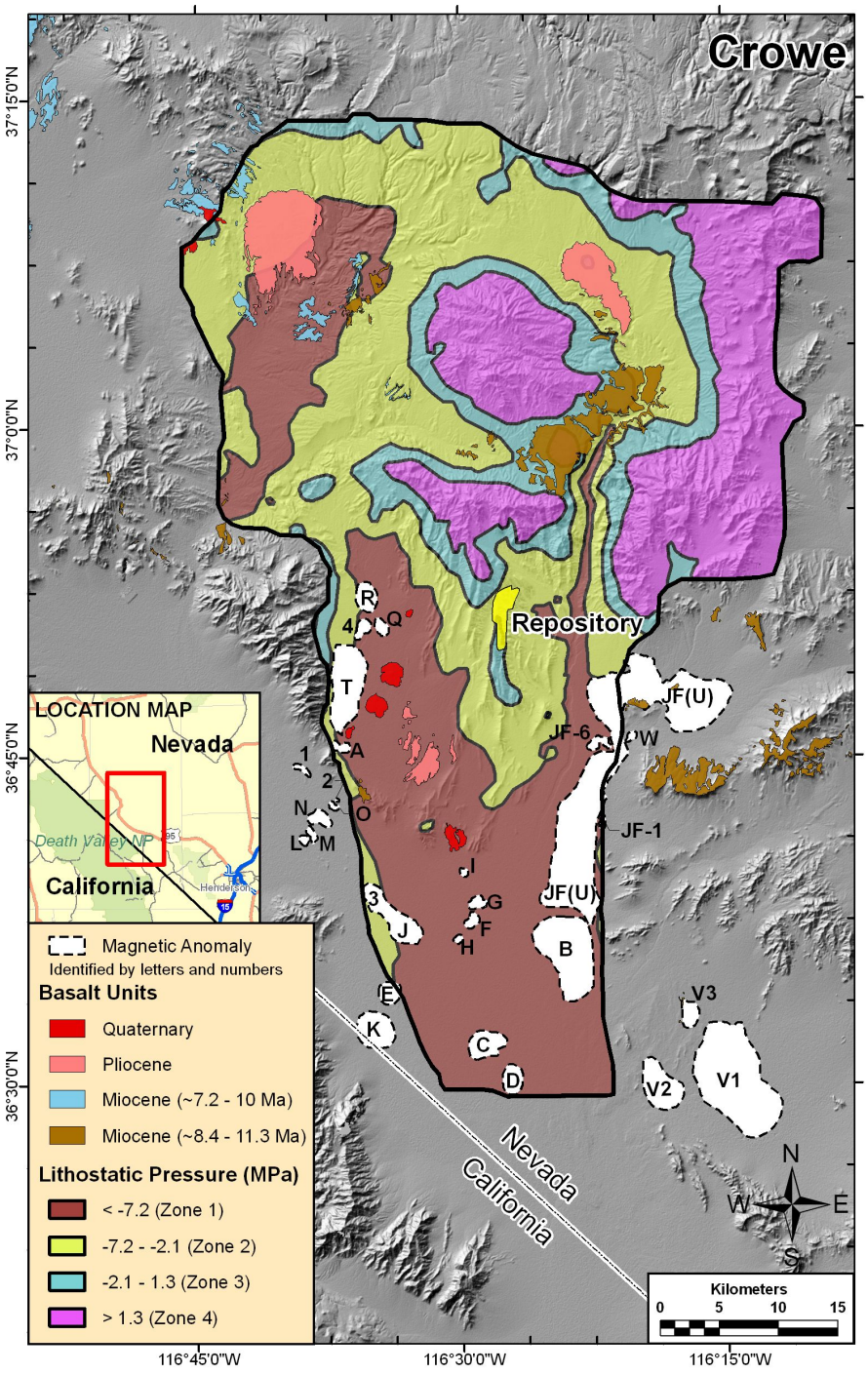

NOTE: Lithostatic pressure values in the map legend correspond to Zones 1, 2, 3, and 4 as lithostatic pressure values increase. Base figure was requested and supplied by the PVHA-U Methodology Development Team.

Figure D.2-8. Event Frequency Zones based on the Lithostatic Pressure Map of the Yucca Mountain Region

D.2.4 TEMPORAL MODELS

As described in Section D.2.1.2, my elicitation model utilizes four alternative rate models that are weighted differently for different models of future volcanic activity and for the 10,000-year and 1-My compliance periods. The development of estimates for recurrence rates involved three steps.

D.2.4.1 Alternative Recurrence Rates

Step one was to identify alternative recurrence rates based on past events for the regions of interest (ROIs). Table D.2-15 summarizes the alternative sets of events and time periods used to estimate past rates within each region of interest, and the weights assigned for estimating the future rate in that ROI. For each alternative, the recurrence rate was estimated by dividing the number of relevant events (those within the ROI and specified time period) by the time between the oldest and youngest such events. Detailed calculations of these rates, as well as other alternatives considered but not used, are provided in Crowe (2007), Excel Worksheet titled *Recurrence Rate Zones.*

Table D.2-15. Estimated Recurrence Rates Based on Alternative Sets of Past Events and Regions of Interest

Alternative Recurrence Rates for Crater Flat Volcanic Field (ROI 1)	**Weight**	**Recurrence Rate[a]**
Quaternary events: Little Cones age estimated as 1.1 Ma	0.25	1.96E-06
Quaternary events: Little Cones age estimated as 0.7 Ma	0.25	2.93E-06
Average rate from past volcanic cycles	0.50	3.07E-06
Alternative Recurrence Rates for Crater Flat/Amargosa Valley Volcanic Field (ROI 2)		
Pliocene cycle: all ~3.8-Ma events interpreted as a single large-cluster event	0.25	3.0E-06
Pliocene cycle: ~3.8-Ma event interpreted as separate events	0.25	5.0E-06
Average rate from past volcanic cycles	0.50	3.07E-06
Alternative Recurrence Rates for Quaternary Full Amargosa Trough (ROI 3)		
Quaternary events: Little Cones age estimated as 1.1 Ma	0.23	2.9E-06
Quaternary events: Little Cones age estimated as 0.7 Ma	0.23	3.9E-06
Pliocene cycle: all ~3.8-Ma events interpreted as a single large-cluster event	0.05	2.6E-06
Pliocene cycle: ~3.8-Ma event interpreted as separate events	0.05	3.6E-06
Average rate from past volcanic cycles	0.45	3.1E-06
Recurrence Rates for Past Volcanic Cycles		
Frenchman/Yucca volcanic cycle (1)	equally-weighted	2.31E-06
Frenchman/Yucca volcanic cycle (2)		3.08E-06
Pliocene volcanic cycle of the Amargosa Trough		2.59E-06
Pliocene volcanic cycle of the Amargosa Trough, with Anomalies C&D and cluster as seprate events		3.63E-06
Quaternary volcanic cycle of the Amargosa Trough (LC = 1.1 Ma)		2.93E-06
Quaternary volcanic cycle of the Amargosa Trough (LC = 0.7 Ma)		3.91E-06

[a] Recurrence rate was estimated for each model by dividing the number of relevant events in that ROI by the time between the oldest and youngest of those events (event duration).

An important feature of the above rate estimates is they are calculated for the *duration* of individual volcanic cycles, defined by the oldest event in the cycle minus the youngest event in the cycle. This approach avoids *dilut*ing recurrence rates by averaging rates across intervals of background volcanic activity *between* volcanic cycles. The estimates are treated as most likely future recurrence rates based on sampling theory (they reflect small data sets that are unlikely to sample upper and lower distribution percentiles).

D.2.4.2 Estimating Future Rates

After the rate estimates given in Table D.2-15 were developed, the next step was to decide how to use those rates to estimate the future rate for each ROI, for each alternative volcanic state, and for the 10,000-year and 1-My compliance periods. As described in Section D.2.1.2, I defined four alternative models of expected patterns of future volcanic activity (steady-state, increasing rate, background rate, and new volcanic cycle).

For the 10,000-year compliance period, three of those rate models are considered relevant: the YMR is assumed to be *within* the current Quaternary cycle of the Crater Flat volcanic field (under either steady-state or increasing rates) or within a cycle of background volcanic activity *following* the Quaternary cycle.

Because the possibility of a new volcanic cycle exists for the 1-My compliance period, all four alternate rate models may be relevant. These alternative models are modified slightly for each ROI. For ROI 1 (Quaternary Crater Flat volcanic field), all alternative models apply. For ROI 2 (Pliocene Crater Flat and Amargosa Valley volcanic field), the increasing rate alternative is not applied, because there is no evidence of decreased repose intervals. For ROI 3 (Quaternary and Pliocene Full Amargosa trough), the increasing rate alternative is not applied for the 1-My compliance period.

The first two columns of Table D.2-16 show the weights for each rate model specific to each ROI and compliance period.

Table D.2-16. Estimated Recurrence Rates for Each Region of Interest, Rate Model, and Compliance Period

Alternatives for ROI 1	Model Weights	Minimum	25th Percentile	50th Percentile	75th Percentile	Maximum
For 10,000-Year Compliance Period						
Steady-State Rate Model[a]	0.60	5.0E-07	7.5E-07	2.8E-06	5.0E-06	8.0E-06
Increasing Rate Model	0.30	5.0E-07	1.5E-06	4.1E-06	6.5E-06	1.0E-05
Background Rate Model	0.10	1.3E-07	2.0E-07	6.9E-07	1.0E-06	2.0E-06
For 1-My Compliance Period						
Steady-State Rate Model	0.25	5.0E-07	7.5E-07	2.8E-06	5.0E-06	8.0E-06
Increasing Rate Model	0.13	5.0E-07	1.5E-06	4.1E-06	6.5E-06	8.0E-06
Background Rate Model	0.35	1.3E-07	2.0E-07	6.9E-07	1.0E-06	2.0E-06
New Volcanic Cycle Rate Model	0.27	5.0E-07	8.0E-07	3.1E-06	7.0E-06	1.3E-05
Alternatives for ROI 2	**Model Weights**	**Minimum**	**25th Percentile**	**50th Percentile**	**75th Percentile**	**Maximum**
For 10,000-Year Compliance Period						
Steady-State Rate Model	0.80	5.0E-07	8.5E-07	3.5E-06	6.0E-06	8.0E-06
Background Rate Model	0.20	1.3E-07	2.0E-07	6.9E-07	1.0E-06	2.0E-06
For 1-My Compliance Period						
Steady-State Rate Model	0.25	5.0E-07	8.5E-07	3.5E-06	6.0E-06	8.0E-06
Background Rate Model	0.40	1.3E-07	2.5E-07	8.8E-07	1.0E-06	2.0E-06
New Volcanic Cycle Rate Model	0.35	5.0E-07	8.0E-07	3.1E-06	7.0E-06	1.3E-05
Alternatives for ROI 3	**Model Weights**	**Minimum**	**25th Percentile**	**50th Percentile**	**75th Percentile**	**Maximum**
For 10,000-Year Compliance Period						
Steady-State Rate Model	0.60	5.0E-07	8.2E-07	3.2E-06	6.5E-06	8.0E-06
Increasing Rate Model	0.30	5.0E-07	1.6E-06	6.5E-06	8.0E-06	1.0E-05
Background Rate Model	0.10	1.3E-07	2.5E-07	8.1E-07	1.0E-06	2.0E-06
For 1-My Compliance Period						
Steady-State Rate Model	0.25	5.0E-07	8.2E-07	3.2E-06	6.5E-06	8.0E-06
Background Rate Model	0.40	1.3E-07	2.5E-07	8.1E-07	1.0E-06	2.0E-06
New Volcanic Cycle Rate Model	0.35	5.0E-07	8.0E-07	3.1E-06	7.0E-06	1.3E-05

[a] For all ROIs, the 50th percentile of the recurrence rate estimate for the steady-state rate model is equal to the weighted average of the recurrence rate for each relevant characterization of past events, as shown in Table D.2-14.

D.2.4.3 Recurrence Rate Distributions

The third step in developing estimates for recurrence rates involved weighting the alternative models and integrating those weighted models to estimate a distribution of recurrence rates for each ROI, volcanic state, and compliance period. The uncertainty in the estimate of the steady-state rate is defined using the weighted average of the recurrence rates from Table D.2-14 as the mid-point of the distribution. Then professional judgment is used to assign upper and lower bounds and 25th and 75th percentiles for the distributions, thereby quantifying structural or conceptual model uncertainty. In general, the assignments are designed to be consistent with a skewed distribution (skewed toward higher rates) that is bounded by realistic minimum and maximum rates. Under a future volcanic state of increasing rates, the rates are estimated to be 1.5 to 2 times higher than under a steady-state rate. Under a future state of background rate, rates are estimated to be about 4 times lower than under a steady-state rate. And under a future state of a new volcanic cycle, rates are estimated based on the average rates of past cycles, but the distribution is skewed toward higher rates having a higher upper bound (bounds are discussed below).

Minimum bounding values are assigned to the rate distributions for models of a steady state, increasing rate, and future volcanic cycle using estimates of background rates of volcanic activity in the Amargosa trough and the southern Great Basin—specifically from a rate consistent with one event in the Amargosa trough in the Quaternary. For a future volcanic state of the background rate, the minimum bound is one-fourth of the minimum bound under the other rate models. Additional detail on alternative bounding calculations is provided in Crowe (2007), Excel Worksheets titled *Probability Bounds* and *ROI Adjusted Recurrence*.

Maximum bounding rates are assigned by assessing recurrence rates for the Cima (California) and Lunar Crater (Nevada) volcanic fields.

The limited characterization data for aeromagnetic Anomalies C and D affect the model assignments. The age and composition of the anomalies was not established through exploratory drilling and chronology studies of recovered basalt samples. Thus event characteristics must be assigned both with and without Anomalies C and D, which affects calculations of the duration and recurrence rate for the Pliocene volcanic cycle. The indeterminate geochronology data for Little Cones affects assessments of the duration of the Quaternary volcanic cycle and the number of volcanic events for multiple sets of recurrence rate calculations. The resulting alternative assignments of event characteristics (whether two or three events for the Quaternary volcanic cycle) increase the uncertainty in the estimates of recurrence rates. Instead of calculating separate rates for the Quaternary and Pliocene cycles for ROI 3, a single weighted recurrence rate is calculated that integrates the Quaternary and Pliocene rates (10% weight for Pliocene rates, 45% for Quaternary rates, and 45% for the average cycle rates).

The probabilities of repository disruption specific to each ROI will be estimated by simulation. These probabilities will be developed by the PVHA-U Methodology Development Team. Each ROI has its own estimated recurrence rate for each of the two compliance periods, as shown in Tables D.2-15 and D.2-16 and discussed above. The combined model for the conditional probability of recurrence of a future volcanic event and the probability of that event intersecting the repository are weighted as follows:

1. 10,000-year compliance period
   a. ROI 1: 60%
   b. ROI 2: 15%
   c. ROI 3: 25%

2. 1-My compliance period
   a. ROI 1: 40%
   b. ROI 2: 30%
   c. ROI 3: 30%

D.2.5 REFERENCES

Anderson, M.P., and Woessner, W.W., 1992. *Applied Groundwater Modeling—Simulation of Flow and Advective Transport.* San Diego, CA, Academic Press, 381 p.

Crowe, B.M., 2007. Microsoft Excel spreadsheets supporting PVHA-U Elicitation Summary, DTN: TBD.

Crowe, B.M., Valentine, G.A., Perry, R.V., and Black, P.K., 2006. Volcanism—the continuing saga, in Macfarlane, A.M., and Ewing, R.C. (eds.), *Uncertainty Underground—Yucca Mountain and the Nation's High-Level Nuclear Waste:* Cambridge, The Massachusetts Institute of Technology Press, pp. 131-148.

Fridrich, C.J., Whitney, J.W., Hudson, M.R., and Crowe, B.M., 1999. Space-time patterns of late Cenozoic extension, vertical axis rotation, and volcanism in the Crater Flat basin, southwestern Nevada, in Wright, L.A., and Troxel, B.W. (eds.), *Cenozoic Basins of the Death Valley Region*. Boulder, Colorado: Geological Society of America Special Paper 333, pp. 197-212.

Grauch, V.J.S., Sawyer, D.A., Fridrich, C.J., and Hudson, M.R., 1999. *Geophysical framework of the southwestern Nevada volcanic field and hydrogeologic implications*. U.S. Geological Survey Professional Paper 1608.

Keating, G.N., Valentine, G.A., Krier, D.J., and Perry, F.V., 2008. *Shallow plumbing systems for small-volume basaltic volcanoes.* Bulletin of Volcanology, v. 70, pp. 563-582, DOI 10.1007/s00445-007-0154-1.

Manning, M.R., M. Petit, D. Easterling, J. Murphy, A. Patwardhan, H-H. Rogner, R. Swart, and G. Yohe (eds), 2004. *IPCC Workshop on Describing Scientific Uncertainties in Climate Change to Support Analysis of Risk and of Options*: Workshop report, Intergovernmental Panel on Climate Change (IPCC), Geneva.

National Research Council, Committee on Models in the Regulatory Decision Process, 2007. *Models in Environmental Regulatory Decision Making.* Washington, D.C., National Academies Press, available online at http://nap.edu/catalog/11972.html.

Parsons, T., Thompson, G.A., and Cogbill, A.H., 2006. *Earthquake and volcano clustering via stress transfer at Yucca Mountain, Nevada*. Geology, v. 34, no. 9, p. 785-788, September.

Slate, J.L., Berry, M.E., Rowley, P.D., Fridrich, C.J., Morgan, K.S., Workman, J.B., Young, O.D., Dixon, G.L., Williams, V.S., McKee, E.H., Ponce, D.A., Hildenbrand, T.G., Swadley, W.C., Lundstrom, S.C, Ekren, E.B., Warren, R.G., Cole, J.C., Fleck, R.J., Lanphere, M.A., Sawyer, D.A., Minor, S.A., Grunwald, D.J., Laczniak, R.J., Menges, C.M., Yount, J.C., Jayko, A.S., Mankinen, E.A., Davidson, J.G., Morin, R.L., and Blakely, R.J., 1999. *Digital Geologic Map of the Nevada Test Site and Vicinity, Nye, Lincoln, and Clark Counties, Nevada, and Inyo County, California, Revision 4; Digital Aeromagnetic Map of the Nevada Test Site and Vicinity, Nye, Lincoln, and Clark Counties, Nevada, and Inyo County, California; and Digital Isostatic Gravity Map of the Nevada Test Site and Vicinity, Nye, Lincoln, and Clark Counties, Nevada, and Inyo County, California*. U.S. Geological Survey Open-File Report 99-554-A, -B, and -C.

Valentine, G.A., and Perry, F.V., 2006. *Decreasing magmatic footprints of individual volcanoes in a waning basaltic field*. Geophysical Research Letters, v. 33, no.14, p. L14305.

Wainwright, J., and Mulligan, M. (eds.), 2004. *Environmental Modelling—Finding Simplicity in Complexity*. Chichester, England, John Wiley & Sons, LTD, 408 p.

SUPPLEMENT A

MODELING PROTOCOL

The approach used to develop my PVHA-U elicitation models follows the guidance provided for modeling protocols summarized in modeling textbooks such as Wainwright and Mulligan, 2004; Anderson and Woessner, 1992; and National Research Council, 2007. This supplement briefly summarizes my implementation of each of the modeling steps.

Purpose of Modeling

This PVHA-U expert panel member developed a model of the probability of volcanic/magmatic disruption of a repository site in the Yucca Mountain region (YMR). The elicitation model utilizes the record of cycles of post-caldera small-volume basaltic volcanic activity (8.6 Ma to recent). The hazard model assumes that past volcanic patterns are the most reasonable predictor of future volcanic hazards.

Conceptual Model

The Yucca Mountain site lies within the Amargosa trough, a major tectonic feature that has influenced the location of (1) silicic volcanic activity in the YMR during the Miocene and (2) basaltic volcanic activity in the trough for the past 5 Ma. The boundaries of the trough are taken from a combination of references and subjective interpretations of the geologic and tectonic features of the southwest Nevada volcanic field.

A critical assumption of the developed conceptual model for the PVHA-U is that future basaltic volcanic activity will occur within the Amargosa trough, as described in the main text.

Governing Equations and Computer Code

The current understanding of the processes leading to the future generation, ascent, and eruption of basaltic magma in the Amargosa trough cannot be quantified using a predictive, process-based model. The hazards of future volcanic activity can be evaluated as an empirical model using a conditional probability equation:

$$Pr(d) = Pr(E2 \text{ given } E1)Pr(E1)$$

where

E1 is the recurrence rate of volcanic events in the Amargosa trough
E2 is an event that intersects/impacts the repository

Model Design

The model design started with an influence diagram developed before the start of the PVHA-U studies (Crowe et al., 2006). It was modified to include changes specific to this PVHA-U elicitation. All model components were designed for the structural framework of the Amargosa trough and identified regions of interest (ROIs) in the trough. The model components were

adapted to volcanic cycles, alternative models of future volcanic events, and the 10,000-year and 1-My compliance periods.

Minimum rates for the recurrence of volcanic activity and probabilities of repository disruption were estimated by establishing background rates for the Amargosa trough and the southern Great Basin and Mojave Desert and assuming that a repository is located randomly within those regions. Maximum disruption ratios were established using maximum recurrence rates and locating a repository footprint within the Quaternary Crater Flat volcanic field. The elicitation model was designed to yield results that are consistent with and remain within the estimates of minimum and maximum probability [see Crowe (2007), Excel Worksheet titled *Probability Bounds*].

Recurrence rates were developed from a matrix of alternative representations of Quaternary and Pliocene volcanic cycles of the YMR. The resulting rates were adapted to the ROIs and two compliance periods, then weighted by alternative models of the future state of the YMR. The probability density functions (PDFs) assigned to the alternative models were adjusted to reflect the uncertainty associated with the small size of available data sets.

A volcanic event is based on recognition of synchronous pulses of Pliocene and Quaternary basaltic volcanic activity. Events were divided into four types based on observed variability in the volcanic record. Separate sub-definitions were used for estimating the number of feeder dikes for each event type and the number of vents along feeder dikes.

The probability of disruption for the repository was estimated by simulating event locations and characteristics within the ROIs weighted by the observed frequency of occurrence of basaltic volcanoes in alluvial basins, range fronts, and range interiors. These frequency zones were defined by adapting lithostatic pressure maps for the ROIs. Disruption probabilities for each ROI and compliance period were combined with the applicable recurrence rate to define the hazard of future volcanism for the Yucca Mountain site (the probability of volcanic events intersecting the repository footprint).

Calibration

The empirical volcanic hazard model does not have data that allow for quantitative model calibration (no data measurements can be identified as calibration targets). The volcanic record for the three volcanic cycles was used to define expected PDFs. Minimum and maximum limits (tail estimations for PDFs) are established from personal knowledge of volcanic processes. A qualitative form of calibration was used whereby the tail parts of PDFs are constrained to be within physical limits or plausibility ranges established from combinations of knowledge of volcanic processes and observations of patterns of basaltic volcanism in the YMR and the Great Basin and Mojave Desert.

Calibration Sensitivity Analysis

Calibration sensitivity analysis is not possible with an empirical volcanic hazard model.

Model Verification

Model verification is difficult with an empirical volcanic hazard model (and in fact with almost all environmental models) because of limited data. All available data are used in the model, and no independent data can be identified for verification. Rather, simulation results are back-compared with the geologic record to confirm that recurrence rates and disruption probabilities are not inconsistent with the volcanic record and/or volcanic processes.

Prediction

Bounding estimates for the probability of magmatic disruption of the repository site were developed for: (1) background rates for the Amargosa trough and the southern Great Basin and Mojave Desert assuming a random location of a repository within those regions, and (2) maximum recurrence rates based on locating a repository within the Quaternary Crater Flat volcanic field [see Crowe (2007), Excel worksheet titled *Probability Bounds*]. The elicitation model was designed to yield results that should be consistent with and remain within these minimum and maximum probability estimations. Bounding estimates for the probability of disruption of a 6-km^2 site in the Amargosa trough range from a minimum background disruption rate of 5.6×10^{-9} events per year (random location of a repository in the trough) to 1.4×10^{-7} events per year for a repository located in the Crater Flat volcanic field (less than 2 orders of magnitude difference). The probability of disruption for the repository site is estimated subjectively to be skewed slightly toward the maximum bounding values because of the site's location within the Amargosa trough and near the active Crater Flat volcanic field. Subjective estimates for repository disruption based on the bounding estimates are 3 to 4×10^{-8} events per year.

A cross section of disruption rates developed for the repository setting using bounding estimates for the Amargosa trough and background includes the following (rates as probability of disruption per square kilometer).

1. Crater Flat basin: 2.3×10^{-8} events per year
2. Yucca Mountain range front: 7.8×10^{-9} events per year
3. Yucca Mountain interior: 5.0×10^{-10} events per year
4. Jackass Flats: 1.4×10^{-10} events per year (outside the trough).

Prediction Sensitivity Analysis

The PVHA-U methodology development team will conduct sensitivity and uncertainty analyses of model results. Qualitative assessments of the major components of uncertainty for my elicitation model are described below.

Statistical Uncertainty

Natural variability is observed in the nature (type) of volcanic events, in the local structural controls for the setting of events, and in event frequencies assigned to ROIs. Knowledge uncertainty derives from a combination of the following factors:

1. Measurement errors, reproducibility, and interpretation of geochronology data

2. Incomplete characterization of all aeromagnetic anomalies in the YMR (primarily knowledge uncertainty, but possible structural uncertainty depending on the age of the uncharacterized anomalies)

3. Subjective judgment in interpreting cones, vents, dikes, and eruptive processes that formed volcanic events

4. Uncertainty in the subsurface geometry of basalt feeder systems (dikes, sills, plugs/conduits) because of the small number of sites at which basalt intrusions can be observed reliably

5. Difficulty in interpreting geophysical data because of limitations in measurement methods and multiple permissive alternative interpretations of the data.

Structural Uncertainty

Conceptual uncertainty derives from applying an empirical probability model that is statistically non-robust (based on limited data) without model calibration. There is uncertainty in having many permissive alternative models of the spatial controls on the locations of volcanic events and in using subjective judgment to select model approaches. The processes that control event formation in alluvial valleys, range margins, and range interiors can be inferred but not tested adequately. There are multiple alternative models of future volcanic activity, including being within the current cycle, being between cycles, and being within a new volcanic cycle (representing uncertainty in conceptual model). The 1-My compliance period is sufficiently long to allow the possibility of changes in the tectonic setting of future basaltic volcanic activity that could alter conceptual models for the hazard assessments.

Model Results

The PVHA-U model results were evaluated at two PVHA-U workshops and two individual elicitation reviews with the PHVA-U methodology development team (MDT). Model documentation is provided in this report, in associated Excel spreadsheets, and in the summation of results that will be produced by the PVHA-U MDT.

Post-audit

The post-audit results will be produced by and are the responsibility of the PVHA-U MDT.

Model Redesign

My elicitation model was redesigned through an iterative process during numerous stages of development of the model. Model development evolved through discussions at several PVHA-U workshops, through elicitation interviews, and through evaluations of interim model results. The concept of separating and using results from assessments of individual basaltic volcanic cycles was developed as an outgrowth of developing presentations for one of the early PVHA-U workshop meetings. The development and redefinition of ROIs and frequency zones involved many stages. The final emphasis on ROIs within the Amargosa trough evolved through a combination of (1) assessing spatial patterns of basaltic volcanism in the YMR and (2) integrating the results of refined gravity and aeromagnetic data for the basins of Crater Flat, Jackass Flats, and the Amargosa Valley. Temporal subdivisions used to establish volcanic cycles were developed through analysis of spatial and temporal patterns of volcanic activity. Boundaries for the Amargosa trough were modified using the PVHA-U geophysical map and geologic, structural, and geophysical data for the Nevada Test Site region. Data on temporal and event patterns of past basaltic volcanic cycles were developed through several workshops. The cycle ages and event patterns were refined at various stages using new geochemistry and chronology data obtained by the PVHA-U MDT.

Bounding probabilities for disruption of a repository were estimated originally for the southern Great Basin. They subsequently were refined primarily for the Amargosa trough, with secondary constraints based on background data for the southern Great Basin and Mojave Desert [see Crowe (2007), Excel Worksheet titled *Probability Bounds*].

Recurrence rates were estimated originally for the Quaternary Crater Flat volcanic field, the Plio-Quaternary Crater Flat/Amargosa Valley volcanic field, and the Quaternary and Plio-Quaternary Amargosa trough (ROIs). These rates were refined and restricted to rates *within* volcanic cycles. The Plio-Quaternary Crater Flat/Amargosa Valley volcanic zone was redefined for the duration of the Pliocene event cycle, and the Amargosa trough ROIs were redefined as the duration of two separate Quaternary and Pliocene volcanic cycles. Estimates of mean recurrence rates for the three volcanic cycles were added to the weighted estimates of recurrence rate. Various approaches were used to weight alternative recurrence models and cycle intervals and to estimate bounding and quartile values for weighted recurrence rates. Final values for the PVHA-U elicitation model are based on multiple alternative models of the current and possible future states of volcanic cycles for the YMR.

Event characteristics were revised through numerous attempts to fit data to combinations of simulation distributions and regression models that account for correlated parameters. Regression models initially used event length as the independent variable to estimate cone densities (dependent variable). Estimated cone densities then were used to develop regression estimates of vent and dike densities. Observed complications in the regression models included small data sets, non-normal data distributions, and outlier values for Little Cones, Anomalies C and D, and large-footprint volcanic events. Because numerous attempts using robust regression failed to give plausible values of regressed dependent variables, the regression approaches were rejected. Final values were obtained by fixing the number of cones/clusters according to the event categories and developing simulation distributions that maintained a relationship whereby

the numbers of cones/clusters are less than or equal to the number of dikes, which are less than or equal to the number of vents.

Distribution values derived from the volcanic event tables initially were categorized by compliance period. The MDT's repeated examination of the simulation results showed that results could be improved by categorizing distributions of event type by alternative models of future volcanic states, consistent with the approach used for recurrence rates.

Cone spacing within volcanic events correlates strongly with event length. Initial attempts to define cone spacing as a probability density function (PDF) resulted in values that were inconsistent with event lengths. This problem was resolved by developing a linear regression fit between event length and cone spacing. This regression equation can be applied to all event types. Dike and vent spacing initially were described as independent PDFs. These data were re-evaluated after preliminary simulations showed results inconsistent with the volcanic record. When dike spacing was re-measured relative to cone locations, the data did not correlate to event type. The revised data are described by a PDF that is applied to all event types. Vent spacing was re-measured relative to cone locations and correlated to associated feeder dikes. Separate distribution data for vent spacing are defined for the alternative conceptual models of future volcanic states.

Large-footprint volcanic events initially were treated like other volcanic events. Resulting simulations were inconsistent with the observed record of the characteristics of volcanic events >28 km. Large-footprint events were re-described using PDFs representing event lengths and widths. Internal clusters of cones, dikes, and vents were dispersed within the large-event rectangles, and separate distributions were developed for the features of the clusters.

Spatial models of the controls on the locations of basaltic volcanoes evolved from iterative assessments, including:

1. Combinations of the effects of topography
2. Controls from past and current extensional deformation
3. Evaluations of cluster analysis of event locations
4. Evaluations of teleseismic tomography data
5. Contouring zones from lithostatic pressure maps and fitting the zones to observed data for events in the Amargosa trough.

A final preferred approach was developed by matching the contour zones for three sets of lithostatic pressure maps to spatial patterns of the locations of basaltic volcanoes in alluvial valleys, along range fronts, and in range interiors.

SUPPLEMENT B

SPREADSHEETS AND SUGGESTED SIMULATION SEQUENCE

This supplement describes the Microsoft Excel spreadsheets and workbooks I developed in support of my assessment of the PVHA-U. It also proposes a suggested sequence for performing disruption simulations.

SPREADSHEETS AND WORKSHEETS

Volcanic Event Tables Crowe.xls

This Excel spreadsheet contains the following worksheets.

Worksheet: *All Event Summary*: table listing of event frequencies; conduit widths; events by event types with characteristics for vent estimates (minimum, expected, and maximum); event lengths, widths, and areas; event orientations; cone spacing; dike lengths (minimum expected and maximum); dike numbers; dike orientations; dike spacing; and vent spacing. Distributions (PDFs) for simulation sampling of event characteristics are compiled by event type.

Worksheet: *> 30 km Events*: sampling sequence, diagram, and distributions for assigning volcanic dimensions to large-footprint events, sampling cluster numbers and locating clusters within event rectangles, and distributions for sampling volcanic features of clusters.

Worksheet: *Cone Vent and Dike Locations*: sequence for sampling the event characteristics from the worksheet, *All Event Summary,* for the four event types.

Worksheet: *Cone Spacing Data*: compilation of cone spacing and event length data for the four events types (excluding large-footprint events); test data set for regression model; plots of event length versus cone spacing; and the linear regression fit to the data.

Worksheet: *Cone Space Regression*: summary output of regression model of event length versus cone spacing.

Worksheet: *Vent Spacing*: vent spacing data for the Quaternary and Pliocene volcanic cycles and PDFs for vent spacing based on alternative models of the future state of volcanic activity in the YMR.

Worksheet: *Event and dike orient*: compilation data for event and dike orientations.

Recurrence Rate Spreadsheet Crowe.xls

This Excel spreadsheet contains the following worksheets.

Worksheet: *Probability Bounds*: calculations of probability bounds for background and maximum disruption rates for the Amargosa trough and the southern Great Basin;

alternative calculations of background event rate for adjusting recurrence rates; disruption rates per 6 km^2 and per km^2 areas; and disruption rates (per km^2) across Crater Flat, Yucca Mountain, and Jackass Flats.

Worksheet: *Recurrence Rate Zones*: matrices of recurrence rate estimates for seven alternative models.

Worksheet: *ROI Adjusted Recurrence*: summation table of adjusted recurrence rates by Region of Interest, by compliance periods, and by alternative models of the future state of volcanic activity. This worksheet includes model weights, weighted recurrence rates, and distribution parameters for alternative models.

Worksheet: *Cycle Patterns*: summations of data and assumptions for basaltic volcanic cycles.

Zone Percentages in ROIs.xls

This Excel spreadsheet contains the following worksheet.

Worksheet: *Zone frequencies:* summations of alternative models used to assign event frequencies to lithostatic pressure zones; includes table of zone distributions for performing simulations.

SUGGESTED SIMULATION SEQUENCE

The following sequence of steps is suggested for use in performing simulations, starting with sampling a volcanic event from the event tables.

1. Sample the event type using the frequency percentages for the four event types.

2. Randomly locate the center point of a volcanic event in the sampled frequency zone (ROI).

3. Test for repository intersection.

4. If there is no intersection, record a sampled event without intersection.

5. If there is an intersection, sample the event characteristics (length, width, and orientation); number of dikes and vents (cone numbers are established by event type); and the characteristics of cones, vents, and dikes (dike lengths and orientations; cone, vent, and dike spacing).

6. Record the number of intersections per total realizations to establish the disruption probability for each ROI.

Large-footprint volcanic events require the simulation sequence to be modified starting with step 5 above.

1. If there is repository intersection, *and*
   a. the event is from the 1-My compliance period, *and*
   b. the future volcanic state is a new volcanic cycle,
   c. then 20% of the sampled events for event types 3 and 4 are drawn from large-footprint volcanic events.

2. Sample the event length, width, orientation, and number of clusters for cluster events.

3. Sample the location of the centroid of a volcanic cluster by sampling distributions for cluster spacing parallel and perpendicular to the event axis from the worksheet titled *> 28 km Events*.

4. Assign three aligned cones to the cluster, then sample the orientation from the event orientation frequencies.

5. Sample required attributes of features in the cluster.

6. Repeat for the number of clusters sampled in step 2.

D.3 WILLIAM HACKETT'S ELICITATION SUMMARY FOR PVHA-U PROJECT

D.3.1 OVERVIEW

This section summarizes new data that have become available since the initial Probabilistic Volcanic Hazard Analysis (PVHA) was performed in 1996. The section also outlines the general principles and concepts underlying this author's modeling of hazards for the updated PVHA.

D.3.1.1 Advances since 1996

Since the 1996 PVHA several major advances have occurred in the understanding of igneous disruptive events of the Yucca Mountain region (YMR, the region within a radius of about 50 km centered on Yucca Mountain). These advances fall into three categories: data quality, quantity, and presentation; availability of magnetic data; and detailed investigations of basaltic volcanoes in the region.

Data Quality, Quantity, and Presentation

The Methodology Development Team (MDT) invited and responded to requests from the current expert panel for data compilations, many of which were unavailable or not requested in 1996. The data products were provided in a timely and useful fashion as electronic data files, colored maps, diagrams, and other visual renderings of geologic and geophysical data, supplemented with publications from the Yucca Mountain Project (YMP), from peer-reviewed professional journals, and from analytical white papers disseminated by the MDT.

Magnetic Data

High-resolution aeromagnetic data were obtained for the expert panel in the form of written documents and map products (e.g., Cogbill, 2006; Perry et al., 2006; Perry et al., 2005). Based on the aeromagnetic data, a thorough program of subsurface drilling was undertaken that incorporated input from the panel members. Investigations of the materials encountered in the boreholes included lithostratigraphic descriptions of subsurface materials, geochemical analyses of buried basalts, and argon-isotopic age-dating of buried and surficial basalts.

The magnetic data and modeling of those data have greatly improved the panel's ability to perform an updated volcanic hazard analysis. The data led to the identification of buried basaltic volcanoes or intrusions in the YMR and provided information on the ages, compositions, and volumes of subsurface basaltic materials. The magnetic and borehole data have improved understanding of the spatial and temporal evolution of YMR basaltic volcanism and of the relationship between the magmatic system and the regional tectonics of the Crater Flat basin during the past 12 Ma. The magnetic data failed to identify any subsurface basaltic dikes associated with mapped Pleistocene volcanic centers. Subsequent modeling showed that magnetic surveys (assuming reasonable, even conservative, magnetic contrast between basalt and host rocks) should have detected any basaltic dikes 1 to 2 m thick within about 200 m of the surface. Together with geologic data and detailed mapping at individual volcanic centers, the magnetic data impose limits on the likely dimensions, notably lengths, of basaltic dikes that may exist in the shallow subsurface of the YMR.

Investigations of Basaltic Volcanoes

Although excellent maps, lithostratigraphic information, geochemical data, and age dates were available in 1996, more detailed and quantitative investigations of basaltic volcanic centers in the YMR were performed during the past decade. In particular, the Pleistocene volcanic centers of Crater Flat and Lathrop Wells were investigated, in most cases with an eye toward providing practical information to the expert panel that was assembled for the PVHA update. The results, which have been published as peer-reviewed professional journal articles and in the YMP literature, greatly improved understanding of the eruptive processes and dynamics of shallow magma intrusion at basaltic volcanoes of the YMR.

D.3.1.2 General Principles Underlying Analysis

The following sections describe the primary principles and approaches underlying my assessment of the probability of igneous events occurring in the YMR during the future 10,000- and 1-million-year time frames.

Region of Interest

I define the region of interest for this analysis as the approximately 3,200-km^2 area for which I have compiled event counts, event volumes, cumulative erupted magma volume, geophysical observations, and other data used directly in my analysis. This analysis also considers data and interpretations from a much larger area, notably the southwestern Great Basin and analog volcanoes worldwide.

Emphasis on Most Recent Volcanism

I apply the principle that "the recent geologic past is the key to the future." I focus on basaltic volcanism of the past 1.1 and 5 Ma, although the time period of interest extends back to 12 Ma.

Emphasis on Repository Depth

Although my analysis incorporates geologic and geophysical data related to the total magmatic system, my focus is on magmatic phenomena occurring at or above the depth of the repository; that is, within several hundred meters of the surface. The petrogenesis and physical properties of alkali basalts in the YMR are well understood. Given the viscosities and volatile contents of basaltic magma in the YMR (viscosity of about 200 poise, which is about the consistency of peanut butter at room temperature; 2 to 4 weight percent of equivalent water), the repository is well above the modeled depths at which magma vesiculates and fragments into a gas-pyroclast mixture (Detournay et al., 2003). In addition, exhaustive investigations of the host rhyolitic tuffs of the repository site have shown that the host tuffs are highly porous, fractured, and gas-permeable.

Characteristics of the magmas and host tuffs present several implications for hazard and consequence analysis. First, the volatile-rich alkali basaltic magma of the YMR is highly eruptible when it reaches depths of less than about 1 km. A dike that ascends to repository depth (about 300 m), therefore, is assumed to vent at the surface. Second, the magma is likely to intersect repository openings as a mixture of expanding gas, frothy pyroclasts, and devolatilized

magma. Third, given the gas-permeable nature of the highly fractured host tuffs, basaltic magma is likely to enter the repository openings in much the same fashion as past eruptions have vented into the atmosphere; that is, as a mixture of expanding gas; pyroclasts (likely to be emplaced into repository drifts as a basaltic scoria flow and surficially as a scoria cone); and effusive lava. Thus, I expect that if magma were to enter repository openings, the same general phenomena and degree of explosivity would occur as have been deduced or modeled from the observed sub-aerial products of Pleistocene basaltic volcanism in the YMR. These phenomena include the likelihood of violent Strombolian eruptions.

Waning Magmatic System

Both the estimated rates of crustal extension and the cumulative volume of erupted basalt have decreased exponentially during the past 14 Ma in the Crater Flat basin, an area that includes the Yucca Mountain block (Fridrich et al., 1999). The Yucca Mountain block was the site of one or more igneous events associated with the Solitario Canyon dike system at about 11 to 12 Ma. Since that time, however, the area has undergone high-angle normal faulting but has not been the site of volcanism or magma intrusion. In contrast, the southwest part of the Crater Flat basin has undergone great amounts of cumulative extension and volcanism during the last 12 Ma.

Since the late Miocene, the Crater Flat basin tectonic-magmatic system has been waning exponentially in terms of decreasing eruptive volumes and cumulative slip along extensional faults. The decreasing cumulative volume and volumes per eruption may reflect conductive cooling of the lithospheric-mantle source region, which previously yielded about 40 batches of alkali-basaltic partial melts beneath the region of interest. Progressively smaller areas (and volumes) of partial melt in the lithospheric mantle apparently have generated progressively smaller batches of basaltic magma, which have ascended to the shallow crust as progressively smaller dike systems and have fed volcanic centers showing decreasing areas and volumes of erupted basalt. This "decreasing magmatic footprint," as described by Valentine and Perry (2006), is among the most important concepts to influence my analysis of volcanic hazards in the YMR. An important implication for hazard analysis is that the magnitude of volcanic events—the physical scale of basaltic volcanism, and by inference the scale of associated shallow intrusion—has decreased significantly in the YMR during the past 12 Ma. Volcanism also has become more focused spatially. From about 12 to 9 Ma, basaltic volcanism was widespread across my region of interest. Since 1.1 Ma, however, basaltic volcanism generally has been confined to southern Crater Flat (Makani Cone, Black Cone, Red Cone, and Little Cones) and the northernmost Amargosa Desert (Lathrop Wells volcano).

Two types of igneous events are identified as having the potential to disrupt the Yucca Mountain radioactive waste repository: a dike intrusion into the repository, or a conduit passing through it. The probability that either type of event would disrupt the repository is a function of the spatial and temporal distribution of volcanism in the area and the physical geometry of igneous events. These factors, and the relationships among them, are illustrated in Figure D.3-1. Models and assessments of the geometry of dikes, dike systems, and conduits are summarized in Section D.3.2, followed by models and assessments of the spatial and temporal distributions of igneous events.

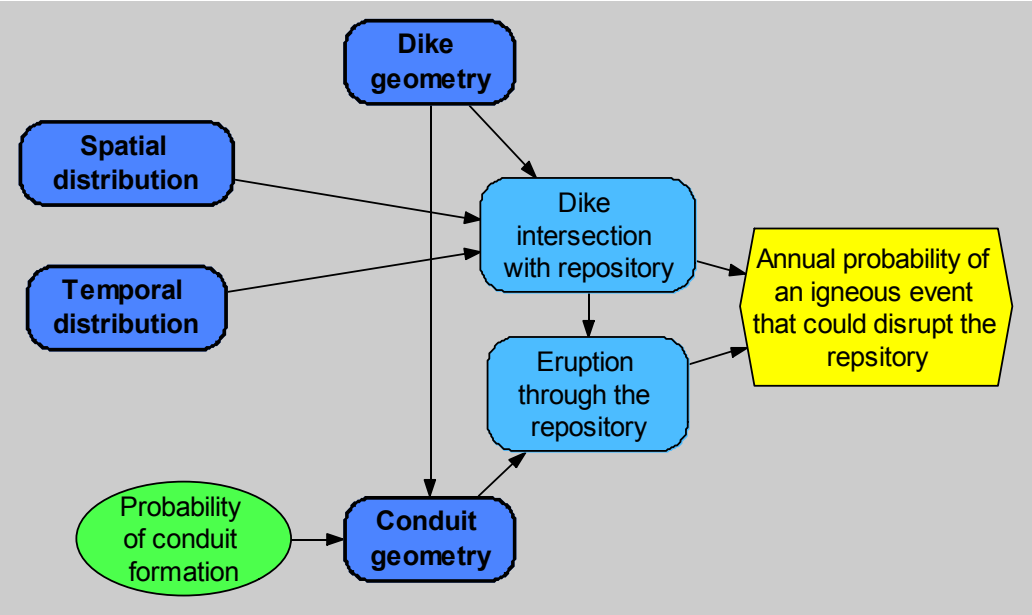

NOTE: The yellow hexagon represents the final result of the assessment. Green ovals represent information or variables for which assessments have been made. Bolded blue rounded rectangles represent sub-models; light blue rounded rectangles represent values calculated from other inputs; and arrows represent influences of one variable on one or more others.

Figure D.3-1. Overall Structure of Model

D.3.2 EVENT DEFINITION

I define an event as a temporally distinct batch of magma that reaches the upper kilometer of crust. The time frame for an event includes the time it takes for a batch of magma to ascend and then solidify in the upper crust or erupt, a process that may involve years, decades, or centuries. This geologically brief time frame for an individual volcanic event generally is beyond the precision of the best geochronologic methods. Thus, I combine geochronology with lithostratigraphic, geochemical, geophysical, and other information in order to identify volcanic events.

Because my event definition is based on the conceptual model of distinct magma batches, my event counts are those of a "splitter" rather than a "lumper," as illustrated by my assessment of the Pleistocene Crater Flat cones. The ages of the cones, which form a prominent northeast-trending vent alignment, cannot be resolved using even state-of-the-art geochronology. Despite their apparent age-equivalence and a geographic alignment that might indicate a common feeder dike, I consider each cone to represent a separate volcanic event. Even if the cones formed during synchronous eruptions, I would still assess them as separate events, given their compositional and geophysical differences. Bulk-rock geochemical data from the cones, notably incompatible trace-element ratios, strongly suggest that each cone represents a separate batch of magma. The cones are separated by 3 to 4 km, and their deposits do not intersect. Aeromagnetic and ground magnetic data show no evidence for a northeast-trending master dike in the shallow subsurface. Rather, the magnetic data suggest that short feeder dikes, if present, do not extend beyond the sub-aerial volcanic deposits. In places these dikes have been observed

or inferred to have NNW orientations controlled by north-trending dilational faults in the rhyolitic tuff bedrock. At Makani Cone, for example, the sub-aerially exposed eruptive fissure (and therefore the feeder dike) is north-trending. At Black Cone, aeromagnetic data show that the pyroclastic cone lies above a north-trending fault in the underlying rhyolitic tuff. This combination of observations and inference suggests the feeder dikes were short and unconnected within several hundred meters of the surface. For these reasons I assess the Pleistocene Crater Flat cones as separate events. In my opinion, the northeast alignment of those cones reflects an elongate (and compositionally heterogeneous) zone of partial melting in the lithospheric mantle, which generated separate magma batches that ascended and erupted along a common alignment but that were not connected by a common, northeast-trending dike.

Our understanding of dike dimensions is based primarily on outcrops of dikes exposed at older, eroded volcanoes of the YMR. My assessments of the geometry of potential future dikes are based on published data related to the YMR and analog regions, mostly within the Southwest Nevada Volcanic Field or the southern Great Basin.

The physical features and inferred processes at Quaternary volcanoes in the YMR provide the primary basis for my assessments of the characteristics of future events. The Quaternary volcanoes are smaller and less voluminous than were the Mio-Pliocene volcanoes. The more voluminous eruptions of the latter involved proportionately larger dike-conduit systems and greater sub-aerial coverage by the eruptive products. This change underlies the "decreasing magmatic footprints" of Valentine and Perry (2006). It is noteworthy that Hidden Cone is located on top of a topographic high. For an eruption to have occurred at this location, the lateral extent of the dike controlling the eruption must have been limited, with a length on the order of 1 km. Had the dike been longer, the eruption would have occurred in the adjacent valley rather than atop a narrow ridge.

Considering the two types of igneous events that could disrupt the repository, an eruption through the repository would require that the repository be intersected by a conduit occurring along a dike. Most dikes that might intersect the repository likely would erupt, leading to the formation of a conduit.

D.3.2.1 Characterization of Past Events

My definition of an event could support alternative characterizations of past events in the YMR. Table D.3-1 shows my assessment of the number of events represented by each cone and magnetic anomaly in the YMR. The table includes my assessment of the age and volume of each event. Where multiple interpretations of the number of events are possible, I provide weights for those alternative interpretations. Because dikes in the region are interpreted to be a few kilometers long, volcanic centers more than about 4 km apart are considered separate events. Based on this interpretation, Makani Cone, Red Cone, and Black Cone in Crater Flat represent discrete volcanic events. This interpretation is consistent with both the geographic separation and geochemical differences among the cones (specifically, incompatible trace-element ratios that indicate separate batches of magma originating from a compositionally heterogeneous source region; Perry et al., 1998). The two Little Cones may represent either one or two events.

Older events are of much less importance to the hazard analysis than are the younger Pliocene and Quaternary events, as discussed below regarding my spatial and temporal models.

Table D.3-1. Relevant Volcanic Events in the Region of Interest

Center	Number of Events[a]	Estimated Age[b] (Ma)	Estimated Volume (km^3)
Lathrop Wells	1	0.08	0.05
Hidden Cone	1	0.35	0.03
Little Black Peak	1	0.35	0.01
Little Cones NE	1 (weight = 0.3) 2 (weight = 0.7)	1.1	0.014
Little Cones SW		1.1	0.012
Makani Cone	1	1.1	0.002
Black Cone	1	1.1	0.06
Red Cone	1	1.1	0.06
Buckboard Mesa	1	2.9	0.84
SE Crater Flat (North Vent, Middle Vent, and South Vent)	3	3.8	0.6 total
Anomaly F	1	3.9	0.03
Anomaly G	1	3.9	0.03
Anomaly H	1	3.9	0.006
Anomaly B	1	3.85	1.28
Thirsty Mountain	1	4.6	2.63
Anomaly C	1	4.8	0.12
Anomaly D	1	4.8	0.07
Borehole V1	1	9.6	0.7
Borehole V2	1	9.6	0.2
Borehole V3	1	9.6	0.1
Jackass Flats	1 (weight = 0.5) 2 (weight = 0.5)	9.5	4.1
Anomaly A	1	10.0	0.06
Dome Mountain	1 (weight = 0.7) 2 (weight = 0.2) 3 (weight = 0.1)	10.0	10
Little Skull Mountain	3 (weight = 0.3) 6 (weight = 0.7)	11.3	2.2
Solitario Canyon Dikes	1 (weight = 0.5) 2 (weight = 0.5)	10.0 (weight = 0.5) or 11.7 (weight = 0.5)	0.001
Anomaly E	1	11.1	0.01
Anomaly 1	0 (weight = 0.8)[c] 1 (weight = 0.2)	11.1	0.001
Anomaly 2	0 (weight = 0.8) 1 (weight = 0.2)	11.1	0.001

Table D.3-1. Relevant Volcanic Events in the Region of Interest (Continued)

Center	Number of Events[a]	Estimated Age[b] (Ma)	Estimated Volume (km^3)
Anomaly 3 and Anomaly J	0 (weight = 0.5) 1 (weight = 0.5)	11.1	0.2
Anomaly K	0 (weight = 0.4) 1 (weight = 0.6)	11.1	0.2
Western Crater Flat (Anomalies R, Q, 4, T, and T Outcrops)	2, 3, 4, or 5 assigned equal weights	11.2	2.3

[a] Some centers can be interpreted as representing more than one event. When I consider multiple interpretations, I provide a weight for each interpretation.
[b] Age and volume estimates are based on consideration of data in a table developed by Los Alamos National Laboratory investigators for the PVHA-U and published as Keating et al., 2008.
[c] Some anomalies may not indicate basalt. For such cases, I include the possibility that the "center" does not indicate a past event by having it represent zero events (assigned a specified probability).

D.3.2.2 Dike and Dike System Geometry

Dike geometry is defined by several variables: the number of dikes in an event/dike system; their relative spacing and locations; and the length, width, and azimuth of individual dikes or dike segments. Figure D.3-2 illustrates these variables as directly influencing the probability of a potential future dike intersecting a drift in the repository. Assessments were made for each variable.

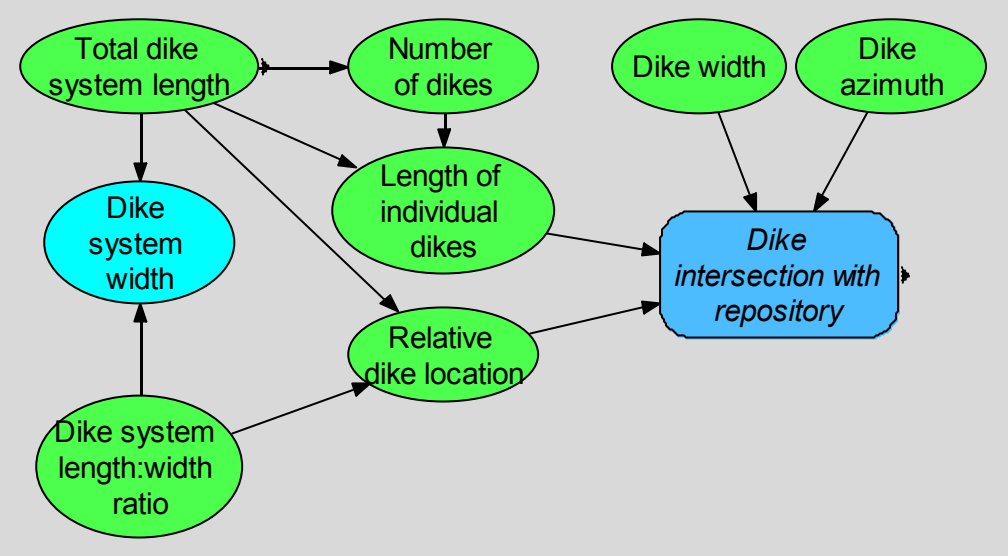

Figure D.3-2. Variables Defining Dike System Geometry

Dike System Length, Number of Dikes, and Dike Geometry

The number of dikes in an event/dike system and the total length of the system are related to magma volume, because more voluminous magma is more likely to ascend along multiple dikes. Expected eruptive volumes and effusion rates provide a basis for considering whether multiple

dikes will occur in the future. Given the small eruptive volumes associated with Quaternary centers in the YMR, a single short dike is more likely than are multiple dikes having a great total length. To address the correlation between number of dikes and the total length of dikes in a system, I first assess the total length of dikes in an event, then assess the number of dike segments to be expected for various total dike lengths.

Dike shapes in the shallow subsurface at repository depth (~300 m) are modeled as having semi-circular or elliptical dike tips (Maaloe, 1999). Based on geologic mapping and magnetic data, dikes in the region of interest appear to extend beyond the area of eruptive products (pyroclastic cone and lava flows) by no more than a few hundred meters. High-resolution aeromagnetic data were obtained throughout a wide area around Yucca Mountain in an attempt to identify buried basalts, including subsurface dikes. No dikes were identified in the subsurface. Modeling has shown that basaltic dikes that are 1 to 2 m thick and lie within about 200 m of the surface should be detectable, assuming reasonable (conservative, actually) magnetic properties for the basalt and host rocks (Cogbill, 2006). By "conservative" I mean that the magnetic contrast chosen for modeling basalt and host rock was taken from the low-contrast end of a range of possible values. Dikes intruded into alluvium, such as that in the shallow subsurface across much of Crater Flat, would be particularly detectable. Ground magnetic data collected near outcropping Pliocene dikes of southeastern Crater Flat show that the dikes do not continue in the subsurface a few tens of meters beyond the limits of their outcrops. These shallow Pliocene dikes therefore appear to have steep sides; they were intruded vertically; and the radius of dike-tip curvature is small. Pleistocene volcanoes in the region of interest generally are not sufficiently eroded to have exposed their underlying dikes and conduits. However, Hidden Cone, a Pleistocene volcano in the region of interest that erupted on a topographically high area, provides evidence for a short feeder dike about 500 m long at the surface (Valentine and Keating, 2007). I estimate that dike length in the shallow subsurface is 1 to 1.5 km.

Dike Length. Dike lengths can be inferred from maximum eruptive fissure lengths, based on our understanding of the subsurface geometry of dikes—specifically, the curved tip described above. Observations of eroded dikes at pre-Quaternary analog sites indicate that dikes are two to three times longer than are their associated eruptive fissures. Based on the assumption that the scaling factor stays constant through time and is applicable to all dikes in the upper few hundred meters of crust, the same proportions can be applied to Quaternary events. Thus, the estimated dike length at repository depth (several hundred meters) is a function of the estimated eruptive fissure length and the estimated scaling of fissure length to dike length.

The length of an eruptive fissure can be estimated based on the diameters of either pyroclastic cones or lava flows. The measured cone diameters of Quaternary centers in the YMR range from 0.2 to 0.8 km. The measured lava flow diameters for these events range from 0.4 to 1.8 km (Valentine and Perry, 2006). For my estimate that dike length is two to three times fissure length, I emphasize cone diameter more than lava flow diameter as an indicator of fissure length. I developed this emphasis because field investigations have shown that Quaternary lava flows in the YMR commonly issued from the bases of pyroclastic cones or from vents near the cones. Cone diameter therefore serves as an indicator of eruptive fissure length.

Figure D.3-3 illustrates my assessment of the length of a potential future dike in the YMR. My assessment assumes (1) elliptical shapes for ascending dike tips (Maaloe, 1999) and (2) the

diameters of cones and flows described above. This distribution has the following characteristics: 1.5 km is the most likely length, with a most likely range from about 0.6 to 2.5 km. The 95th percentile is 5 km, and the maximum total length (100th percentile) is 13 km. My estimate of maximum dike system length is based on the entire 11-km length of the Quaternary Crater Flat alignment plus 2 km to account for the continuation of such a dike in the subsurface. Although a dike of this length is inconsistent with my assessment that each Crater Flat cone represents a distinct event, I assign a very low probability to a 13-km-long dike by placing it at the extreme tail of my length distribution. I would characterize such a dike as being "the longest hypothetical dike that can be imagined in the region of interest. Such a dike is extremely unlikely, but perhaps not impossible."

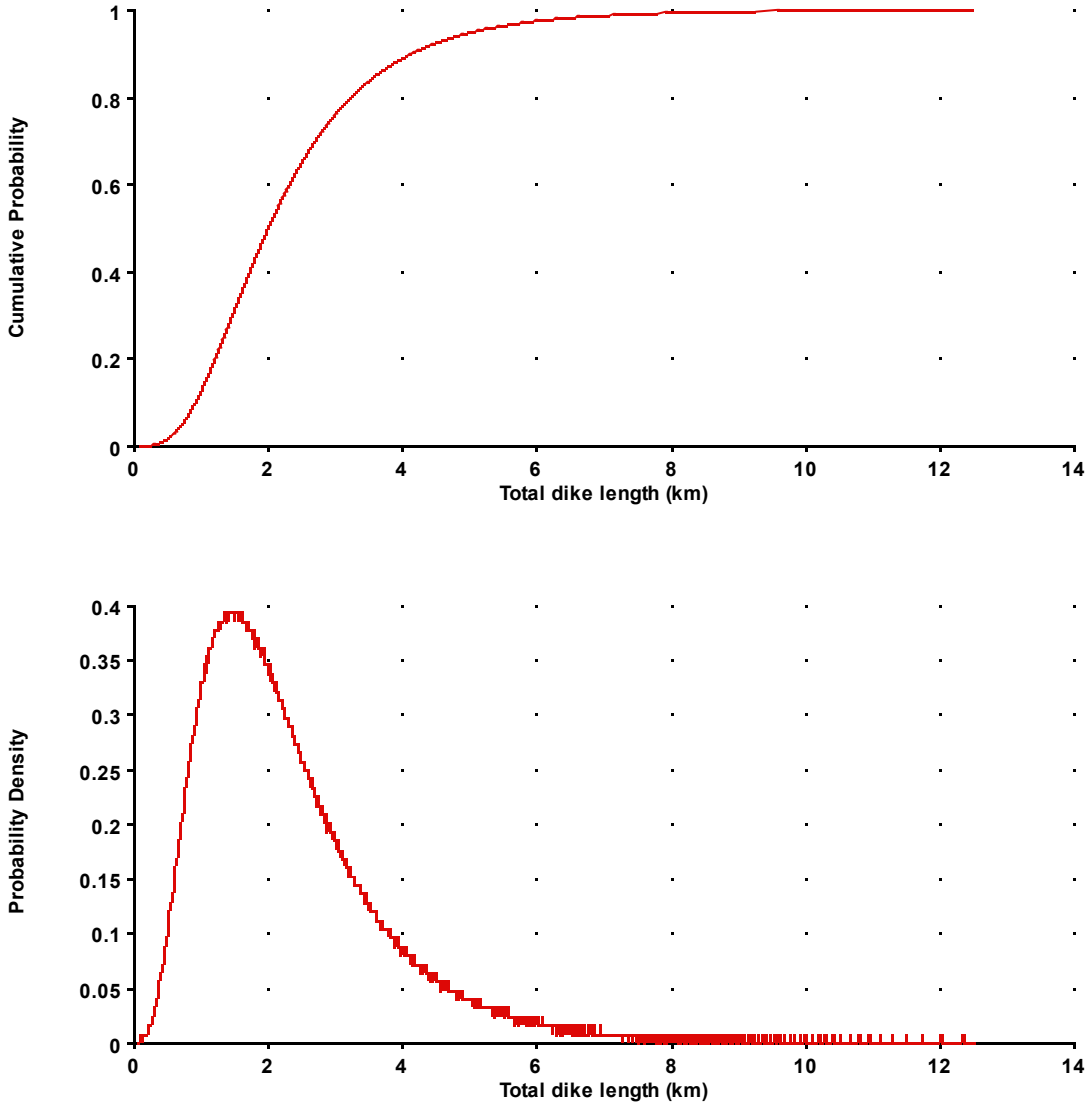

NOTE: Upper graph is a cumulative distribution function; lower graph is a probability density function.

Figure D.3-3. Assessment of the Total Length of Dikes in an Event or Dike System

In keeping with the concept of a decreasing magma footprint (Valentine and Perry, 2006), I apply this distribution to the length of a single dike or the total length of all dikes in a system that might be produced during a single future event.

Number of Dikes. I assess the number of dikes in a potential future dike system as a function of the total length of the system. Longer systems tend to have more dikes. For a given total system length, the probabilities associated with various numbers of dike segments are given in Table D.3-2 below.

Table D.3-2. Probability of Number of Dikes as a Function of Total Dike System Length

	Number of Dikes				
Total System Length	**1**	**2**	**3**	**4**	**5**
0.5 km	0.90	0.1	0	0	0
1.5 km	0.7	0.2	0.1	0	0
5 km	0.1	0.2	0.5	0.1	0.1
8 km	0	0.1	0.2	0.4	0.3
13 km	0	0.1	0.2	0.3	0.4

If a dike system were to comprise more than one dike, I would expect all the dikes to be of approximately equal length, with the maximum difference in length being a factor of about three. Figure D.3-4 shows my assessment of the ratio of the longest dike segment length to the shortest within a system. As shown, the highest weight is on a 1:1 ratio, but the ratio could be as high as 3:1. It is about six times more likely that the dike lengths would be equal than that they would have a 3:1 ratio.

I expect that multiple dikes in a potential future event would be arranged in en echelon patterns involving minimal overlap. Overlap could range from 25 percent to an underlap (gap) of 25 percent. Multiple sub-parallel dikes displaying a greater overlap would imply a larger magma supply and greater extensional strains than I expect within the YMR.

The fan-like opening of the Crater Flat Basin (Fridrich et al., 1999) and the right-lateral component of extensional faulting associated with Walker Lane imply that right-stepping en echelon patterns of dikes are more likely (0.8) than are left-stepping patterns (0.2). I model a potential future dike system as having a rectangular footprint that has the total length defined above, en echelon patterns of dikes, and a total system width defined by length-to-width aspect ratios ranging from 10:1 to 5:1. Narrower dike systems are more likely than are wider ones. My assessment of the length-to-width ratio of dike systems is shown in Figure D.3-5, which reflects my judgment that a 10:1 ratio is about twice as likely as a 5:1 ratio. Dikes are assessed to be evenly spaced across the width of an event.

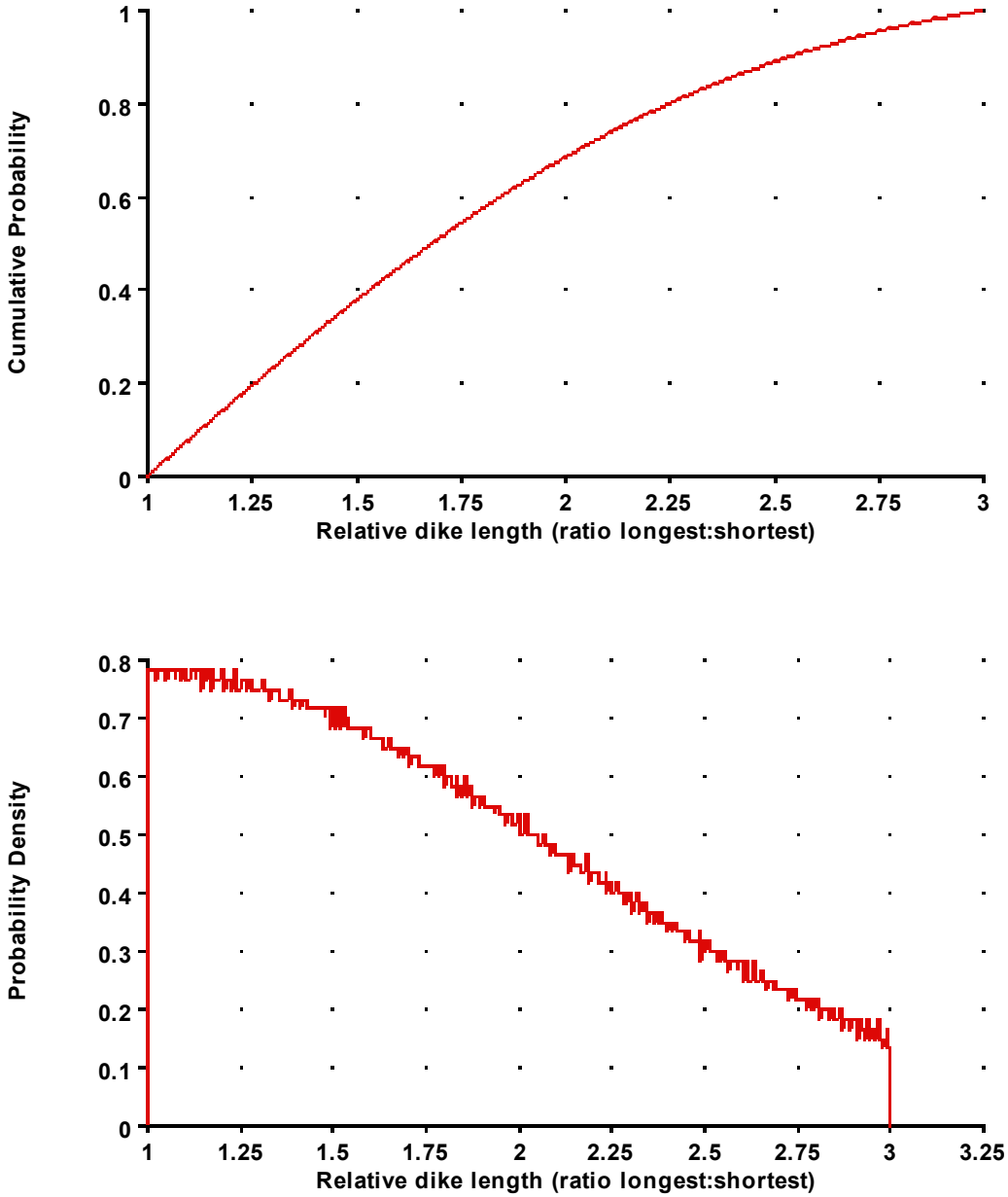

Figure D.3-4. Assessment of the Relative Lengths of Dikes in a Dike System, Expressed as the Ratio of the Length of the Longest Dike to the Length of the Shortest Dike in the System

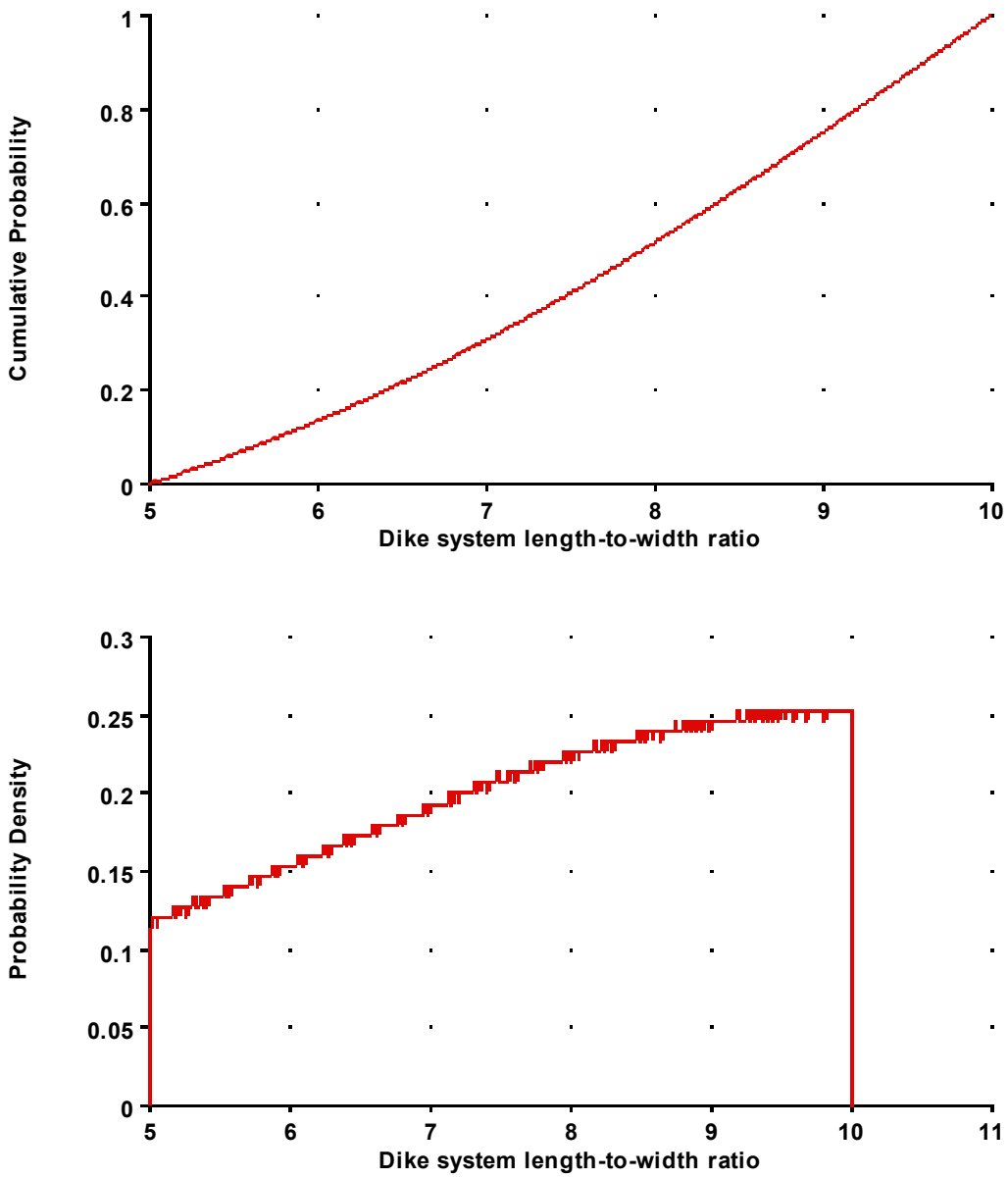

Figure D.3-5. Assessment of the Length-to-Width Ratio of a Dike System

Dike Width. Dike widths for Pleistocene basaltic volcanoes in the YMR are difficult to assess, because the dikes are neither exposed at the surface nor detected geophysically in the subsurface. Observations of dikes exposed at older, eroded volcanoes in the region can be used for estimating the dike widths of young volcanoes, bearing in mind that the scale of volcanism and igneous intrusion (including dike width) in the YMR has decreased from the Miocene to the Pleistocene (Valentine and Perry, 2006). My assessment therefore emphasizes the lower (narrower) end of dike-width distributions derived from observations at older and more voluminous analog centers. Crowe et al. (1983) report dike widths at eroded YMR volcanic centers ranging from 0.3 to 4 m. At Paiute Ridge, late Miocene dikes range in width from 1.2 to 9 m, with most being from 2 to 6 m wide (Valentine and Krogh, 2006). Several hundred measurements of Tertiary basaltic dikes of the San Rafael Swell, Utah, range from 0.1 to 6.5 m wide, with a median value of 1.1 m (Delaney and Gartner, 1997). Observational data and thermal considerations indicate that dikes less than about 0.2 m wide cannot propagate for significant distances, because the magma solidifies in response to conductive heat loss. Thus, 0.2 m is a good lower bound for dike width. Many of the 1996 PVHA experts estimated the dike width associated with future volcanism to be about 1 m. Because width varies along the length of a dike, my assessment is for average dike width.

My assessment of the width of a potential future dike in the YMR, as shown in Figure D.3-6, has the following characteristics: the 5th percentile is 0.3 m; the 95th percentile is 4 m; and the most likely value is about 1 m.

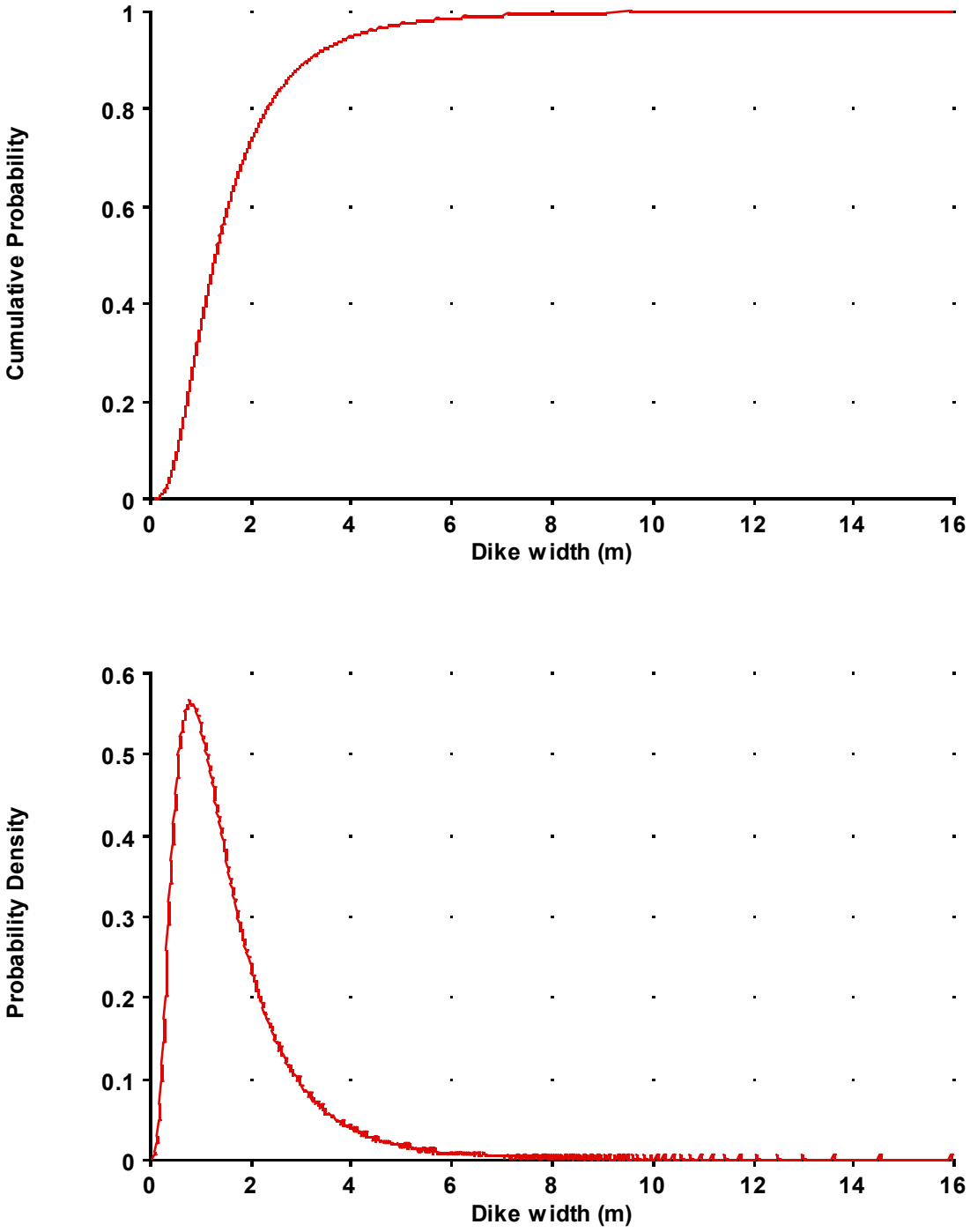

Figure D.3-6. Assessment of Dike Width

Dike Azimuth. In the mid-crust, dike intrusion can be understood using the principles of fracture mechanics, which show that dikes (magma-filled cracks) will be oriented perpendicular to the least-principle horizontal stress in the region. Based on Yucca Mountain borehole breakouts (Stock and Healy, 1988), the expected azimuth of dikes at depth (below a few kilometers) in the YMR is N25°E +/-20.

In the upper crust of the YMR, dike orientation is affected by extensional faults. Here shallow dikes tend to follow north-trending dilational faults. There is much observational evidence that dikes in the shallow subsurface have followed NNW-trending dilational, intrablock faults. Six of the nine Pliocene-Quaternary volcanic centers in the YMR show geologic or geophysical (subsurface magnetic) evidence of NNW-oriented fissures. Specifically, Makani Cone and Black Cone, Lathrop Wells, and all three Pliocene southeast Crater Flat eruptive fissures appear to be oriented about N5°W to N10°W, reflecting local structural control by NNW-trending faults. Most of the mapped and geophysically identified faults in these areas have NNW trends. Accordingly, I use a bimodal distribution for the azimuth of a potential future dike in the YMR. Both are modeled as Gaussian distributions: (1) N5°W +/-10 degrees, representing azimuths controlled by dilational faults in the shallow crust (about the upper 1 km), and (2) N25°E +/-20 degrees, representing dike azimuths controlled by regional stress at greater depths. "Plus or minus 20 degrees" should be interpreted to represent about two standard deviations. I assign greater weight to the NNW trend (0.67) than to the NE trend (0.33), because the repository lies at a depth of a few hundred meters, where potential dikes likely would follow paths of opportunity afforded by dilational faults. The combination of the two azimuth distributions is illustrated in Figure D.3-7.

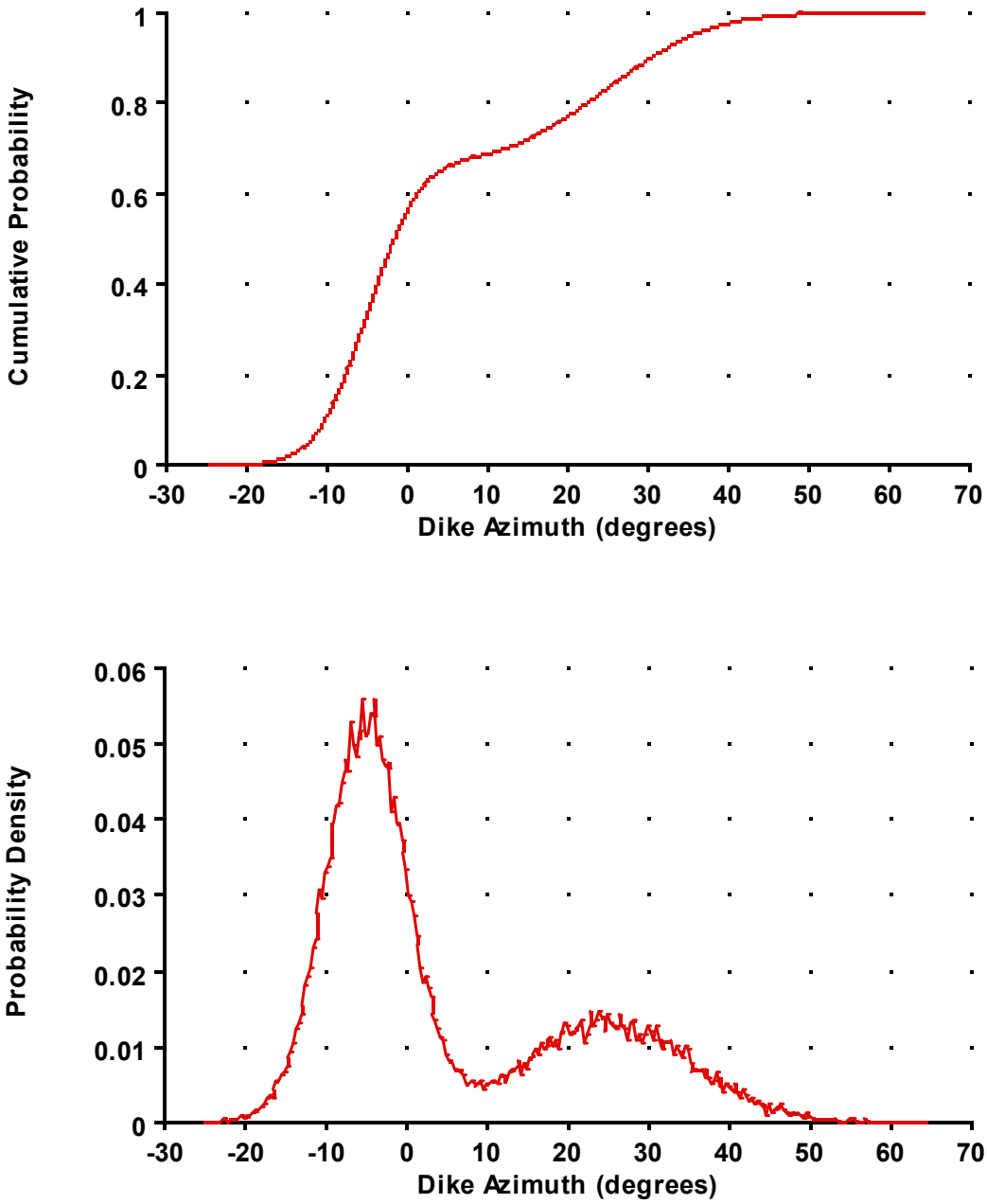

NOTE: This distribution is the weighted combination of two Gaussian distributions. Roughness in the density function (bottom graph) is a result of simulation noise and is not an important feature of the assessment.

Figure D.3-7. Assessment of Dike Azimuth (zero represents north-south)

D.3.2.3 Conduit Formation and Geometry

The venting of magma at a free surface causes the magma to focus, creating a conduit. The low viscosity and high volatile content of the basaltic magmas of the YMR make them very eruptible upon ascending to depths of less than about 1 km (the approximate depth of vesiculation; Detournay et al., 2003). The associated expanding volume will accelerate the rate at which magma ascends. If magma ascends to within a few hundred meters of the surface (the depth of the repository), an eruption likely will occur and a conduit form to the surface. In my assessment, venting to the surface is necessary to form a conduit, and one vent is associated with one conduit. A conduit can range from a slight widening of a dike (due to mechanical and thermal erosion) to roughly cylindrical features several tens of meters in diameter that include zones of dense magma, zones of vesicular magma, and mixed zones of magma and brecciated wall rock.

My assessments of the number and locations of potential future conduits are made for a dike system, which may contain one or more dikes. Because the YMR basaltic magma is highly eruptible and because venting is required for a conduit to form, the probability that a conduit would form somewhere along a potential future dike system at repository depth is weighted 0.9. I assign a weight of 0.1 to an intrusion that reaches repository depth but does not erupt. I consider there is only a small potential for a conduit to develop without a dike reaching repository depth.

As shown in Figure D.3-8, conduit geometry is defined by the number and location of conduits in a dike system and the diameter of each conduit. Assessments were made for each of these variables.

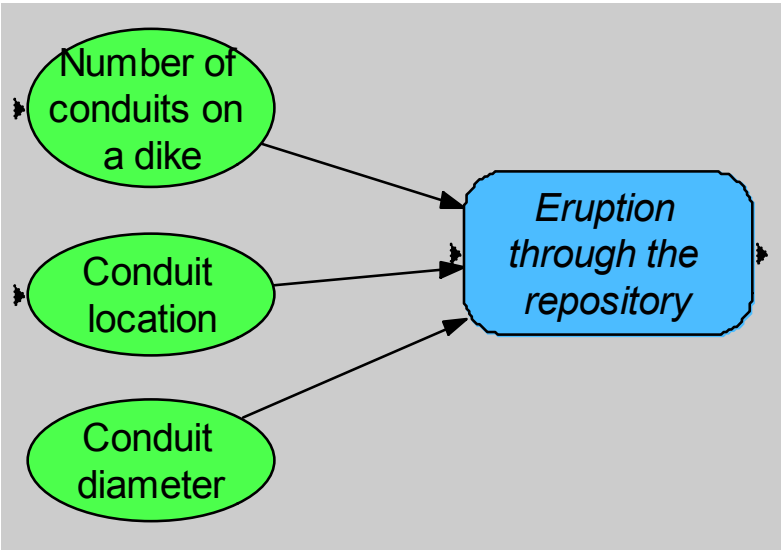

Figure D.3-8. Variables Defining Conduit Geometry

Based on the record of small-volume, monogenetic Pleistocene volcanism in the YMR, if a conduit were to occur in the future, there most likely would be only one conduit per dike system (assigned a weight of 0.8). A conduit could occur anywhere along the dike system, although it most likely would be centered on the dike system. Conduit location(s) along the dike are represented with a triangular distribution, the same distribution I use for the locations of vents along a feeder dike. Pre-Quaternary analogs show evidence of multiple conduits, so a second conduit (weighted 0.15) or even a third (0.05) might form. If there were more than one conduit in a dike system, the location of each conduit would be defined by a triangular distribution, although a minimum spacing equivalent to the spacing between dikes must be maintained. In modeling, these factors are combined with a 10% probability of a future dike that has no conduit. The result is a 10% probability of zero conduits, a 72% probability of one conduit, a 13.5% probability of two conduits, and a 4.5% probability of three conduits.

Keating et al. (2008) characterize the sub-volcanic geometry of five small-volume Miocene and Pliocene basalt volcanic centers exposed by erosion in the southern Great Basin. At Basalt Ridge and East Basalt Ridge, Nevada, the feeder dikes flare upward into conduits. At depths of 150 to 250 m below the eruptive surface, observed conduit diameters range from 4 to 15 m. Conduits formed at the eruptive surface (the Pliocene volcanoes of southeast Crater Flat) and at depths less than 100 m are much wider (perhaps several hundred meters) because of the effects of the free surface. A potential future conduit would be narrower at repository depth than at the surface. I estimate the most likely diameter of a potential conduit at repository depth to be between 5 and 20 m, and the 5th and 95th percentiles to be 2 m and 50 m, respectively. Figure D.3-9 illustrates my assessment.

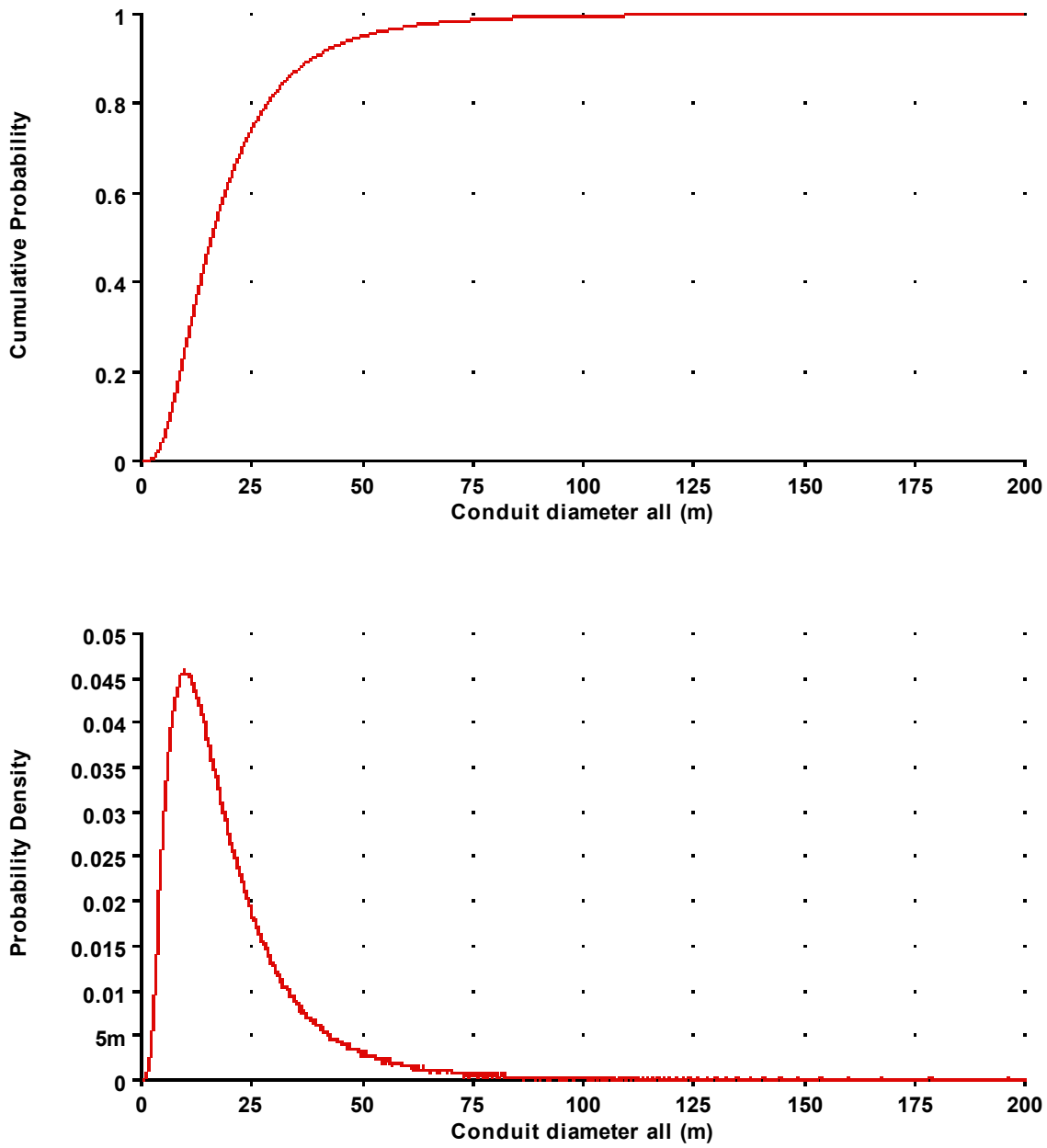

NOTE: For values less than 0.01 on the y-axis, suffix notation is used (m = 10^{-3} and u = 10^{-6}, so 5m = 0.005).

Figure D.3-9. Assessment of the Diameter of a Conduit at Repository Depth

Column-Producing Conduits

A sustained eruptive column (one that sustains buoyancy in the atmosphere) is a defining feature of violent Strombolian eruptions. Within the YMR, the Lathrop Wells cone displays clear evidence of this type of eruption (Valentine et al., 2005), and the pyroclastic deposits of the Quaternary Crater Flat cones also show evidence of violent Strombolian behavior (Valentine et al., 2006; Valentine and Keating, 2007). I therefore conclude that at least one conduit in a potential future eruptive event likely would be column-producing (80% likelihood). For multiple conduits, the collective probability of a column-producing conduit also is 0.8.

Multiple column-producing conduits can occur as an ephemeral condition early in the history of an event, eventually focusing in a single, stable, and central conduit. Once a mature stage of dynamic equilibrium is reached, the central conduit usually produces sustained eruption of volatile-rich magma as pyroclastic material. The central conduit or other conduits that are part of the event simultaneously can produce lava flows or normal-Strombolian pyroclastic deposits.

D.3.2.4 Sill Formation and Geometry

In this section I address the characteristics and likelihood of sill formation (loosely used to refer to a sub-horizontal intrusion of a sheet of magma).

Two conditions must exist for a sill to form. First, the magma overpressure must exceed the strength of the host rock plus the lithostatic pressure at the level of sill injection. Second, the local least-compressive stress (sigma-3) must have a sub-vertical orientation. Because feeder dikes require that sigma-3 be oriented sub-horizontally, the presence of sills emanating from feeder dikes implies a localized rotation of the stress field as a result of magma overpressure during dike intrusion.

There are about 40 events in my region of interest, only one of which (Anomaly A) is likely to be a sill. A sill also has been recognized at Paiute Ridge (outside the region of interest; Valentine et al., 2006). Both of these features (one possible, one certain) are Miocene in age. During the Miocene, eruptions were more voluminous; sill injection occurred locally as a result of forceful dike intrusion in the shallow subsurface (e.g., Paiute Ridge). For the smaller Quaternary (and potential future) eruptions, however, sills are less likely to form. I judge that magma volumes and overpressures will be insufficient to locally rotate sigma-3 to a vertical orientation. I therefore assign a maximum probability of 0.01 that a potential future event would generate a sill (based on Miocene events) and an expected probability of 0.001 (based on comparatively smaller Quaternary events).

If a sill were to form, it likely would be a semicircular, sub-horizontal sheet having a length ranging from a few hundred meters up to 1 km (the length of the largest Miocene sill at Paiute Ridge). Quaternary and potential future sills are expected to be smaller than Miocene analogs, given the lower magma volumes of eruptive events. My assessment of the lengths of potential future sills is based on the smaller Miocene examples: 100 m minimum to 1 km maximum, with a mode of 300 m, as illustrated in Figure D.3-10.

Sills are emplaced along dike segments, occurring randomly on either side of the dike. A sill is more likely to occur near the center of a dike, because that is where the greatest magma

overpressure and magma flux are expected to occur. The location of a sill along the length of a dike can be described by a triangular distribution having the mode in the center of the dike and tapering to zero at the ends.

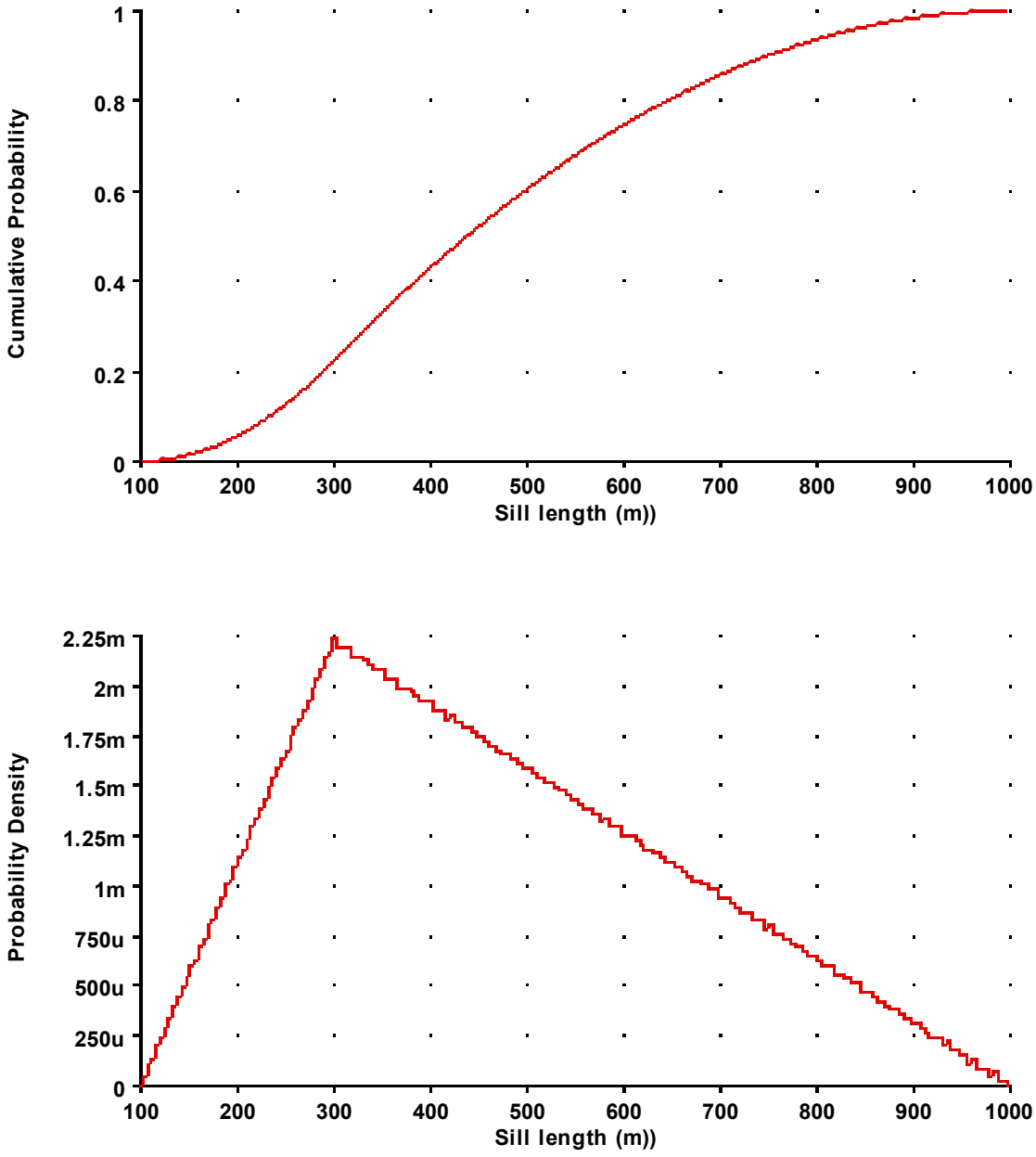

NOTE: For values less than 0.01 on the y-axis, suffix notation is used (m = 10^{-3} and u = 10^{-6}, so 5m = 0.005).

Figure D.3-10. Assessment of the Length of a Sill

D.3.3 SPATIAL MODEL

In this section I describe in detail my region of interest, discuss the possibility of hidden or undetected events, and then present models for estimating the locations of potential future events in the YMR.

D.3.3.1 Region of Interest

The region of interest for my assessment is shown in Figure D.3-11. This region is defined by past events in the post-silicic period of basaltic volcanism in the YMR, specifically post-12 Ma events. The area purposely includes the volcanic centers of Thirsty Mountain, Buckboard Mesa, Sleeping Butte, Hidden Cone, Little Black Peak, and Crater Flat; the Solitario Canyon dikes; and the aeromagnetic anomalies in the northern Amargosa Valley and Jackass Flats. My assessment depends on the inclusion of Miocene events, even though they are weighted far less than are Quaternary and Pliocene events. The older events are included because they demonstrate that volcanism has been waning exponentially in the Crater Flat basin and my region of interest throughout the past 12 Ma.

Regional geophysical data from the YMR (as described in Connor et al., 2000) indicate that Plio-Pleistocene events are restricted to the Amargosa Trough, a north-trending area of largely negative gravity anomalies (and relatively low lithostatic pressure in the upper crust) that extends southward from Crater Flat through the Amargosa Desert. In contrast to the widespread Miocene basaltic volcanism that occurred in the region of interest, Plio-Pleistocene volcanism (of the past 5 Ma) has been confined to the Amargosa Trough. The Amargosa Trough therefore is considered the most likely area of potential future volcanism, with a lower probability of future volcanism outside that area.

Bare Mountain's high topography and high lithostatic pressure (higher than in any other part of the Crater Flat domain) are unfavorable to volcanism. I exclude Bare Mountain from my region of interest, because (1) possible future volcanism on Bare Mountain is unlikely to impact the repository (too distant) and (2) the "infinite" extension of Bare Mountain reported by Fridrich et al. (1999) as due to its major vertical displacement cannot logically be construed as requiring an "infinite likelihood of volcanism" there. I eliminate Bare Mountain from my spatial model, instead relating the spatial probability of volcanism to the rate of crustal extension across the Crater Flat basin (as described below in the section titled *Cumulative Extension Data*).

My spatial models calculate relative spatial intensity based on the locations of past events in my region of interest. As noted above, Table D.3-1 lists past events within my region of interest; the locations of those events are shown on Figure D.3-11. My spatial models incorporate kernel smoothing and closely follow the approach of Connor et al. (2000) for probability models based on the distribution of individual vents. I take this approach because my event definition emphasizes individual magma batches and individual vents, rather than alignments that comprise multiple vents.

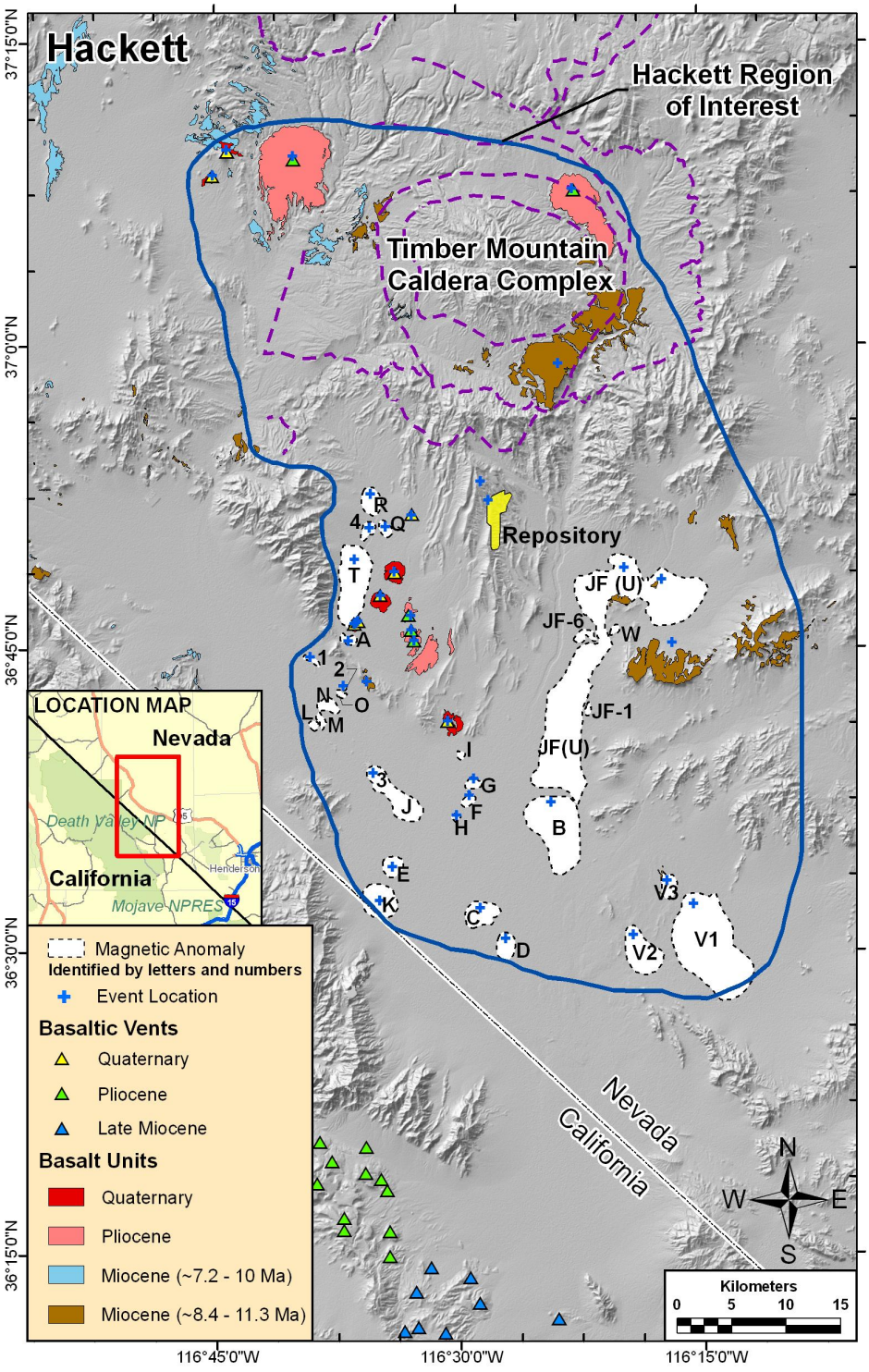

NOTE: Locations of events having a known vent exposed at the surface are shown as triangles. Blue crosses indicate the locations of all events within the region of interest, including events that are buried or are interpreted where eroded lava flows on the surface have no known vent location.

Figure D.3-11. Region of Interest and Events within the Region

D.3.3.2 Undetected Events

The region around Yucca Mountain has been examined thoroughly using geologic, geochemical, and geophysical techniques. In particular, high-resolution aeromagnetic data recently were obtained and modeled. I believe that all basaltic materials at the surface or within a few hundred meters of the surface likely have been accounted for. Because basaltic magma of the YMR is highly eruptible upon ascent to within a few hundred meters of the surface (i.e., repository depth), I am confident that few if any events have escaped our attention. If any dikes have intruded the crust of the YMR without erupting, I assess that their stagnation occurred deeper than the estimated depth of vesiculation for those volatile-rich magmas—i.e., deeper than about one kilometer. An event at such a depth, which is well below that of the repository, would be unlikely to affect the facility. Therefore my spatial smoothing model and rate estimates are based only on the events shown in Table D.3-1 and on Figure D.3-11, all of which are observational.

I also wish to establish a broader context for my assessment of possibly hidden events by addressing the general idea of magma intrusion without eruption. This process undoubtedly is common at large, polygenetic central volcanoes. Such volcanoes, which have protracted life spans, integrated magma-supply systems, and high cumulative volumes, are observed to grow as much by intrusion as by eruption. This situation, however, is not expected in a waning volcanic system such as in the YMR, which displays small (less than 0.1 km^3 each), monogenetic, widely dispersed scoria cones and lava fields composed of highly eruptible magma.

Given the eruptive style of the YMR, it is understandable that the area lacks volcanic rift zones. Rift zones are belts of volcanism and magma-induced extensional deformation, commonly tens of kilometers long. These belts are underlain by bladed dikes intruded horizontally from voluminous reservoirs beneath central volcanoes (as in Hawaii and Iceland) or intruded along extending regions that have abundant magma supply (as in Iceland and along the mid-ocean ridge system). The YMR lacks the magma supply and extension rate to sustain large, central volcanoes that have integrated magma-storage systems and associated rift zones underlain by bladed, horizontally intruded dikes. Like the small monogenetic volcanoes they feed, YMR basaltic dikes are small in volume, are limited in lateral extent (length), and have intruded the shallow crust primarily vertically rather than horizontally.

D.3.3.3 Spatial Smoothing

Using the principles and approach described above, I calculate the conditional spatial intensity of potential future events based on the locations and ages of past events. I use a Gaussian kernel function in order to generate non-zero spatial intensities across the region of interest, as opposed to using a truncated kernel (e.g., Epanechnikov kernel). My smoothing parameter of 5 km follows the approach and explanation of Connor et al. (2000), who adopt "a natural definition of conservatism for a site-specific hazard analysis." They further demonstrate that "a 5-km smoothing parameter is conservative for probability models based on individual vent distributions," based on the mean distance between observed nearest-neighbor volcanic events.

I developed the smoothing distance by considering the mean and standard deviation of a nearest-neighbor analysis of five sets of events. Connor et al. (2000) also used such a nearest-neighbor

approach to arrive at a smoothing distance of about 5 km for Quaternary-Pliocene events in the YMR.

I evaluated the spatial patterns of volcanism in the Quaternary, Pliocene, and Miocene time periods to gain insight into the space-time evolution of volcanism in the region of interest. The space-time relationship is as important as the age-volume relationships that have been developed (Valentine and Perry, 2006). In my spatial smoothing model, I weight recent events higher than older events, reflecting my assessment that the locations of Quaternary events are more informative of the locations of potential future events than are the locations of older events. Within my spatial smoothing model Quaternary, Pliocene, and Miocene events are weighted according to their relative ages as 11:4:1.

D.3.3.4 Incorporating Geologic Data Sets

In developing my spatial approach, I interpret specific geologic data (regional lithostatic pressure and cumulative extension within the Crater Flat Basin) to obtain information about the spatial distribution of potential future events. I use these interpretations to exert a bias on the spatial distribution calculated using the smoothing approach described above.

Lithostatic Pressure Data

Crustal extension is accommodated via two mechanisms, faulting and dike intrusion. Dike intrusion requires a supply of magma from a source region and the ascent of that magma to the surface. Areas of lower lithostatic pressure may experience increased magma supply via decompression melting of enriched lithospheric mantle. This scenario is described by Connor et al. (2000), who state, "the direct link between crustal extension and magmatism relies on the possibility that density variations in the crust produced during extension are sufficient to initiate decompression melting at much greater depths within the mantle." This relationship is tenuous, because the estimated effects at mantle depths are less than 10 MPa, a small fraction of the total pressure at mantle depths. Decompression melting therefore is credible only for hydrous lithospheric mantle that is already at the point of anatexis. Small batches of basaltic magma would be generated, consistent with the observed small volumes of the most recent volcanic events in the YMR.

A second, more compelling reason that decreased lithostatic pressure may increase the likelihood of dike intrusion in the shallow crust was given by George Thompson at PVHA-U Workshop 3 (written report distributed to the expert panel in September 2006). To paraphrase Thompson's written and verbal presentation: "Topography alone defines only the shortest route to the surface, short in basins and long in mountains, but the free-air anomaly (from which lithostatic pressure is calculated at depth) accurately defines the rock pressure in the upper few kilometers, which must be overcome for intrusion to take place. The effects of lithostatic pressure can be overcome, given sufficient magma volume (and overpressure), as in the Reveille Range and volcanic field. In such areas of strong magmatism, lithostatic pressure may not have much influence. But in an area such as the YMR, which exhibits weak, waning volcanism, lithostatic pressure can have a significant effect. Because the effects of lithostatic pressure due to topography and upper-crustal density contrasts (as in the YMR) are attenuated at depth, lithostatic pressure is largely a guide to magma intrusion in the shallow crust."

I therefore adopt the general principle that the higher the gravity values (lithostatic pressure) in a given area of the YMR, the greater the bias against magma intrusion. An example of such a location is Bare Mountain. The reverse rationale also applies, with lower gravity values (lithostatic pressure) indicating higher probabilities of magma intrusion. An example of such a location is the Amargosa Trough.

The values of lithostatic pressure across my region of interest provide a basis for my assessment of the relationship between lithostatic pressure and the locations of potential future events. Figure D.3-12 illustrates this assessment. It shows the value of lithostatic pressure at each past event in my region of interest (from Table D.3-1), along with my assessment of the likely value of lithostatic pressure at a hypothetical location in the region where a future event is assumed to occur. The red line/bars show the pressure at past events that I have identified. Because of the small number of events, I modified that distribution (as shown by the blue line/bars) to reflect my judgments about the relationship between events and lithostatic pressure. I added a longer tail on the high end to reflect my judgment that high pressure values suppress magmatic activity. I also extended the lower tail slightly to reflect my judgment that low pressure values increase the probability of magmatic activity, even beyond the limits of the empirical data. This extended lower tail represents the probability that magmatism would continue to increase for hypothetical areas of even lower lithostatic pressure than observed at vents in the area of interest.

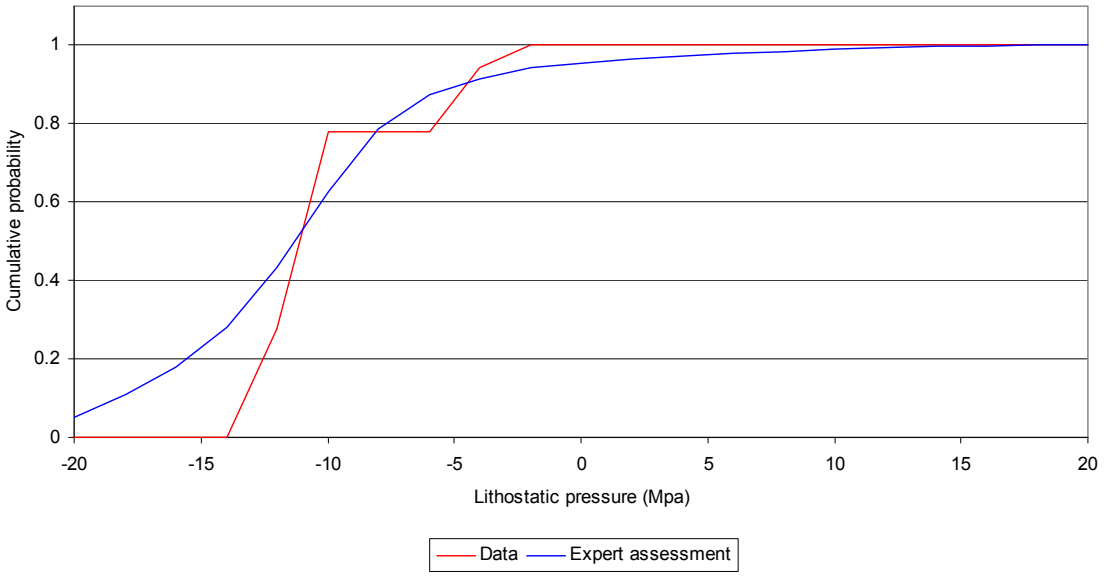

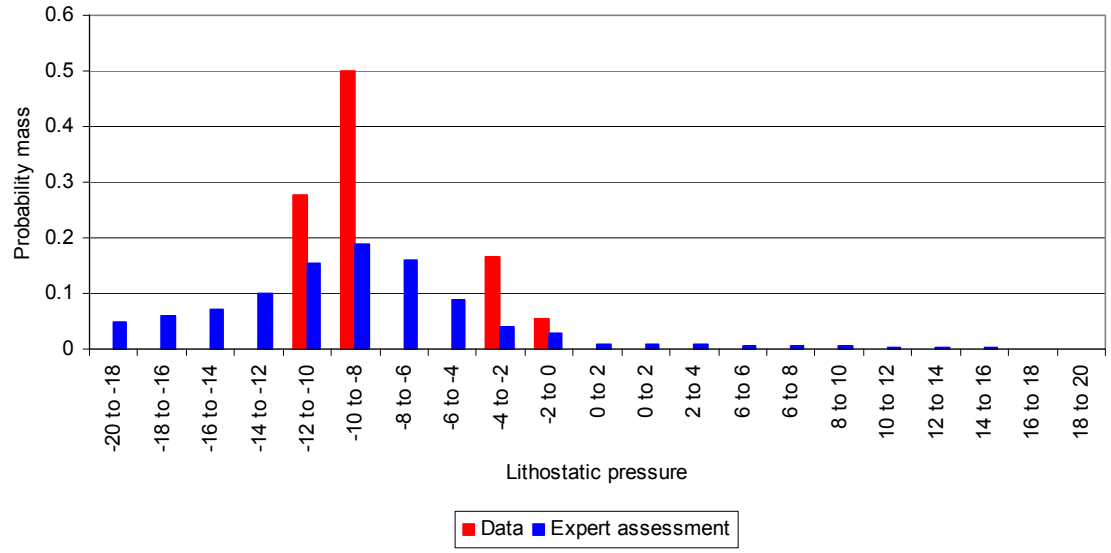

NOTE: The red line/bars represent the empirical distribution of pressure at past events in the region that are younger than 5 Ma; the blue line/bars represent my assessment of the likely value at a future event.

Figure D.3-12. Assessment of Lithostatic Pressure at a Hypothetical Future Event in William Hackett's Region of Interest

Cumulative Extension Data

Investigations by Fridrich et al. (1999) indicate that the Crater Flat structural basin, which includes Yucca Mountain, has experienced a fan-like pattern of extension during the past 11 to 12 My. The greatest amount of extension has occurred in the southwest part of the basin. Both extension and volcanism have waned exponentially in the basin during the past 14 Ma. I therefore expect that any future volcanic events would be located preferentially in those parts of the region that experience the greatest amount of extension. Cumulative extension data (from Fridrich et al., 1999) indicate that Crater Flat volcanism has occurred in the area that has undergone a cumulative extension of more than 50 percent. There is a decreased probability of future volcanism in areas that show a cumulative extension of less than 50 percent (which include the Yucca Mountain block). The extension data indicate that the Yucca Mountain block has undergone less than half the cumulative extension of areas to the south and west.

As shown in Figure 5A of Fridrich et al. (1999), the cumulative extension data do not cover my entire region of interest. To use those data in a quantitative model it is necessary to extrapolate the data to cover my region of interest. I assume that the cumulative extension for all areas not covered by the Fridrich et al. data is the same as the value at the location of the repository. This assumption is consistent with my assumption that, without knowing cumulative extension rates, the potential for future volcanism is everywhere identical to the potential at the repository. Figure D.3-13 shows the extension values used in my spatial model.

A higher cumulative extension rate indicates a higher potential for volcanism. My assessment is that the potential for volcanism is related directly to cumulative extension. For example, a future event is nine times more likely to occur at a location that has a cumulative extension of 90 percent than at a location having a cumulative extension of 10 percent.

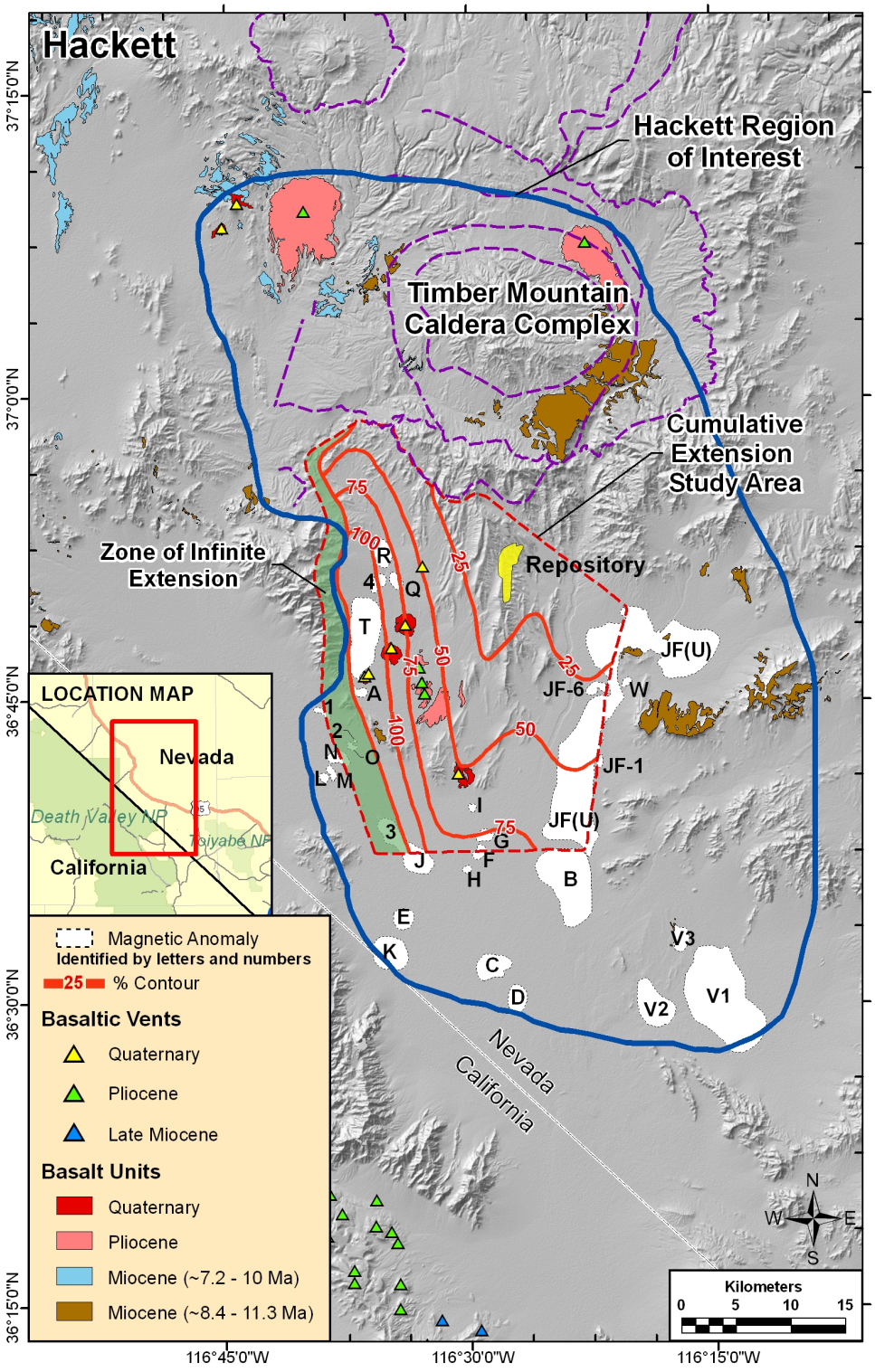

Figure D.3-13. Extrapolation of Extension Data of Fridrich et al. (1999) across William Hackett's Region of Interest

Other Geologic Data

Based on the work of Fridrich et al. (1999), most of the cumulative extension in Crater Flat occurred during the Miocene; the late Quaternary rate of extension is less than 1 percent of that initial rate. The southwest part of Crater Flat has experienced the most extension. Quaternary fault data show that extension there is ongoing, and that horizontal slip rates along individual faults are higher in the southern segments of the faults (Figure 6 of Fridrich et al., 1999). These observations qualitatively support my analysis, again suggesting that rates of Quaternary extension are greater in the south part of the basin. From this conclusion I deduce that potential future volcanism would be more likely to occur in the southern part of Crater Flat basin than in the northern part. The dynamic relationship between extensional faulting and volcanism in the southern part of the basin is described by Parsons et al. (2006), based on the synchronicity of Lathrop Wells volcanism and slip along the Stagecoach Road fault.

Tomographic data, like other geophysical data from the deep crust or mantle, are too ambiguous to be useful in my analysis. Interpretations of deep tomographic data are non-unique. That is, in addition to the possible presence of partial melt, slow seismic velocities in the mantle may reflect slightly elevated water content in olivine or other compositional differences. The available tomographic data are not useful for resolving the differences between possible volcanism in Crater Flat versus the Yucca Mountain block, which are only about 10 km apart.

I do not apply the bivariate Gaussian approach to the volcanic field shape in my model. It is difficult to define centroids when applying this method to the YMR, because the geology does not fit this model closely.

D.3.3.5 Combining Geologic Interpretations with Spatial Smoothing

The best predictor of the location of potential future volcanism is the locations of past Pliocene and Quaternary events, to which I add a bias imposed by lithostatic pressure and cumulative extension data. Accordingly, I combine the spatial smoothing approach with the spatial distributions based on geologic data, using weights of 2:1. Because I believe the lithostatic pressure data and the data on cumulative extension are equally informative of the spatial distribution of future events, I assign them equal weights.

D.3.4 TEMPORAL MODEL

I use two approaches to assess the temporal distribution of potential future igneous events in the YMR: (1) a homogeneous Poisson process model that incorporates rate estimates based on Quaternary volcanism (post-1.1 Ma), and (2) a time-volume model that considers the changes in erupted volume during the past 5 Ma. The homogenous Poisson model based on Quaternary events acknowledges the recent past as the best predictor of the near future, whereas the time-volume model acknowledges the declining eruptive volumes throughout a longer period, which is an important feature of the regional volcanism. I weight the two temporal models equally.

I expect the frequency of volcanism to be about the same within the two future time periods of interest (10 ka and 1 Ma). The Quaternary pattern of volcanism in the YMR, involving perhaps

more frequent events but smaller volumes per event, should persist, continuing the waning pattern of volcanism that has occurred since the Miocene.

D.3.4.1 Bounding Rates

I want to ensure that any recurrence rates derived from my spatial and temporal models are bounded by the following two cases: (1) a maximum rate of 1×10^{-6}/yr/km^2, based on Connor et al.'s (2000, p. 429) estimate of 10^{-5} to 10^{-6}/yr /5 km^2 for the most active volcanic fields in the western United States; and (2) a minimum rate of 4.3×10^{-10}/yr/km^2, calculated for my 3,200 km^2 area of interest, assuming spatial homogeneity across the region and excluding the Crater Flat/Lathrop Wells volcano cluster. I base the latter, minimum-rate calculation on the following:

1. For the post-4.8-Ma time period I use (each = one event) Hidden Cone; Little Black Peak; Buckboard Mesa; Thirsty Mountain; and Anomalies B, C, D, F, G, and H, for a total of 10 events. The rate calculation is thus (n–1 = 9 events) /4.8 Ma/3,200 km^2 = 5.8×10^{-10}/yr/km^2.

2. For the post-1.1-Ma time period I obtain a similar result: Hidden Cone and Little Black Peak are two events within the area of interest, not part of the Crater Flat volcano cluster. This approach gives (n–1 = 1 event)/1.1 Ma /3,200 km^2 = 2.8×10^{-10}/yr/km^2.

The average of these two similar results (a, b) is the 4.3×10^{-10} minimum estimated recurrence rate for the region of interest.

D.3.4.2 Homogeneous Poisson Model

Volcanism in the YMR appears to be episodic (temporally clustered). Although volcanic fields commonly demonstrate episodic activity, there is no compelling reason to use this information for future predictions for the YMR, because it is unknown whether we currently are inside or outside a temporal cluster of volcanism. It is highly uncertain whether the youngest event at Lathrop Wells occurred at the beginning or end of a cycle of volcanism. In any case, the Quaternary event data set is the most important for assessing future volcanism. In the next 1 Ma, volcanism should be similar to what has occurred in the past 1 Ma (the recent past is the key to the future). Rather than a temporal cluster model, I prefer a more simple and straightforward Poisson model that considers the overall recurrence rate during the Quaternary. This model is especially appropriate for the 10,000-year assessment, because this period is considerably shorter than the average recurrence interval. It is also appropriate for the 1-Ma assessment, because I consider the time scale of significant change in regional tectonics and the magma system to be longer than the 1-Ma period.

Using a simple Poisson model and my characterization of past events shown in Table D.3-1, the estimated mean recurrence rate in my region of interest is 5.45×10^{-6}/yr to 6.36×10^{-6}/yr (average recurrence interval is from 183 ka to 157 ka), depending on whether Little Cones is interpreted as one or two events. For comparison to the maximum (1×10^{-6}/yr/km^2) and minimum (4.3×10^{-10}/yr/km^2) bounding rates, the simple Poisson recurrence rate from my

model is 1.9×10^{-9} events/yr/km^2 for the region of interest, assuming a homogeneous spatial distribution across the region.

D.3.4.3 Time-Volume Model

The volume of basaltic magma erupted in the YMR has decreased during the past 14 Ma, as documented by Fridrich et al. (1999), and during the past 5 Ma, as documented by Valentine and Perry (2006). The regional tectonic setting provides no evidence of a waxing volcanic system, nor of increasing volumes in the future. Based on cumulative magma volume, there is no question that volcanism in the YMR is in an advanced stage of decline. The most credible temporal models, therefore, will incorporate specifically the observation of exponentially decreasing magma volume during the past 12 Ma. The past 5 Ma has seen a decrease in the volume per event. But the past 1.1 Ma has seen an apparent increase in frequency of volcanism. This is useful information in a qualitative sense. It is especially useful for projecting into the future and particularly relevant when considering the 1-Ma future time frame of interest.

In developing models of the change in cumulative volume and in volume per event over time, I considered several alternative approaches and models. I then selected the simplest model that fits the data.

I chose to model cumulative volume over time using a linear regression of cumulative volume as a function of the log of the time over the past 5 Ma. The regression fit is statistically significant and provides a good visual fit to the data. The log of time vs. cumulative volume curve is similar in form to the square root of time vs. cumulative volume curve, but provides a better fit to the data. The root-of-time function has a physical basis because it expresses the expected relationship for a conceptual model that incorporates conductive cooling. The log-of-time function has no physical basis but is true to the "exponentially decreasing magma volume through time" that is evident from YMR time-volume data for the past 14 Ma. Figure D.3-14 illustrates the cumulative volume vs. time data for the past 5 Ma and my chosen model fit to that data.

The time-volume model also requires an estimate of the mean volume per event for potential future events. The volumes of past events identified in Table D.3-1 display no statistically significant trend that can be used to predict future event volume as a function of time. I anticipate that future events, in either the 10-ky or 1-My period, will be of similar volume to Quaternary events. Thus, I estimate the mean volume per future event based on the average and variance in Quaternary event volumes.

Based on the log-time fit of cumulative volume and the volume per event, this model results in the following recurrence rates that can be compared to the bounding rates described above:

- The 50th percentile of the recurrence rate is 3.1 e-09 events/yr/km^2 in the region of interest, with Little Cones interpreted as one event and assuming a homogenous spatial distribution across my region of interest.

- The 5th and 95th percentiles of the recurrence rate are 1.2 e-09 events/yr/km^2 and 7.5 e-09 events/yr/km^2, respectively, again assuming a homogenous spatial distribution across my region of interest.

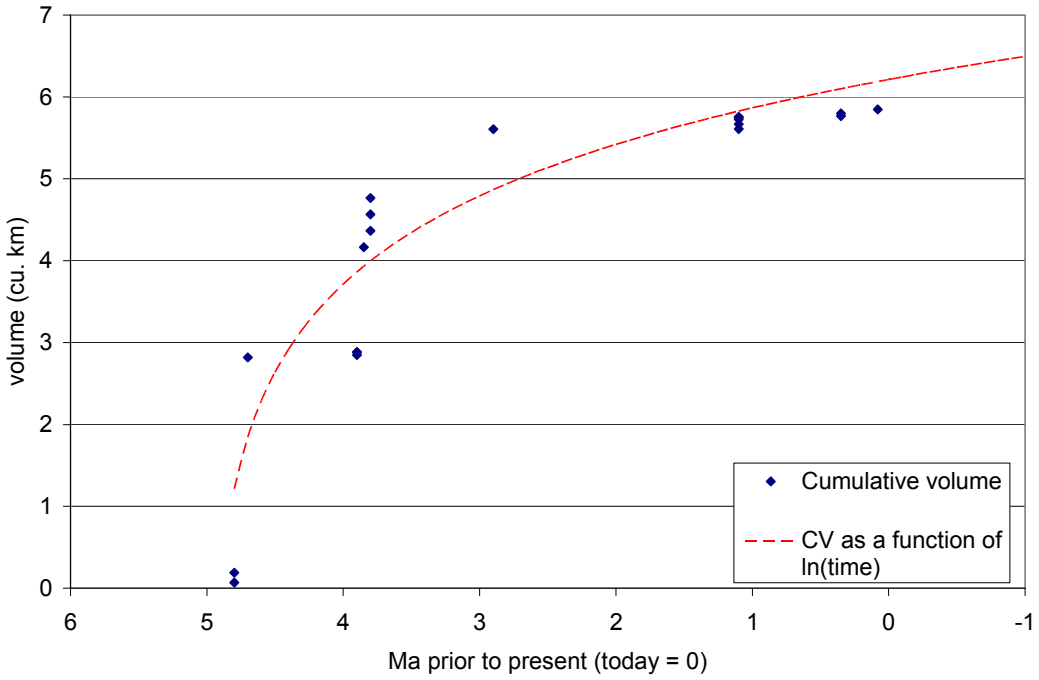

NOTE: Markers represent individual events. Line represents my assessment for a model of cumulative volume over time.

Figure D.3-14. Cumulative Volume and Volume per Event over Time for Events in the Past 5 Ma

D.3.5 REFERENCES

Cogbill, A.H., 2006. *Detectability of basaltic dikes using the 2004 Yucca Mountain aeromagnetic survey*: Unpublished report distributed to the PVHA-U Panel, dated June 2006, 11 p.

Connor, C.B., Stamatakos, J.A., Ferrill, D.A., Hill, B.E., Ofoegbu, G.I., Conway, F.M., Sagar, B., and Trapp, J., 2000. *Geologic factors controlling patterns of small-volume basaltic volcanism—Application to a volcanic hazards assessment at Yucca Mountain, Nevada*: Journal of Geophysical Research, vol. 105, pp. 417-432.

Crowe, B., Self, S., Vaniman, D., Amos, R., and Perry, F., 1983. *Aspects of potential magmatic disruption of a high-level radioactive waste repository in southern Nevada*: Journal of Geology, vol. 91, pp. 259-276.

Delaney, P.T., and Gartner, A.E., 1997. *Physical processes of shallow mafic dike emplacement near the San Rafael Swel*l, Utah: Geological Society of America Bulletin 109, pp. 1,177-1,192.

Detournay, E., Mastin, L.G., Pearson, J.R.A., Rubin, A.M., and Spera, F.J., 2003. *Final Report of the Igneous Consequences Peer Review Panel, with Appendices.* Las Vegas, Nevada: Bechtel SAIC Company. ACC: MOL.20031014.0097; MOL.20030730.0163.

Fridrich, C.J., Whitney, J.W., Hudson, M.R., and Crowe, B.M., 1999. *Space-time patterns of late Cenozoic extension, vertical axis rotation, and volcanism in the Crater Flat basin*, southwest Nevada, in Wright, L.A., and Troxel, B.W. (eds.), Cenozoic Basins of the Death Valley Region: Boulder, Colorado, Geological Society of America Special Paper 333, pp. 197-212.

Keating, G.N., Valentine, G.A., Krier, D.J., and Perry, F.V., 2008. *Shallow plumbing systems for small-volume basaltic volcanoes*: Bulletin of Volcanology, v. 70, pp. 563-582, DOI 10.1007/s00445-007-0154-1.

Maaloe, S., 1999. *Shape of ascending feeder dikes and ascent modes of magma*: Journal of Volcanology and Geothermal Research, vol. 81, pp. 207-214.

Parsons, T., Thompson, G.A., and Cogbill, A.H., 2006. *Earthquake and volcano clustering via stress transfer at Yucca Mountain, Nevada*: Geology, vol. 34, pp. 785-788.

Perry, F.V., Cogbill, A., Kelley, R., Lewis, C., Cline, M., Fleck, R, and Peterman, Z., 2006. *Preliminary results and interpretations of a high-resolution aeromagnetic survey and drilling program to investigate buried volcanic features near Yucca Mountai*n: Unpublished Report to the PHVA-U Expert Panel, dated June 30, 2006: 18 p. with appendix of lithologic logs.

Perry, F.V., Cogbill, A., and Kelley, R.E., 2005. *Uncovering buried volcanoes at Yucca Mountain*: Eos, vol. 86, pp. 485-488.

Perry, F.V., Crowe, B.M., Valentine, G.A., and Bowker, L.M., eds., 1998. *Volcanism Studies*: Final Report for the Yucca Mountain Project, Los Alamos National Laboratory Report LA-13478.

Stock, J.M., and Healy, J.H., 1988. Stress field at Yucca Mountain, Nevada, in Carr, M.D. and Yount, J.C. (eds.), *Geologic and Hydrologic Investigations of a Potential Nuclear Waste Disposal Site at Yucca Mountain, Southern Nevada: Denver, Colorado*, U.S. Geological Survey Bulletin 1790, pp. 87-93.

Valentine, G.A., and Keating, G.N., 2007. *Eruptive styles and inferences about plumbing systems at Hidden Cone and Little Black Peak scoria cone volcanoes (Nevada, U.S.A.)*: Bulletin of Volcanology, vol. 70, pp. 105– 113. DOI 10.1007/s00445-007-0123-8.

Valentine, G.A., and Krogh, K.E.C., 2006. *Emplacement of shallow dikes and sills beneath a small basaltic volcanic center—the role of pre-existing structure (Paiute Ridge, southern Nevada, USA)*: Earth and Planetary Science Letters, vol. 246, pp. 217-230.

Valentine, G.A., and Perry, F.V., 2006. *Decreasing magmatic footprints of individual volcanoes in a waning basaltic field*: Geophysical Research Letters, vol. 33, p. L14305.

Valentine, G.A., Perry, F.V., Krier, D.J., Keating, G.N., Kelley, R.E., and Cogbill, A.H., 2006. *Small-volume basaltic volcanoes—Eruptive products and processes, and post-eruptive geomorphic evolution in Crater Flat (Pleistocene), southern Nevada*: Geological Society of America Bulletin, vol. 118, pp. 1313-1330. DOI 10.1130/B25956.1.

Valentine, G.A., Krier, D.J., Perry, F.V., and Heiken, G., 2005. *Scoria cone construction mechanisms, Lathrop Wells volcano, southern Nevada, USA*: Geology, vol. 33, pp. 629-632.

INTENTIONALLY LEFT BLANK

D.4 MEL KUNTZ'S ELICITATION SUMMARY FOR PVHA-U PROJECT

Two types of igneous events are identified as having the potential to disrupt the Yucca Mountain radioactive waste repository: an igneous intrusion into the repository (which could be a dike, a sill, or both), or a conduit through the repository. The probability that either of these events would disrupt the repository is a function of the spatial and temporal distribution of volcanism in the area and the physical geometry of each type of igneous event. These factors, and the relationships among them, are illustrated in Figure D.4-1. Models and assessments of the geometry of dikes, dike systems, and conduits are summarized in Section D.4.1, followed by models and assessments of the spatial and temporal distributions of igneous events.

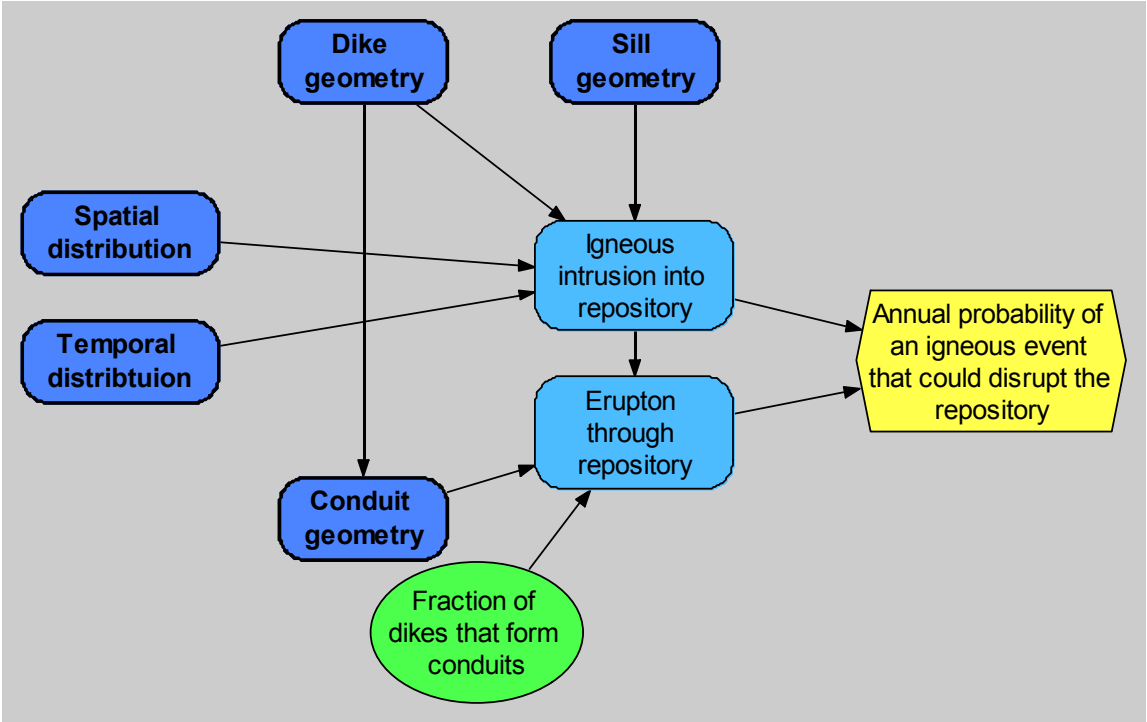

NOTE: The yellow hexagon represents the final result of the assessment. Green ovals represent assessed variables; dark blue rounded rectangles represent sub-models; light blue rounded rectangles represent values calculated from other inputs; and arrows indicate influence of one variable on one or more others.

Figure D.4-1. Overall Structure of the Model

D.4.1 EVENT DEFINITION

An event is defined as a sequence of processes that includes development or aggregation of magma in a source zone in the mantle, transfer of magma from that source zone to the upper part of the crust, and delivery of magma to a shallow depth in the crust or to the surface. Potential future igneous events to be expected in the Yucca Mountain region (YMR) would be basaltic, likely forming from magma derived from decompression melting that perhaps is related to tectonic events. For this project, the YMR is defined as the region within a radius of about 50 km centered on Yucca Mountain.

Two types of events may occur in the repository area: an eruption at the surface or an intrusion (a dike and/or a sill) that does not erupt. A critical question related to dikes is how close to the surface they can ascend without erupting. The repository lies about 300 m below the surface of Yucca Mountain, so we must consider the possibility that dikes could rise to that depth without erupting. Dikes in the Snake River Plain are known to be present at shallow depth for long distances from eruptive centers (Kuntz et al., 2002), but the Snake River Plain might not be a good analog to the YMR. General models suggest that dikes that ascend to depths of about 1 km will continue to ascend to the surface, moving upward largely by propulsion caused by exsolution of gases from the magma. Dikes, however, may ascend to depths of several kilometers, then stagnate at those depths without erupting at the surface. The Idaho dikes referred to above produced non-eruptive features, such as fractures and small faults, at the surface. Similar structures could affect the repository if dikes were to stagnate at a depth of several kilometers below the repository. Since these features are not observed in the YMR, I conclude that such dikes probably are not present in the shallow subsurface.

An interesting topic of discussion in PVHA-U workshops was whether non-erupted dikes in the shallow subsurface could be recognized by magnetic methods. Cogbill (2006) concludes that dikes having widths of about 1 m could be detected in alluvium at a depth of about 100 m; dikes having a width of 4 m could be detected at a depth of about 200 m. Magnetic methods have detected no dikes in Crater Flat. Because no dikes have been detected, I consider that dikes probably are not present in the shallow subsurface. If future geophysical techniques should identify basalt dikes in the shallow subsurface that did not erupt, then those dikes should be considered for hazard analysis.

Once magma approaches the surface, an event is defined both by the characteristics of the dike system and by the style of the eruption. I believe that any future volcanic event in the YMR would occur rapidly in geologic terms. By rapidly, I mean that the volcanic event would occur within a period of days, months, or a few years, but probably not over decades or centuries. Valentine et al. (2007) suggest that the Lathrop Wells cone and flows could have formed in only seven months. The study of the ~1-Ma volcanoes in Crater Flat provides evidence that the several aligned vents all formed within a short period, because all of the vents have the same paleomagnetic direction. This fact strongly suggests that the aligned cones formed during a single temporal event, even though the cones are relatively widely spaced over a distance of about 10 km. Valentine et al. (2006) suggest that all the ~1-Ma volcanoes formed in a single eruptive episode lasting as long as a few years. I believe that the tendency toward decreasing volumes throughout past volcanic events in the YMR also suggests that potential future eruptions would consist of single dikes, one or a few cones, and small-volume lava flows (<0.01 km^3), all being produced in less than a decade.

I am not a proponent of long and complicated eruptive episodes in the YMR, such as single events that consist of several dike systems and numerous cones and flows that occur over centuries or millennia. During Workshop 4, some members of the panel expressed support for this type of complex, longer-duration event definition. Some members also offered interpretations of the eruptive history in the YMR that comprise multiple events spread throughout a period of several hundred thousand years, with long periods of repose between event clusters. I believe that the radiometric age data available for past volcanic events are not robust enough to suggest anything other than relatively simple volcanic events in the YMR.

Such simple events would have involved one or several cones and flows that are relatively widely separated both temporally and spatially. I, therefore, do not use the cluster approach.

D.4.1.1 Characterization of Past Events

My assessment of the number of past events (based on my definition of an event) in the region of interest is presented in Table D.4-1. Because there are alternative interpretations of the number of events in the region, I have selected and provided weights for such alternatives in the event table. I generally interpret cones of the same or reasonably similar radiometric age to be part of a single event. In some instances, however, when there are other indicators of significant differences between cones (such as significant chemical differences or large spatial dispersion, as seen among the volcanic centers that are 3.8 Ma in age), I have provided weights for multiple alternative interpretations.

Table D.4-1. Relevant Events in the Region of Interest

Center	Number of Events	Age* (Ma)	Volume* (km^3)
Lathrop Wells	1	0.08	0.048
Sleeping Butte[†]			
Hidden Cone	1 (p = 0.3)	0.35	0.032
Little Black Peak	or 2 (p = 0.7)	0.35	0.014
Quaternary Crater Flat	1 (p = 0.9)		
Makani Cone	2 (p = 0.05)	1.07	0.002
Black Cone	4 (p = 0.05)	1.07	0.06
Red Cone		1.07	0.055
Little Cones NE	If 2 events, Little Cones are 1 event; Black Cone, Red Cone, and Makani Cone are a separate, single event	0.78	0.014
Little Cones SW		0.78	0.02
	If 4 events, Little Cones are combined in 1 event; Red Cone, Black Cone, and Makani Cone each are separate events		
Mio-Pliocene Centers			
Buckboard Mesa	1	2.87	0.838
Pliocene Basalt of Crater Flat[‡]	1 (p = 0.3)	3.8	0.585
Anomaly B	3 (p = 0.7)	3.8	1.227
Anomalies F, G, and H	If 3 events, Pliocene CF is 1 event; B is 1 event; F, G, and H together are 1 event	3.9	0.063
Thirsty Mountain	1	4.63	2.28 to 2.63
Dome Mountain	1	10.5	~10
Anomaly C	1 (p = 0.5)	4.8	0.117
Anomaly D	2 (p = 0.5)	4.8	0.073
Jackass Flats	1	9.5	4.1

Table D.4-1. Relevant Events in the Region of Interest (Continued)

Center	Number of Events	Age* (Ma)	Volume* (km^3)
Western Crater Flat (Anomalies R, Q, 4, and T)	1 (p = 0.85) 2 (0.05) 3 (0.05) 4 (0.05)	11.2	2.3
Solitario Canyon	1 (p = 0.3) 2 (p = 0.7)	11 (10 or 11.7)	Unknown
Anomaly A	1	10	0.06

* Age and volume estimates are based on consideration of Los Alamos National Laboratory (LANL) (2007).

† For Sleeping Butte, similar ages suggest one event; chemistry suggests two; geometry also suggests two N-S trending faults. I assign greater weight to two events.

‡ For the ~3.8 Ma events (Pliocene basalt of Crater Flat, Anomaly B, and Anomalies F, G, and H), one event is possible based on similarity in ages, but is unlikely given the geographic distribution and large magma volume required. There most likely were three events, based on mineralogical differences between Anomalies B and G.

D.4.1.2 Event Characteristics and Geometry

The following sections describe my assessments of the characteristics of potential future events in the YMR. The features of potential dikes, sills, and conduits are discussed, along with additional considerations.

Dike Geometry

Dike geometry is defined by the length, width, and azimuth of dikes and by their number and spacing, as illustrated in Figure D.4-2.

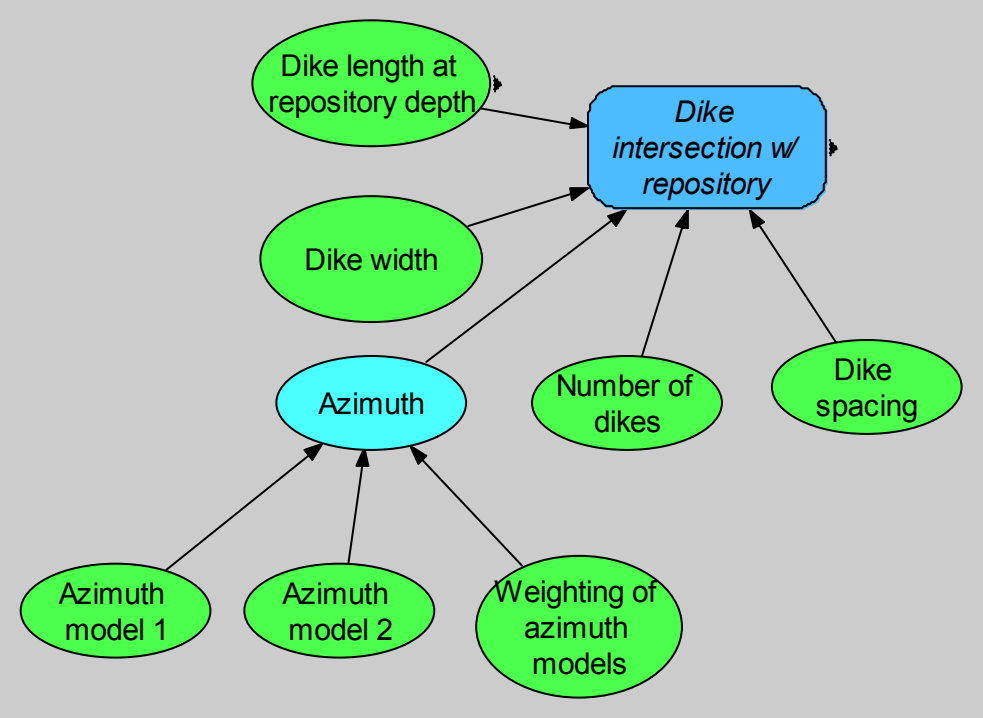

Figure D.4-2. Components of the Model for Dike System Geometry

Dike Length. In the YMR, dikes and fissures are observed to be less than about 5 km long, although at repository depths dikes may be longer than the features observed at the ground surface. Analog events in the YMR show typical dike lengths of 1 to 2 km; 5 km is at the upper bound of dike lengths observed in the field. In the YMR, shorter dike lengths are associated with more recent (Quaternary) volcanic events. If the Quaternary cones in Crater Flat are connected by a single dike, that dike would be about 11 km long. Based on comparisons with other basaltic fields, dikes longer than 10 km are unlikely but possible in the YMR.

I believe that ascending dikes have aspect ratios that suggest the shape of a very thin popsicle stick; that is, the dikes are several kilometers long, several meters wide, and approximately 40 km tall. Whether the dike extends as a single dike or a plexus of dikes from the base of the crust is a moot point for our analysis. As the dike ascends, its upper surface probably has a circular shape. That is, the crest of the dike reaches the surface first and then lengthens in opposite directions as the dike's "shoulders" reach the surface progressively away from the first outbreak.

My assessment of the length of potential future dikes at repository depth, shown in Figure D.4-3, is based on the following: minimum dike length is 0.2 km; maximum length (to be treated as an upper bound) is 15 km. Two kilometers represents the 50th percentile; 8 km represents the 95th percentile.

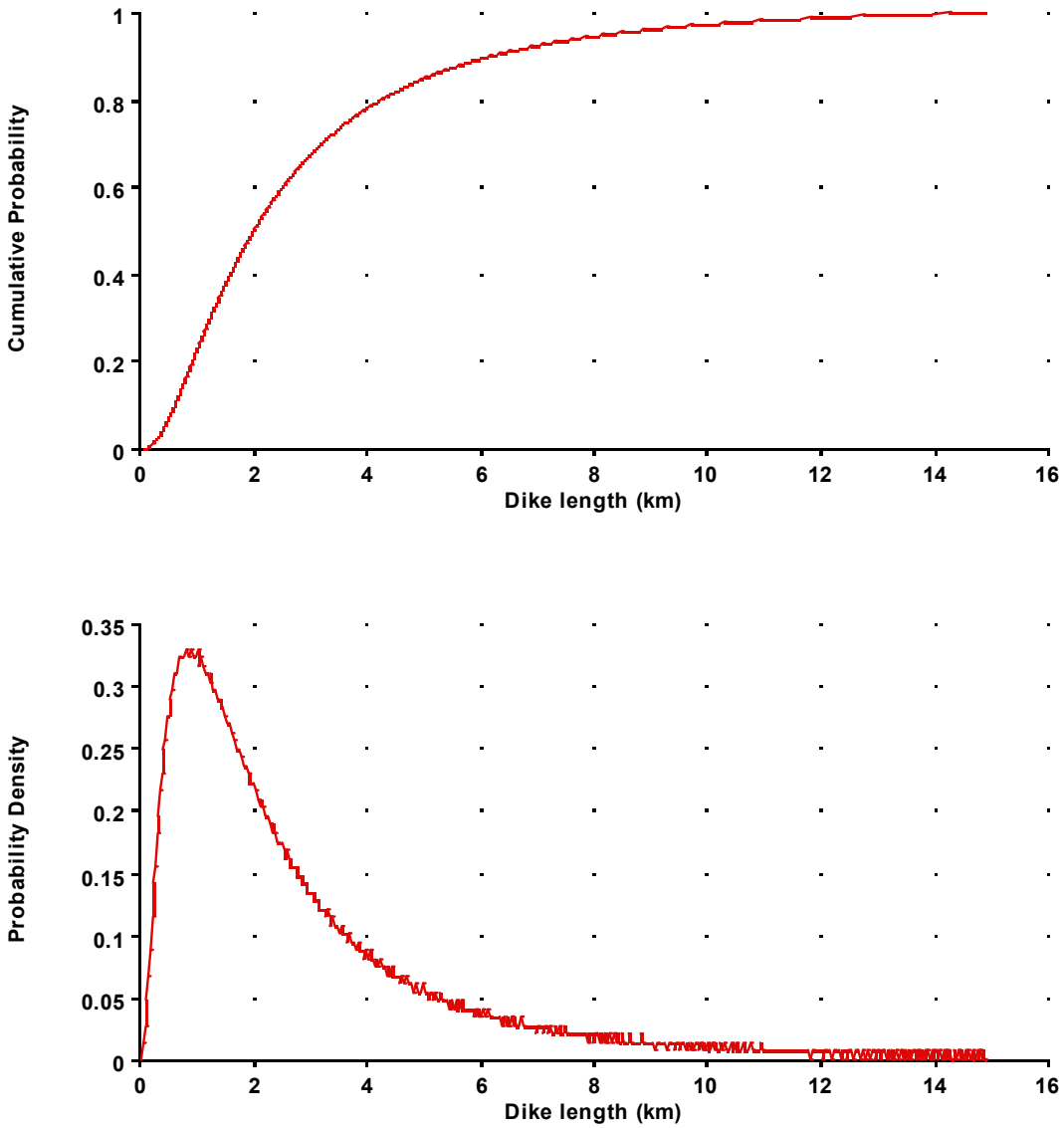

NOTE: Top graph is a cumulative distribution function; bottom graph is a probability density function.

Figure D.4-3. Assessment of Dike Length

Dike Width. Estimates of dike width are complicated by possible dike budding and/or the formation of conduits. Five meters is the maximum dike width expected at repository depth. Dike widths of more than 5 m probably reflect widening effects in the near-surface. Minimum dike width is affected by the cooling and heat transfer properties of magma.

Based on analogs in the YMR (data from an analog table developed by LANL investigators for the PVHA-U and published as Keating et al., 2008), my assessment is that the surface width of a potential future dike would range from a minimum of about 0.5 m to a maximum of about 10 m. Two meters represents the 50th percentile. My assessment of dike width is illustrated in Figure D.4-4.

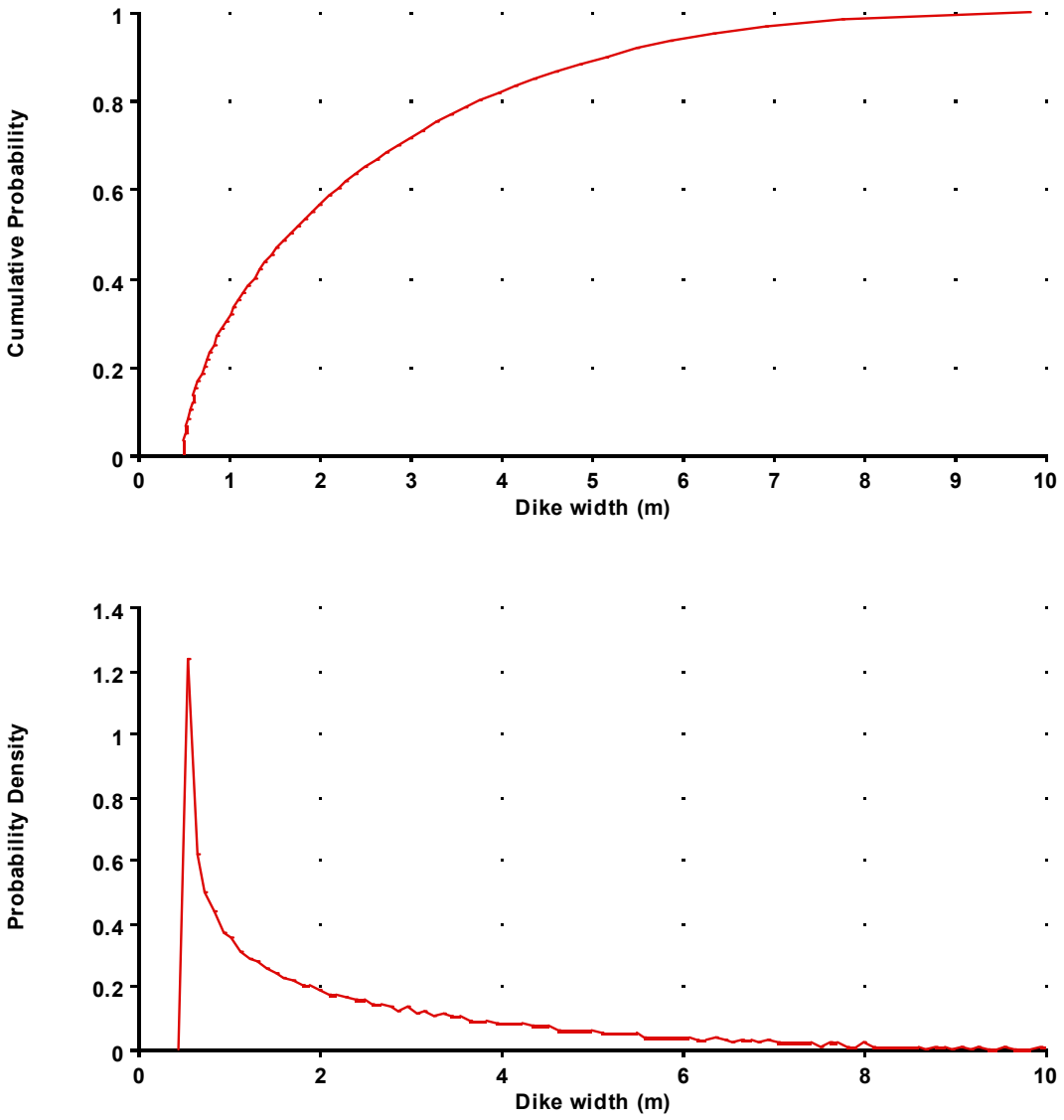

Figure D.4-4. Assessment of Dike Width

Dike Azimuth. The orientations of observed and interpreted dikes associated with analog volcanoes in the YMR, as well as the regional orientation of tectonic stress, provide the basis for my assessment of the azimuth of potential future dikes in the YMR. Most analog dikes are oriented about N-S (e.g., Pliocene Crater Flat dikes), although the alignment of the dike at Lathrop Wells is assumed to be about N10°W, and dikes at Paiute Ridge also are oriented about N10°W. I use two alternatives for my assessment of dike azimuth: (1) an azimuth similar to the alignment of Lathrop Wells and Paiute Ridge (N10°W), and (2) an azimuth more strongly influenced by the direction of least principal regional stress. For the second case, the direction of least principal stress in the YMR is about N60°W, so that dikes are oriented about N30°E (Parsons et al., 2006). Fault capture of dikes in the near surface may be an important factor. Most faults in the YMR have a N-S to NW orientation (Slate et al., 1999).

For the first alternative, N5°W is the most likely dike azimuth, with +/-15 degrees capturing about 90% of the distribution. For the second alternative, N30°E is the most likely azimuth, with +/-15 degrees capturing about 90% of the distribution. I estimate that an azimuth of N5°W would be more likely than one of N30°E, by a 2:1 ratio (weights of 0.67 and 0.33).

Figure D.4-5 illustrates both assessments for dike azimuth, as well as the weighted combination of the two distributions.

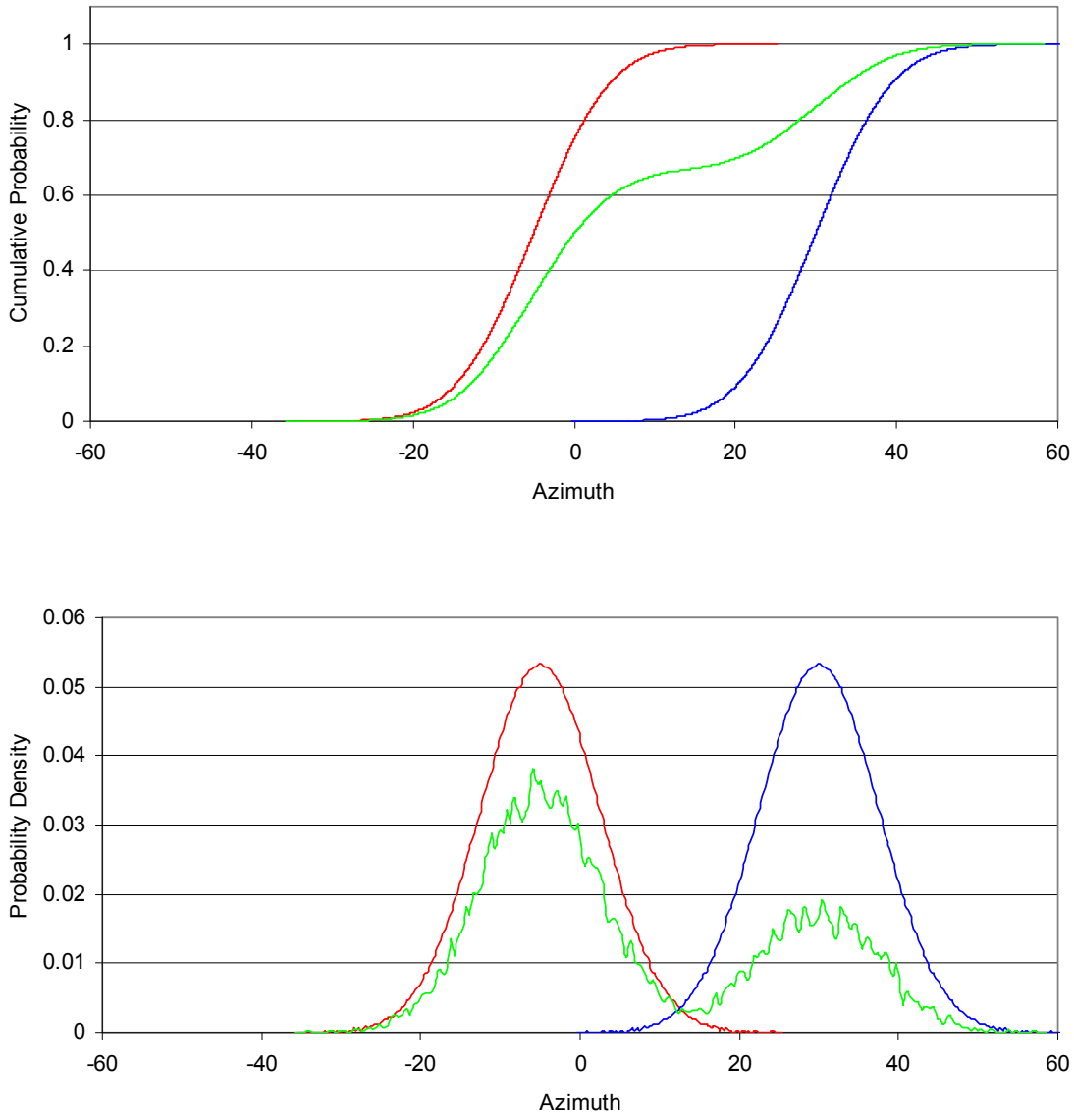

NOTE: Zero degrees represents north. Red and blue lines represent two alternative models; green line represents the weighted combination of those models.

Figure D.4-5. Assessment of Dike Azimuth

Number and Spacing of Dikes. Although it is most likely that a single dike would occur in the repository area, two or more dikes are possible during an individual event. Valentine et al. (2007) suggest that the Lathrop Wells cone was fed by a single dike, but Keating et al. (2008) observe that feeder dikes for more voluminous Pliocene and Miocene volcanoes commonly occur in sets that are several hundred meters wide, each set consisting of two to six sub-parallel or en echelon dikes. Six primary sets of dikes are observed at Paiute Ridge, and as many as five dikes are observed at Pliocene Crater Flat.

I estimate that the number of potential dikes that might occur at the surface in the YMR ranges from one to five, with one being the most likely. Based on consideration of the YMR analogs, my assessment of the number of dikes in an event at repository depth and their relative weights is: one (0.40), two (0.25), three (0.15), four (0.10), five (0.05), or six (0.05).

My assessment of the perpendicular spacing between multiple dikes in a single event is based on a consideration of analog areas such as Paiute Ridge and Basalt Ridge, as well as the horizontal (east-west) distance between features in Quaternary Crater Flat. My assessment of the spacing between potential future dikes, as illustrated in Figure D.4-6, is based on the following: minimum of 0.05 km; 95th percentile of 3 km; and 10th, 20th, and 50th percentiles of 0.2, 0.5, and 1 km, respectively.

Sub-parallel dikes would be expected to be offset in an en echelon pattern, but could have either an overlap or an underlap (gap) of as much as 50 percent of the length of the shortest dike. Based on the geometries of features in Quaternary Crater Flat; Pliocene Crater Flat; Anomalies F, G, and H; and Nye Canyon, it is expected that any en echelon dikes would be right-stepping (weight of 0.75) rather than left-stepping (weight of 0.25).

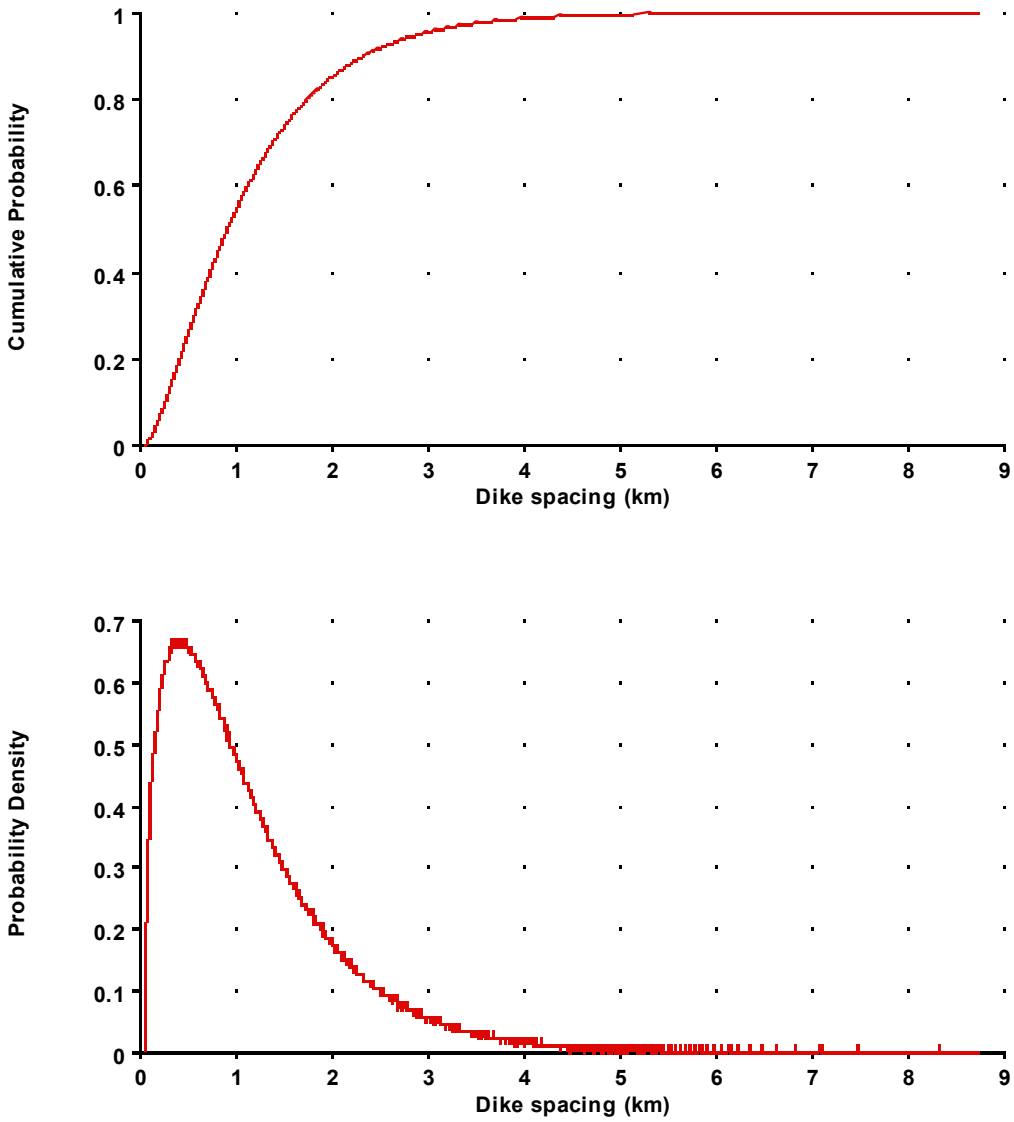

Figure D.4-6. Assessment of the Perpendicular Spacing between Dikes in an Event Composed of Multiple Dikes

Additional Considerations. Dikes are buoyantly driven, and unless buoyancy forces exceed lithostatic forces, they may not reach the surface. Thus, it is possible that if a dike were to ascend to repository depth, it might not reach the surface. Little information is available for assessing the ratio between eruptive and non-eruptive dikes in the YMR. Expected exsolution depths of magmas in the YMR suggest that dikes that ascend to within 1,000 m of the surface likely would erupt, although some segments of dikes that reached the surface might terminate below ground. I estimate, therefore, that a relatively small fraction of potential dikes would reach repository depth but not reach the surface (0.05). The small volumes expected for potential future events are close to the volumes needed to fill a dike and not much more. Given the decreasing volumes of eruptions in the YMR, we may be approaching a time when the

volumes of magma generated will be insufficient to fill a dike. The volume of a dike having dimensions of 2 km long, 2 m wide, and 40 km tall is approximately 0.15 km^3. For comparison, this volume is approximately three times the estimated volume of volcanic material erupted for the Lathrop Wells cone, approximately equal to the estimated volume of volcanic material in the Quaternary Crater Flat cones, and about 20 percent of the estimated volume of the Buckboard Mesa lava field.

Sill Formation and Geometry

Figure D.4-7 illustrates the factors that define sill geometry. Sills can be observed in the YMR where erosion is sufficiently deep. Given the geology and stress conditions within the repository area, sills could form during a potential future event. Paiute Ridge provides a useful analog for sill formation, because sills at that locality formed near (above) contacts between ash-flow and bedrock units. The Paiute Ridge sills have a diameter of about 0.5 to1 km.

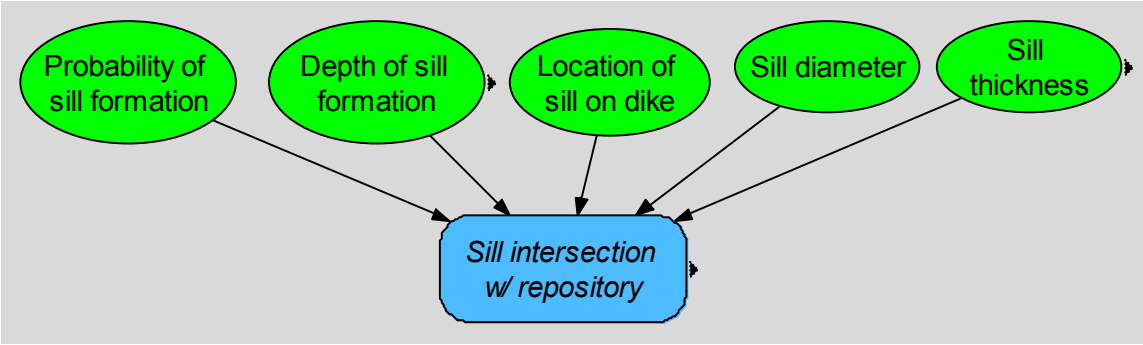

Figure D.4-7. Components of the Model for Sill Formation and Geometry

Estimating the likelihood of a sill forming at repository depth involves several factors. A simple probability distribution of sills over a range of depths assumes that the intruded medium is homogeneous and that sills are simply a function of driving pressure versus lithostatic pressure. Valentine and Krogh (2006) demonstrate that sill formation is affected more by local inhomogeneities along the fault/dike plane than by simple, model-based pressure relations. Factors important to sill formation include contact relationships, rock strength (welded vs. nonwelded), and dip of bedding. My assessments of sill parameters are based on the expectation that any future eruptions would involve small volumes of magma.

I estimate that about 1 in 10 potential future events in the YMR would produce a sill at some depth. The number of events producing sills could be as low as 1 in 25, or as high as 1 in 2. If a sill were to develop, there is uncertainty about the depth at which it would form. My assessment is that a depth of 150 to 200 m is most likely, based on the Paiute Ridge analog (Valentine and Krogh, 2006), but I consider that sills could form between depths of 400 m (maximum) and 100 m (minimum). Figures D.4-8 and D.4-9 illustrate my assessments of the fraction of potential future events that would include a sill and the depth at which a sill would form on a dike, respectively.

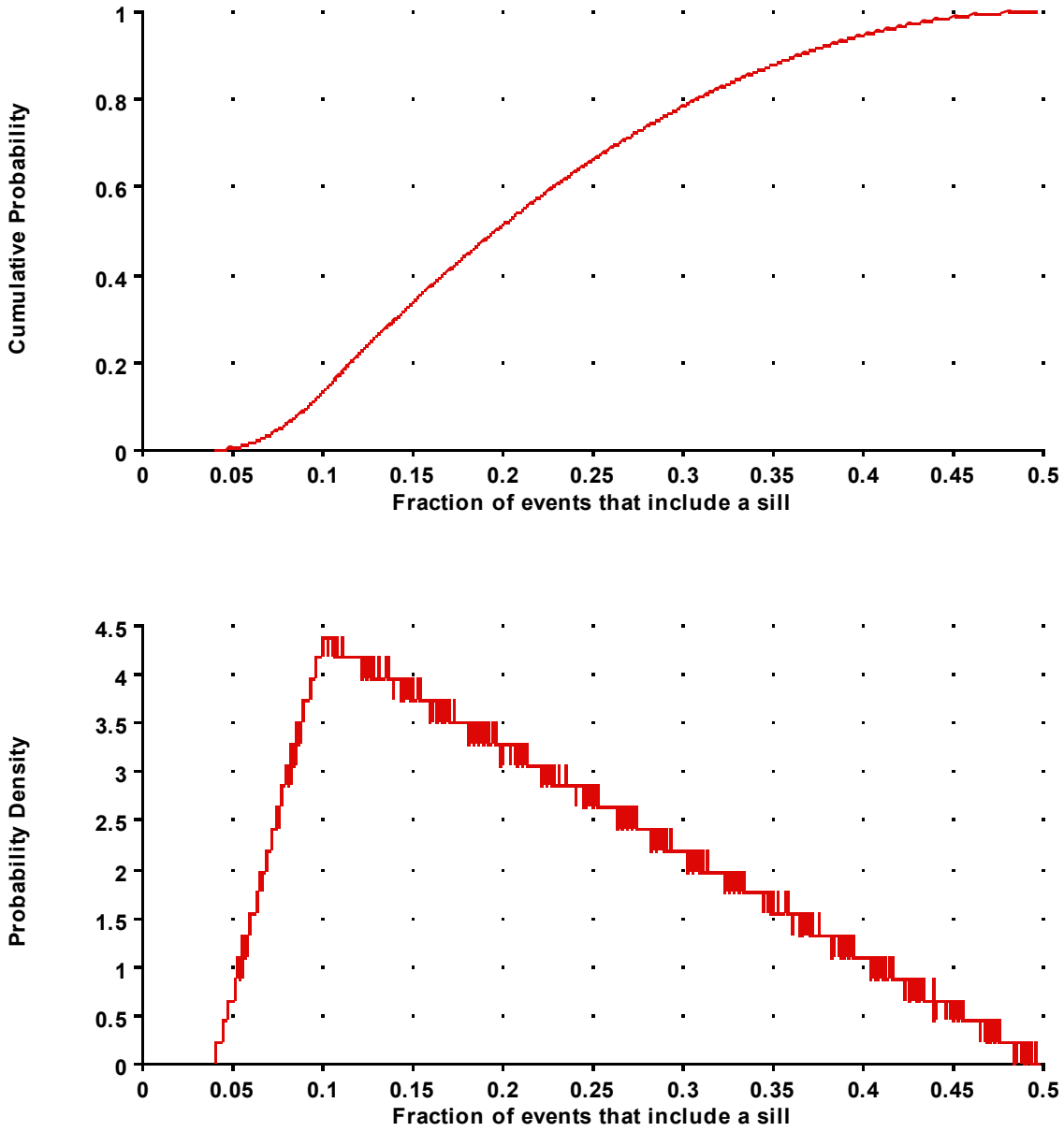

Figure D.4-8. Assessment of the Fraction of Events That Include a Sill

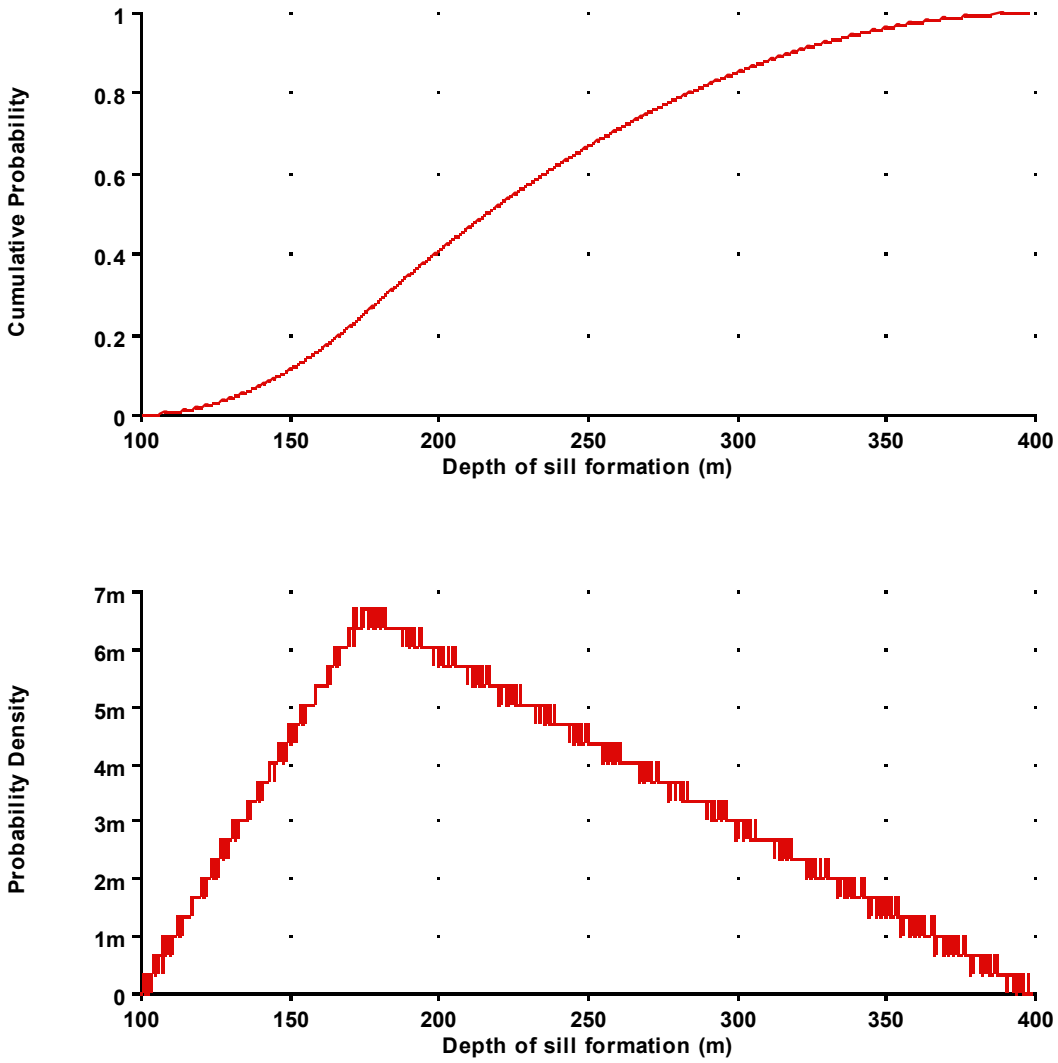

NOTE: For values less than 0.01 on the y-axis, suffix notation is used (m = 10^{-3} and u = 10^{-6}, so 5m = 0.005).

Figure D.4-9. Assessment of the Depth of Sill Formation on a Dike

Sill Geometry. Sills can be modeled as ellipses having an approximately constant thickness. The aspect ratio of a sill should be modeled as anywhere from 1:1 to 3:1 (length is three times the width of the ellipse). Given my assessment that potential future events in the YMR would involve a small volume of magma, I estimate that the length of a sill (assuming one occurs) most likely would be about 500 m. The length could be as small as 20 m (minimum) or as large as 1 km (maximum). Uncertainty in the length can be modeled using a triangular distribution.

Studies of sills such as those at Paiute Ridge suggest that sills occur on the hanging-wall side of normal faults. In the YMR, however, it usually is not clear which side is the hanging wall, so potential sills should be assumed to occur randomly on either side of associated dikes. Sills can be located anywhere along the length of a dike, but are more likely to be located toward the center. Figure D.4-10 illustrates my assessment of the location of a sill along the length of a

dike. Based on the Paiute Ridge analog, I assess the azimuth of sills to be oriented parallel (0.3) or perpendicular (0.7) to their associated dikes.

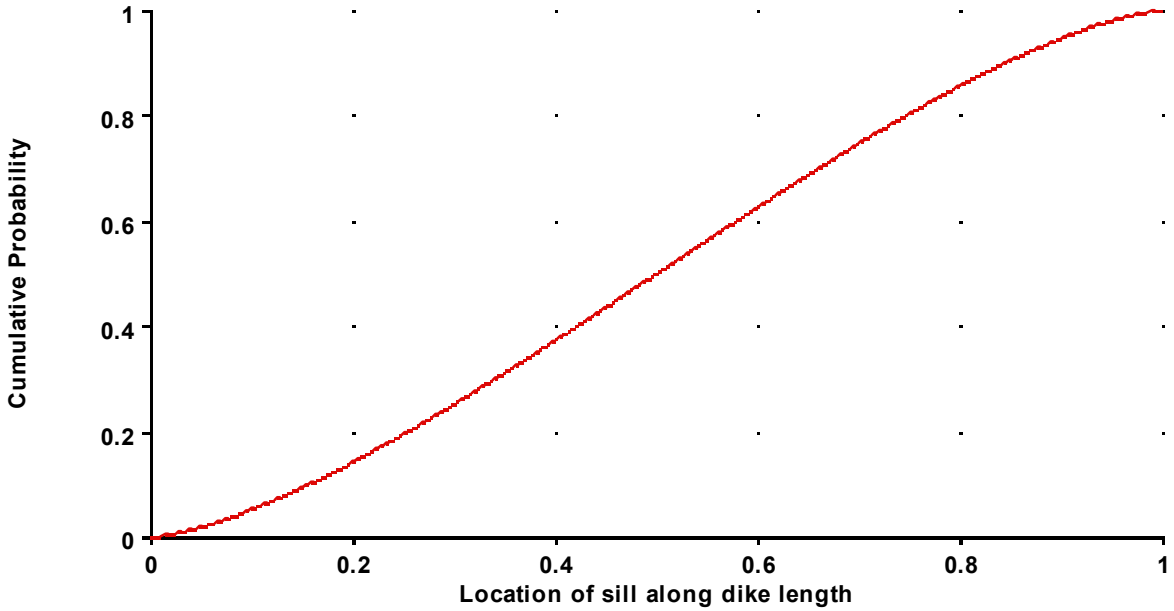

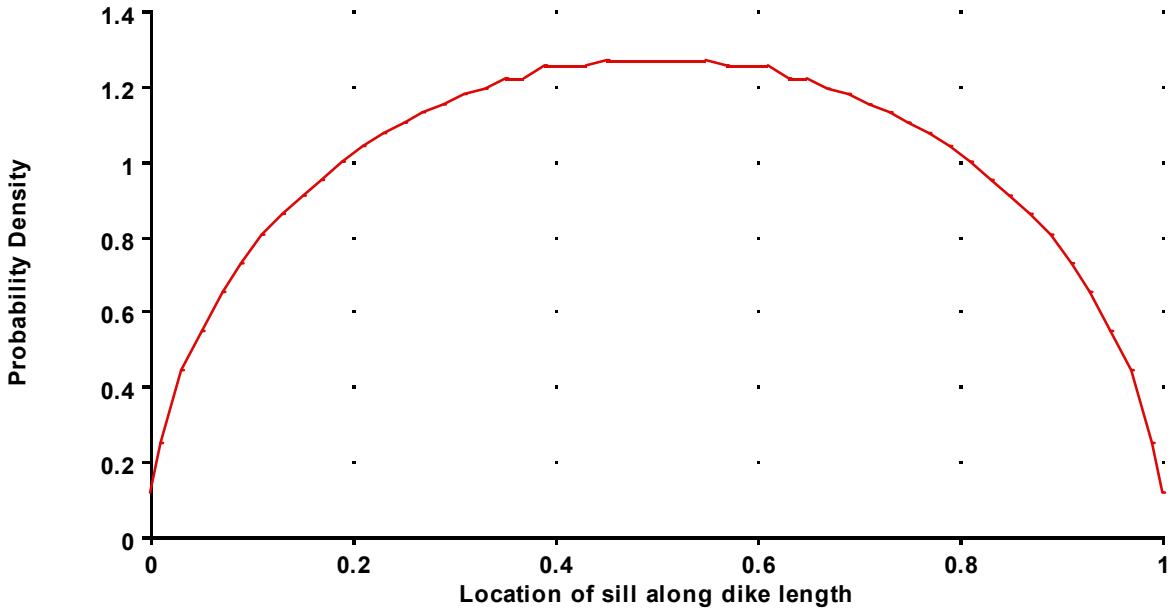

NOTE: Zero and 1 represent the ends of the dike.

Figure D.4-10. Assessment of the Location of a Sill along the Length of a Dike

The thickness and length of sills are correlated because both are functions of the volume of magma (longer lengths should be associated with thicker sills). My assessments are based on analogs at Paiute Ridge and Basalt Ridge. The most likely value for the thickness of a potential future sill is 50 m, but a sill could be as thin as 5 m (minimum) or as thick as 200 m (maximum). Figure D.4-11 illustrates my assessment of sill thickness.

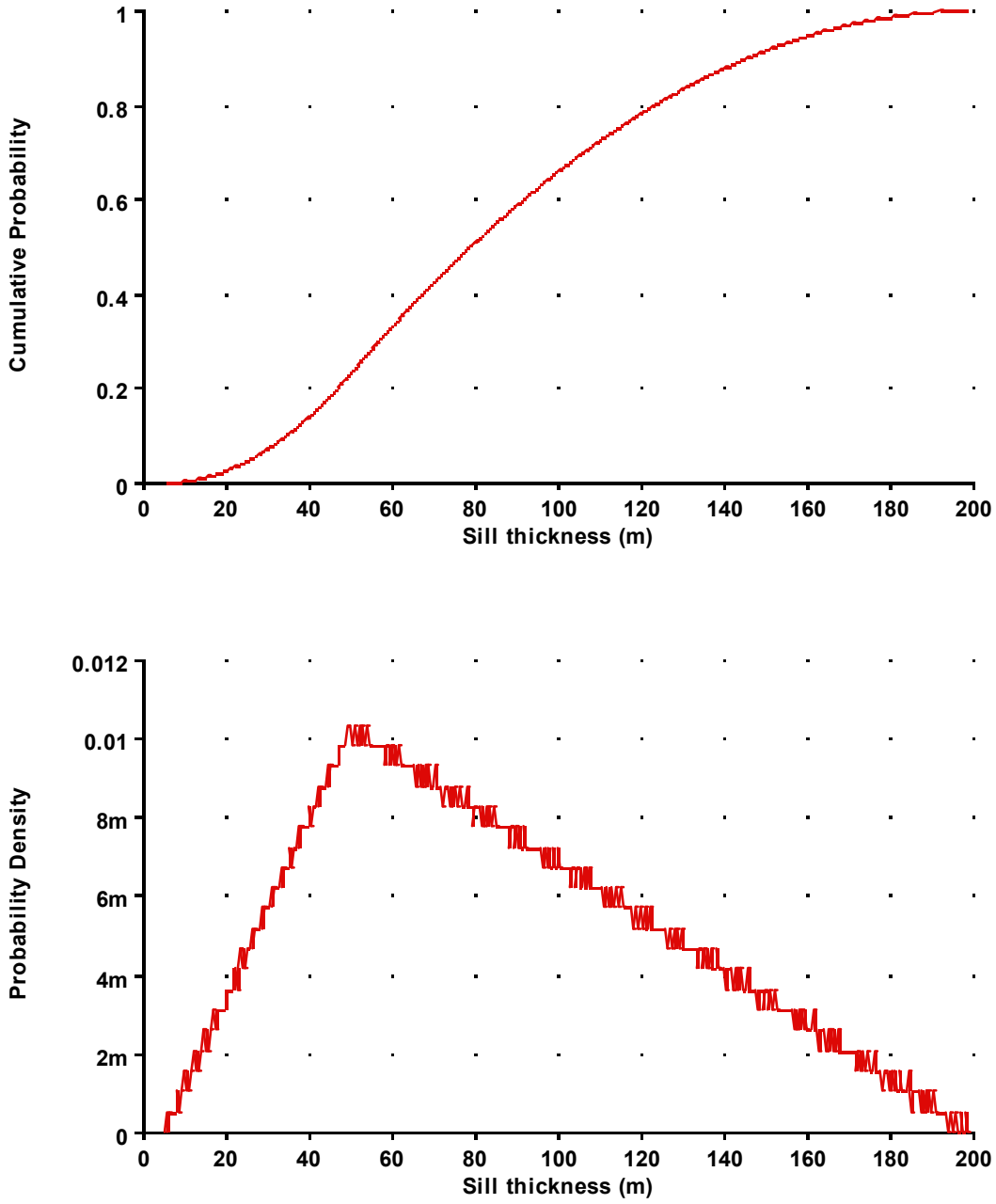

NOTE: For values less than 0.01 on the y-axis, suffix notation is used (m = 10^{-3} and u = 10^{-6}, so 5m = 0.005).

Figure D.4-11. Assessment of Sill Thickness

Conduit Formation and Geometry

A conduit forms when a fissure has formed at the surface and the eruption continues until it is localized in one or more eruptive conduits. A dike that ascends to the surface, however, will not necessarily contain a conduit, depending on the volume of magma in the dike and the length of time that the eruption continues. Shorter-duration eruptions are likely to produce fewer conduits, whereas longer-duration eruptions are likely to produce more conduits. The probability that a conduit would occur without a dike at repository depth is negligibly small.

Conduit geometry is defined by conduit diameter and the number and spacing of conduits on a dike, as shown in Figure D.4-12.

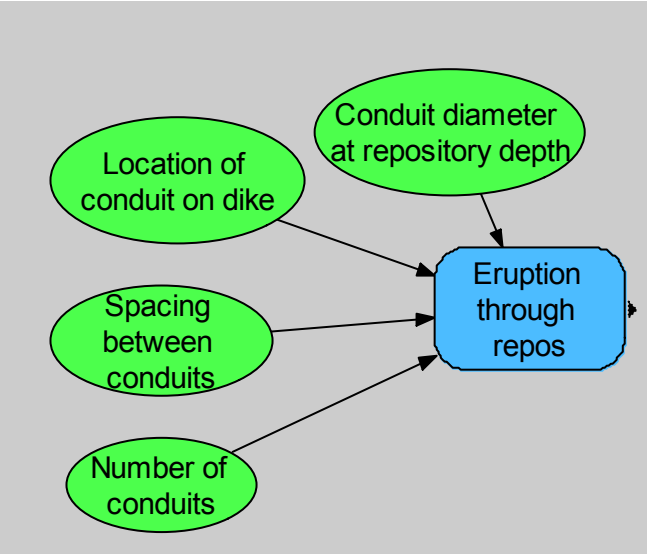

Figure D.4-12. Components of the Model for Conduit Geometry

Number of Conduits. The number of conduits that can occur on a dike is a function of dike length, which in turn is related to the volume of magma. Quaternary analogs in the YMR indicate that a single conduit is associated with most events, except for the Quaternary Crater Flat cones, which may represent four conduits. An eruption in Saudi Arabia was observed to involve six conduits on a 3- to 5-km-long dike. Evidence of multiple conduits typically is erased by later eruptive phases (for example, Lathrop Wells today reflects conditions present when the eruption ceased and may not reflect what happened during the early stages of eruption).

To estimate the number of conduits as a function of dike length, I developed assessments for various dike lengths. These assessments can be interpolated and extrapolated to other dike lengths. Based on my field observations, the chance that zero conduits will occur on a dike is greater on a shorter dike. The number of conduits is dependent on total dike length, but not in a linear way. I believe that for total dike lengths as long as about 8 km, the number of conduits generally increases with dike length, because dikes having a total length of about 0.5 to 8 km are associated with Strombolian or violent Strombolian eruptions. As total dike length increases beyond about 8 km, however, I believe that the nature of the eruption begins to tend toward a fissure type, which is associated with fewer discrete conduits. In Table D.4-2, therefore, I show

that as dike length increases beyond 8 km, the number of conduits begins to decrease. For a dike length of 16 km, I show a high probability that there would be no conduits on the dike system.

Table D.4-2. Number of Conduits as a Function of Total Dike Length

Number of Conduits	Total Dike Length						
	0.2 km	0.5 km	1 km	5 km	8 km	12 km	16 km
0	0.7	0.2	0.05	0.02	0	0.4	0.7
1	0.3	0.5	0.475	0.2	0.1	0.3	0.2
2		0.2	0.2375	0.3	0.2	0.2	0.1
3		0.1	0.1425	0.2	0.3	0.1	
4			0.0665	0.1	0.2		
5			0.0285	0.09	0.1		
6			0	0.05	0.05		
7			0	0.03	0.03		
8			0	0.01	0.02		

NOTE: The values for number of conduits on a 1-km dike are calculated from a conditional assessment. I estimate a 5% probability of no conduits on a 1-km dike. If there are any conduits (95% probability), there is a 50% probability of one conduit, 25% probability of two conduits, 15% probability of three, 7% probability of four, and 3% probability of five.

Location of Conduits. Analog data indicate that conduits typically are located at the centers of dikes, because magma flux is highest in that area. Conduits, however, may occur anywhere along a dike. A single conduit is likely to be located on the "middle half" of the dike, but can occur anywhere along the length of the dike. Figure D.4-13 illustrates my assessment of the probable location of a conduit along a dike. This distribution puts a 60% probability of the conduit being in the center part of the dike, and a 40% probability of it being toward one end.

In multiple-dike systems, conduits are more likely to occur on longer rather than shorter dikes, because magma flux is higher in longer dikes. If a potential future event were to involve multiple dikes but a single conduit, my assessment is that the conduit most likely would be located on a longer dike (probability = 0.75) than on a shorter dike (probability = 0.25). If an event were to involve multiple dikes and multiple conduits, one conduit would occur on the longest dike. Second and subsequent conduits might occur with equal probability on that same (longest) dike or on any other dike. My assessment of conduit spacing along a dike, based on consideration of analog data (developed by LANL investigators and published as Keating et al., 2008), is that a minimum spacing between conduits is 250 m; most likely spacing is about 500 m; and maximum spacing is 1 km.

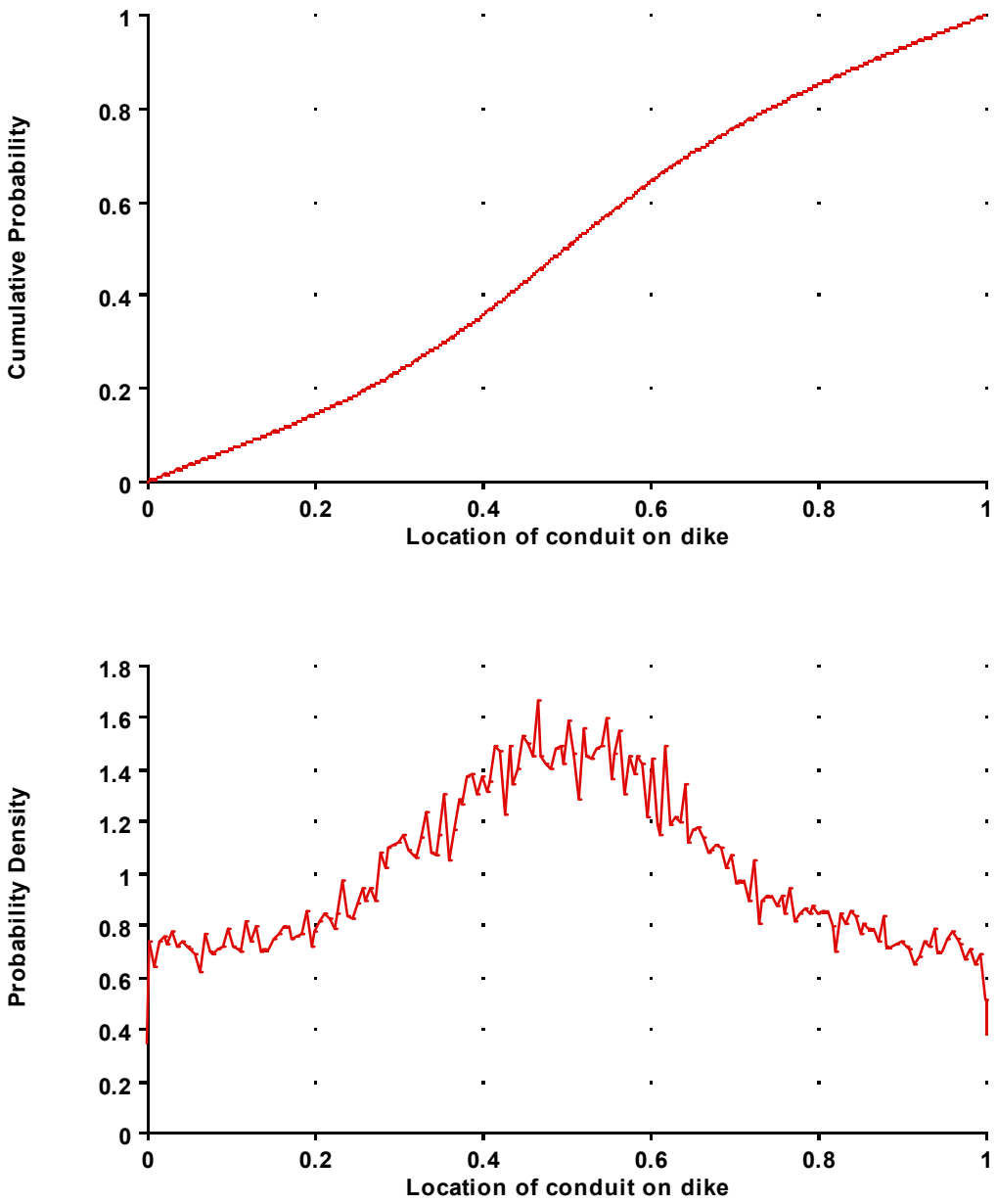

NOTE: Zero and 1 represent the endpoints of the dike. The distribution function is a combination of a uniform and a Gaussian distribution. The roughness, or "spikiness," of the density function is an artifact result of simulation and is not an important feature of my assessment.

Figure D.4-13. Assessment of the Location of a Conduit along the Length of a Dike

Conduit Diameter. Little analog information is available on dimensions of conduits at the depth of the repository. Conduits at the surface typically have diameters of 50 to 100 m. Dimensions at repository depth likely would be less than those at the surface, given the expected upward-flared shape of a conduit.

My assessment of the diameter of a potential future conduit at repository depth is illustrated in Figure D.4-14. It is based on the following estimates: 1.5 m (or the width of the dike) is the minimum diameter; 100 m is the maximum; and 20 m is about the 50th percentile.

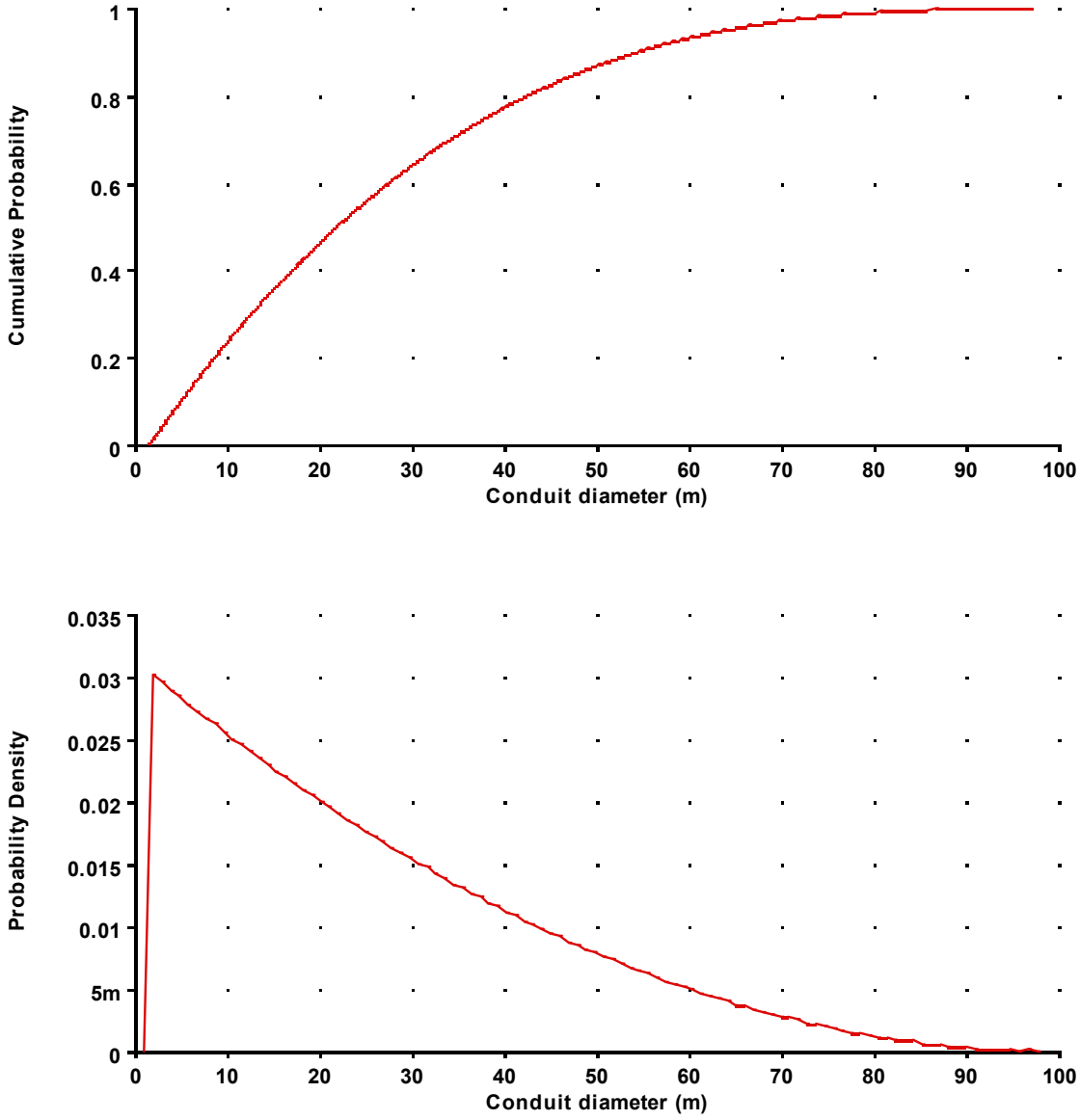

NOTE: For values less than 0.01 on the y-axis, suffix notation is used (m = 10^{-3} and u = 10^{-6}, so 5m = 0.005).

Figure D.4-14. Assessment of Conduit Diameter for a Dike That Is 1.5 m Wide

Column-Producing Conduits. Quaternary analogs in the YMR suggest that about 80 to 90 percent of conduits produce eruptive columns (Valentine et al., 2006, 2007; Valentine and Keating, 2007). Given the expected small volumes of potential future events in the YMR, I would expect that the more conduits on a dike, the smaller the probability that any given conduit would be column producing. The following is my assessed probability that a conduit would be

column producing as a function of the total number of conduits on a dike (extrapolations can be made for intermediate numbers of conduits): 1 conduit (90%), 3 conduits (80%), and 8 conduits (5%). As discussed above, I believe that very long dikes (>8 km) would be associated with fissure eruptions, with a smaller number of conduits for longer dikes. Any conduits in such eruptions are less likely to be column producing: my assessment is that if a conduit occurs on a 12 to 16 km dike, there is a 50% chance of it being column producing.

Additional Considerations

In addition to the features of dikes, sills, and conduits, I consider some other aspects of potential future events.

Style of Eruptions. Some volcanic events in the YMR began as true fissure eruptions that eventually formed cinder cones. An excellent example is the Pliocene Crater Flat vents. Lathrop Wells, on the other end of the spectrum, was a Strombolian to violent Strombolian eruption—although the volume of magma was low, it was delivered to the surface fairly violently and rapidly. Other volcanic events in the YMR were intermediate in eruption type, involving Strombolian eruptions that were less explosive than those observed at Lathrop Wells. Some eruptions certainly involved column-producing conduits, especially the Lathrop Wells and Quaternary Crater Flat eruptions. During the past 10 Ma, relatively large volumes of erupted lava and relatively high mass/eruption rates have produced several fissure eruptions such as the one at Thirsty Mountain. Because there has been a progressive shift toward lower volumes and lower mass/eruption rates during more recent eruptions in the YMR, there has been a shift toward Strombolian and violent Strombolian types of eruptions. My assessment of potential future eruption types therefore is skewed toward violent Strombolian eruptions that involve low volumes of magma erupted within a period of days to months.

Maar Eruptions. Maar eruptions are common at some locations in the Great Basin, but there is little evidence they have occurred in the YMR. The future occurrence of a maar eruption, therefore, is considered unlikely. Maar-type eruptions generally are produced where magma intersects water-saturated sediments. Although all dikes intersect a water table at some depth, in most cases the type of eruption is not affected. Yucca Mountain is underlain chiefly by welded and non-welded ash-flow tuffs and not by loose sediments (Day et al., 1998). My assessment for the 10,000-year time frame is a 1% probability that any future eruption would be of the maar type. Modeling of future climate indicates that intermediate and monsoon states (one to three times current precipitation) are likely to occupy 67 percent of the next million years, and interglacial and glacial (1.5 to 3.5 times current) states will occupy about 33 percent (BSC 2003). These expected increased precipitation states suggest that there may be a slightly greater chance of a maar eruption in the next one million years. Given the potential for climate change and groundwater rise in the Yucca Mountain area during the 1-My time frame, I estimate that the probability of a maar eruption increases to about 3% for that time frame.

D.4.2 SPATIAL MODEL

I use two conceptual approaches to model the conditional spatial intensity of potential future volcanism within the region of interest: (1) a uniform distribution within defined zones, and (2) spatial smoothing around past events combined with my interpretation of various geologic data.

My region of interest contains the events and structural characteristics of importance to the spatial distribution of potential future volcanism. Within the region of interest I define a smaller Crater Flat zone, reflecting my assessment that volcanism will continue to be concentrated in that zone. As described previously, Table D.4-1 lists identified centers in the region of interest, my assessment of the number of events each center represents, and the estimated age and volume of each event. I consider only events younger than 4 Ma for my 10-ky assessment; my 1-My assessment incorporates both post-11-Ma events (weight of 0.2) and post-4-Ma events (weight of 0.8).

As discussed below, I consider two alternative models for the spatial distribution of potential future igneous events: a zone model, and a spatial smoothing model. I prefer the zone model (weight of 0.7) over the spatial smoothing model (weight of 0.3), because it better reflects the differences between Crater Flat and the surrounding region regarding the locations of past events and the potential for future events. These weights are applicable to both the 10-ky and 1-My assessments.

D.4.2.1 Zone Model

Two zones are defined that incorporate volcanic events relevant to the repository. The larger zone (my region of interest) contains events that represent the range of eruption types to be considered; the smaller zone encompasses the higher density of past events in Crater Flat. Figure D.4-15 illustrates both my region of interest and the Crater Flat zone. Each zone includes volcanic events having a range of ages. The anticipated frequency of future events differs for each defined zone.

The region of interest, which is defined based primarily on gravity data, incorporates the Amargosa Trough. The northern boundary of the zone was drawn specifically to include the larger-volume events of the Thirsty Mesa, Buckboard, Timber Mountain, and Sleeping Butte areas. The southern boundary is located north of the Greenwater Mountains along the Stateline fault, which is a major tectonic boundary. The region of interest thus incorporates older volcanic events and the larger-volume eruptions that I believe may be relevant for the 1-My assessment.

The smaller zone includes only the Pliocene-Quaternary events of Crater Flat. Crater Flat is expected to have a higher rate of future volcanism because its rate has been higher more recently than any other area in the YMR. Also, those youngest events are concentrated in a relatively small geographic area. The events of Sleeping Butte and Anomalies F, G, H, and B are specifically excluded from this zone because of their location outside Crater Flat.

Although I expect the rate of future volcanism to be higher in the Crater Flat zone than in the larger region of interest, the rate changes gradually, rather than as a step-function, across the zone boundary. The distance over which the change in rate occurs is uncertain, but ranges from about 0.5 to 20 km. My assessment of the rate-transition distance is illustrated in Figure D.4-16 based on a minimum of 0.5 km, a maximum of 20 km, a 60th percentile of about 2 km, and a 95th percentile of about 10 km.

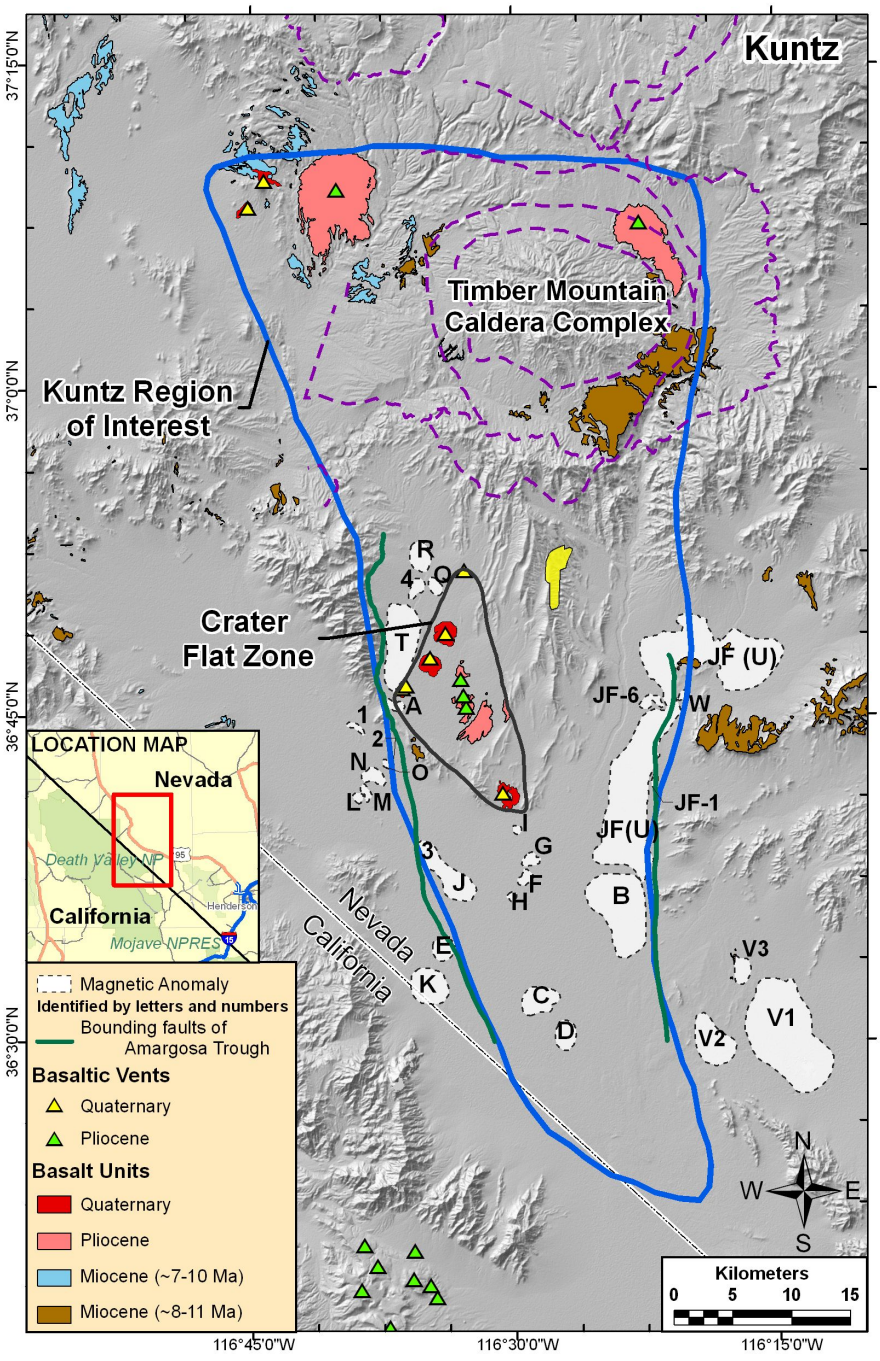

NOTE: The outer blue line delineates my region of interest. The inner black line outlines the boundaries of the Crater Flat zone.

Figure D.4-15. Region of Interest and the Crater Flat Zone

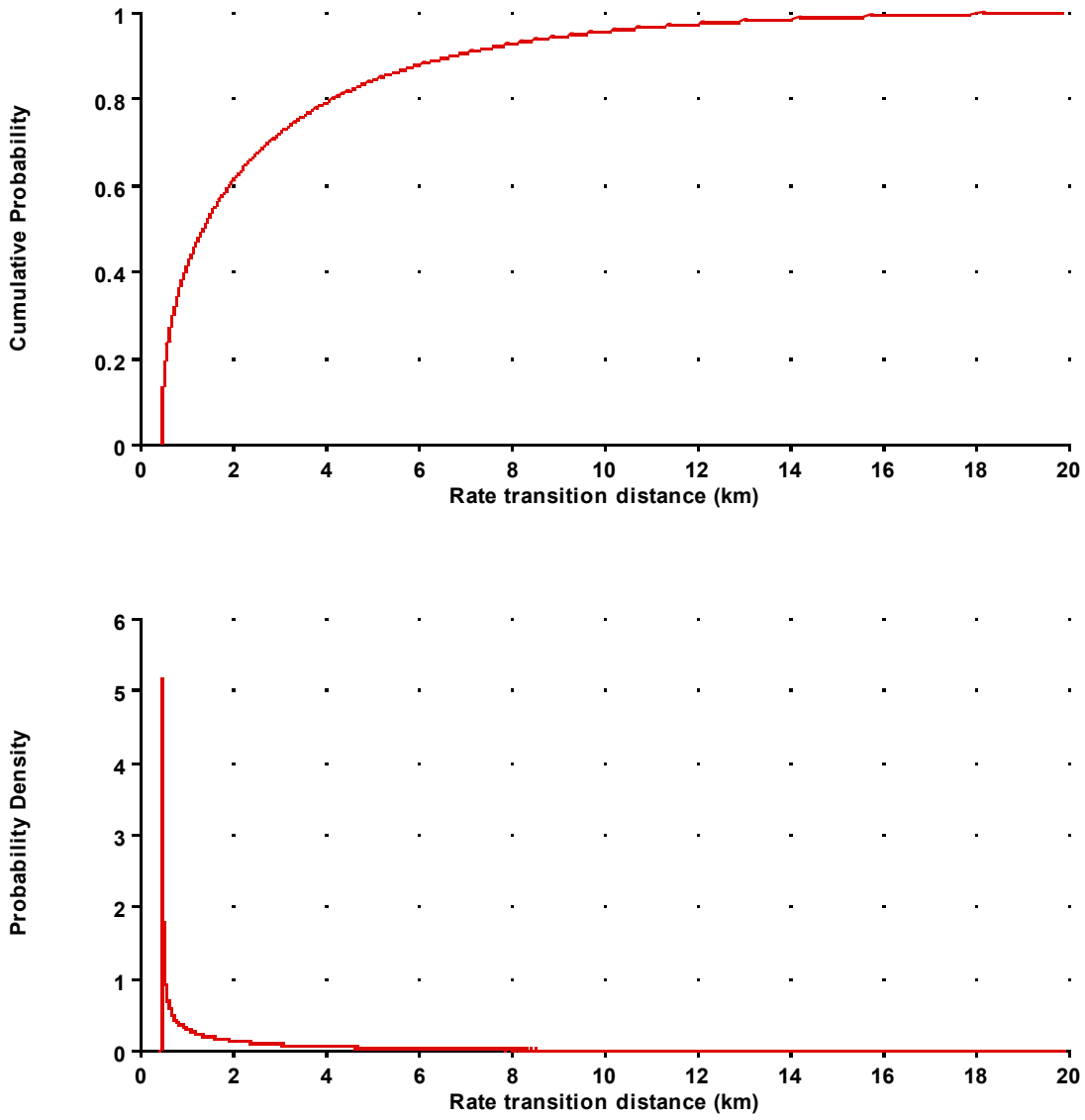

Figure D.4-16. Assessment of the Distance over Which the Rate of Volcanism Changes between Zones

D.4.2.2 Spatial Smoothing Model

Because more recent events better indicate the locations of potential future events than do older events, my spatial smoothing utilizes weights based on the inverse of the age of each event. After exploring various smoothing models, I selected a Gaussian kernel and the range of smoothing distances described below.

For the 10-ky assessment, I use spatial smoothing around post-4-Ma events in the Crater Flat zone only. After evaluating alternative smoothing distances (h), including those considered by Connor et al. (2000), I use a smoothing distance of 5 km. I prefer smaller h values, because

these reflect my belief that potential future events in the YMR most likely would occur near past events.

For the 1-My assessment, spatial smoothing is used around all events in my region of interest. Smoothing around post-4-Ma events is weighted 80%. Smoothing around post-11-Ma events is weighted 20%. Again, I use a smoothing distance of 5 km.

D.4.2.3 Incorporating Geologic Data

The spatial models derived from the smoothing approach are combined with my interpretation of several geologic data sets, as described below. This approach utilizes my interpretations of geologic data sets, including lithostatic pressure and tomography, which are combined with the spatial intensities derived from the spatial smoothing models to define the spatial distribution of potential future events.

Lithostatic Pressure. Lithostatic pressure, which is derived from free-air gravity data, appears to provide reliable data for assessing the distribution of potential future events. Based on the relationship between past events and lithostatic pressure within my region of interest, I developed the assessment illustrated in Figure D.4-17. This figure illustrates the lithostatic pressure I would anticipate at the location of a hypothetical future event in the region. The figure was developed based both on a general assessment that events tend to be associated with lower lithostatic pressure values, and on the empirical distribution of pressures at past events (the red line). Because of the small number of data points that comprise the empirical distribution, the distribution was then smoothed. The background distribution of lithostatic pressure across the region of interest represents my assessment of the lithostatic pressure value I would expect at a randomly chosen location where no future event occurs (see Figure D.4-18). Given the large number of data points in this background distribution, I was able to use directly the empirical distribution of lithostatic pressure values across the region of interest.

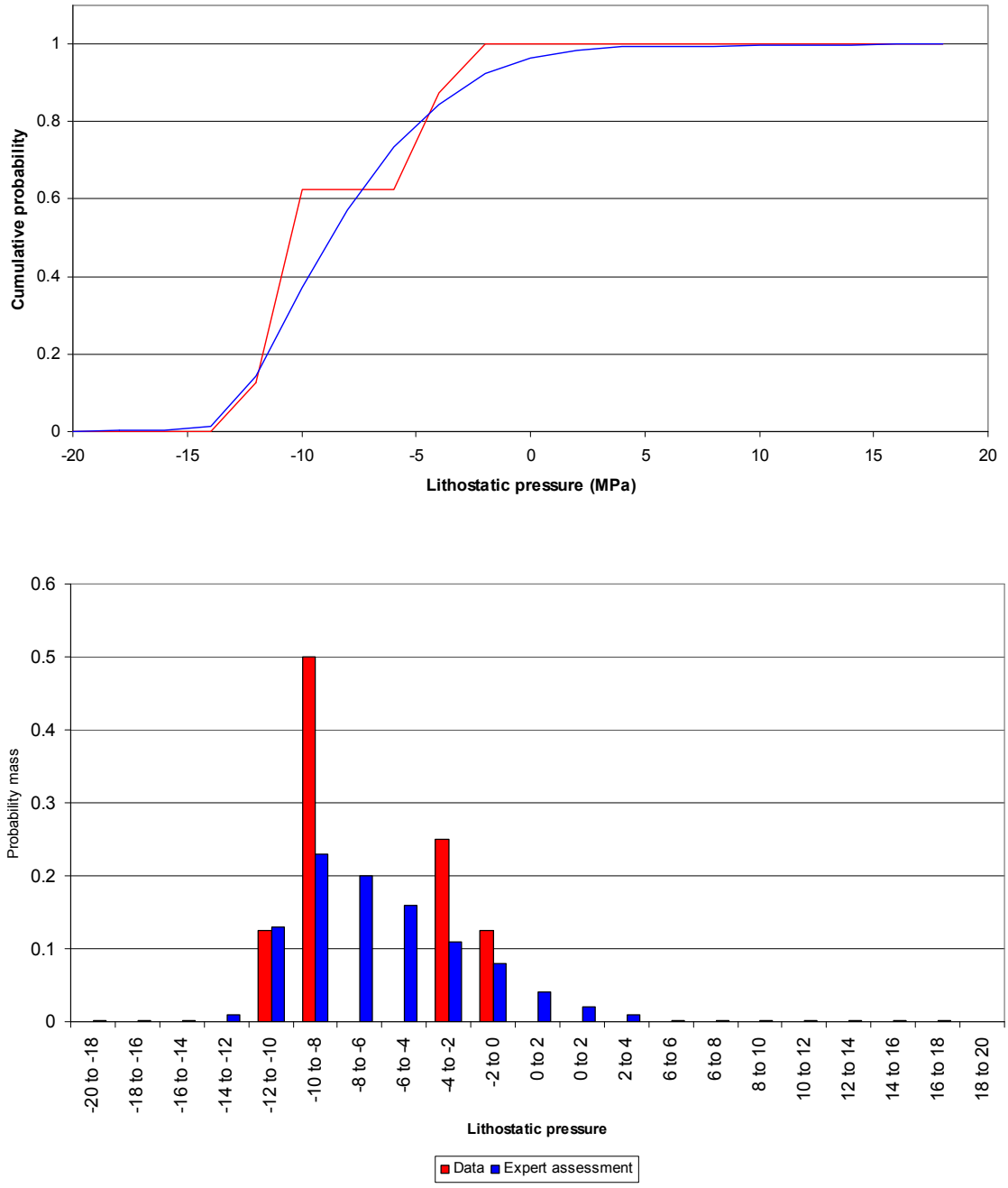

NOTE: The red line/bars represent the empirical distribution of pressure at past events in the region; the blue line/bars represent my assessment of the likely value at a future event.

Figure D.4-17. Assessment of Lithostatic Pressure at a Hypothetical Future Event in Mel Kuntz's Region of Interest

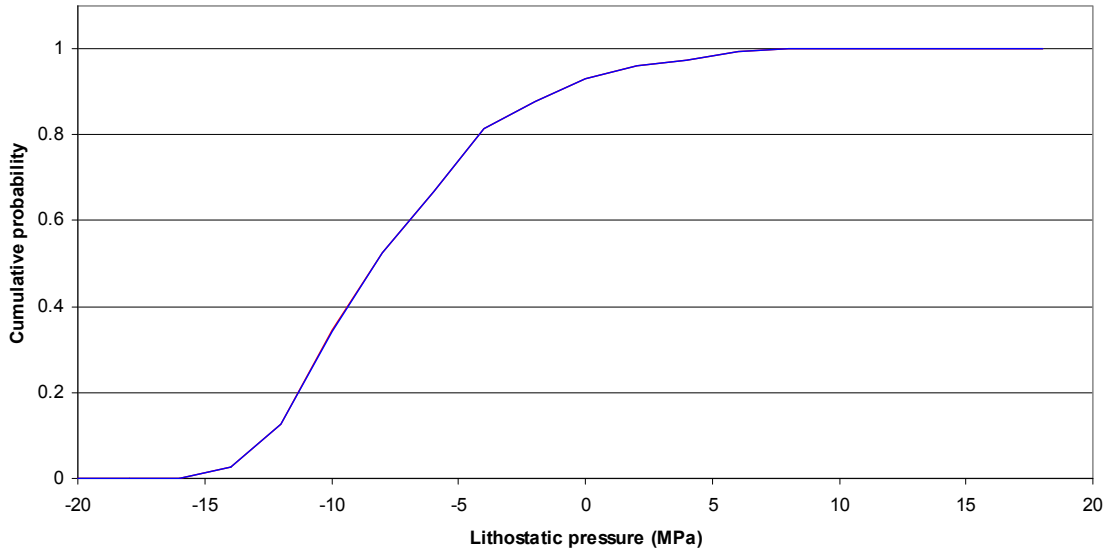

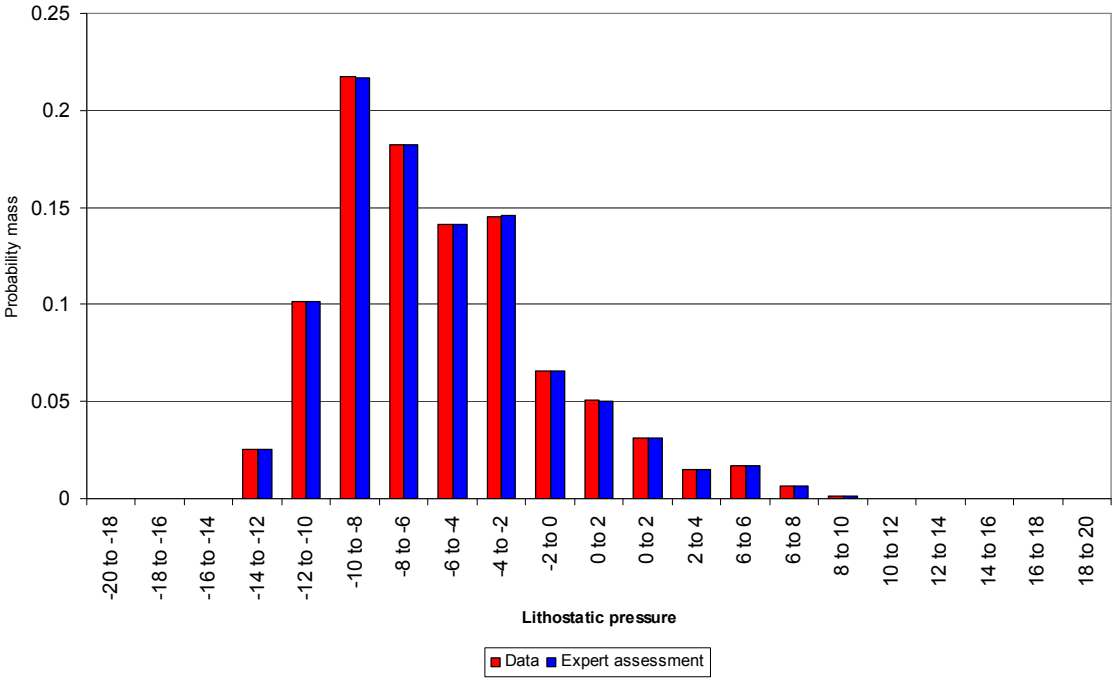

NOTE: Assessment utilizes the background distribution of lithostatic pressure in the region of interest. (Data and expert assessment lines overlie in the top figure, so only one line appears.)

Figure D.4-18. Assessment of Lithostatic Pressure in the Region of Interest at a Random Location Where No Future Event Occurs

Tomographic Data. Data regarding spatial variations in seismic velocity may indicate locations of melting in the mantle and, when combined with data on the structural geology of the surface, may help predict where future events are likely to occur. According to Glen Biasi of the University of Nevada (presentations at PVHA-U Workshops 1 and 2), present-day volcanism is occurring around the margins of Biasi's defined root zone, a zone of high seismic velocity that coincides with Miocene caldera systems. In his assessment of Biasi's data, Gene Humphreys of the University of Oregon suggests that an E-W-trending boundary at approximately the latitude of the repository divides the region into a high-velocity area to the north and a low-velocity area to the south (Humphreys, 2006). Because the low-velocity zone may be indicative of partial melt in the mantle, the area south of the boundary may have a higher probability of future volcanism.

Figures D.4-19 and D.4-20 show how I contoured the Biasi and Humphreys inversions of the tomographic data into regions of higher and lower seismic velocity. I reviewed the distributions of velocities at the locations of past events and at locations without events in my region of interest, as shown below. I conclude that only Humphreys' interpretation gives meaningful information about the likely locations of potential future events, so those are the data I use in my spatial model (Table D.4-3).

Table D.4-3. Two Tomographic Inversions and Event Locations

	Fraction of Events in Low-Velocity Region	Fraction of My Region of Interest in Low-Velocity Region
Humphrey's Inversion	17/18 = 94%	67%
Biasi's Inversion	14/18 = 78%	69%

My assessment is that if a future event were to occur within my region of interest, it more likely would occur in an area of low seismic velocity than in one of high velocity, as characterized by the map in Figure D.4-20. Specifically, I estimate that the probability of a low seismic velocity at the location of a hypothetical future event in my region of interest is 90%.

Both the lithostatic pressure data and tomographic data provide useful information on the likely locations of potential future events. I assign equal weights to both data sets. The spatial model derived from my interpretations of the geologic data sets should be combined with a model based on spatial smoothing, assigning weights of 0.5 to the smoothing model and 0.5 to the interpretation of the geologic data sets.

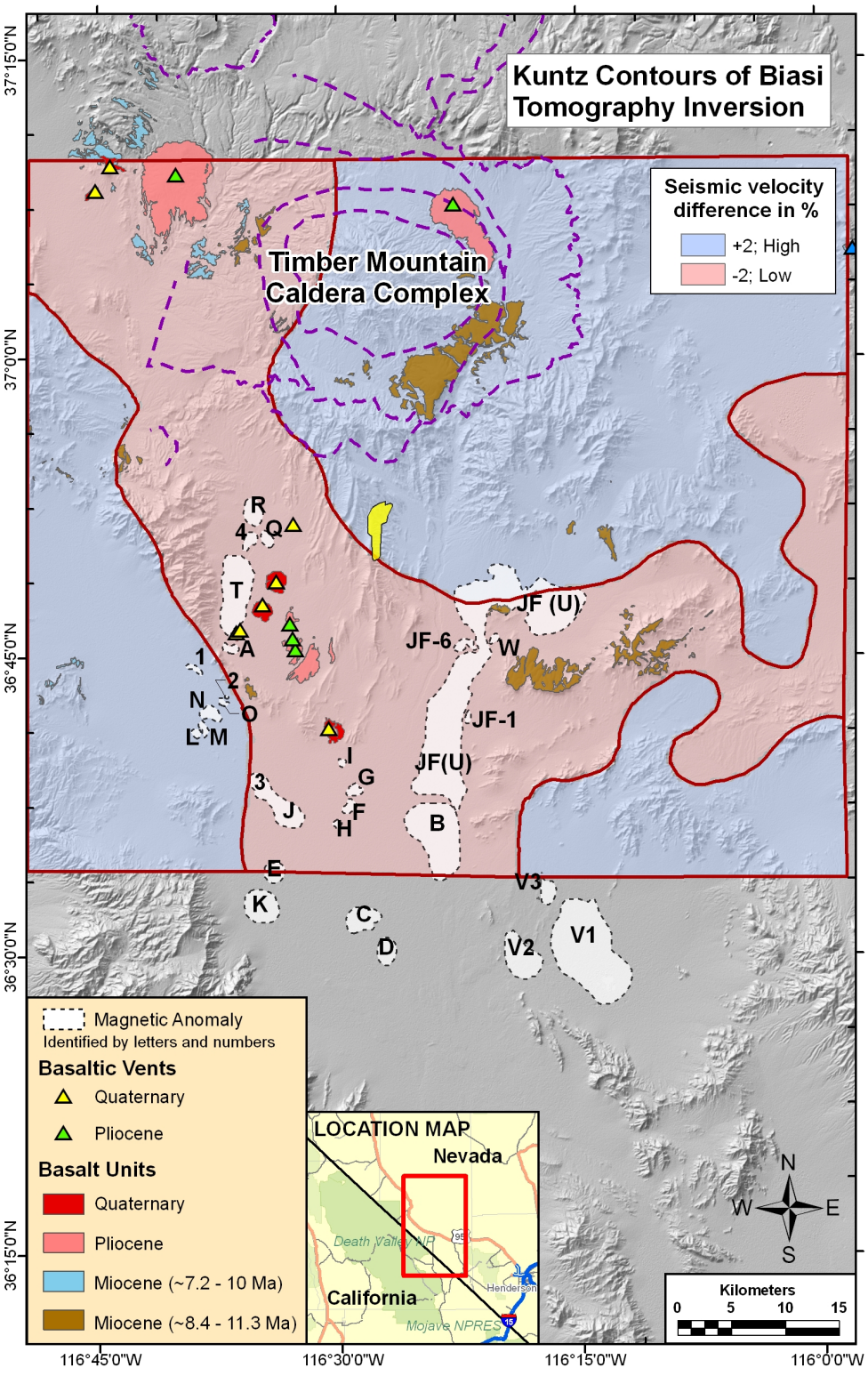

Figure D.4-19. Contouring of Biasi's Inversion of Tomographic Data into Regions of High (blue) and Low (red) Seismic Velocity

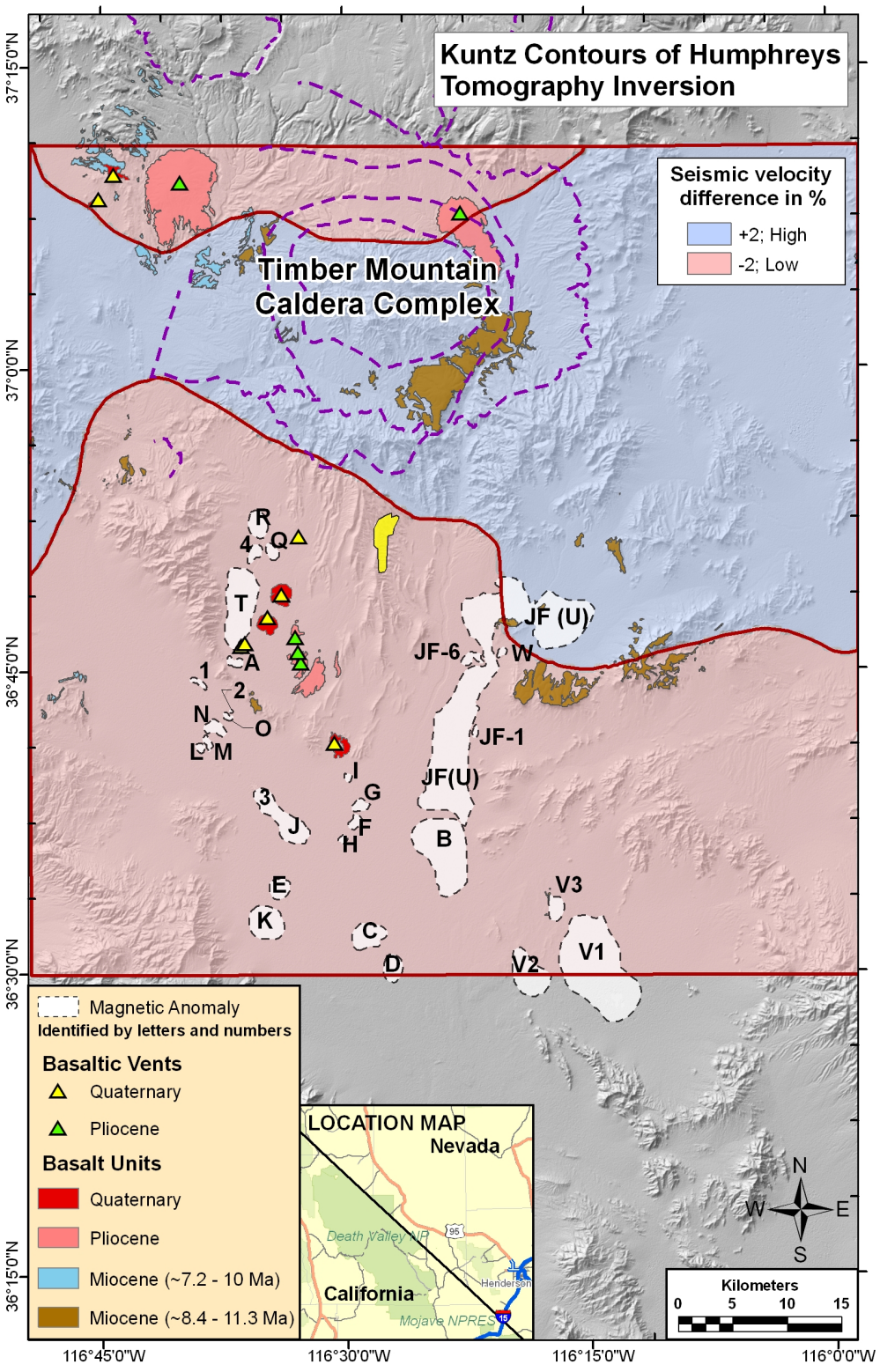

Figure D.4-20. Contouring of Humphreys' Inversion of Tomographic Data into Regions of High (blue) and Low (red) Seismic Velocity

Additional Data Sets. I considered data on extension within my region of interest. Volcanic events should be located within the area of greatest extension (that is, above the subsurface locus of extension), but the cumulative extension maps may not show this. A contour map constructed from cumulative extension data for Crater Flat (per Fridrich et al., 1999) indicates that post-4-Ma centers lie within regions that show more than 45-percent extension, although areas that show less extension reveal the presence of older events, such as the Solitario Canyon dike. Because of the limited spatial extent of the Fridrich et al. map, I do not use crustal extension data directly to modify my spatial intensity map.

D.4.3 TEMPORAL MODEL

I use two approaches to describe the temporal distribution of potential future events. For the 10-ky assessment, my rate estimates are based on post-4-Ma events only. For the 1-My assessment, I consider rates based both on post-4-Ma events (weight of 80%) and on post-11-Ma events (weight of 20%)

The first approach assumes a homogenous Poisson process in which recurrence rates within each zone are estimated based on past events in that zone. For the zone-based spatial model, this temporal model is weighted 100%. For the spatial smoothing model, I also consider use of a time-volume model, which incorporates the reduction in event volumes over time, to estimate the recurrence rate in the region of interest (described below). For that spatial model, I weight the homogenous Poisson temporal model 60% and the time-volume model 40%.

This second approach, the time-volume model, considers changes in cumulative volume and volume per event over time. Table D.4-1 provides my estimates of volumes associated with events in the region of interest. I use several approaches to assess the relationship between volume and time:

1. Figure D.4-21 shows the cumulative volume over time for the event set I consider most likely, along with the fit of three alternative models to that data. The three models incorporate (a) cumulative volume as a linear function of time, fit to the 2.87-Ma and later events; (b) cumulative volume as a function of the log of time, fit to post-4-Ma events; and (c) cumulative volume as a function of the square root of time, fit to post-4-Ma events. For the rate estimate I assign weights of 0.3, 0.45, and 0. 25 to models (a), (b), and (c), respectively.

2. Similar models were fit to the post-11-Ma events. For the rate estimate based on those events, I weight the log-time model 0.70 and the linear model 0.30.

3. Finally, the time-volume model requires an estimate of the volume per event for potential future events. After considering several forms to represent volume per event as a function of time, I decided that none of the available models is a good predictor of future event volumes as a function of time. Because I believe that the volume of future events will most resemble the volume of Quaternary events in my region of interest, I use those volumes as the basis for estimating volume per potential future event.

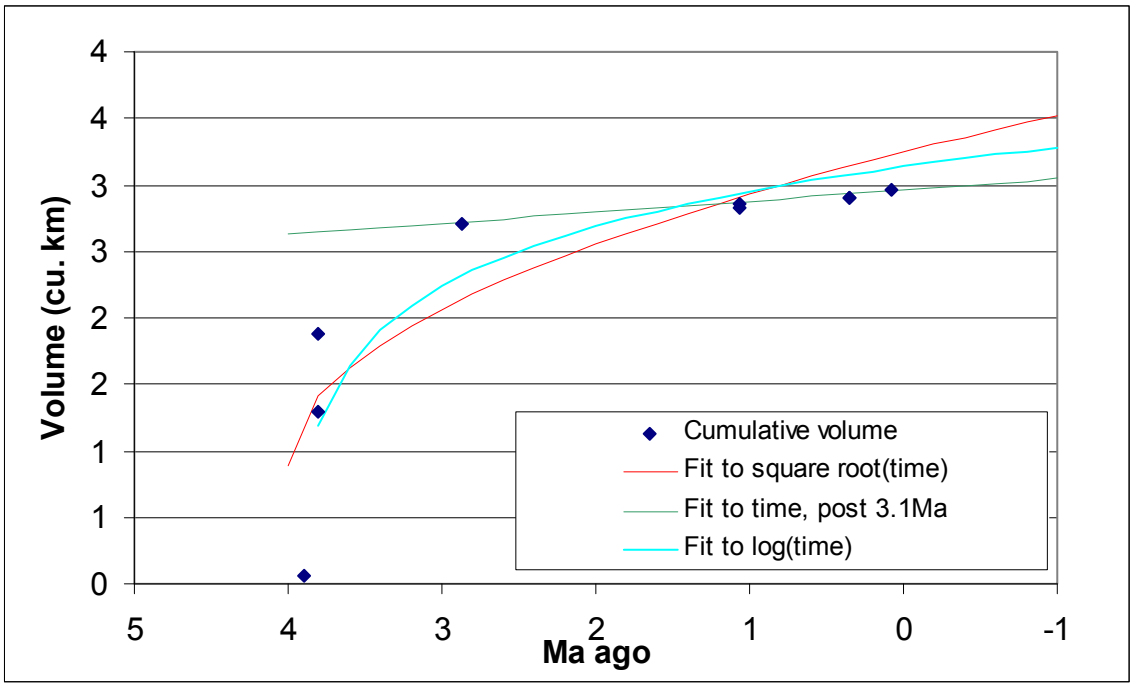

NOTE: Also shown are alternative models fit to that data

Figure D.4-21. Cumulative Volume of Post-4-Ma Events in Mel Kuntz's Region of Interest for His Most Likely Event Set

The time-volume approach provides a good estimate of potential future volcanism for the 10-ky and 1-My time periods, based on the long-term history of volcanism in the YMR. Because there is no evidence for episodic or rapid changes in tectonic rate, I envision no change that would affect the rate at which magma is generated during the next 1 My.

D.4.4 REFERENCES

Bechtel SAIC Company (BSC), 2003, Analysis and modeling report—future climate analysis 10,000 years to 1,000,000 years after present: MOD 01 001 Rev 01; MOL 20030407.0055.

Cogbill, A.H., 2006, Detectability of basaltic dikes using the 2004 Yucca Mountain aeromagnetic survey: Memorandum to the PVHA-U expert panel, 11 p.

Connor, C.B., Stamatakos, J., Ferrill, D., Hill, B.E., Ofoegbu, G., and Conway, F.M., 2000, Volcanic hazards at the proposed Yucca Mountain, Nevada, high-level radioactive waste repository: Journal of Geophysical Research, vol.105, p. 417-432.

Day, W.C., Potter, C.J., Sweetkind, D.S., Dickerson, R.P., and San Juan, C.A., 1998, Bedrock geologic map of the central block area, Yucca Mountain, Nevada: U.S. Geological Survey Miscellaneous Investigations Series Map I-2601, scale 1:6,000.

Fridrich, C.J., Whitney, J.W., Hudson, M.R., and Crowe, B.M., 1999, Space-time patterns of late Cenozoic extension, vertical axis rotation, and volcanism in the Crater Flat basin, southwest Nevada, in Wright, L.A., and Troxel, B.W. (eds.), Cenozoic Basins of the Death Valley Region: Boulder, Colorado, Geological Society of America Special Paper 333.

Humphries, E., 2006, Assessment of Glenn Biasi's P-wave tomography of the upper mantle beneath the NTS Region: White Paper Provided to PVHA-U Expert Panel, July 2006, 8 p.

Keating, G.N., Valentine, G.A., Krier, D.J., and Perry, F.V., 2008, Shallow plumbing systems for small-volume basaltic volcanoes: Bulletin of Volcanology, v. 70, pp. 563-582, DOI 10.1007/s00445-007-0154-1.

Kuntz, M.A., Anderson, S.R., Champion, D.E., Lanphere, M.A., and Grunwald, D.J., 2002, Tension cracks, eruptive fissures, dikes, and faults related to late Pleistocene-Holocene basaltic volcanism and implications for the distribution of hydraulic conductivity in the eastern Snake River Plain, Idaho: Geological Society of America Special Paper 353, p. 111-133.

Los Alamos National Laboratory (LANL), 2007, Ar/Ar age determinations, volume, location, and elevation of Plio/Pleistocene volcanoes in the Yucca Mountain region, Rev. 3: Excel spreadsheet titled Volcano_volume_age_location_Rev03.xls.

Parsons, T., Thompson, G.A., and Cogbill, A.H., 2006, Earthquake and volcano clustering via stress transfer at Yucca Mountain, Nevada: Geology, v. 34, no. 9, p. 785-788, September.

Slate, J.L., Berry, M. E., Rowley, P. D. and others, 1999, Digital geologic map of the Nevada Test Site and vicinity, Nye, Lincoln, and Clark counties, Nevada, and Inyo County, California: U.S. Geological Survey Open-File Report 99-554A.

Valentine, G.A., and Keating, G.N., 2007, Eruptive styles and inferences about plumbing systems at Hidden Cone and Little Black Peak scoria cone volcanoes (Nevada, USA): Bulletin of Volcanology, vol. 70, p. 105– 113, DOI 10.1007/s00445-007-0123-8.

Valentine, G.A., and Krogh, K.E.C., 2006, Emplacement of shallow dikes and sills beneath a small basaltic volcanic center—the role of pre-existing structure (Paiute Ridge, southern Nevada, USA): Earth and Planetary Science Letters, v. 246, p. 217-230.

Valentine, G.A., Krier, D.J., Perry, F.V., and Heiken, G., 2007, Eruptive and geomorphic processes at the Lathrop Wells scoria cone volcano: Journal of Volcanology and Geothermal Research, v. 161, p. 57-80.

Valentine, G.A., Perry, F.V., Krier, D., Keating, G.N., Kelley, R.E., and Cogbill, A.H., 2006, Small-volume basaltic volcanoes—eruptive products and processes and post-eruptive geomorphic evolution in Crater Flat (Pleistocene), southern Nevada: Geological Society of America Bulletin, v. 118, p. 1313-1330.

D.5 ALEXANDER R. MCBIRNEY'S ELICITATION SUMMARY FOR PVHA-U PROJECT

Two types of igneous events are identified as having the potential to disrupt the Yucca Mountain radioactive waste repository: an igneous intrusion into the repository (which could be either a dike or a sill), or an eruption through the repository. The probability that either type of event would disrupt the repository is a function of the spatial and temporal distribution of volcanism in the area and the physical geometry of each type of igneous event. These factors, and the relationships among them, are illustrated in Figure D.5-1. Models and preliminary assessments of the geometry of dikes, dike systems, and conduits are summarized in Section D.5.1, followed by models and preliminary assessments of the spatial and temporal distributions of igneous events.

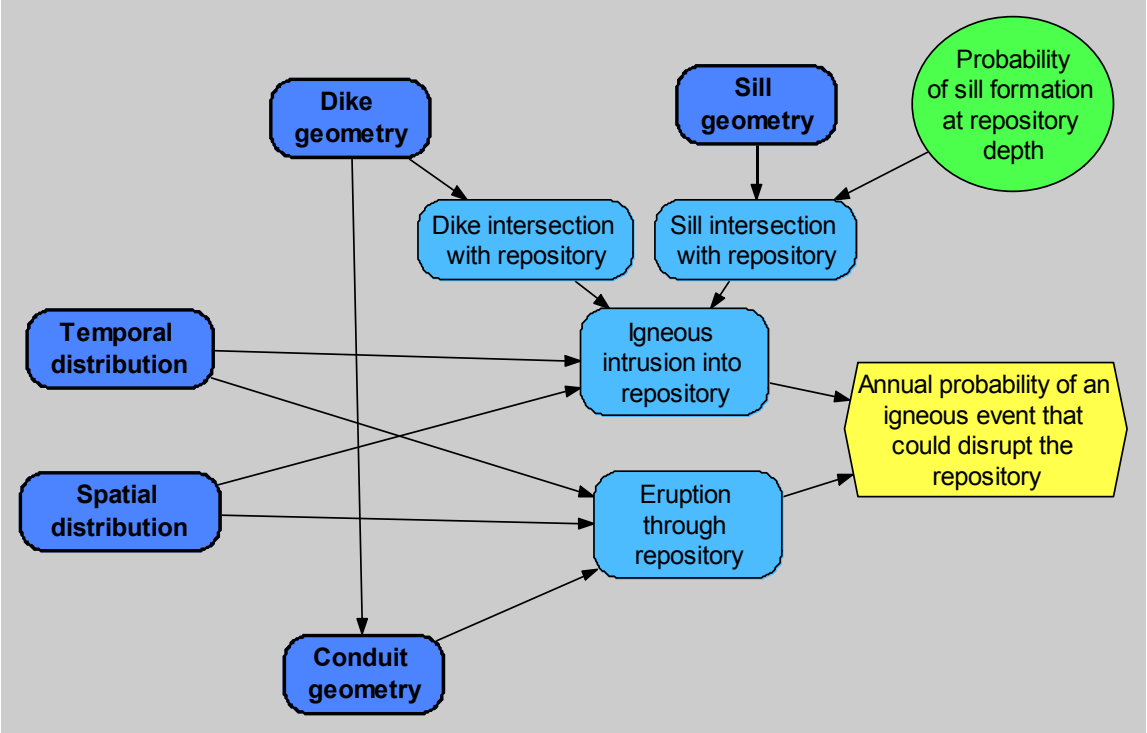

NOTE: The yellow hexagon represents the final result of the assessment. Green ovals represent assessed variables; dark blue rounded rectangles represent sub-models; light blue nodes represent values calculated from other inputs; and arrows indicate influences of one variable on one or more others.

Figure D.5-1. Overall Structure of Model

D.5.1 EVENT DEFINITION

What constitutes an event depends on the size of the volcanic center that creates it. A single event at Mt. Hood, for example, could be a series of closely spaced eruptions lasting for a few weeks to as long as 1,000 years depending on the purpose of the analysis. The small events typical of the Yucca Mountain region (YMR; defined as the region within a radius of about 50 km centered on Yucca Mountain) involve temporally distinct batches of magma that are erupted or intruded during brief periods and that are relatively small in volume. The data show a

clear decrease in the volumes of eruptions at the YMR from the Miocene to the Quaternary. My assessments therefore discount observations of Miocene volcanism, except when considering the influence that Miocene structures could have on more recent events. Volcanism in the future is likely to be related to changes in mantle temperatures or pressures and their effects on zones of partial melting. Stress changes due to extension are the most likely triggering mechanism for volcanic activity in the region. In all my assessments, an igneous event is one that ascends to the shallow depths of the repository (~300 m) or less.

D.5.1.1 Characterization of Past Events

Given my definition of an event, I have assessed the number, volumes, and ages of past events that are relevant to my spatial and temporal models. Tables D.5-1 and D.5-2 list the events in my region of interest: Table D.5-1 lists events in my Crater Flat zone and Table D.5-2 lists events in my background zone. These two zones are described below in Section D.5.2. Uncertainties in the number of events or whether an aeromagnetic anomaly represents an event are expressed in the table.

Table D.5-1. Relevant Events in the Region of Interest: Crater Flat Zone

Past Event	Number of Cones or Vents	Age* (Ma)	Number of Events	Volume* (km^3)
Lathrop Wells	1	0.08	1	0.048
Makani Cone	1	1.07	1	0.002
Black Cone	1	1.07	1	0.06
Red Cone	1	1.07	1	0.055
Little Cones NE	1	1.07	1	0.014
Little Cones SW	1	1.07	1	0.02
Anomaly G	1	3.9	1 (0.25), 2 (0.33), or 3 (0.42) based on relative weights of 3, 4, and 5	0.028
Anomaly F	1			0.029
Anomaly H	1			0.006
Pliocene Crater Flat	3	3.8	3	Total volume is 0.585
Anomaly B	1	3.85	1	1.227
Anomaly C	1	Between 3.8 and 5.8	40% chance anomaly is young enough to be included as a relevant event	0.117
Anomaly D	1		40% chance anomaly is young enough to be included as a relevant event	0.073
Anomaly E	1	Unknown	30% chance anomaly is basalt and young enough to be included	Unknown
Anomaly K	1	Unknown	30% chance anomaly is basalt and young enough to be included	Unknown

* Age and volume estimates are based on consideration of Los Alamos National Laboratory (LANL) (2007).

Table D.5-2. Relevant Volcanic Events in the Region of Interest: Background Zone

Location	Age* (Ma)	Number of Events
Sleeping Butte: Hidden Cone	0.35*	1
Sleeping Butte: Little Black Peak	0.35*	1
Buckboard Mesa	2.9*	1
Thirsty Mountain	4.6*	1
Clayton Valley Cone	0.39**	1

* Age based on consideration of LANL (2007).
** Age based on Wood and Kienle (1990).

Younger events are more relevant to predicting future events than are older events. I consider events older than Thirsty Mountain (4.6 Ma) to be part of a prior period of volcanism and thus irrelevant to the current rate or to estimates of future rates. There is uncertainty about the ages of both Anomalies C and D. Based on the range of ages considered possible for Anomalies C and D, I assign a weight of 0.4 to those events being relevant to current and future volcanism.

Similarly, there is uncertainty about whether Anomalies E and K are basalt and, if so, their ages. I assign a weight of 0.3 to the possibility that each anomaly is basalt and young enough to be relevant to the event counts.

D.5.1.2 Event Characteristics and Geometry

The following sections describe my assessments of the characteristics of possible future events in the YMR. The features of potential dikes, sills, and conduits are discussed, along with additional considerations.

Dike Geometry

As shown in Figure D.5-2, dike geometry is defined by several components: length, width, and azimuth of each dike and the number, pattern, and spacing of dikes in a dike system. I have assessed all these variables as appropriate for repository depth (~300 m). The length, width, and spacing of dikes reflect the extensional strain across a zone of transverse shear and are functions of the magnitude of this strain and the physical properties of the rocks.

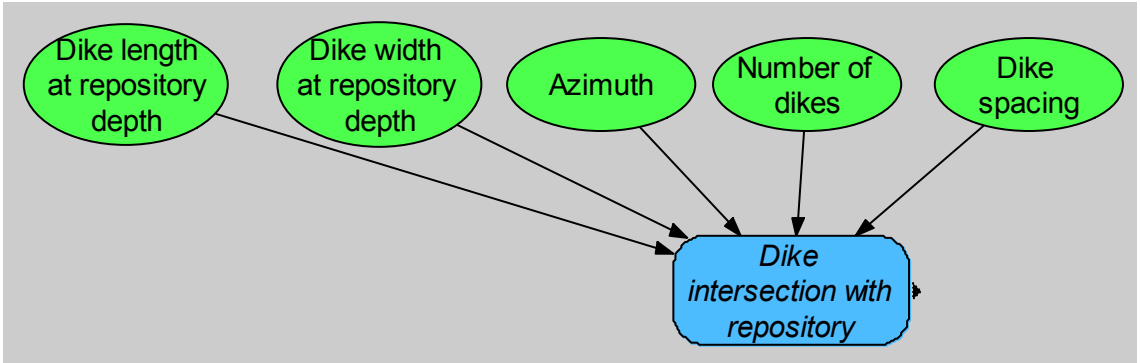

Figure D.5-2. Components of the Model for Dike System Geometry of Dike Systems

Dike Length. My assessment of the lengths of potential dikes at repository depth is based on the lengths of dikes observed in the geologic record for analog events. Based on data from an analog table developed by investigators at Los Alamos National Laboratory (LANL) for the PVHA-U (published as Keating et al., 2008), dikes as long as 5 km have been measured in the region. My estimates are based on observations at volcanic fields around the margin of the Colorado Plateau (including a field near Mt. Taylor, which is similar to, although larger than, the YMR). I have observed similar relations in mines and deeply eroded terrains of high relief where one can see the three-dimensional forms of such intrusions.

Five km is about the maximum dike length expected in the YMR; I estimate that 95% of potential future dikes would be shorter than 5 km. The most likely dike length is 1 km; the minimum expected length is 200 m (95% of dikes would be longer). Figure D.5-3 illustrates this assessment.

Dike Width. The lower limit of dike width, which is determined primarily by the rate of heat loss and the physical properties of the rocks and magma, is about 0.1 m.

The maximum width of potential future dikes is 2 m, with the most likely width being 0.5 m, based on observations at eroded analog volcanic fields and considering the depth of the repository. Figure D.5-4 illustrates this assessment.

Dike Azimuth. The azimuths of potential future dikes would reflect the orientation of pre-existing fractures (faults and joints) in the region, because dikes tend to propagate along structural features in the near surface. Modeling by Itasca (2006) supports this conclusion.

The most likely azimuth of potential future dikes is north-south. At least half of future dikes would occur within the azimuth range of N20°E to N20°W; 90% would occur within the range of N30°E to N30°W. Figure D.5-5 illustrates this assessment.

Multiple Dikes. Although only one dike is likely to be found at depth, shorter, sub-parallel dikes can diverge from that dike in the shallow subsurface (below the depth of the repository). Because I believe that most multiple dikes at shallow depth join at greater depth, the maximum length of a dike system is the same as the maximum length of any individual dike (see dike length distribution given above). If a dike occurs in multiple segments, the lengths of the segments can vary greatly.

A dike that formed at the depth of the repository most likely would be a single, continuous dike. A single dike at the repository horizon is as likely as more than one. The probability of three dikes is about half the probability of two, and so on. Ten is the maximum number of dikes that could develop. Based on these assessed values, I have assessed the number of dikes in a potential future event, as given below.

Table D.5-3. Number of Dike Segments in an Event

Number of Dikes in an Event	1	2	3	4	5	6	7	8	9	10
Relative Probability	0.5	0.25	0.125	0.063	0.031	0.016	0.008	0.004	0.002	0.001

Perpendicular spacing between dikes most likely would be about 50 to 100 m. Dikes would not be closer together than 10 m or farther apart than 1,000 m (99th percentile). The distribution based on these assessed values is shown in Figure D.5-6.

A set of multiple dikes is most likely to be arranged in an en echelon manner. Based on the observed alignments of Anomalies G, F, and H and other en echelon dike systems, the maximum overlap between dike segments would be about 20 percent of the dike length, and the minimum would be no overlap between segments. The offsets of en echelon dikes in the YMR typically are toward the right, because they result from a right-lateral regional stress field, and there is no apparent condition that would lead to the opposite offset.

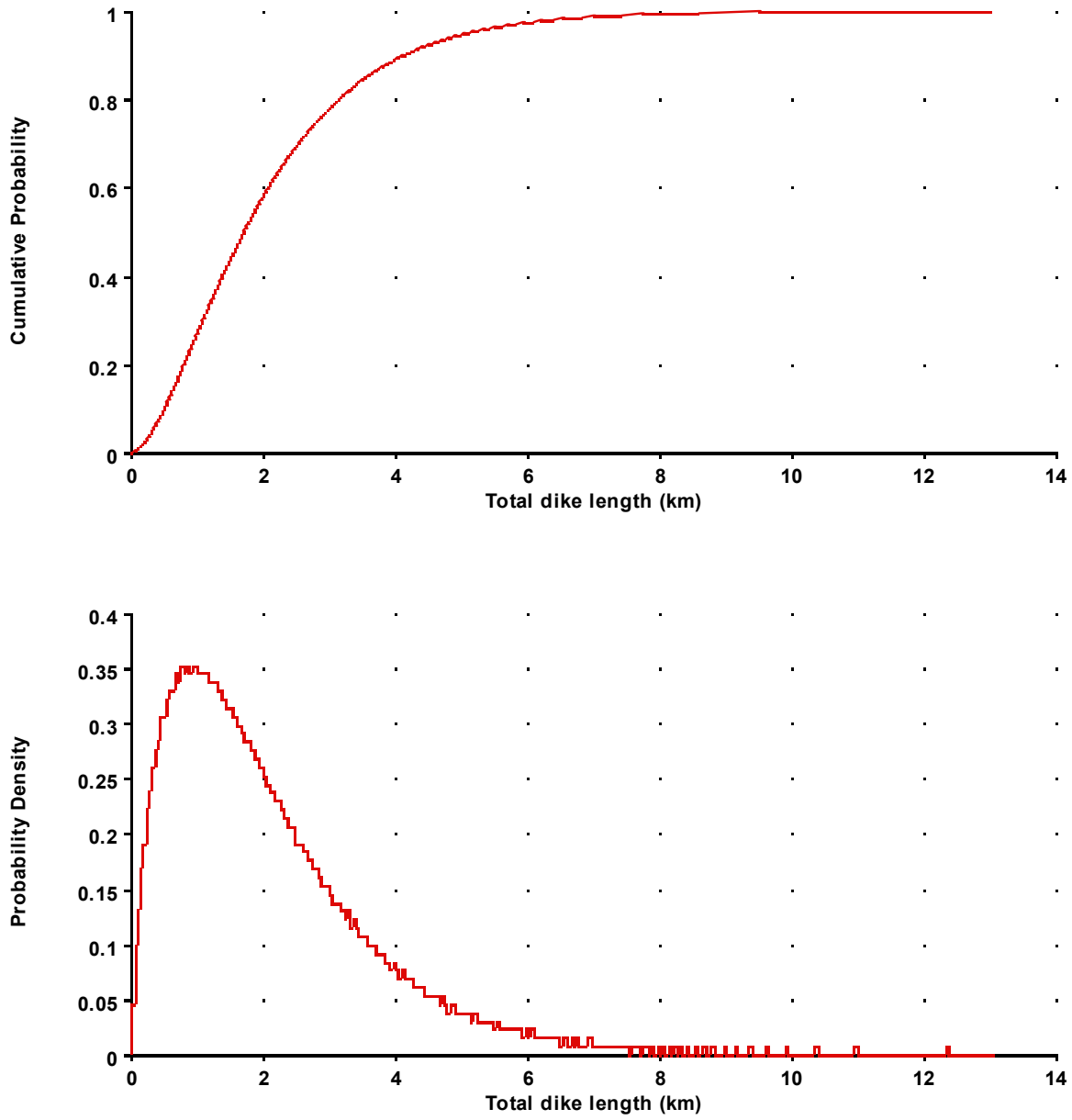

NOTE: The top graph is a cumulative distribution function; the bottom graph is a probability density function.

Figure D.5-3. Assessment of Total Dike Length

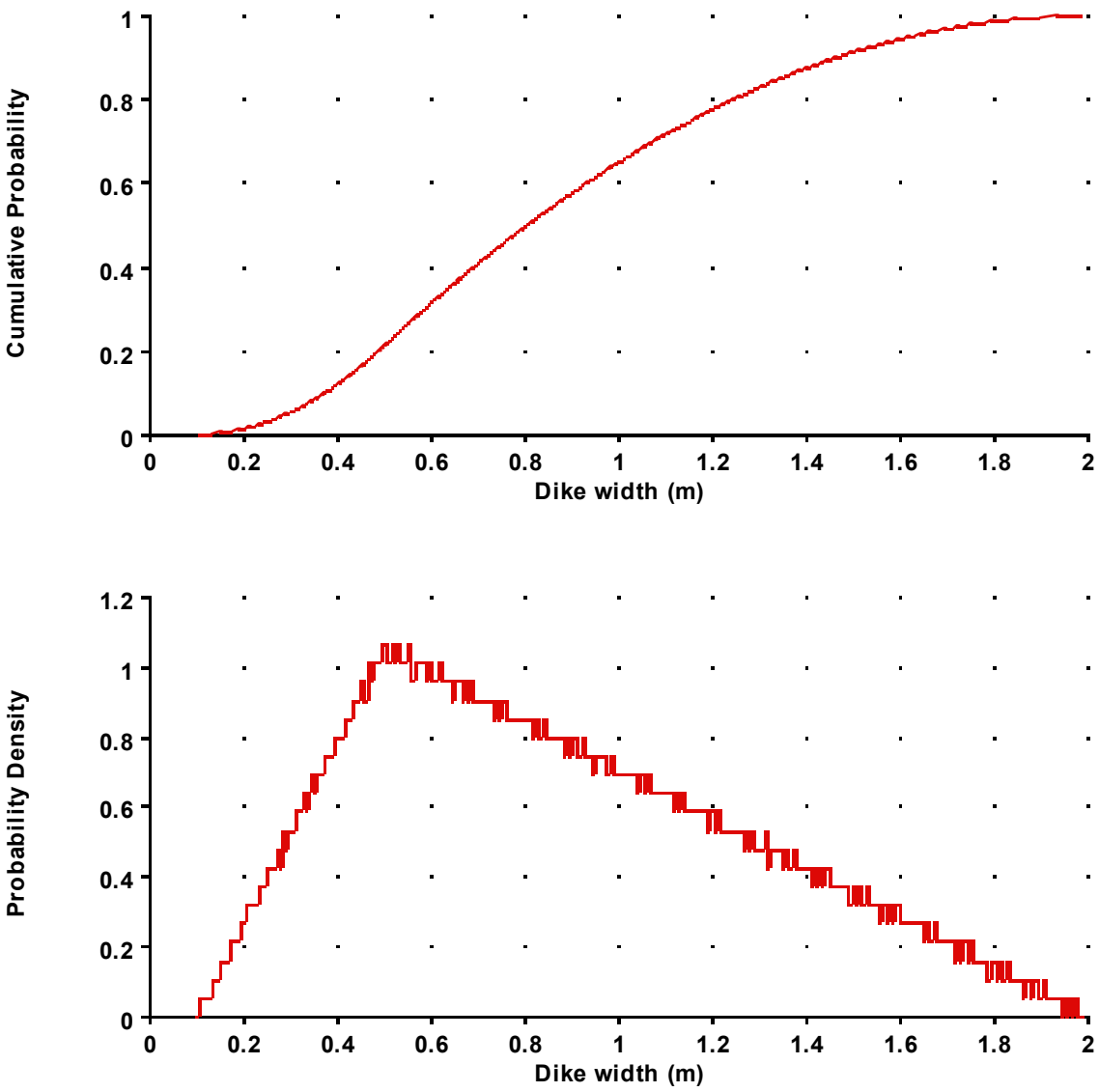

Figure D.5-4. Assessment of Dike Width

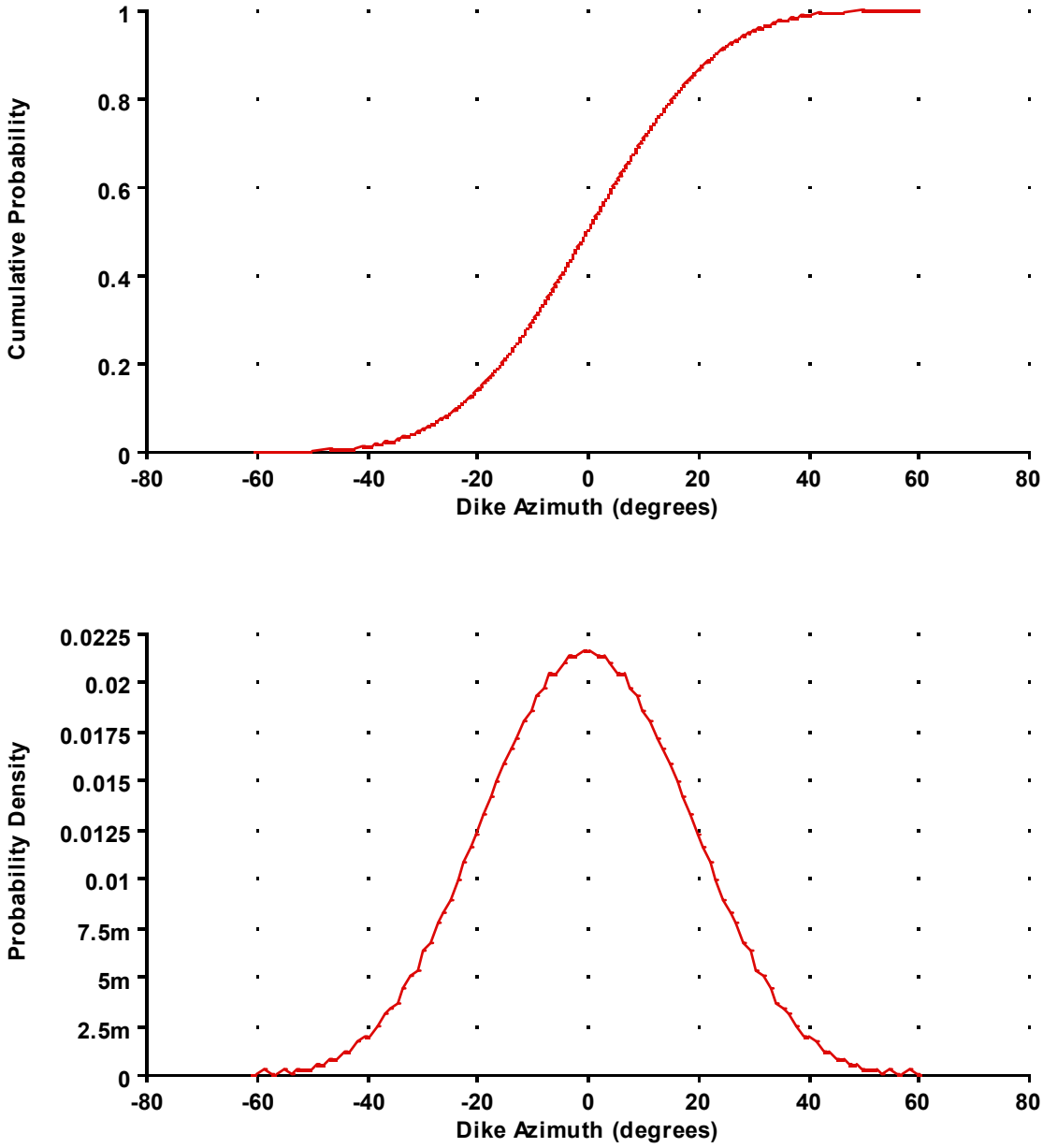

NOTE: Zero represents north. For values less than 0.01 on the y-axis, suffix notation is used (m = 10^{-3} and u = 10^{-6}, so 5m = 0.005).

Figure D.5-5. Assessment of Dike Azimuth

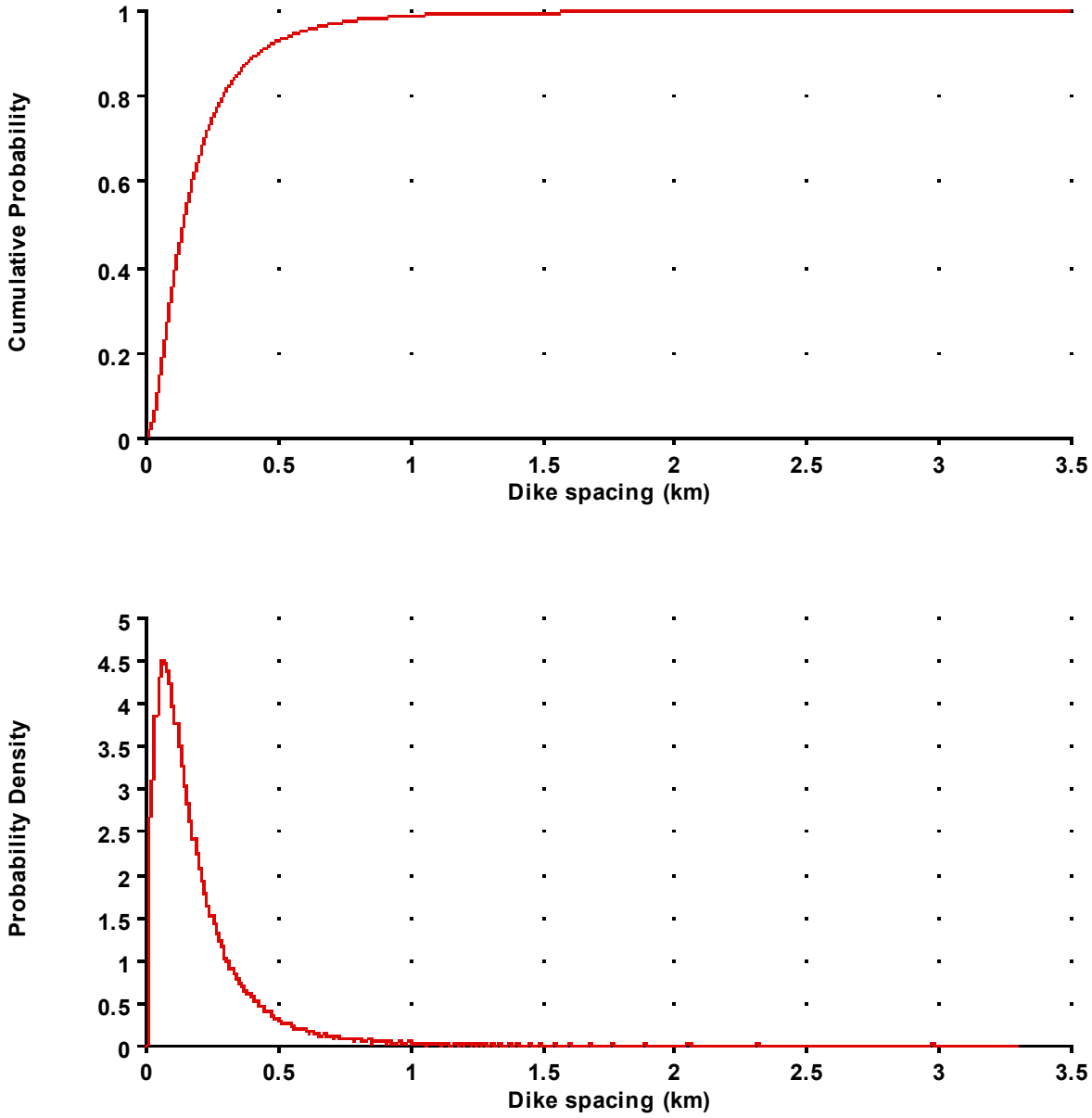

Figure D.5-6. Assessment of the Perpendicular Spacing between Dike Segments

Sill Geometry

A sill presents a mirror image of the surface topography. Thus, a dike crossing Yucca Mountain would propagate sills more deeply beneath higher elevations than beneath valleys. Because the repository lies below the elevation of Crater Flat, sills could form at repository depth. Observations of past events in the region suggest that any sill would be relatively small. If a sill were to intersect a drift, it likely would terminate there, so extension into an adjacent drift would be unlikely. Figure D.5-7 illustrates the factors that define sill geometry.

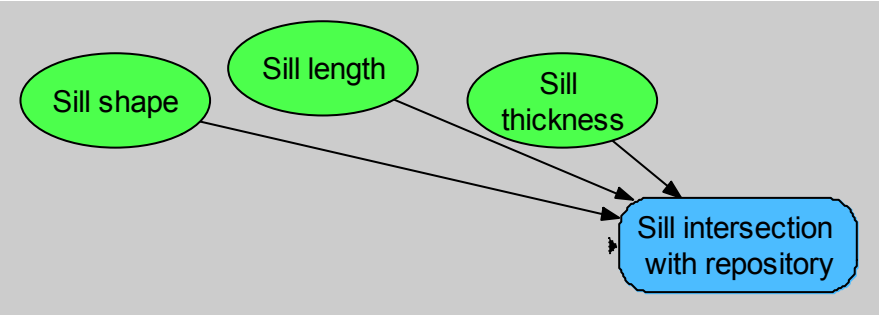

Figure D.5-7. Components of the Model for Sill Geometry

In estimating the likelihood of a sill developing, much depends on the structure of the surrounding rocks, especially whether there are horizontal discontinuities such as bedding planes. The vertical stress at the relatively shallow depth of the repository will be quite low. This low level of stress would make it easy for magma to be injected laterally, but the hydrostatic head on the magma and hence the driving force also would be low. In fact, if a dike were to intersect a repository drift, that force would be essentially zero. So if a dike intersected an open space, the probability of a sill forming would be zero; if not, the probability of a sill forming could be as high as 10%.

If a sill were intruded, its location on a dike and its dimensions would depend primarily on the local stress field and the structure of the rock. In general, a sill tends to be centered on a dike, but can occur anywhere along the length of the dike. Generally a sill will not extend much beyond the length of a dike. Sills tend to be elongated in the same direction as the host dike, and will be approximately almond-shaped. For the purposes of modeling a potential sill, a value of about 2:1 is reasonable for the length-to-width ratio of a sill, although considerable variability exists in this ratio. For the small volumes that would be characteristic of future events in the YMR, the maximum length of a sill would be about 1 km and the most likely length is 500 m long. Figure D.5-8 illustrates my assessment of sill length.

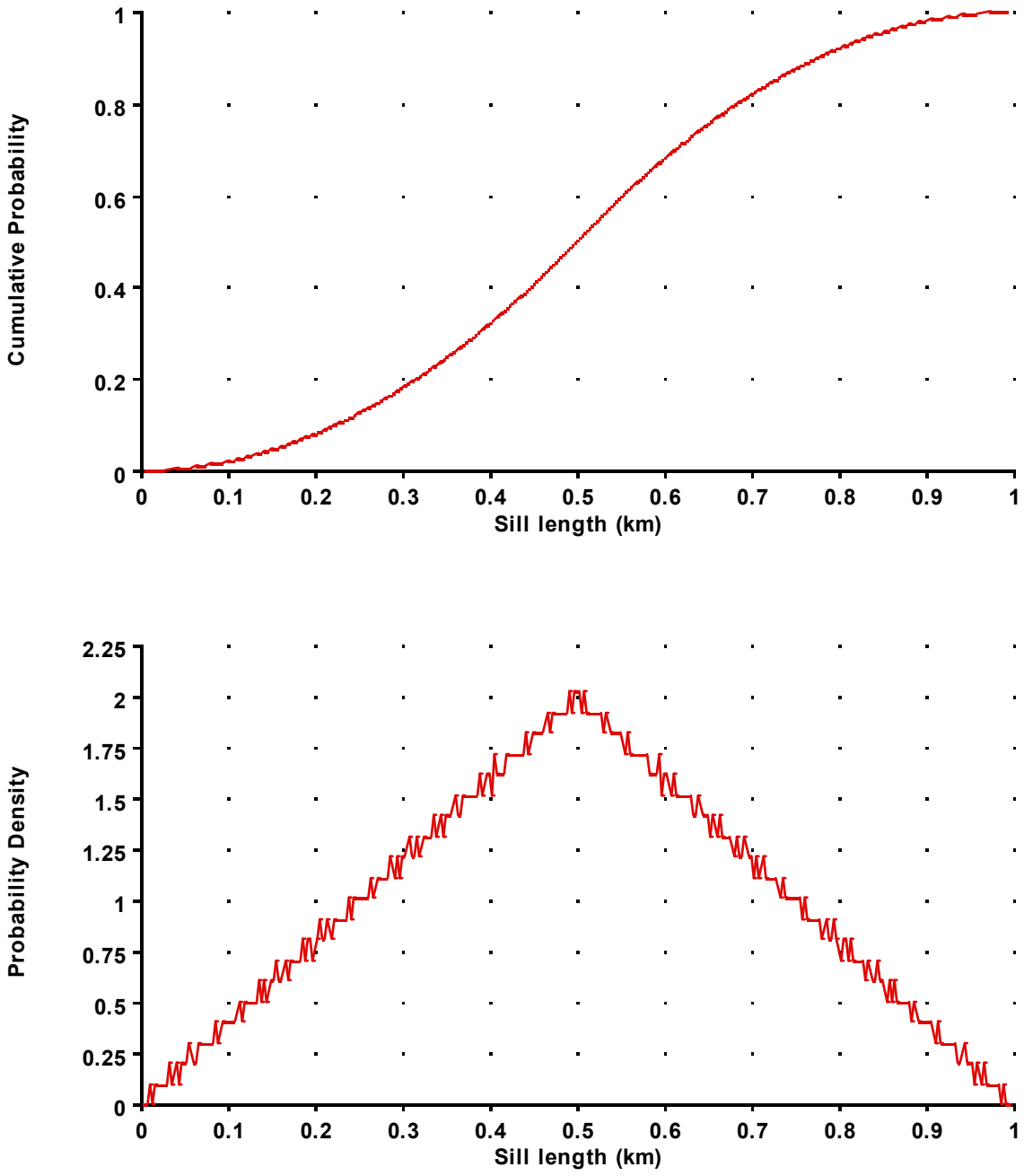

Figure D.5-8. Assessment of the Length of a Sill

Conduit Formation and Geometry

Conduit geometry is defined by the diameter of a conduit and the number and locations of conduits on a dike or within a dike system, as shown in Figure D.5-9. Each of these variables is assessed below.

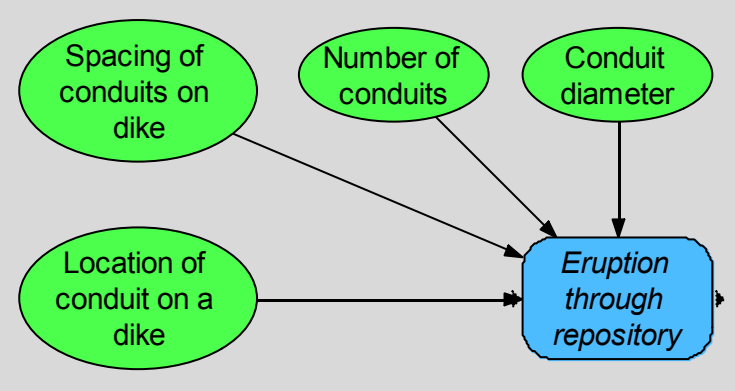

Figure D.5-9. Components of the Model for Conduit Geometry

Conduit Diameter. Conduits typically are rooted in dikes. A conduit at repository depth would be expected to resemble most conduits. At depth, conduits tend to have elliptical shapes and be smaller than near the surface, where they are larger and more cylindrical. Cylindrical conduits propagating from great depths have been observed in only a few localities, such as in deep diamond mines. Assuming that no high water table develops beneath Yucca Mountain, no deep cylindrical conduit would form. Instead, conduits would form from dikes that reach repository depth or higher. The greater the magma flow in a dike, the larger the conduit that would develop. My assessment considers dimensions of analog conduits measured in the YMR. The diameters measured at East Basalt Ridge seem too large for a future event in the Yucca Mountain area.

At the time it was first formed, a conduit would not exceed about 1 m in diameter (or the dike width). The diameter could be as great as 10 m at the ground surface. At repository depth, the most likely diameter would be 4 to 5 m. There is a 95% probability that the final diameter would be 10 m or less, while the narrowest a conduit could be is the width of the dike. Figure D.5-10 illustrates this assessment.

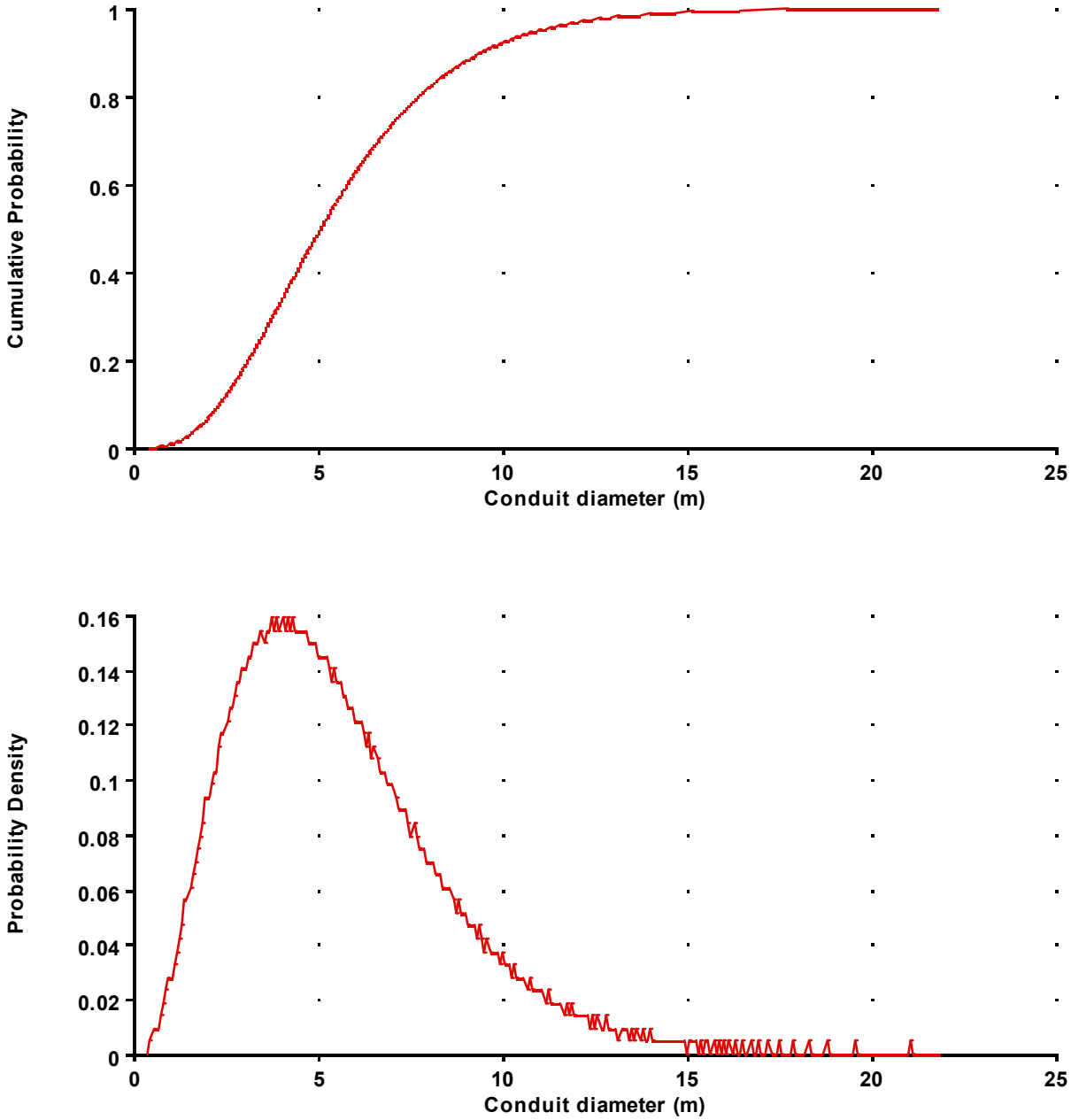

Figure D.5-10. Assessment of the Diameter of a Conduit at Repository Depth

Number of Conduits. The number of conduits on a dike or dike system is related to the length of the dike system and the spacing of conduits along it, both of which are functions of the rate and volume of magma flow. In Hawaii, for example, small vents develop early in an eruption and then close when one conduit becomes the focus for the eruption. Initially, conduits at Hawaiian volcanoes typically are on the order of tens of meters apart. With time and continued magma flow, the spacing between conduits increases to about one conduit per kilometer. Minimum final spacing of multiple conduits on a dike is 500 m; maximum spacing is 1 km.

The most likely number of conduits on any dike is about one per kilometer of dike length, but there can be as many as one conduit per 500 m of dike length. If a dike is 1 km long, for example, one conduit is most likely (75%), but two or three conduits are possible (10%). If a dike is 2 km long, the most likely number of conduits is three, with decreasing likelihoods of two or four conduits, and even lower likelihoods of a single or five conduits. If a dike is 5 km long, the most likely number of conduits is five, but there may be fewer or as many as 11, with decreasing probability as the number increases or decreases. A 5-km-long dike is likely to have more rather than fewer than five conduits. Table D.5-4 below reflects my assessment of the probable number of conduits associated with events of various total dike lengths. This assessment can be interpolated or extrapolated as necessary for an assessment of the number of conduits associated with an event of any length.

Table D.5-4. Number of Conduits as a Function of Total Dike Length

Number of Conduits	Total Dike Length				
	0.5 km	1 km	2 km	3 km	5 km
1	1	0.7	0.15	0.08	0.02
2		0.25	0.5	0.15	0.04
3		0.05	0.2	0.42	0.08
4			0.1	0.2	0.16
5			0.05	0.1	0.26
6				0.05	0.23
7				0.01	0.11
8					0.06
9					0.03
10					0.01
11					0.01

Conduits tend to develop where there are large volumes of magma flowing through the fissure, so if an event involves multiple dikes, conduits are more likely to develop on wider rather than narrower segments of dikes. If there also are multiple conduits, they are more likely to be distributed among dike segments than clustered on a single dike segment.

The most likely location of a conduit is the center of a dike segment, although the distribution of fractures in the bedrock surrounding the dike can affect location. Conduits are commonly located at the intersection of fractures, and if the dike terminates at a cross-fracture, then a conduit could be located at the very end. Based on observed conduits at the ends of dikes at Paiute Ridge and near Boulder Dam, the distribution should taper toward and decrease to zero at

each end of the dike. As illustrated in Figure D.5-11, the distribution also should be rounded; it is not a sharp triangular distribution. This assessment also applies to the location of conduits within a dike system.

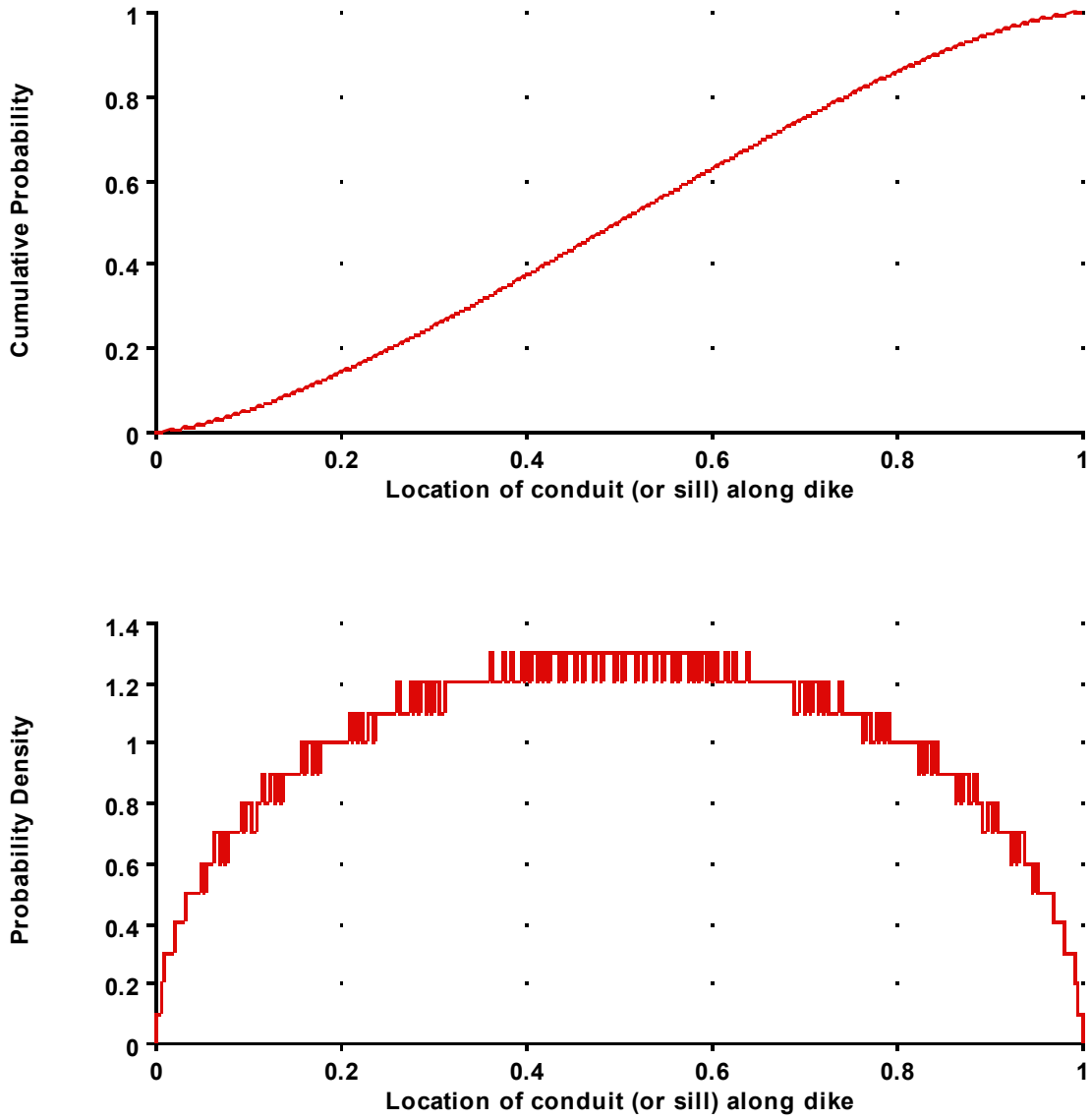

NOTE: Zero and 1 represent the dike endpoints.

Figure D.5-11. Assessment of the Location of a Conduit (or a sill) along the Length of a Dike

Column-Producing Conduits. The volume of magma involved in an eruption, fracture properties of the rocks surrounding a conduit, and other factors influence whether a conduit produces an eruptive column. An ascending dike would fill the relatively small volume of the repository before reaching the ground surface.

Based on the fact that seven or eight of the eruptive centers in Quaternary Crater Flat produced columns, I would assess an 85% probability that any future conduit would be column producing.

D.5.1.3 Additional Considerations

In addition to the geometry of dikes, sills, and conduits, I consider other event characteristics.

Magnitude of Eruption. Monogenetic basaltic cinder cones are the expected type of any future volcanic events in the vicinity of Yucca Mountain. Silicic domes and ignimbrites are not expected, because most such eruptions are associated with regions that contain large-volume magma sources. Crater Flat has a high potential for hydromagmatic volcanism because of the presence of alluvium and the relatively shallow water table, especially if the future climate becomes wetter. This type of eruption would not be expected in the Yucca Mountain block, however, because the rocks there have a low permeability and the water table is too deep, even assuming a climate-induced rise of the water table. An eruption through the repository more likely would have a violent Strombolian character such as that of past eruptions in the immediate vicinity.

Undetected Events. If there was a previous, buried hydromagmatic event in Crater Flat, it would leave little evidence because few maars produce a near-surface magnetic signal. A plug of basalt should be apparent at some depth, but would be buried deeply, so that the magnetic signature would be weak and hard to detect.

Some dikes could ascend to a shallow depth but fail to reach the surface. This would be less likely to happen under Crater Flat than at Yucca Mountain simply because of the higher elevation of the latter. Any intrusion that spanned the transition between Crater Flat and Yucca Mountain would find its first outlet at the lower elevation of Crater Flat. Flow would increase at that point at the expense of further rise of a dike under Yucca Mountain. The number of such potential intrusive events would be negligibly small.

D.5.2 SPATIAL MODEL

My primary spatial model for potential volcanism in the YMR is a zone model. I have identified a background zone and a smaller zone that is structurally distinct from that background zone. That smaller zone encompasses the Crater Flat-Amargosa Desert area. Each of these two zones is expected to experience a different rate of future volcanism. Figure D.5-12 shows the background zone, and Figure D.5-13 shows the Crater Flat-Amargosa Desert zone. Although the background zone and the Crater Flat-Amargosa Desert zone have different rates of volcanism, the transition between the two is gradational. The width of that transition is greater in the east and southeast than at the western edge of the zones. Figure D.5-13 illustrates both the boundary between zones (the inner blue line) and the outer edge of the transition distance over which the rate changes (the outer black dashed line).

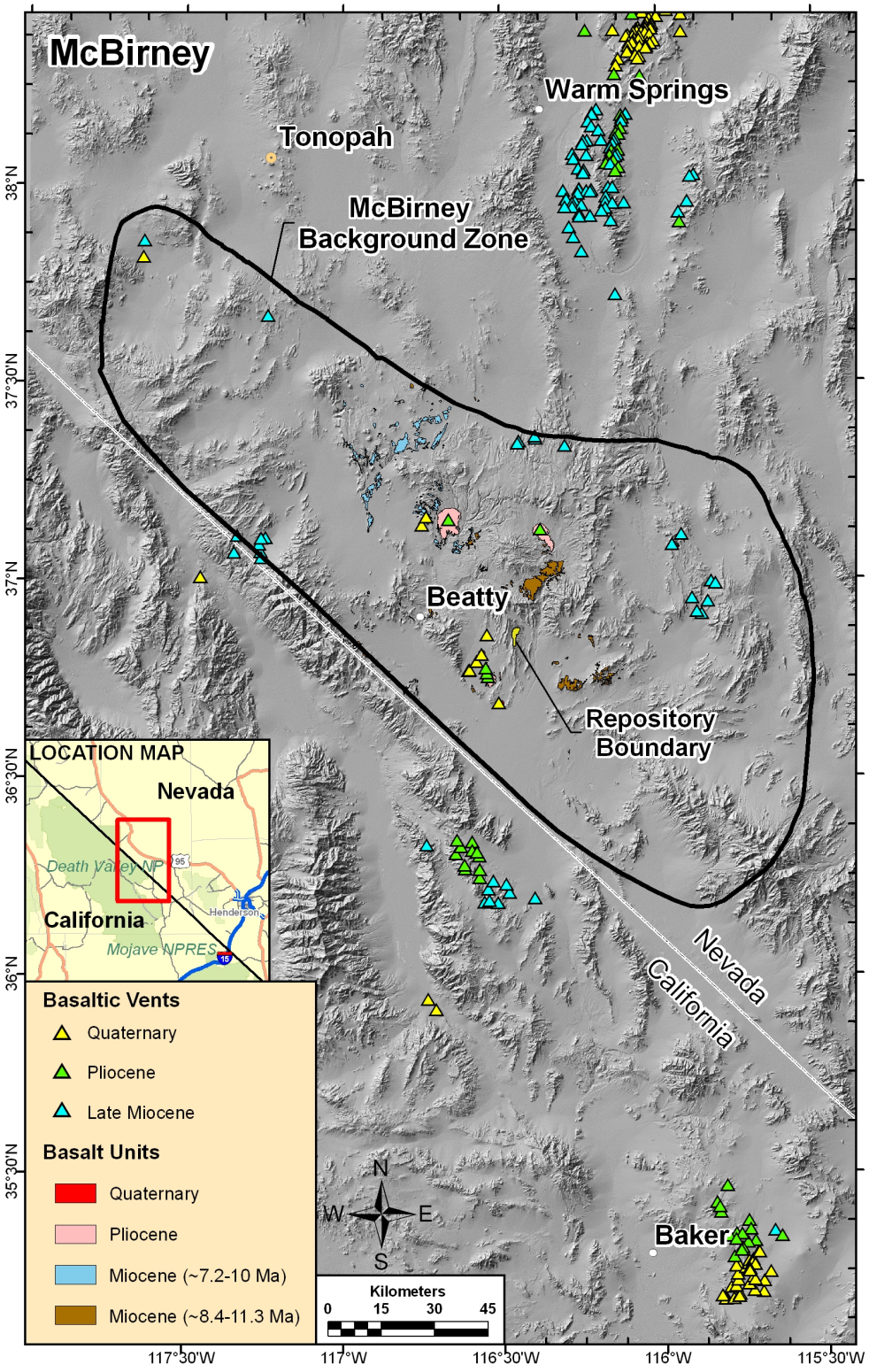

Figure D.5-12. Background Zone

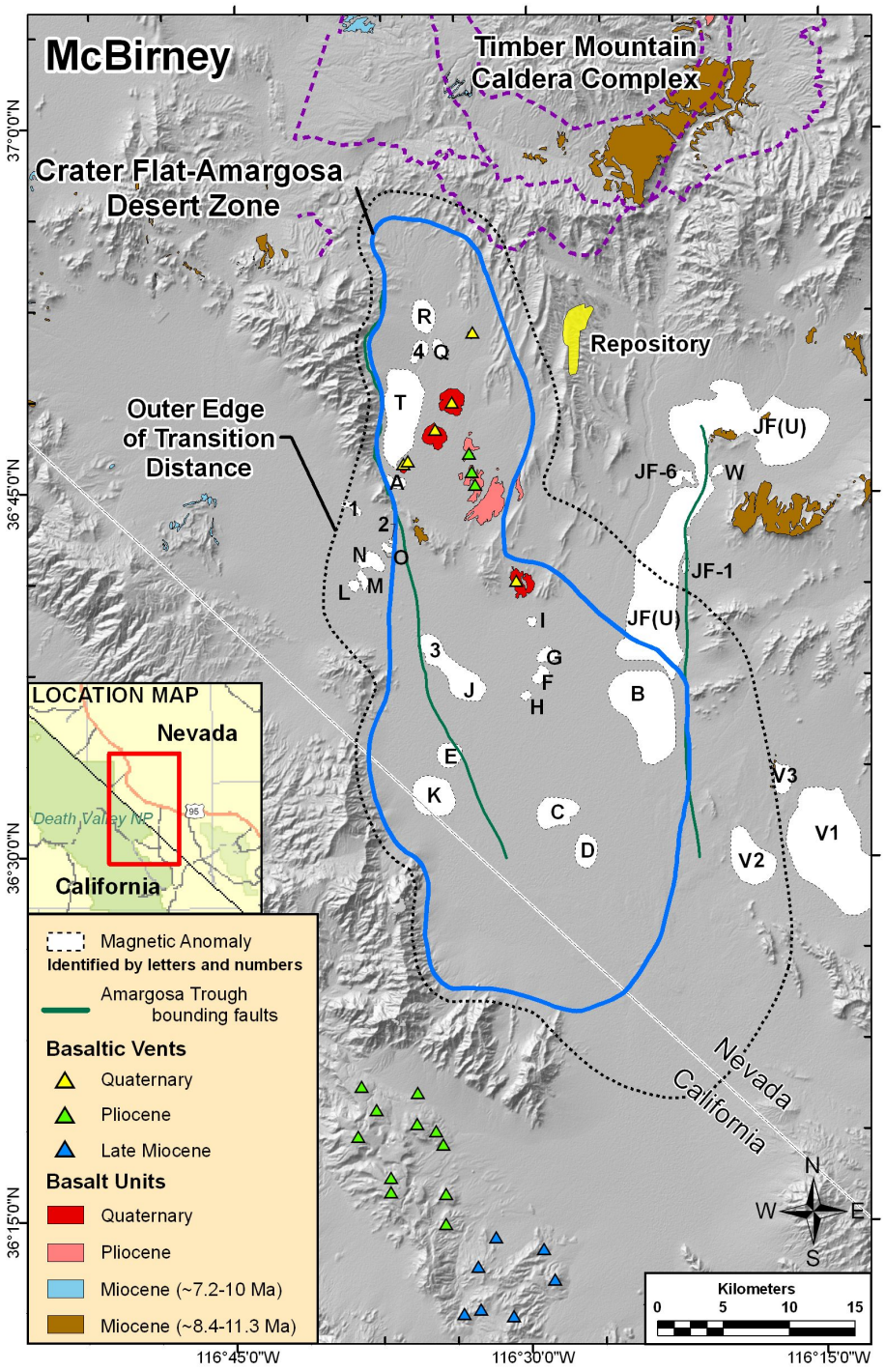

NOTE: Rate changes gradually between zones: the red line represents the zone boundary; the dashed black line indicates the distance over which the rate changes.

Figure D.5-13. Crater Flat-Amargosa Desert Zone

D.5.2.1 Definition of Crater Flat-Amargosa Desert Zone

The Amargosa Trough, a structural feature defined primarily by geophysical data, includes Crater Flat and the Amargosa Desert. Because the Amargosa Trough has a higher potential for future volcanism than do areas outside it, it defines the principal area considered for this assessment. The topographically high Yucca Mountain area is considered separate from Crater Flat and the Amargosa Desert. The northwestern part of the Amargosa Trough region (which includes the Quaternary centers of Sleeping Butte and Thirsty Mesa) similarly is considered to be structurally separate from Crater Flat, as seen in the different velocities evident in the tomographic data.

Quaternary cones outside the YMR are located far from Yucca Mountain, suggesting that YMR volcanism is a local phenomenon. The closest Quaternary volcanic fields (the Cima field to the south and the Lunar Crater field to the north) are roughly 150 km distant.

The Quaternary-active Rock Valley fault intersects the Amargosa Trough, suggesting that a higher level of volcanism may occur in the southern part of the trough. Although the structural setting seems favorable, some other factor, such as distance from the magma source, has inhibited activity in that area. Because Lathrop Wells shares structural characteristics with the Crater Flat-Amargosa Desert area, it is included in that zone.

Events north of the northern Amargosa Trough (Thirsty Mountain, Buckboard Mesa, and the Sleeping Butte volcanoes) are included in the background region.

D.5.2.2 Definition of Background Zone

My background zone includes the area that appears to have a similar structural setting, excluding areas such as the Greenwaters near Death Valley, which are associated with a more active tectonic environment. Fields containing large numbers of Quaternary vents, such as Lunar Crater, also are excluded because I prefer to define a background rate rather than the rate associated with any given field. Only events less than 4.7 Ma in age are included in the recurrence rate estimate (see Section D.5.3).

D.5.2.3 Rate Transition between Zones

Because Bare Mountain creates a well-defined boundary, the transition between the Crater Flat-Amargosa Desert zone and the background zone occurs close to this feature (within 1 km). Along the eastern boundary of Crater Flat, the transition distance is about 2 km. At approximately the latitude of Lathrop Wells, the transition zone has a width of about 5 km (Figure D.5-13). The transition distance is greatest (10 km) in the Amargosa Valley, because the Amargosa Trough is not as clearly defined in this area.

D.5.2.4 Conditional Spatial Intensity within Crater Flat Zone

The volumes of magma associated with events within my zone of interest are important clues to the present state of the system. They recently have been decreasing, and the accompanying trend toward compositions that are more enriched in excluded (incompatible) trace elements indicates that the volcanic system is waning. The high seismic velocities found under the Timber

Mountain caldera complex can be interpreted to reflect depletion of the mantle source under that region.

Table D.5-1 lists past volcanoes or basalt-based aeromagnetic anomalies in the Crater Flat zone. I use this information in a spatial smoothing model to estimate the spatial intensity within this zone. The smoothing model should use a Gaussian kernel function and a smoothing distance of 7 km. The ages and volumes of the listed events strongly affect my estimate of future spatial distribution. I weight the events in Table D.5-2 by (1) the inverse of their ages (younger events are weighted more heavily), and (2) their volumes (higher-volume events are weighted more heavily). When considering a short time frame (<0.5 My), volume is the more important factor, whereas age is more important for a longer period. A large-volume eruption within a cluster provides a favorable thermal regime for future volcanic events. Over time, however, the heat decays, and event ages become better predictors of future volcanism. Overall, I consider the ages of past events to be more important than their volumes in estimating future spatial intensity. Thus I weight the inverse-age factor 0.75 and the volume factor 0.25 in the spatial smoothing model.

D.5.2.5 Additional Geologic Data

The rate of extension in a region is another factor that could affect future volcanism, as this rate reflects the structural setting of the region. The data on extension used by Fridrich et al. (1999) show that the amount of extension in Crater Flat increases to the south. Extension data are incomplete across the region of interest, however, and are a less significant factor than either age or volume for both future periods of interest. Moreover, if magma is locally depleted, then the amount of extension that is occurring is irrelevant. Extension data are not used directly in my spatial model.

I used the interpretations of tomographic data to assist in defining my zone and the distance over which the rate changes between zones. The data are not sufficiently well resolved, however, to be useful in defining the variation in spatial intensity within a zone.

D.5.3 TEMPORAL MODEL

I use two temporal models to develop a recurrence rate for future events: a homogeneous Poisson model, and a time-volume model.

D.5.3.1 Homogeneous Poisson Model

In this approach, events are assumed to occur according to a Poisson model, and a future rate is estimated from the frequency of past events. Table D.5-1 lists events within the Crater Flat zone that form the basis for my estimate of the recurrence rate for that zone.

The recurrence rate for the background zone is defined by the post-4.7-Ma events identified within the zone. Table D.5-2 lists all known Plio-Quaternary events in the background zone, which form the basis for my estimate of a rate for that zone.

I have considered two models for estimating a recurrence rate for volcanism in the region of interest: (1) one based on the recurrence rate of Quaternary events only, and (2) one based on the recurrence rate of both Pliocene and Quaternary events.

I believe the Quaternary rate is more predictive of the future rate of volcanism than is the rate based on both Pliocene and Quaternary events. I assign a weight of 2/3 to the estimate based on the Quaternary rate and a weight of 1/3 to the estimate based on the Plio-Quaternary rate.

Miocene events, such as the Solitario Canyon dike or the flows in Jackass Flats, should not be used to assess recurrence rate because they are related to an earlier magmatic episode that ended 4 or 5 million years ago and are too old to be relevant.

D.5.3.2 Time-Volume Model

I also consider a time-volume model to estimate a recurrence rate for the Crater Flat-Amargosa Desert zone. The long-term effects of such time-dependent forces means that the decrease in eruptive volume could be more or less pronounced than that shown on Figure 2 of Valentine and Perry (2006).

The time-volume model requires estimating the eruptive volumes of individual events and the cumulative volumes of eruptions throughout the period of interest. In considering the change in cumulative volume over time, the conceptual model of conductive heat loss described by Richard Carlson (PVHA-U Workshop 2) seems appropriate. A model of cumulative volume as a function of time should be fit to the events identified in Table D.5-1.

I prefer using the time-volume model rather than the homogeneous Poisson model to estimate a recurrence rate for the Crater Flat-Amargosa Desert zone, because the time-volume model takes into account the variation in behavior throughout the period of interest rather than simply reflecting a long-term average. I assign relative weights of 0.95 to a time-volume model and 0.05 to a homogeneous Poisson model.

D.5.4 REFERENCES

Fridrich, C.J., Whitney, J.W., Hudson, M.R., and Crowe, B.M., 1999, Space-time patterns of late Cenozoic extension, vertical axis rotation, and volcanism in the Crater Flat basin, southwest Nevada, in Wright, L.A., and Troxel, B.W. (eds.), Cenozoic Basins of the Death Valley Region: Boulder, Colorado, Geological Society of America Special Paper 333, p. 197-212.

Itasca, 2006, Dike/fault interaction below Yucca Mountain: internal memo dated May 18, 2006.

Keating, G.N., Valentine, G.A., Krier, D.J., and Perry, F.V., 2008, Shallow plumbing systems for small-volume basaltic volcanoes: Bulletin of Volcanology, v. 70, pp. 563-582, DOI 10.1007/s00445-007-0154-1.

Los Alamos National Laboratory (LANL), 2007, Ar/Ar age determinations, volume, location and elevation of Plio/Pleistocene volcanoes in the Yucca Mountain region, Rev. 3: Excel spreadsheet titled, Volcano_volume_age_location_Rev03.xls.

Valentine, G.A., and Perry, F.V. (2006), Decreasing magmatic footprints of individual volcanoes in a waning basaltic field: Geophysical Research Letters, vol. 33, L14305, DOI:10.10292006GL026743.

Wood, C.A., and Kienle, J., 1990, Volcanoes of North America: United States and Canada: Cambridge University Press, Cambridge.

D.6 MICHAEL SHERIDAN'S ELICITATION SUMMARY FOR PVHA-U PROJECT

Two types of igneous events are identified as having the potential to disrupt the Yucca Mountain radioactive waste repository: an igneous intrusion into the repository, or a conduit passing through it. The probability that either type of event would disrupt the repository is a function of the spatial and temporal distribution of volcanism in the area and the physical geometry of igneous events. These factors, and the relationships among them, are illustrated in Figure D.6-1. Models and assessments of the geometry of dikes, dike systems, and conduits are summarized in the Section D.6.1, followed by models and assessments of the spatial and temporal distributions of igneous events.

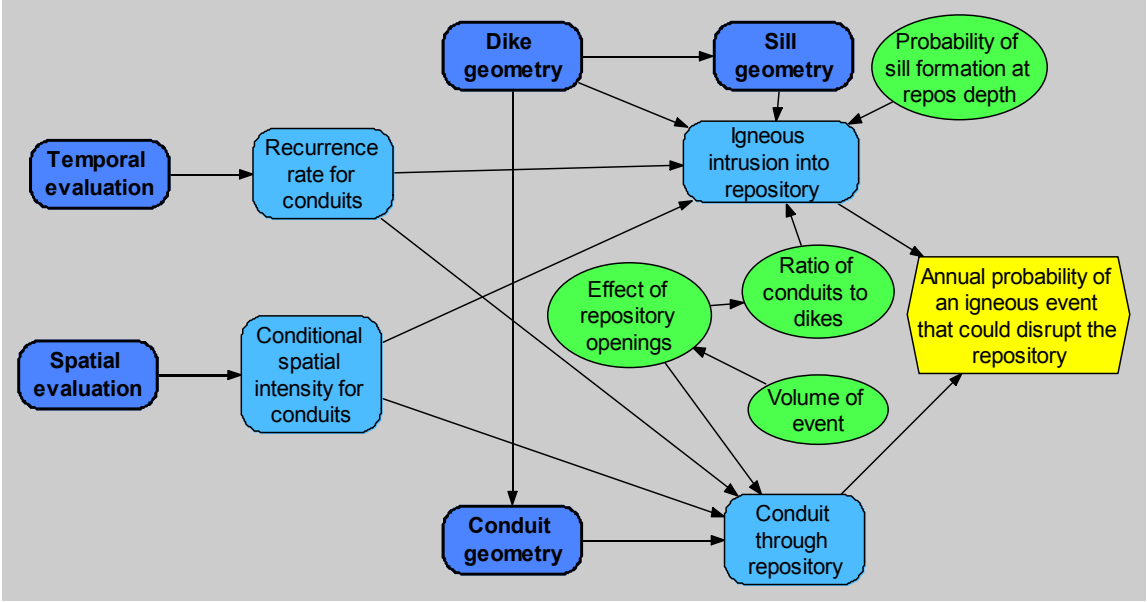

NOTE: The yellow hexagon represents the final result of the assessment. Green ovals represent information or variables for which assessments have been made. Dark blue rectangles represent sub-models; light blue nodes represent values calculated from other inputs; and arrows represent influence of one variable on one or more others.

Figure D.6-1. Overall Structure of the Model

D.6.1 EVENT DEFINITION

An event is a temporally and spatially distinct pulse of magma that reaches the ground surface. I consider a single event to have a duration at the surface of a few hours to a maximum of about 20 to 50 years. This relatively short time frame means that although the ages of some past cones cannot be distinguished by radiometric dating, they do not necessarily represent a single event. A large spatial separation between cones also indicates that they may represent separate events.

Observations of the 1970 eruption of Hekla in Iceland are relevant for assessing characteristics of igneous events worldwide. In that eruption, cones formed from conduits located along an en echelon fissure system. Fissures released gas, but not lava, at the surface; multiple conduits were widely spaced along the fracture system. At many localities we observe that lava does not erupt from fissures, but only from conduits.

Not all dikes in an event necessarily ascend to the ground surface to form a fissure. If a fissure does occur, it may develop into a conduit that brings magma to the surface, subsequently forming a cinder cone. A conduit will form where the upward velocity of magma is greatest in a dike. The center of a cone is directly above a conduit.

As magma ascends, lower parts of dikes likely seal off as the pulse of magma passes through. Although a dike having fingers that connect at depth differs from a single dike, at the depth of the repository there would be little difference between a dike that ascends from mantle depths and a dike that fingers from a larger dike well below the repository.

The Quaternary volcanoes in Crater Flat demonstrate that it is difficult to see a dike in the near surface. The important question is the depth at which a conduit may bud off from a dike. At the depth of the repository, a conduit could be located above a dike that does not reach the surface. In the volcanic system observed near Hoover Dam in Arizona, conduits apparently budded from dikes within 10 to 20 m of the surface.

Eruptive volume is key to determining the characteristics of an event. First, a minimum volume of magma is required for any eruption to occur. Small-volume basaltic eruptions have occurred during the past few million years in the Yucca Mountain region (YMR, defined as the region within a radius of about 50 km centered on Yucca Mountain). Total erupted volume consists of lava, close-in fallout (scoria cone), and the tephra blanket. These three components are considered sub-equal. The minimum volume for an eruption approximates 106 m^3 (0.001 km^3). Although the Makani "Cone" is the smallest-volume eruption in the vicinity of Yucca Mountain, it is the product of a fissure event (fire fountain) rather than a cone, based on the presence of ribbon bombs and scoria (Valentine et al., 2006). The volume of Makani is about 0.002 km^3, or more than one order of magnitude smaller than the volume of Lathrop Wells. I anticipate that potential future events in the region also would be small-volume basaltic events.

D.6.1.1 Characterization of Past Events

Table D.6-1 lists cones and igneous centers in the YMR that I consider to be part of a Crater Flat volcanic field, along with estimated ages of the events and my interpretation of how many events each center represents. These events define my time period of interest, which includes all events since the Miocene (post-5 Ma).

As discussed above and shown in Table D.6-1, I believe the cones in the region likely represent separate events (that is, they were separated by at least 20 to 50 years), rather than a single event that produced multiple sub-parallel dikes. It is possible that the cones are part of a single event involving multiple dikes or represent multiple conduits occurring on a single dike. The cones are arranged in more of an en echelon pattern than strictly sub-parallel dikes would be. The 3.8-Ma Pliocene centers appear to be related to perhaps three sub-parallel dikes, although magma volumes were larger during the Pliocene than during the Quaternary. I think multiple sub-parallel dikes are unlikely to occur in the future.

Table D.6-1. Relevant Events in the Region of Interest

Center	Number of Events	Age* (Ma)
Lathrop Wells	1	0.08
Makani Cone	1, 2, or 3 events (weights of 0.05, 0.20, and 0.75)	1.07
Black Cone		1.07
Red Cone	If 2 events, Red Cone and Black Cone are one event; Makani Cone is a separate event	1.07
Little Cones	1 or 2 events (weights 0.75 and 0.25) Most likely 1 event with two cones, but there is not enough evidence to reject the possibility of 2 events that cannot be separated by radiometric data	0.78
Pliocene Basalt of Crater Flat	1, 2, or 3 events (weights 0.05, 0.20, and 0.75)	3.8
Anomaly B	1	3.85
Anomaly F	1, 2, or 3 events (weights 0.05, 0.20, and 0.75)	3.9
Anomaly G		3.9
Anomaly H		3.9
Anomaly C	0, 1, or 2 events (weights 0.8, 0.1, and 0.1)	4.8
Anomaly D		4.8

* Age estimate based on consideration of Los Alamos National Laboratory (LANL) (2007).

D.6.1.2 Event Characteristics and Geometry

Events consist of a collection of conduits, dikes, and possibly sills. Dike geometry is defined by estimates of dike length, width, and azimuth and by the number and spacing of dikes in an event, as illustrated in Figure D.6-2. Conduit geometry is described by estimates of the number of conduits per event, the locations of conduits relative to dikes, and the conduit diameter or dimensions, as illustrated in Figure D.6-3. All assessments discussed below are appropriate for repository depths (~300 m below the surface).

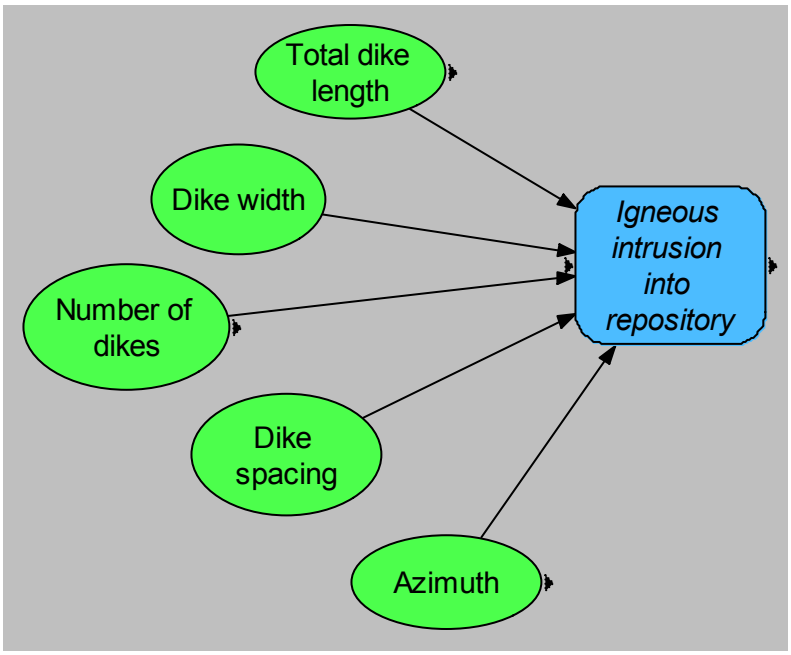

Figure D.6-2. Components of the Model for Dike Geometry

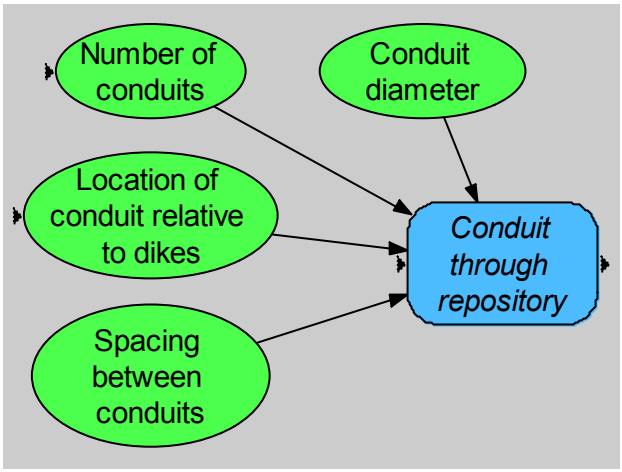

Figure D.6-3. Components of the Model for Conduit Geometry

Number of Conduits and Dikes in an Event

Large volcanoes may have multiple conduits, or feeder systems, as is typical of Hawaiian volcanoes or composite andesitic volcanoes such as Hekla. Hawaiian volcanoes, which have large magma chambers, are not appropriate analogs for the repository area, however. The number of conduits per event decreases for a smaller volume of magma; ultimately, there is insufficient volume for any eruption to occur. Also, the relatively flat topography that borders the Yucca Mountain block does not provide the large, sloping surfaces along which multiple conduits could migrate downhill (as occurs in Hawaii, which again is not a good analog).

My interpretation of the Crater Flat cones, including Lathrop Wells, is that they most likely represent isolated scoria cones, each having one dike, one conduit, and one cone. This pattern, which appears to be typical of the region, is logical given the small volumes of magma in regional events. When there is sufficient magma pressure to form an eruption, the associated conduit forms at the weakest path to the surface. The formation of a conduit reduces the pressure in other parts of the dike, thereby reducing the likelihood that a second conduit will form on that dike. Multiple conduits in an event are likely to be associated with unusual circumstances, such as very long dikes, multiple dikes, blockage of existing conduits, or prolonged eruptions.

Data are sparse regarding the number of conduits in a single event or along a single dike. Based on the discussion above, my assessment of the number of conduits at repository depth for a potential future event and their relative weights is: one conduit (0.75), two (0.2), or three (0.05).

My assessment of the number of sub-parallel or en echelon dikes in an event is conditional on the number of conduits: generally I would expect there to be one dike for every conduit, but I allow for the possibility of several conduits on a single dike, or of a dike that has no conduit. Table D.6-2 below shows my assessment of the probable number of dikes for a given number of conduits.

Table D.6-2. Number of Dikes as a Function of Number of Conduits

Number of Conduits	Number of Dikes						
	0	1	2	3	4	5	6
1	1%	87%	12%				
2		20%	50%	20%	10%		
3		5%	15%	40%	20%	10%	10%

Dike Geometry

The following sections describe my assessments of dike length, width, and azimuth.

Dike Length. Based on observations worldwide, maximum dike length can be more than a thousand kilometers, because dikes carrying large volumes of magma can extend for long distances. Because dikes cool rapidly, short dikes (<10 m) will "freeze" before propagating far. Relatively short dikes are expected to be associated with the type of small-volume basaltic eruptions observed in the YMR. The lower bound for dike length is 100 m, consistent with a dike length-to-width aspect ratio of 1,000:1 and a minimum dike width of 10 cm. It is unlikely that a single dike feeds the Quaternary cones in Crater Flat. My assessments take into account the analog data in Valentine and Perry (2006).

Figure D.6-4 illustrates my assessment of the total length of potential future dikes at repository depth in a single event in the YMR. My assessment is based on the following estimates: 100 m is the lower bound; 8 km is the 95th percentile; and 4 km, 2 km, and 1 km are the 75th, 50th, and 25th percentiles, respectively.

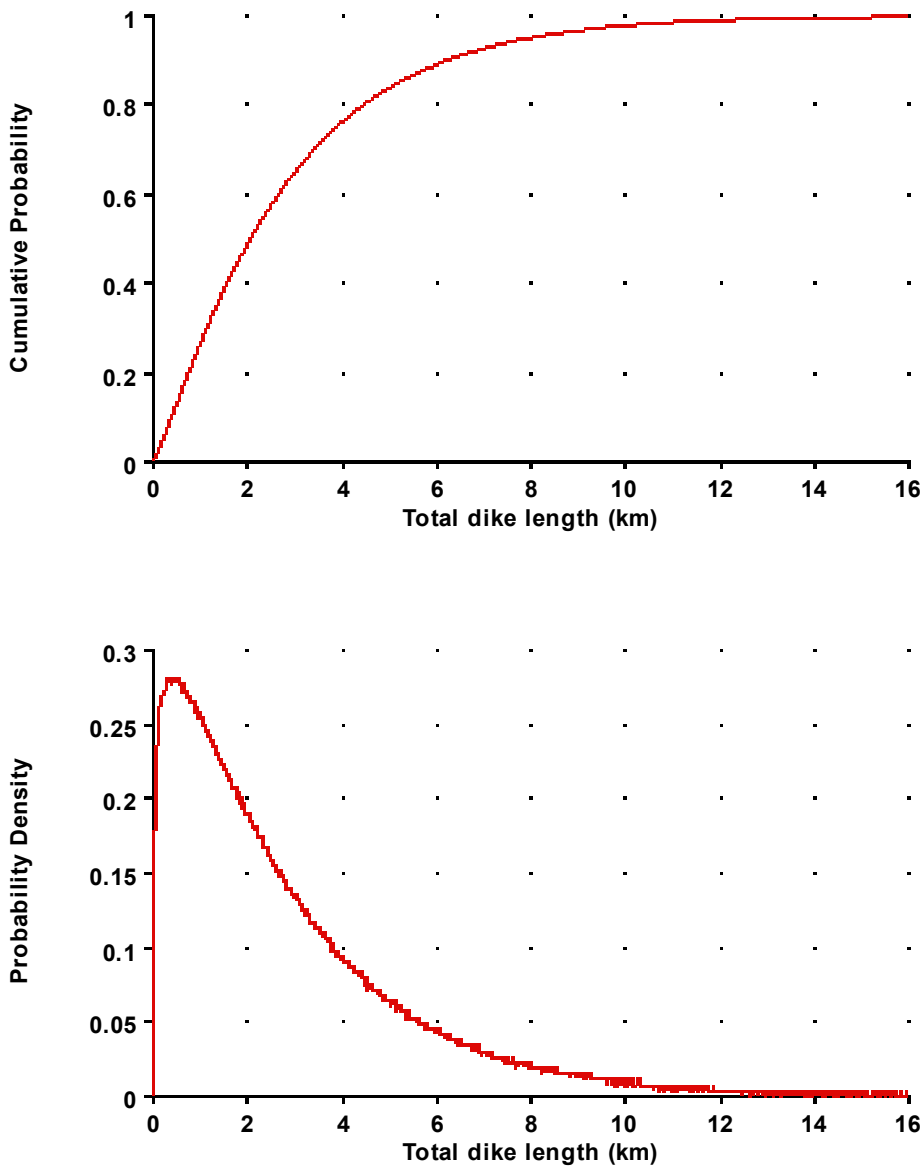

Figure D.6-4. Assessment of the Total Length of Dikes at Repository Depth in an Event

Dike Width. Widths may change along the length of a dike, and in places can be as small as a millimeter. Average dike width must be at least ~10 cm, however, to maintain sufficient heat for magma to rise.

Based on extensive measurements of dike widths in the Boulder Dam area, my assessment of the width of potential future dikes at repository depth in the YMR is a Gaussian distribution having a mean of 1.8 m and a standard deviation of 0.9 m, truncated at the lower bound of 0.1 m. This distribution is illustrated in Figure D.6-5.

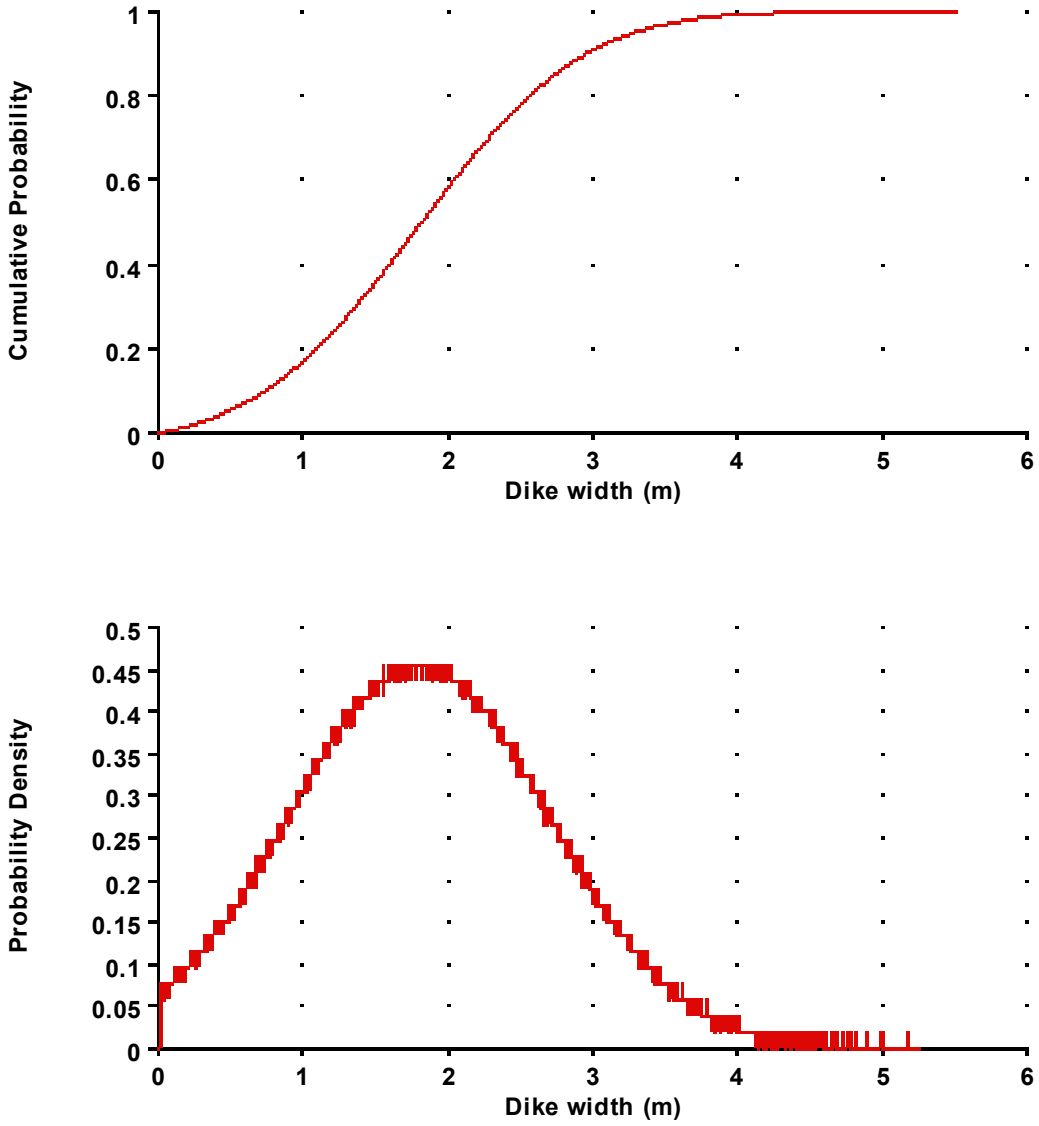

Figure D.6-5. Assessment of the Width of a Dike at Repository Depth

Dike Azimuth. I developed three conceptual models for the orientation of potential future dikes in the YMR. I consider each model to be equally likely.

1. N15°W ±20 based on observations at Lathrop Wells and the alignment of the 3.8-Ma Anomalies F, G, and H. This azimuth follows the general orientation of the Amargosa Trough.

2.. N30°E ±20 based on faults having this orientation. In the shallow subsurface dike orientation tends to be controlled by faults. This belief is influenced by a paper by Valentine and Krogh (2006). Although the stress field may change over the 1-My time frame of this assessment, current major structural orientations are unlikely to change.

3. N-S ±20 based on the dike alignments in southeast Crater Flat and the alignment of feeder dikes for the Quaternary Crater Flat cones, as inferred from the aeromagnetic data.

For each of the above models, uncertainty in azimuth is represented by a Gaussian distribution, and the ± values are one standard deviation. The distributions are truncated in the orthogonal directions. Figure D.6-6 illustrates distributions for all three azimuths. For modeling potential future events, a combined distribution should be used in which each of these three distributions is weighted equally.

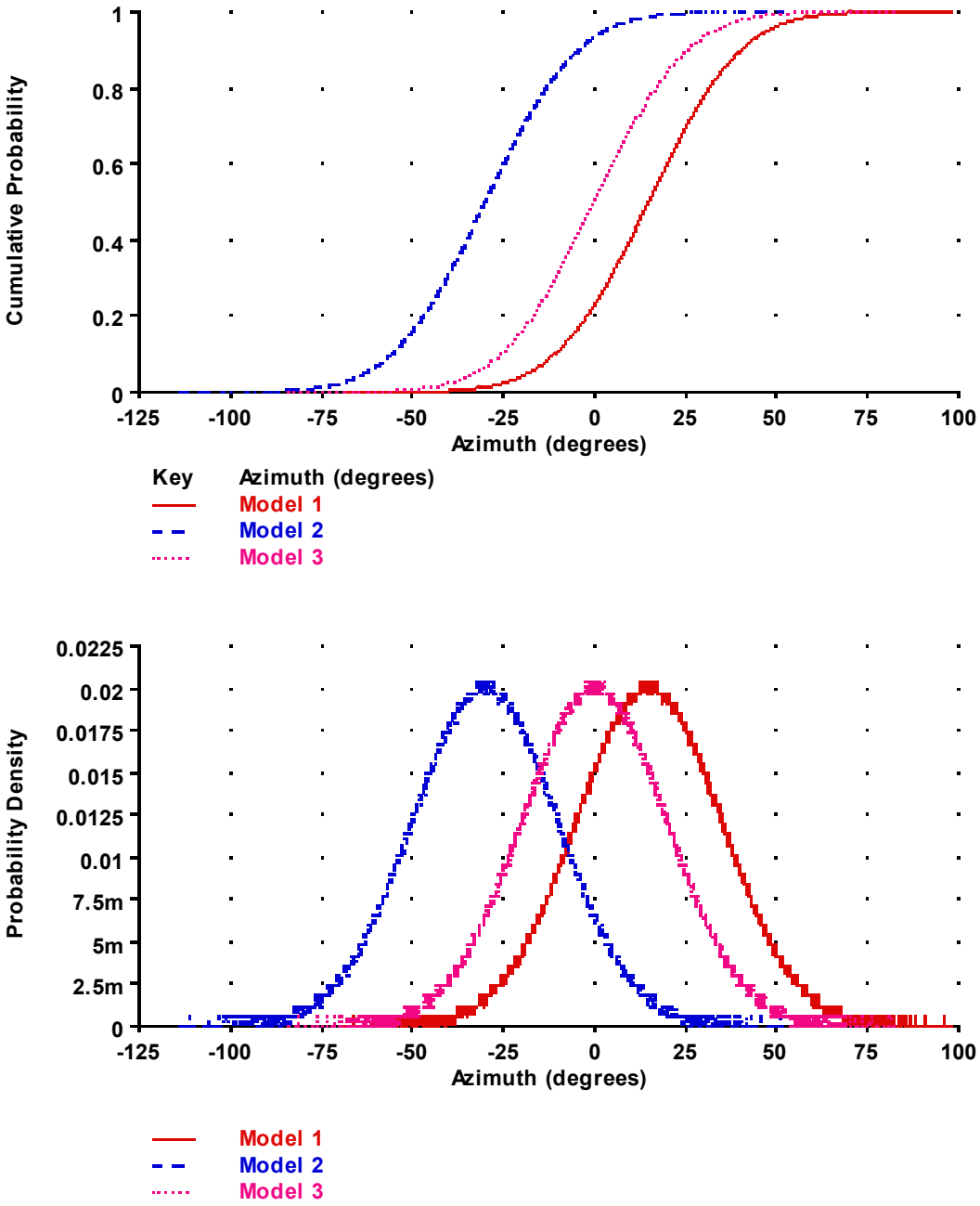

NOTE: For values less than 0.01 on the y-axis, suffix notation is used (m = 10^{-3} and u = 10^{-6}, so 5m = 0.005).

Figure D.6-6. Assessment of Dike Azimuth at Repository Depth: Three Alternative Models to Be Weighted Equally

Conduit Diameter at Repository Depth

Conduits are the pathways in which magma flow to the surface is concentrated. Because there are few field observations of conduits at depths of 300 to 400 m below the surface, dimensions of such conduits must be extrapolated. The diameter will depend on the volume of material ejected. Because the widest conduits are correlated with the longest dikes, the assessment of conduit diameter is given as a function of dike length.

The literature reports various values for conduit size, based primarily on theoretical estimates. All show a decrease in conduit size with a decreasing volume of erupted material. Wilson et al. (1980) give minimum conduit diameters of 5 to 100 m for Plinian eruptions. Melnik et al. (2005) show conduit diameters ranging from 40 to 70 m for large-volume eruptions. Barmin et al. (2002) estimate a conduit diameter of 15 to 25 m for some moderate-volume lava domes. Kazahaya et al. (2002) estimate conduit widths greater than 50 m for model calculations for a basaltic caldera.

There is significant uncertainty about conduit diameters at repository depth. My best estimate is a median diameter of 10 to 20 m, which reflects uncertainty in the size of a potential future event. Mapped plugs that served as conduits for the Hoover Dam dike swarm that I studied are 30 to 50 m wide, and were close to the original surface (less than 10-m-deep) structures.

Figure D.6-7 shows my assessments of the probability distribution for conduit diameter for a 5-km-long dike and for a 1-km-long dike, based on my review of the literature and the Hoover Dam conduits I have studied. These distributions are defined by the following estimates. For a 5-km-long dike, the median conduit diameter is about 20 m; the minimum is the width of the dike; and the maximum is 50 m. Forty meters represents about the 95th percentile. For a 1-km-long dike, the median conduit diameter is about 10 m; the minimum is the width of the dike; and the maximum is 20 m. Fifteen meters represents about the 95th percentile.

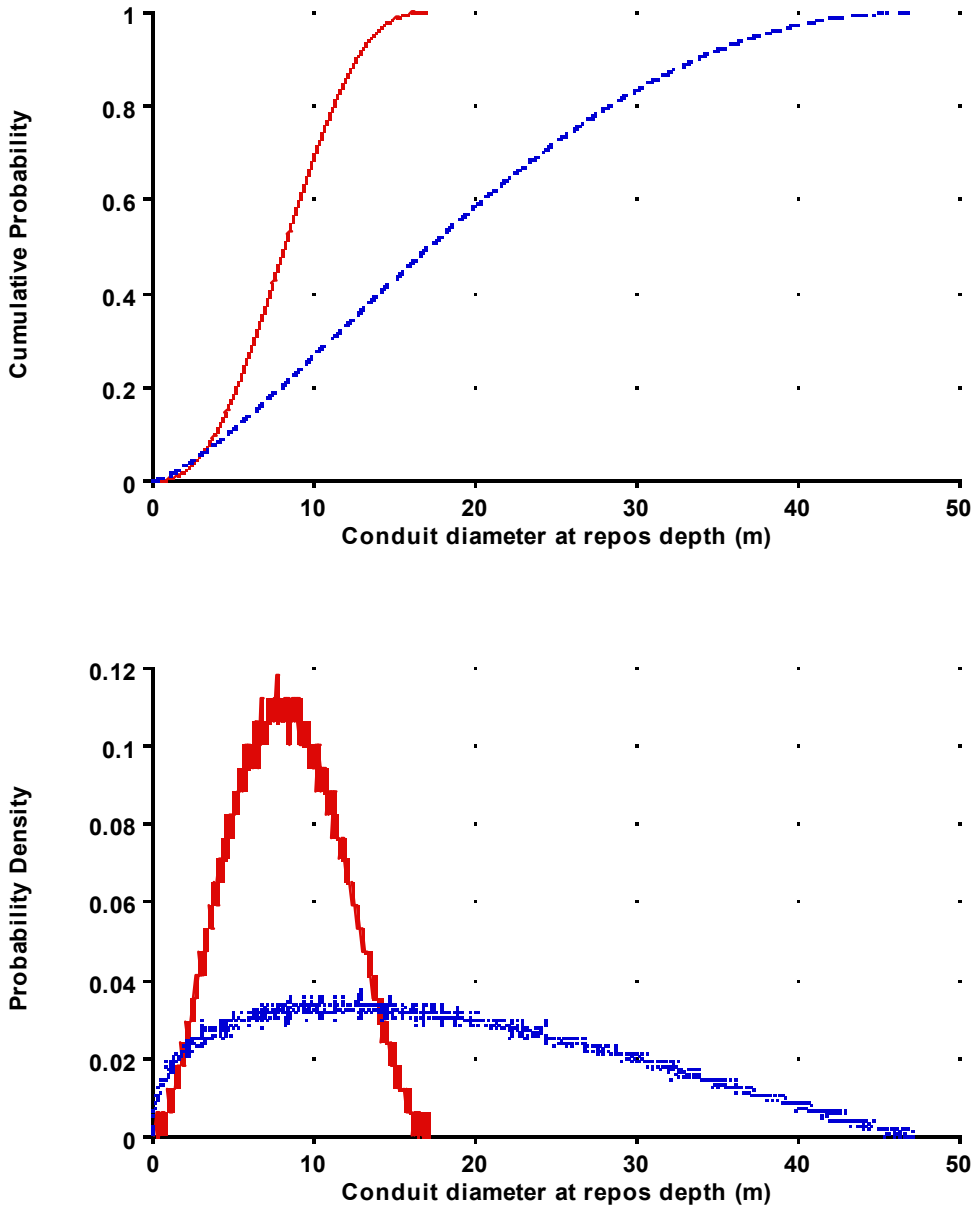

Figure D.6-7. Assessment of the Diameter of a Conduit at Repository Depth for Dike Lengths of 1 km (red line) and 5 km (blue line)

Column-Producing Conduits

Relatively small-volume events are expected in the future in the YMR. Smaller events could be more violent and water-rich, but that is difficult to assess. An eruptive column could be produced at some point during an eruption, given that eruptions change through time. Based on a mapped fallout deposit, Lathrop Wells once had a column. Although no fallout sheet remains at Red Cone, Black Cone, Hidden Cone, or Little Black Peak, the nature of their vent facies suggests strong vesiculation and high gas content, which argue for a column-producing phase. The two Little Cone vents, in contrast, are surrounded by welded spatter, suggesting the lack of a column.

I consider the volume of the 3.8-Ma event in Crater Flat to approximate the largest volume of a potential future event. Thus, the median volume for an eruption in the YMR during the future periods under consideration is about 6×10^7 m^3 (with plume, cone, and flow each representing about 1/3 of this volume). One order of magnitude in each direction represents the 1st and 99th percentiles. If the volume is 6×10^7 m, then a column is likely, but columns are less likely below that volume. Based on the estimated volume of future events and consideration of the Crater Flat cones, my assessment is that if a potential future event has a conduit, there is about a 70% probability it will produce a column.

The maximum height of an eruptive plume would range from 2 to 6 km. The most likely maximum height is 3 km.

Location and Spacing of Conduits and Dikes

The total length of dikes in an event is described above. In events involving multiple sub-parallel or en echelon dikes, the length of an individual dike is random, with the restriction that the length of the longest dike is no more than four times the length of the shortest dike.

There is little evidence of parallel, completely overlapping dikes in past events in the YMR, and some evidence for right-stepping en echelon segments (e.g., if Red Cone, Black Cone, and Makani Cone are considered to represent one event, and similarly if Anomalies F, G, and H are considered to represent one event). Accordingly, my assessment is that, given two or more sub-parallel dikes in a single event, those dikes will be right-stepping in a somewhat widely spaced en echelon pattern, with little to no overlap at the ends of the dike segments. For example, dikes may overlap by as much as 10 percent of the length of the shorter dike, or may be separated by that same distance. Based on field observations, the perpendicular spacing between dikes is between 50 and 1,000 m. For example, the two sets of dikes at Boulder Dam are separated by about 800 m. My assessment of the spacing between potential future dikes is shown in Figure D.6-8, defined based on the following percentiles: 1,000 m = 90th; 500 m = 50th; and 200 m = 10th.

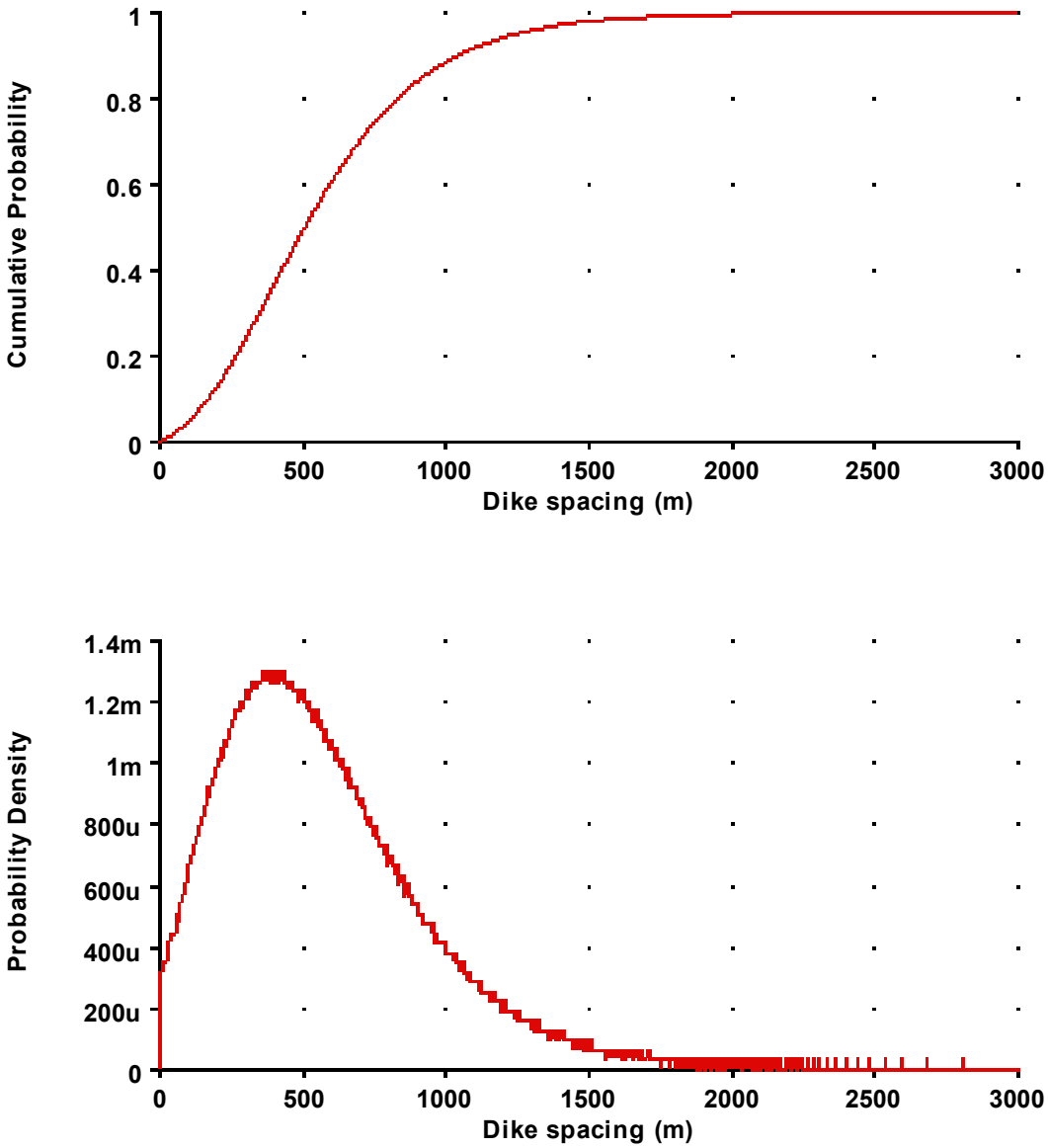

NOTE: Top graph is a cumulative distribution function; bottom graph is a probability density function. For values less than 0.01 on the y-axis, suffix notation is used (m = 10^{-3} and u = 10^{-6}, so 5m = 0.005).

Figure D.6-8. Assessment of the Perpendicular Spacing between Dikes in an Event Involving Multiple Sub-parallel Dikes

A conduit can occur anywhere along the length of a dike, typically forming where a dike is closest to the ground surface. The tendency for a conduit to be located at the lowest topographic elevation along the trace of a dike is incorporated into my spatial evaluation by utilizing a lithostatic pressure map (see Section D.6.2). At the depth of the repository, a feeding dike would be located beneath each conduit. The location of a conduit on a dike is modeled using a uniform probability distribution.

Given the type of monogenetic system prevalent in the YMR, a conduit that reaches the surface most likely would be associated with a dike at repository depth. It is possible, however, that a conduit could form at a depth below that of the repository without the associated dike reaching repository depth. As shown in my assessments of the number of conduits and dikes in a potential future event, my event definition allows for the possibility of an event that includes only a single conduit and no dike at repository depth.

If an event involves multiple conduits, those conduits are located preferentially on longer dikes or longer dike segments. If there is more than one conduit on a dike, the spacing between conduits must be at least 400 m. This minimum spacing is based on the relatively short distance (about 0.5 km) between the two Little Cones and observations from five additional analog sites in the YMR [Basalt Ridge, East Basalt Ridge, Paiute Ridge, Thirsty Mountain, and southeast Crater Flat, for which data were derived from an analog table developed by LANL investigators for the PVHA-U and published as Keating et al. (2008)]. At Paiute Ridge, a conduit has been observed at one end of a dike. A conduit is also present at one end of a dike in the Boulder Dam dike swarm. Although this is an unusual configuration, it must be included in the distribution of possible spacings.

Sill Geometry

Investigators have recognized sills within the YMR (e.g., at Paiute Ridge and possibly at Anomaly A). Magma may form sub-horizontally in sills if the location of dike intrusion is fault-controlled. Sills are most likely to occur where there is a contrast between the strengths of materials across bedding planes—that is, at a major lithologic contact. Many faults in the YMR minimally displace uniform materials, conditions that provide a lower probability of a sill forming than where differing units are juxtaposed. The welded tuffs below the repository are relatively homogeneous. The tuff/bedrock contact at which a sill most likely would occur lies 2 to 3 km below the ground surface.

A sill would form at the depth of the repository in about 5% of the dikes that might occur close to the repository. The probability of a sill forming on a dike is independent of the number of dikes in the event. That is, an event may involve more than one sill if the event includes more than one dike.

Figure D.6-9 illustrates components of the model of sill geometry. A sill can form anywhere on a dike (uniform random distribution along dike length), but would not extend beyond the end of the dike. Sill location is independent of conduit location.

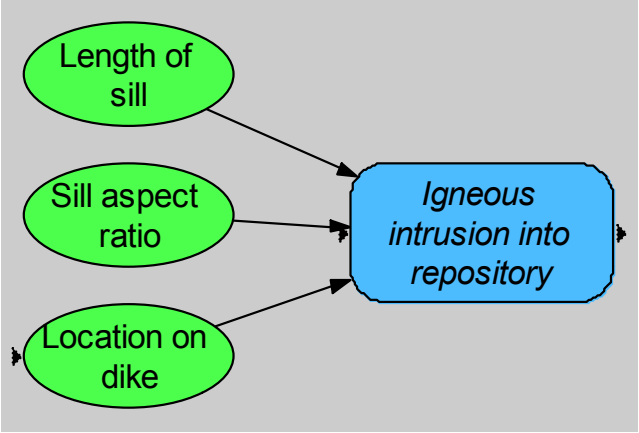

Figure D.6-9. Components of the Model for Sill Geometry

In map view, sills would have a circular to oval shape, with a maximum length-to-width ratio (aspect ratio) of about 2:1. The long axis of an oval sill would be parallel to the dike azimuth. My assessment of the length of the long dimension of a potential future sill is shown in Figure D.6-10, based on an estimate that the most likely length is about 200 m, the smallest is 2 m, and the 95th percentile is about 500 m. Sills would be wedge-shaped in vertical profile and would have a maximum thickness of 30 to 40 m.

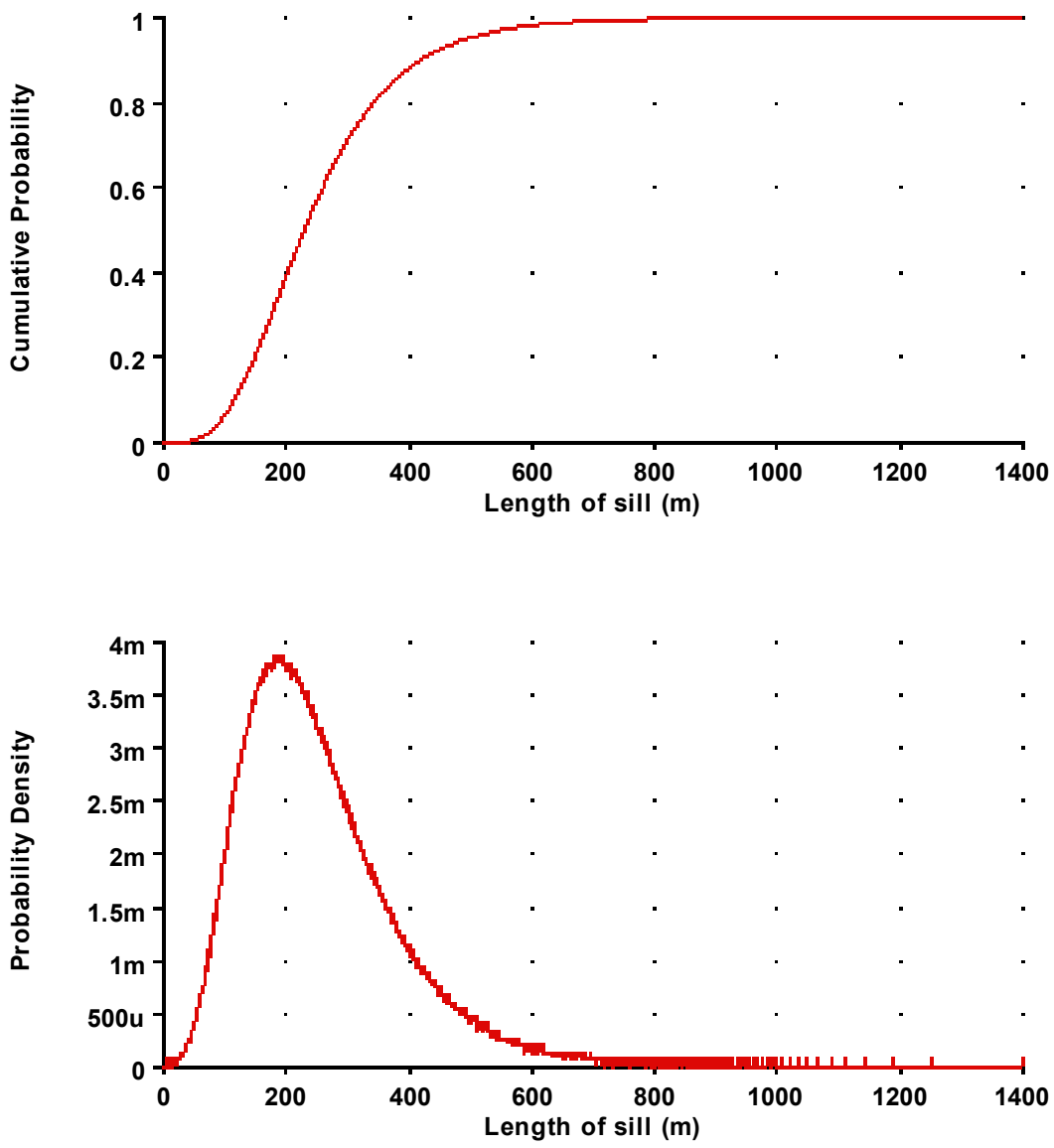

NOTE: For values less than 0.01 on the y-axis, suffix notation is used (m = 10^{-3} and u = 10^{-6}, so 5m = 0.005).

Figure D.6-10. Assessment of the Length of a Sill at Repository Depth

D.6.1.3 Additional Considerations

Style of Eruption. Data regarding the duration of eruption, volume of erupted material, and maximum height of plume are necessary to quantify eruption style. The large set of data I have collected (some published, some unpublished) from events in the Western United States and Mexico provides the basis for my assessments.

Based on my event definition presented above, the duration of any future event in the YMR would be on the order of days to as long as 50 years. Six months represents the median of my assessment of eruption duration. A short-duration eruption would last about one month (5th percentile of my assessment), while a long-duration eruption might last 30 years (95th percentile).

Hydromagmatism is not expected to affect the repository. Hydromagmatism could occur within the larger YMR, especially during the 1-My time frame, in response to possible climate change. Although a major hydrovolcanic event has not been observed in the YMR, hydromagmatism has occurred in nearby Death Valley. These events typically are not seen at higher elevations (although Ubehebe Crater in Death Valley occurs high on an alluvial fan).

D.6.2 SPATIAL MODEL

Figure D.6-11 illustrates the components of the model for spatial distribution of future volcanism. The region of interest is the Amargosa Trough and immediately adjacent areas, extending into the Timber Mountain caldera. Because the western edge of the Amargosa Trough seems to present a barrier to volcanism, the potential for new cones west of it is small, and future spatial intensity should be truncated at that boundary. This region and the line of truncation are shown in Figure D.6-12.

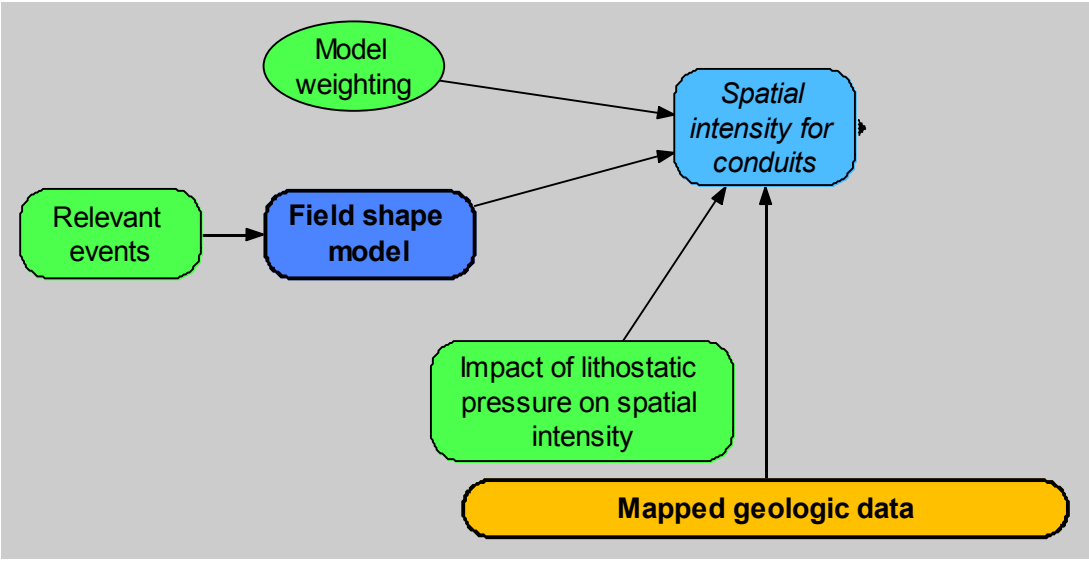

Figure D.6-11. Components of the Model for Spatial Distribution

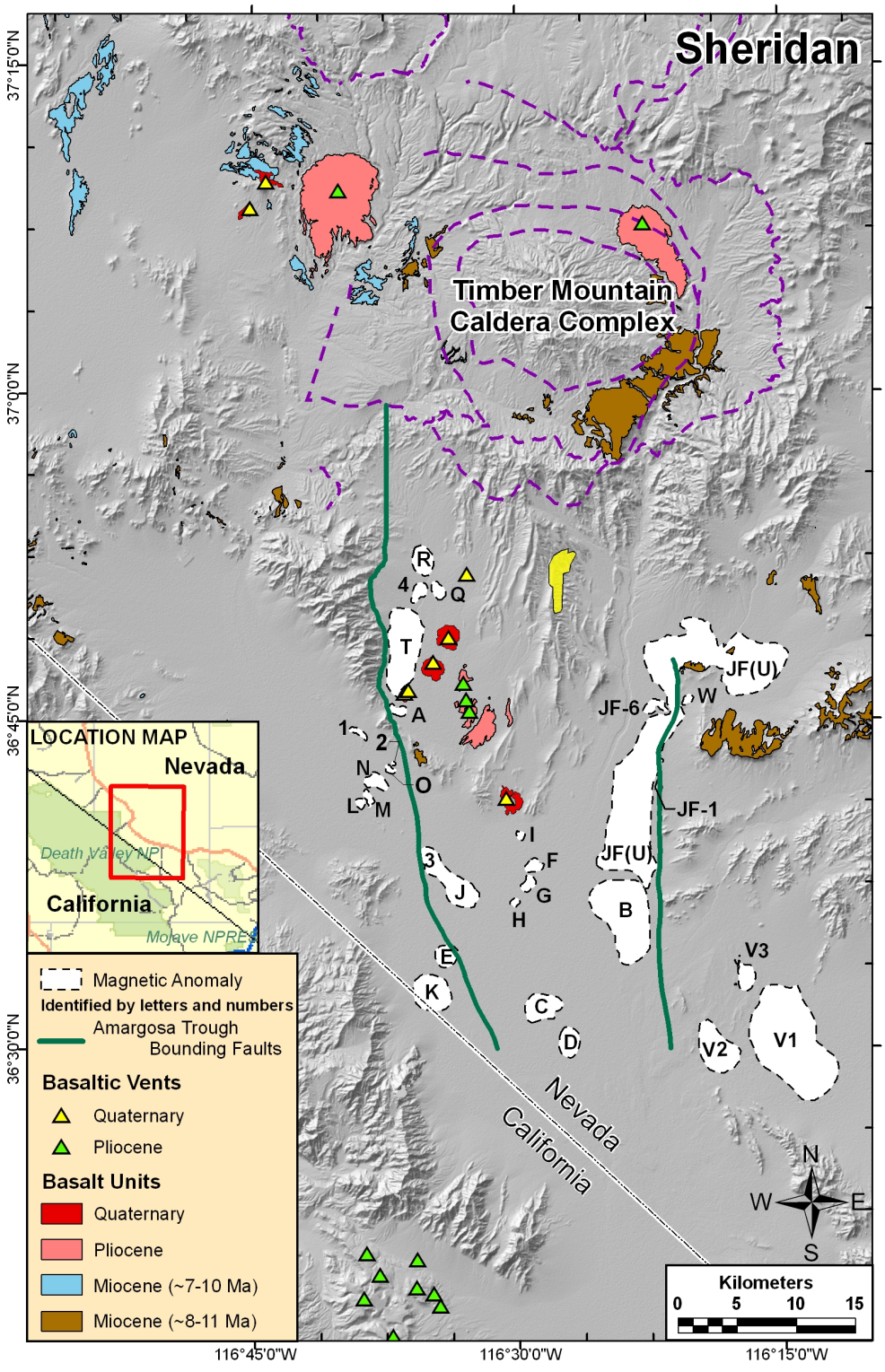

NOTE: Green lines indicate margins of Amargosa Trough determined from geophysical data. Western Amargosa Trough margin indicates the western truncation of the bivariate Gaussian model.

Figure D.6-12. Region of Interest

At about 11 Ma, the tectonic setting of the YMR shifted from one of subduction toward one of strike-slip faulting and extension. During episodes of crustal extension, batches of magma began to ascend, and basalts were erupted within the Basin and Range Province. Over time, the magma supply in the YMR dwindled. In map view, magma source regions in the mantle beneath the YMR could be compared with the shorelines of a large evaporating lake that leaves behind localized areas ("puddles"). Within the mantle these areas represent isolated zones of partial melt. The Crater Flat "puddle" is separate from the Sleeping Butte and Thirsty Mesa "puddles." The Thirsty Mountain area is one of higher heat flow, reflecting its location near the Timber Mountain caldera. Therefore, only events younger than 5 Ma that are south of the Timber Mountain caldera within the Amargosa Trough are considered to be relevant to the spatial distribution of potential future events in the region of interest.

I use two alternative spatial approaches: (1) a bivariate Gaussian field shape, and (2) a bivariate Gaussian field shape modified by (or combined with) lithostatic pressure data.

D.6.2.1 Bivariate Gaussian Field Shape

Because the shape of the Amargosa Trough probably is related to the underlying structural geology, I consider that the bivariate Gaussian shape is an appropriate spatial model for the volcanic field of interest. Support for the bivariate Gaussian shape of volcanic fields comes from studies of basaltic fields in similar tectonic environments. Basaltic volcanic fields that exhibit a geometry that can be described by a bivariate Gaussian distribution include Cima (>30 cones), Taos (~40 cones), Reveille (~50 cones), Unikaret (160 cones), and Pinacate (~275 cones).

Using this approach, past events are assumed to represent one volcanic field, and the parameters of a bivariate Gaussian distribution are derived based on the locations of those events. Separate models are fit to each alternative characterization of past events, as described above and shown in Table D.6-1.

D.6.2.2 Bivariate Gaussian Field Shape Combined with Lithostatic Pressure

As noted above, the bivariate Gaussian approach to field shape is influenced heavily by the locations of past events, which establish the dimensions and orientation of the field. Possible locations of future volcanic events could be overlooked, however, if a forecast were based solely on the locations of past events. Accordingly, additional information may be useful in identifying areas within the region of interest that have a higher or lower probability for future events.

The lithostatic pressure data for the YMR can be used in conjunction with the bivariate Gaussian field shape to identify locations of possible future events. The map of lithostatic pressure for the Amargosa Trough shows an extremely strong correlation between pressure and volcanism—all the Plio-Pleistocene and younger volcanic events in the region are located within the lowest pressure contour intervals. The map shows that the highest gravity values indicate the lowest likelihood of future events, based on the reasonable assumption that there has been little or no change in gravity conditions during the past 3 Ma.

Although the Lunar Crater and Reveille fields also fit a spatial model based on a bivariate Gaussian field shape, the lithostatic pressure maps for those areas show volcanic events distributed throughout a range of lithostatic pressure contours. Although the event location and

lithostatic pressure data do not correlate well for the Lunar Crater and Reveille fields, those areas may not be good analogs to the Yucca Mountain region. The much higher number of events in those fields suggests higher magma pressures and volumes than in the YMR. Tectonic conditions also may differ. The apparent lack of correlation with lithostatic pressure also could mean that there are many buried/unrecognized anomalies in the Lunar Crater and Reveille fields.

I developed two probability distributions to combine lithostatic pressure data with the bivariate Gaussian field shape. Figure D.6-13 illustrates my assessment of the likely values of lithostatic pressure at a point in the region where a future event is assumed to occur. This distribution was developed first by considering the lithostatic pressure values at the locations of observed events. This coarse distribution was then smoothed, and the tails of the distribution were considered in light of available information. Very high values of pressure, such as those beneath Bare Mountain, are consistent with an event probability of zero, because there are no observed events in those areas. Because somewhat lower values are associated with no observed events in the YMR, but with observed events in the Lunar Crater and Reveille fields, the tail of the distribution is shaped to allow for the low probability of events occurring at those values. For the likely values of lithostatic pressure at a point in the region of interest where a future event is assumed not to occur, I use the background distribution directly—that is, the distribution of lithostatic pressure across the region of interest. These two distributions should be used together to develop a conditional spatial intensity based on lithostatic pressure, which will be combined with the conditional spatial intensity from the bivariate Gaussian model.

After reviewing the predicted spatial intensity of events for various weighted combinations of bivariate Gaussian field shape and lithostatic pressure, I believe relative weights 0.75 (bivariate Gaussian) and 0.25 (lithostatic pressure) are appropriate for this general spatial model.

After considering the spatial intensity distributions in the region of interest derived from the two models and comparing those with the pattern of observed events, I believe the bivariate Gaussian field shape modified by lithostatic pressure provides a better assessment of the spatial distribution of potential future events than does the bivariate Gaussian alone. Thus, I assign the combined model a weight of 2/3.

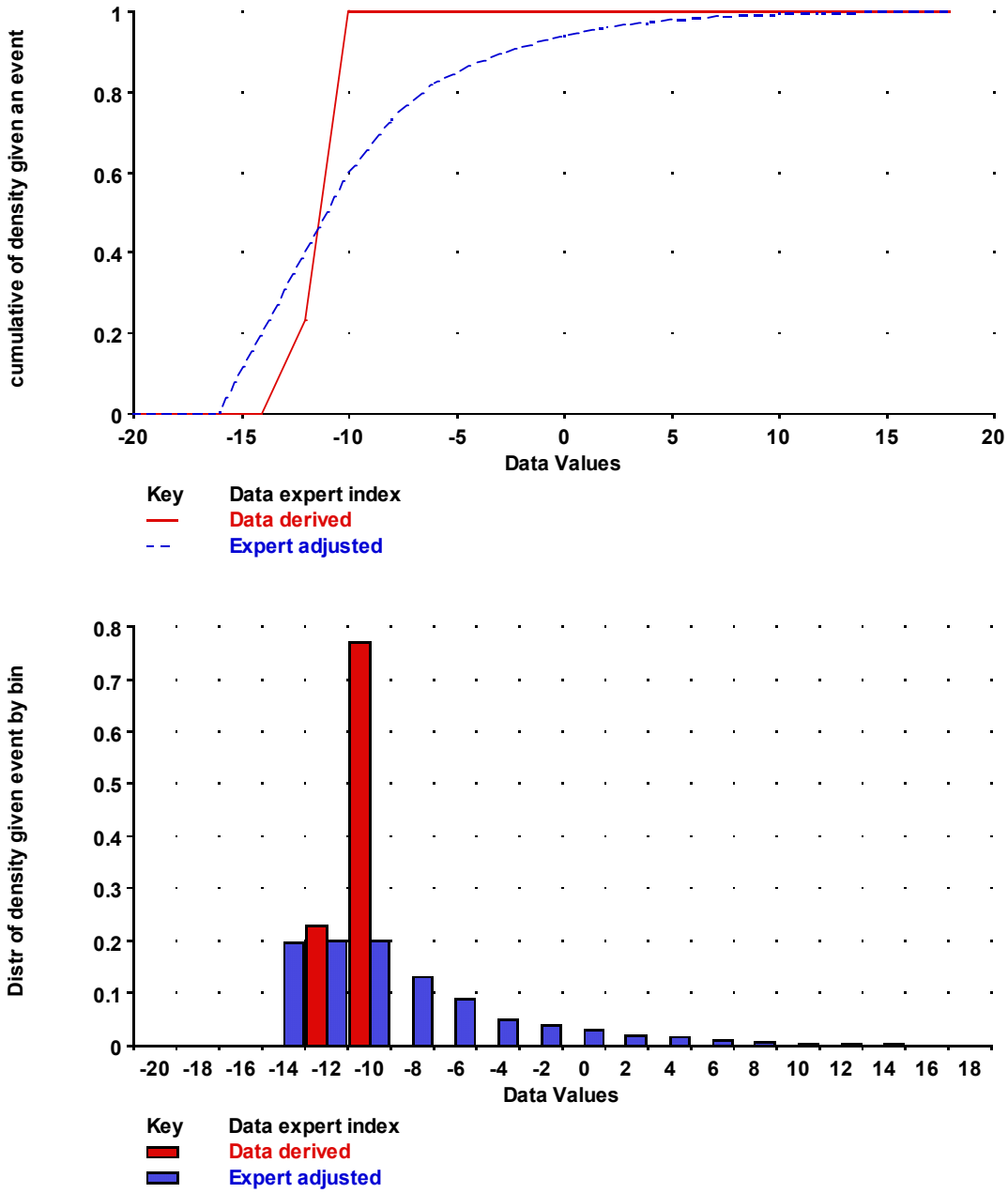

NOTE: Red bars/lines represent the values at the location of past events in the region of interest; blue bars/lines represent the assessment of the probable values at the location of a future event.

Figure D.6-13. Probability Distribution for Lithostatic Pressure at a Hypothetical Location in the Region of Interest Where an Event Is Assumed to Occur

D.6.2.3 Additional Data

Data regarding extension in Crater Flat may be useful in estimating the spatial distribution of potential future events. Structural control of volcanism probably operates in the region, and faulting provides an excellent indicator of structural control. In the absence of other data, information on fault locations is valuable, as zones of faulting reflect thinning of the crust, which are favorable zones for volcanism. The interpretive map of the estimated cumulative percent of extension in Crater Flat (Fridrich et al., 1999, Figure 5) correlates well with volcanic events in Crater Flat, because all events are associated with areas that have experienced at least 50 percent cumulative extension. The data, however, are of limited use because: (1) they are less useful than a detailed map showing all faults and their displacements; (2) they are difficult to reproduce because there are no direct indicators of displacement within Crater Flat; and (3) they cover a very small part of the region of interest. For those reasons, and because the lithostatic pressure data indicate some of the same focusing effects for magma rise that extension data might provide, I elected not to use the available extension data directly in my spatial model.

D.6.3 TEMPORAL MODEL

My temporal approach has two components: an estimated recurrence rate for events within the Crater Flat volcanic field, and an estimated background rate for events in the region of interest but outside the influence of that field.

To estimate a recurrence rate for events within the Crater Flat volcanic field, I apply two alternative models: (1) a homogeneous Poisson model for average recurrence, and (2) a cluster/episodic model.

D.6.3.1 Homogeneous Poisson Model

The recurrence rate is calculated based on the number of events in the region of interest during the period of interest, which I define as all the events listed in Table D.6-1. Alternative characterizations of past events lead to slightly different estimated recurrence rates, a factor that contributes to overall uncertainty in the rate.

D.6.3.2 Clustered/Episodic Model

Volcanic activity can be cyclic—magma can ascend but then be stored before it erupts (for instance, the Long Valley area in eastern California in the 1980s). Once the driving factor is released in a period of volcanism, a period of stability will follow. Evidence indicates that magma volume in the YMR is decreasing. Volcanism has been occurring for 11 Ma, however, so another 1 My of volcanic activity is possible. To address this phenomenon, I use a temporal model wherein events are assumed to occur in clusters.

This model assumes that clusters arrive according to a Poisson process having a rate of λ_c, which can be estimated from past clusters. It further assumes that within a cluster, events arrive according to a Poisson process having a higher rate of λ_w. The within-cluster rate can be estimated from the number of events in past clusters and an assessment of the duration of a cluster.

In Table D.6-3, I identify four temporal clusters of volcanoes in the YMR that are relevant to estimating the recurrence rate within the influence of the Crater Flat field.

Table D.6-3. Temporal Clusters in the YMR

Group	Age Range	Number of Events in Cluster
1	~4.8 Ma	2 (Anomalies C and D)
2	3.8 to 3.9 Ma	3 to 7 (1 to 3 SE Crater Flat events; Anomalies B, F, G, and H)
3	1.1 to 0.78 Ma	2 to 5 (Quaternary Crater Flat cones)
4	0.077 Ma	1 (Lathrop Wells)

Cluster duration could be as long as about 300 ky, based on the ages and age-dating uncertainty in Quaternary Crater Flat. Little Cones is considered to have occurred at the end of the 1-Ma Crater Flat cluster, and could be as much as 300 ka younger than Red Cone and Black Cone. My assessment of the maximum duration of a cluster is therefore 300 ky. My best estimate of the duration of a cluster is about 150 ky, based on the uncertainty in the age dates for events within each of the clusters identified above. This length of time represents the median of my distribution on cluster duration.

The singular occurrence of the Lathrop Wells event raises the question of whether a "single-event cluster" is possible, and if so, whether Lathrop Wells represents a complete cluster or the first event within a new cluster. The time since Lathrop Wells erupted (80 ka) is long compared to the average time for event recurrence within the other three clusters (~50 ka), which suggests that Lathrop Wells could represent a single-event cluster. In addition, the single event at Buckboard Mesa at 2.87 Ma indicates that single-event clusters have occurred in the region. My assessment is that there is about a 20% chance that a cluster has duration of zero—that is, that a single-event cluster occurs. My assessment of the duration of a cluster is illustrated in Figure D.6-14.

There are, of course, few data with which to estimate the parameters for either of the temporal models described above. Because the sparse data are a concern in the temporal clustering model, I have less confidence in that model than in the homogenous Poisson model. Accordingly, I weight the homogeneous Poisson model higher (0.75) than the clustered/episodic model (0.25).

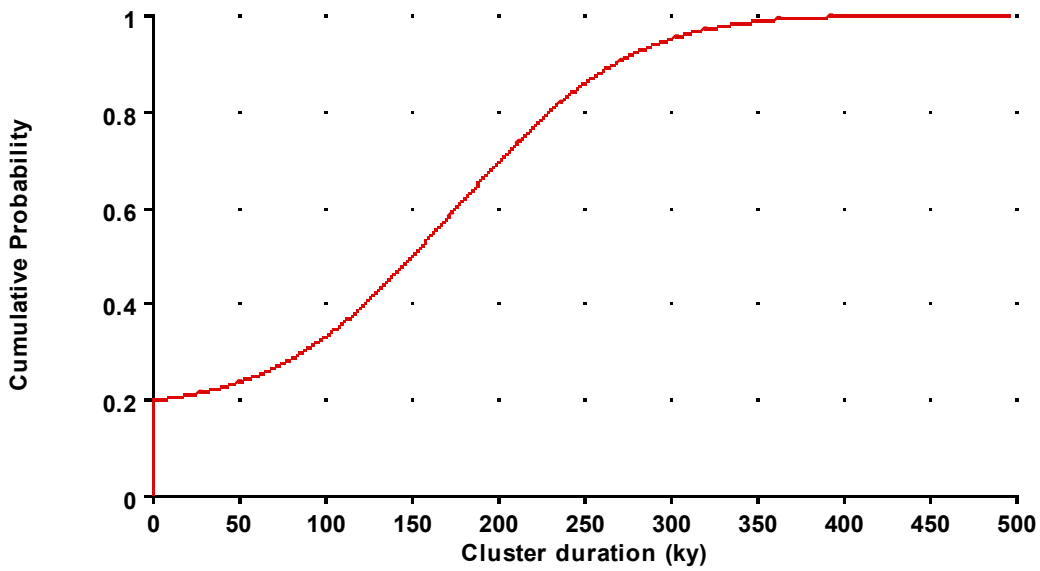

NOTE: Duration of zero implies a single-event cluster.

Figure D.6-14. Assessment of the Duration of a Temporal Cluster

D.6.3.3 Background Rate outside the Influence of Crater Flat Field

Both my models require establishing a recurrence rate for events that are not within the Crater Flat field, as a future igneous event possibly could occur anywhere in the region. To estimate this background rate, I defined a large region in the western Great Basin, as illustrated in Figure D.6-15, then calculated the average event rate throughout that region. This region, which is centered on Yucca Mountain, deliberately excludes the high-density, high-rate areas of the region, as those represent volcanic fields rather than background areas. Table D.6-4 lists the single events in this background zone, which has an area of 79,423 km^2. The resulting estimate gives a mean recurrence rate of about 5×10^{-11} events per year per km^2 outside Crater Flat field.

Table D.6-4. Post-1.5-Ma Events in the Background Region

Location	Number of Cones
Clayton Valley	1
Ubehebe	1
Split Cone	1
Hidden Cone	1
Little Black Peak	1
Total	*5*

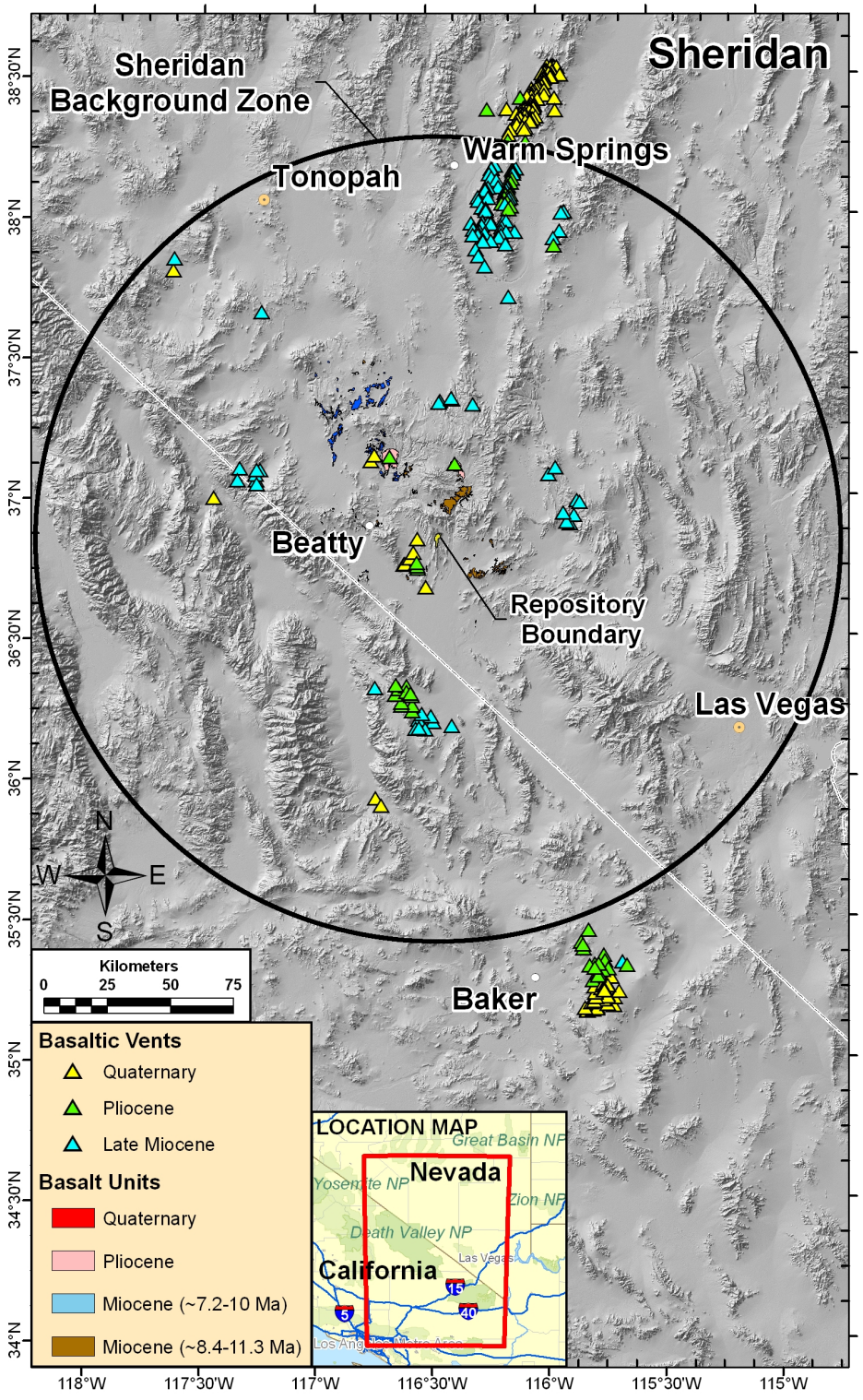

NOTE: Yellow triangles include events < 1.5 Ma counted in background zones.

Figure D.6-15. Background Region

D.6.4 REFERENCES

Barmin, A.A., Melnik, O., and Sparks, R.S.J., 2002, Periodic behavior in lava dome eruptions: Earth and Planetary Science Letters, vol. 199 (1-2), p.173-184.

Fridrich, C.J., Whitney, J.W., Hudson, M.R., and Crowe, B.M.,1999, Space-time patterns of late Cenozoic extension, vertical axis rotation, and volcanism in the Crater Flat basin, southwest Nevada, in Wright, L.A., and Troxel, B.W. (eds.), Cenozoic Basins of the Death Valley Region: Boulder, Colorado, Geological Society of America Special Paper 333.

Kazahaya, K., Shinohara, H., and Saito, G., 2002, Degassing process of Satsuma-Iwojima volcano, Japan—supply of volatile components from a deep magma chamber: Earth, Planets and Space, vol. 54, p. 327–335.

Keating, G.N., Valentine, G.A., Krier, D.J., and Perry, F.V., 2008, Shallow plumbing systems for small-volume basaltic volcanoes: Bulletin of Volcanology, v. 70, pp. 563-582, DOI 10.1007/s00445-007-0154-1.

Los Alamos National Laboratory (LANL), 2007, Ar/Ar age determinations, volume, location and elevation of Plio/Pleistocene volcanoes in the Yucca Mountain region, Rev. 3: Excel spreadsheet titled: Volcano_volume_age_location_Rev03.xls; prepared for PVHA-U.

Melnik, O., Barmin, A.A., and Sparks, R.S.J., 2005, Dynamics of magma flow inside volcanic conduits with bubble overpressure build up and gas loss through permeable magma: Journal of Volcanology and Geothermal Research, vol. 143 (1-3), p. 53-68.

Valentine, G.A., and Krogh, K.E.C., 2006, Emplacement of shallow dikes and sills beneath a small basaltic volcanic center—the role of pre-existing structure (Paiute Ridge, southern Nevada, USA): Earth and Planetary Science Letters, v. 246, p. 217-230.

Valentine, G.A., and Perry, F.V., 2006, Decreasing magmatic footprints of individual volcanoes in a waning basaltic field: Geophysical Research Letters, v. 33, no.14, p. L14305.

Valentine, G.A., Perry, F.V., Krier, D., Keating, G.N., Kelley, R.E., and Cogbill, A.H., 2006, Small-volume basaltic volcanoes; eruptive products and processes, and post-eruptive geomorphic evolution in Crater Flat (Pleistocene), southern Nevada: Geological Society of America Bulletin, v. 118, p. 1313-1330. DOI 10.1120/B25956.1.

Wilson, L., Sparks, R.S.J., and Walker, G.P.L., 1980, Explosive volcanic eruptions IV—The control of magma properties and conduit geometry on eruption column behaviour: Geophysical Journal International, vol. 63, no. 1, p. 117-148.

D.7 FRANK J. SPERA'S ELICITATION SUMMARY FOR PVHA-U PROJECT

Two types of igneous events are identified as having the potential to disrupt the Yucca Mountain radioactive waste repository: an igneous intrusion into the repository, or a conduit passing through it. The probability that either type of event would disrupt the repository is a function of the spatial and temporal distribution of volcanism in the area and the physical geometry of each type of event. These factors, and the relationships among them, are illustrated in Figure D.7-1. Models and assessments of the geometry of dikes, dike systems, sills, and conduits are summarized after Section D.7.1 below, followed by models and assessments of the spatial and temporal distributions of igneous events.

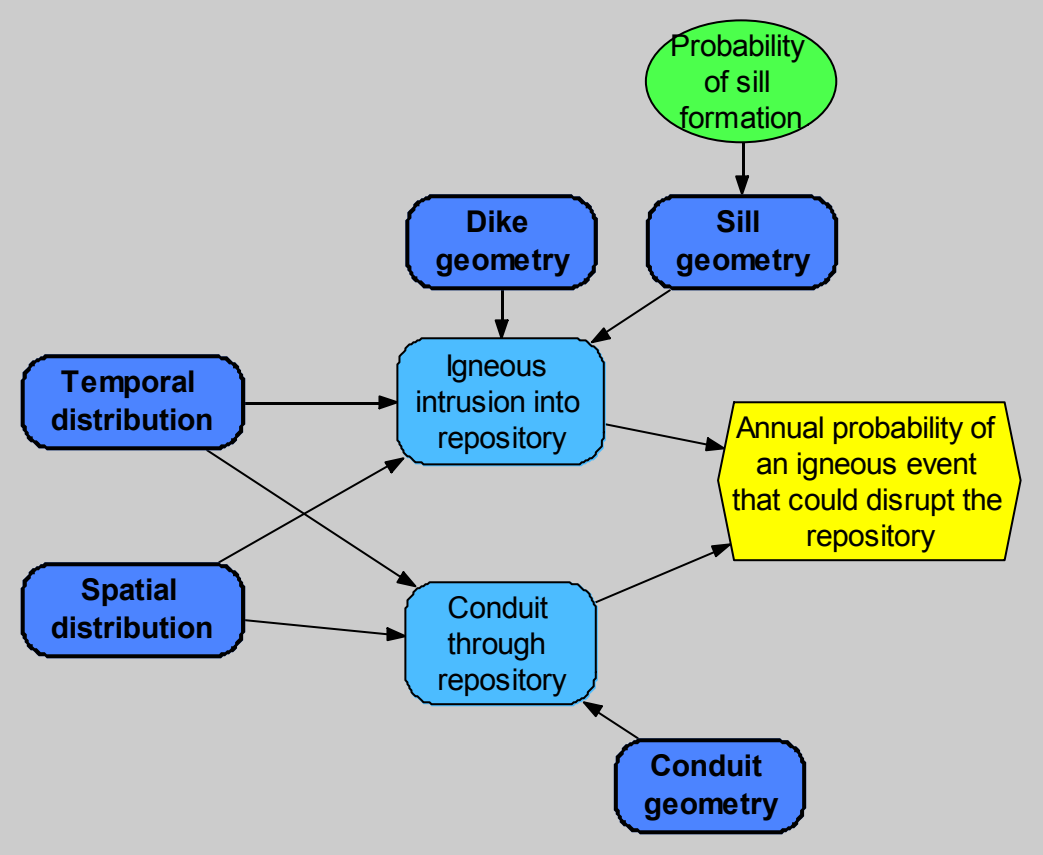

NOTE: The yellow hexagon represents the final result of the assessment. Dark blue rounded rectangles represent sub-models; light blue nodes represent values calculated from other inputs; the green oval represents an uncertain input for which an assessment has been made; and arrows indicate influence of one variable on one or more others.

Figure D.7-1. Influence Diagram Illustrating the Overall Structure of the Model

D.7.1 EVENT DEFINITION

An event is defined as a temporally distinct batch of magma that reaches within 300 m of the ground surface. An event can be defined temporally within the uncertainty of geochronological dating, typically about 50,000 years (5 percent of a million years) for the alkali basaltic rocks typical of the Yucca Mountain region (YMR, defined as the region within a radius of about

50 km centered on Yucca Mountain). Note that most small-volume alkali basalt eruptions that have occurred in extensional terrains are complex-compound events that take place on time scales measured in days to weeks or months. Geochronology generally cannot distinguish or break out these short time intervals.

A propagating crack filled with magma of the type most relevant to a potential future eruption near Yucca Mountain (alkali basalt magma) would originate at a depth of 60 to 120 km. This depth of origin is great compared to the distance of 0.3 km between the repository and the surface, suggesting that a dike, if it reached repository level, likely would continue to propagate upward to the surface. Other factors that would influence the continued propagation of a dike in the upper few hundred meters of the shallow subsurface, and that are considered in my assessment, include the influence of the free surface on the shallow local stress field, the spatial density of fractures in the shallow crust, the concept of dike capture, and the volatile content of magma. Saturation of magma by volatiles occurs at depths between 2 and 4 km, if the volatiles (primarily H_2O) exsolved from rising melt are not separated from the magmatic mixture of volatile-saturated melt plus the coexisting supercritical fluid phase. This depth is well below the 0.3-km depth of the repository. Thus, any dike that reaches repository depth is assumed to reach the surface, unless it becomes arrested and develops a sill. The potential for a sill to develop at repository depth is discussed below.

D.7.1.1 Characterization of Past Events

My assessment of possible future events in the YMR is based in part on the characterization of past events in the region. Table D.7-1 identifies events within my region of interest and gives the estimated age, eruptive volume, breakdown of event count, and additional pertinent comments related to each volcanic center. These events form the primary basis for my estimates of event geometries. The names of the locations of events reflect well-known geographic names used formally and informally on geologic and geographic maps of the region. Each province is associated with a number of events. Where the number of events is uncertain, I have assigned probabilities to various numbers of events. Events within the region of interest that are deemed applicable are less than 5 Ma in age.

Table D.7-1. Relevant Volcanic Events in the Region of Interest

Province (Sub-province or Cone)	Age* (ka; span ±2σ)	Volume* (km^3)	Event Count	Composition; Eruptive Style
Anomalies C and D	4,200 to 5,800 (see text)	0.19	0: C and D are irrelevant (weight: 0.2) 1 (weight: 0.8)	
Thirsty Mountain[1]	4,630 ±60	2.63	1 super-event[2]	Basaltic trachyandesite; fissure/shield eruptions
Pliocene SE Crater Flat (PSECF)	3,800 ±60	0.59	1 super-event[3]	Basalt; low shield/fissure eruptions
Anomalies F,G, and H [Pliocene Amargosa Desert West (PADW)]	3,910 ±220	0.06	1 super-event[4]	Trachybasalt; fissure? eruption; localized tephra along fissure; one to three vents?
Anomaly B Pliocene Amargosa Desert East (PADE)	3,850 ±50	1.2	1 event[5]	Basaltic lava flow?
Buckboard Mesa	2,870 ±120	0.84	1 super-event	Basaltic trachyandesite
Quaternary Crater Flat	Range over 5 cones	Total V = 0.15	1 to 5 events; most likely 4 or 5 separate events (see text for further discussion)	Trachybasalt
Makani Cone	1,090 ±30	0.002		
Black Cone	1,070 ±12	0.06		
Red Cone	1,070 ±20	0.055		
SW Little Cone	950 ±150	0.02		
NE Little Cone	950 ±150	0.014		
Hidden Cone	350 ±30	0.032	1 event	Basalt to trachybasalt
Little Black Peak	350 ±30	0.014	1 event	Basalt to trachybasalt
Lathrop Wells	77 ± 0.012	0.14	1 event	Basalt

* Age and volume estimates are based on consideration of Los Alamos National Laboratory (LANL) (2007).

[1] A single main fissure feeds this shield trachyandesite province; fissure length ~5 km

[2] The term "super-event" in this context means that this author cannot, on the basis of the exposed geologic record, discern a significant volcanic hiatus during Thirsty Mountain volcanism. This fact does not mean that the eruption was continuous; there could have been several or even many pulses. There is no way, however, to know unambiguously the fine temporal-scale sequence of events. From analog studies, a minimum mean volumetric eruption rate of 1 m^3/s implies that the entire eruptive volume of Thirsty Mesa basaltic trachyandesite could have been emplaced in less than a century. Because this interval is well within the uncertainty of radiometric ages, the author considers Thirsty Mountain a single super-event.

[3] The term "super-event" in this context means that this author cannot, on the basis of the exposed geologic record, discern temporally discrete events or a significant temporal hiatus during PSECF volcanism. This fact does not mean that the eruption was continuous; there could have been several or even many pulses. There is no way, however, to know unambiguously the fine temporal-scale sequence of events. From analog studies, a minimum mean volumetric eruption rate of ~1 m^3/s probably is roughly applicable. This rate implies that the entire eruptive volume of PSECF basaltic volcanism could have been emplaced in less than two decades. Because this interval is well within the uncertainty of radiometric ages, the author considers PSECF a single super-event. Minimum volumes are used for consistency. Based on worldwide values, these could be two times larger (combination of tephra and basalt).

[4] The term "super-event" in this context means that this author cannot, on the basis of the geologic record and available drilling and radiometric data, discern temporally discrete events or a significant temporal hiatus during PADW volcanism. Each magnetic anomaly is considered either a buried volcanic cone or simply a thickened part of a buried lava flow or a thickened pile of cinder along a NNE fissure defined by the linear arrangement of magnetic anomalies. From analog studies, a minimum mean volumetric eruption rate of ~0.5 m^3/s is roughly applicable. This rate implies that the entire eruptive volume of PADW volcanism could have been emplaced in less than a decade. Because this interval is well within the uncertainty of radiometric ages, the author considers PADW a single super-event.

[5] Given the absence of constraints, the author assumes this to be a single event.

The number of events represented by the Quaternary Crater Flat cones is uncertain. The source of this uncertainty is the inability to date events by geochronologic means to a precision commensurate with "eye-witness" volcanologic time scales. Even a relatively simple small-volume alkali basalt eruption (such as Black Cone or Lathrop Wells) is a complex-compound event that can exhibit hour-by-hour to minute-by-minute variations in eruptive style. Although the events of interest occurred several tens to hundreds of kiloyears in the past, geochronology provides a resolution that is measured in centuries to millennia. Based on these (and additional) considerations, I made the following assessments. The Little Cones are considered to have formed during either one or two separate events that are independent of the events that formed the other Quaternary cones in Crater Flat. The Little Cones basalts show a trace element composition that differs significantly from the compositions of Red Cone, Black Cone, and Makani Cone. In addition, geochronologic data (Ar-Ar and K-Ar), although not robustly conclusive, hint that Little Cones may be younger than Black Cone, Red Cone, and Makani Cone. The Sr and Nd isotopic composition of Black Cone, Red Cone, and Makani Cone are essentially coincident but differ from Little Cones in that Little Cones is considerably more radiogenic with respect to Sr. This indicates a distinctive mantle source, although no constraint of relative spatial location of the source can be inferred. Although Makani Cone, Black Cone, and Red Cone are aligned, I do not think that these eruptive centers are necessarily connected along a single fracture. The alignment of cones may be related instead to the orientation of the stress field at ~1 Ma. The prevailing stress field at ~1 Ma most probably is reflected in the orientation of the Crater Flat volcanic corridor itself.

Although I believe it unlikely, I allow for the possibility that all five cones in Quaternary Crater Flat represent a single event (probability = 0.05). If the cones represent separate events, my assessment is that Little Cones comprise one event (probability = 0.6) or two events (probability = 0.4), and that Red Cone, Black Cone, and Makani Cone represent either three, two, or one events, to which I assign probabilities of 0.65, 0.1, and 0.25, respectively. Combined, these judgments lead to the following characterization of the number of events represented by the Quaternary Crater Flat cones:

- One event: probability = 0.05.
- Two events (Little Cones, combination of Red Cone, Black Cone, and Makani Cone): probability = 0.14.
- Three events (Little Cones, combination of Red Cone and Black Cone, and Makani Cone): probability = 0.06.
- Four events (Little Cones, Red Cone, Black Cone, and Makani Cone): probability = 0.37.
- Five events (Little Cones SW, Little Cones NE, Red Cone, Black Cone, and Makani Cone): probability = 0.38.

The ages of Anomalies C and D are estimated to be 4.2 to 5.8 Ma, which straddles the temporal period I consider relevant, <5 Ma old. Hence I include these anomalies in my models as a single event having an 80% weight and as "no event" having a probability of 20%.

D.7.1.2 Event Characteristics and Geometry

The following sections describe my assessments of the characteristics of possible future events in the YMR. The features of potential dikes, sills, and conduits are discussed, along with potential effects of the repository openings.

Dike Geometry

Dike geometry is characterized by estimates of dike length, width, and azimuth, as well as by the number and spacing of dikes in a multi-dike system, as illustrated in Figure D.7-2. Several of these factors depend on or are functions of other variables given in the figure and described below. Figure D.7-2 also illustrates factors related to sill formation and geometry, which affect the probability of an igneous intrusion into the repository.

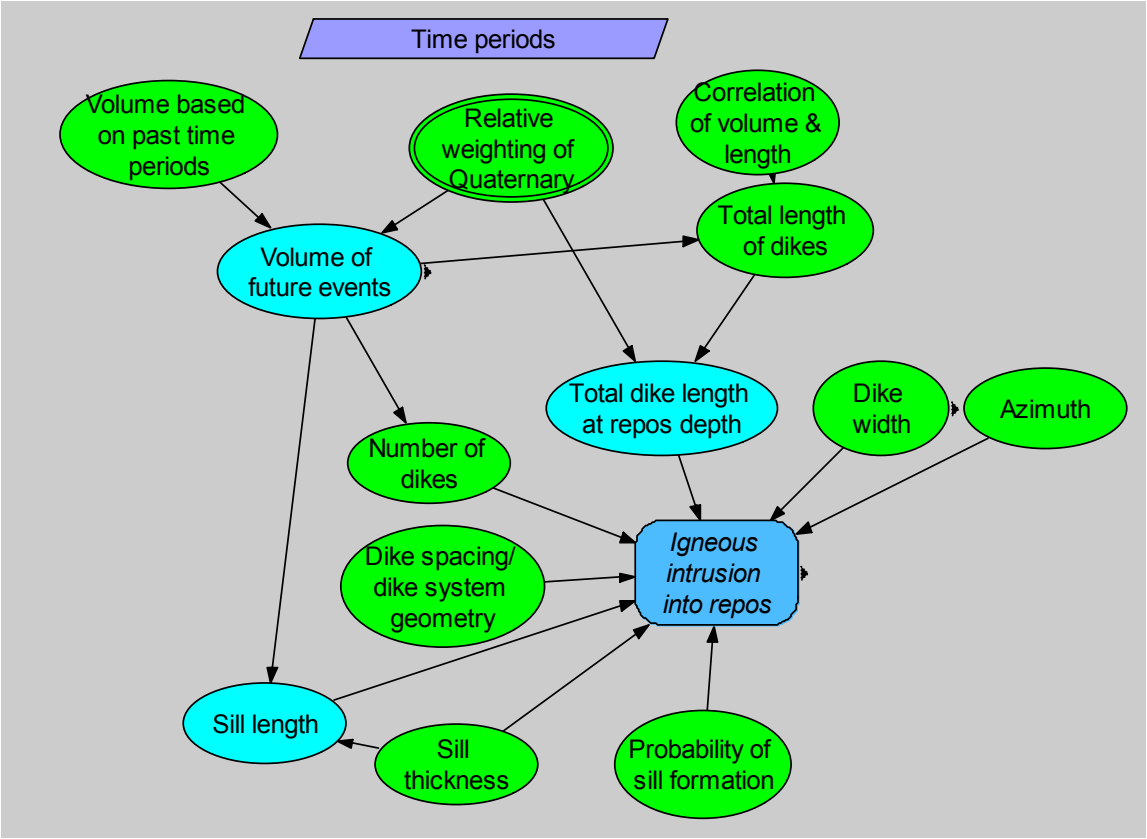

NOTE: Green nodes represent assessed variables; blue nodes represent values calculated from other variables.

Figure D.7-2. Components of the Model for Dike and Sill Geometry

Volume. Several event characteristics are a function of the eruptive volume of magma; that is, larger-volume events generally produce longer and/or a larger number of dikes. The volume of future events is estimated based on events from two periods: (1) Quaternary events, and (2) Pliocene events. Table D.7-1 identifies those events within my region of interest and gives the estimated age and volume of each.

I consider Quaternary events to be more relevant than Pliocene events for estimating the volumes of future events. The final volume assessments used for my models therefore are based on a combination of my assessments of the volume based on Quaternary events (weighted 0.85) and the volume based on Pliocene events (weighted 0.15). These probabilities reflect my assessment that events having low eruptive volumes—more similar to previous Quaternary than Pliocene events—are more likely to occur in the next 10 to 1,000 ky near Yucca Mountain.

If volumes of only Quaternary eruptions are used to estimate volumes of potential future events, my assessment of the volume of a future event ranges from 0.005 km^3 (10th percentile of my uncertainty distribution) to 0.2 km^3 (95th percentile). The mode for the distribution is 0.05 km^3, and the upper bound about 1 km^3. If volumes of only Pliocene eruptions are used to estimate volumes of potential future events, my estimates would be greater by about a factor of 10.

Figure D.7-3, which illustrates the weighted combination of these event volumes, represents my assessment of the volumes of potential future events. This distribution has the following characteristics: a mean value of 0.15 km^3, a median value of 0.057 km^3, and a 5th to 95th percentile range of 0.004 to 0.7 km^3. The mean of this distribution is about the same as the observed volume of all the Quaternary Crater Flat cones, while the median is on the high end of the observed Quaternary volumes for my preferred characterization of past events. Volume estimates provided by Los Alamos National Laboratory (LANL) for Quaternary cones (LANL 2007) do not include volumes of the original tephra sheets, so the actual volumes of magma erupted likely were higher than indicated. Thus, I am satisfied with the distribution on future event volumes I have described here.

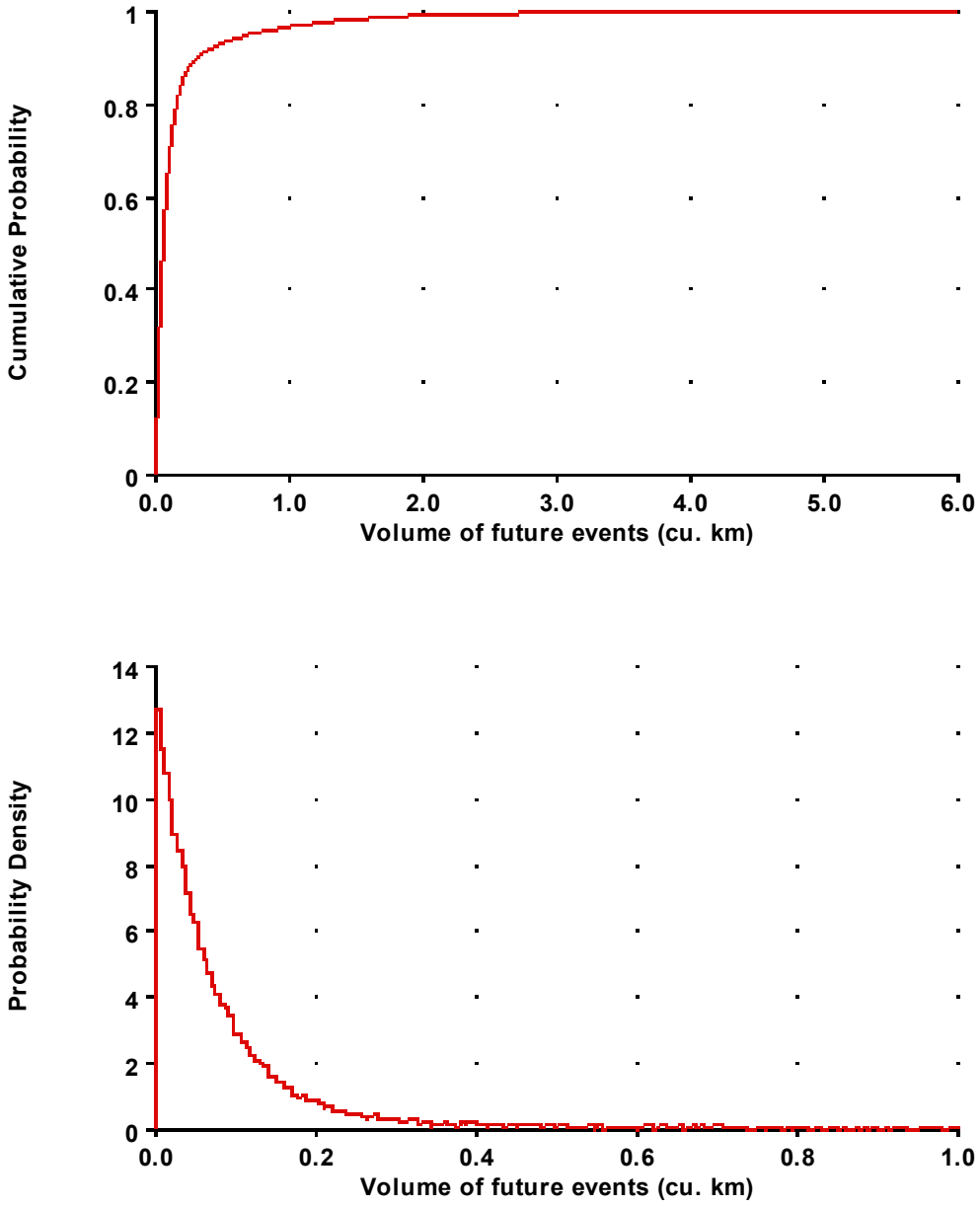

NOTE: Top graph is a cumulative distribution function; bottom graph is a probability density function. (Note change in scale along the x-axis between the two representations.)

Figure D.7-3. Assessment of the Volume of Future Events

My assessment of the volume of potential future events is the same for the 10-ky and 1-My periods. The predominant mode or style of volcanic eruption in the Yucca Mountain vicinity has been roughly constant throughout at least the past one million years, as represented by the Quaternary cones and flows in Crater Flat and at Lathrop Wells. I can present no technical basis to suppose that activity in the next 10 ky will be any different than during the next 1,000 ky.

Total Dike Length. Lengths of potential future dikes will be similar to those associated with Quaternary-Pliocene (5 Ma and younger) volcanism observed in the Yucca Mountain region. Dikes may occur as multiple sub-parallel dikes having cumulative total lengths characterized by the probability distributions developed in this section. The number and geometry of multiple dikes are discussed in the following section.

As with my assessment of the volume of potential future events, my assessment of the total length of dikes in a future event is a weighted combination of my assessments of (1) the length of dikes systems in Quaternary events (weighted 0.85) and (2) the length of dike systems in Pliocene events (weighted 0.15).

Based on the estimated volumes of Quaternary events, I would expect a possible future dike to occur in one or two segments, for a total dike length of about 1 to 2 km. Event volume and dike length are highly correlated: larger-volume events are associated with longer total dike lengths. An observed correlation between eruptive volume and cumulative fissure or dike length is noted by many volcanologists for many volcanic systems in several different tectonic environments. My estimate is that the correlation coefficient between event volume and total dike length is about 0.8.

As a first-order assessment, dike length at repository depth would be the same as fissure length at the surface, given that the 300 m between the repository and ground surface is short relative to the 60- to 70-km depth at which magma originates. The influence of a free surface is neglected in this correlation, because uncertainties are likely to swamp the actual effects.

Based on the analog of Lathrop Wells, the expected fissure length of Quaternary cones is about 1 km, with a very tight distribution around this length. The Quaternary cones in Crater Flat likely did not erupt within a short (say, 100-year) period; thus, it is unlikely that they are associated with a single fissure. Given the known differences in chemical composition among the cones, however, a fissure length of 11 km (the measured distance between Makani Cone and Little Cones) is possible, but unlikely. Further, it appears that Black Cone and Makani Cone are associated with north-south faults, rather than the northeasterly trend defined by the volcanic (topographic) landforms.

Based on the Quaternary data and estimated volumes, lengths of potential future dikes are assessed to be from 0.5 km (representing the 10th percentile of my distribution) to 10 km (representing about the 99.9th percentile). The most likely dike length is about 1.5 km.

Pliocene events in the YMR include (1) geomagnetic Anomalies C and D, which are assumed to be buried basaltic volcanics (lava plus tephra) of an estimated age of 5,800 to 4,200 ka; (2) the flows at Thirsty Mountain (4,630 ka); (3) the Pliocene Crater Flat basalts (3,800 ka); (4) geomagnetic Anomalies G, H, and F (3,900 ka); (5) geomagnetic Anomaly B (3,800 ka); and

finally (6) the basalts of Buckboard Mesa (2,800 ka). The measured fissure length of the Pliocene (3.8 Ma) southeast Crater Flat basalts (estimated volume 0.59 km^3) is 3.5 km. Relative to the Pliocene Crater Flat volcanic activity, Anomaly B likely has a similar or longer fissure length based on a sub-similar volume estimate of about 1.2 km^3. Note that the inferred area of Anomaly B is roughly equal to that of the Pliocene Crater Flat basalts. A single combined measured fissure length of 4 km can be assumed for Anomalies F, G, and H. If each anomaly represents a separate event, the fissure length of each is about 1 km. The estimated volume of the combined Anomalies F, G, and H is about 0.1 km^3, about 10 times smaller than the volume of the Pliocene southeast Crater Flat basalts. The maximum measured fissure length of 5 km at Paiute Ridge is considered to approach the upper end of the range of fissure lengths for Pliocene events.

The distribution of dike lengths based on Pliocene events, then, is similar to that for dike lengths based on Quaternary events, but shifted by 1 km. That is, the distribution for Pliocene events has a mode of 2.5 km, shifted from 1.5 km for the Quaternary distribution.

Figure D.7-4 illustrates my final assessment of the lengths of dikes for potential future events, based on the weighted combination of the two assessments described above.

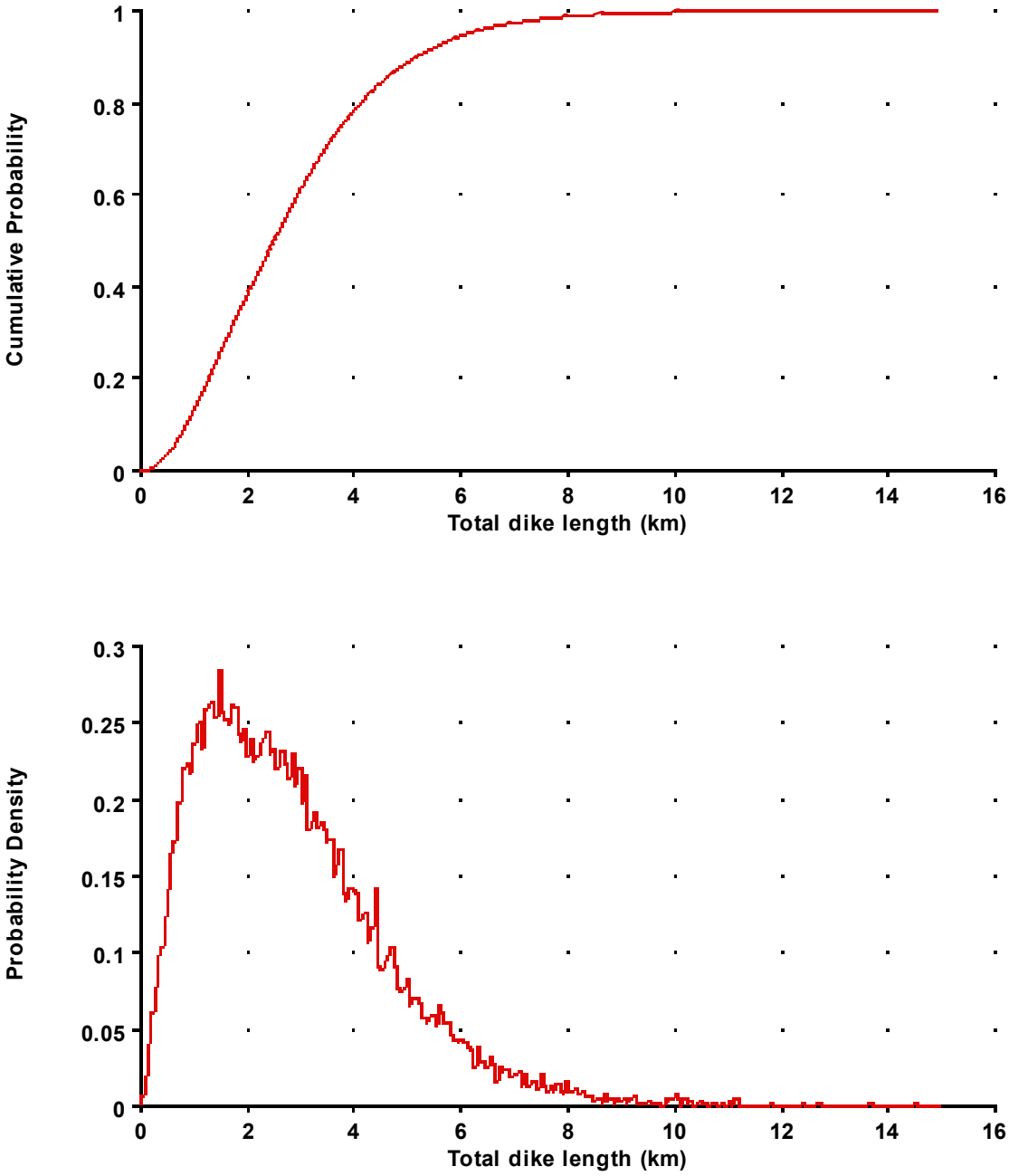

NOTE: The apparent roughness of the bottom curve is a function of the simulation process.

Figure D.7-4. Assessment of the Total Length (at repository depth) of Dikes in a Potential Future Event

Multiple Sub-parallel Dikes. Formation of multiple sub-parallel dikes is controlled by the ambient state of stress of the host crustal rocks, the thermo-physical properties of the wall rock, rock heterogeneity, and magma properties. These factors, which are unique to each region, are too poorly understood to make deterministic assessments. Larger volumes of magma more commonly are associated with multiple dikes. Analogs in the YMR provide the best available data: in Crater Flat each cone is associated with a single dike. The three "camptonite" dike segments (near Boulder Dam), which are separated by about 300 m, have a cumulative length of about 4 km (1.5, 1.5, and 1 km). En echelon segments can be separated by as much as 50 m; dikes must be >50 m apart to be considered distinct dikes.

My assessment of the number of dikes associated with a potential future event is partly a function of expected magma volume. For a 0.1-km^3 event, there is a 70% chance of one dike, a 25% chance of two dikes, and a 5% chance of three dikes. The table below documents my assessment of the number of dikes in an event as a function of the volume of that event.

Table D.7-2. Number of Dikes as a Function of Magma Volume

	Magma Volume (km^3)			
Number of Dikes	0.1	0.5	1	2
1	0.7	0.15	0	0
2	0.25	0.3	0.1	0
3	0.05	0.4	0.3	0.1
4	0	0.15	0.4	0.2
5	0	0	0.2	0.35
6	0	0	0	0.2
7	0	0	0	0.1
8	0	0	0	0.05

If an event involves multiple dikes, the total length of dikes in the system is as described above in the section titled "Total Dike Length," and the dike segments should have approximately equal lengths.

The locations of multiple dikes that occur as a single event are defined by an ellipse in which the length of the long axis is equal to the cumulative lengths of the dikes. The ellipse is elongate, having a minimum aspect ratio of 4:1 and a maximum of 12:1, with a uniform distribution between these two values. The aspect ratio for the ellipse is not correlated with volume. Dike segments can occur anywhere on the ellipse, but will have a minimum separation of 50 m.

Dike Width. Estimates of dike width are informed by heat transfer arguments and observations from analog regions. Observations in similar basalt dike systems, including the "camptonite" (Boulder Dam) analog, indicate dike widths of 1 to 2 m. When a dike becomes too narrow, the magma within it crystallizes. This effect occurs at a width of about 0.1 m, which therefore defines minimum dike width. The chemical composition of a system is important—silicic dikes tend to be wider than basaltic dikes. Alkali basalt dikes typically are 1 or 2 m wide, consistent with observations in the YMR.

My assessment of the distribution of dike widths is illustrated in Figure D.7-5. This distribution is characterized by my estimate of a minimum dike width of 0.1 m, a 99th percentile of about 10 m, a median width of about 1 m, and a lognormal shape.

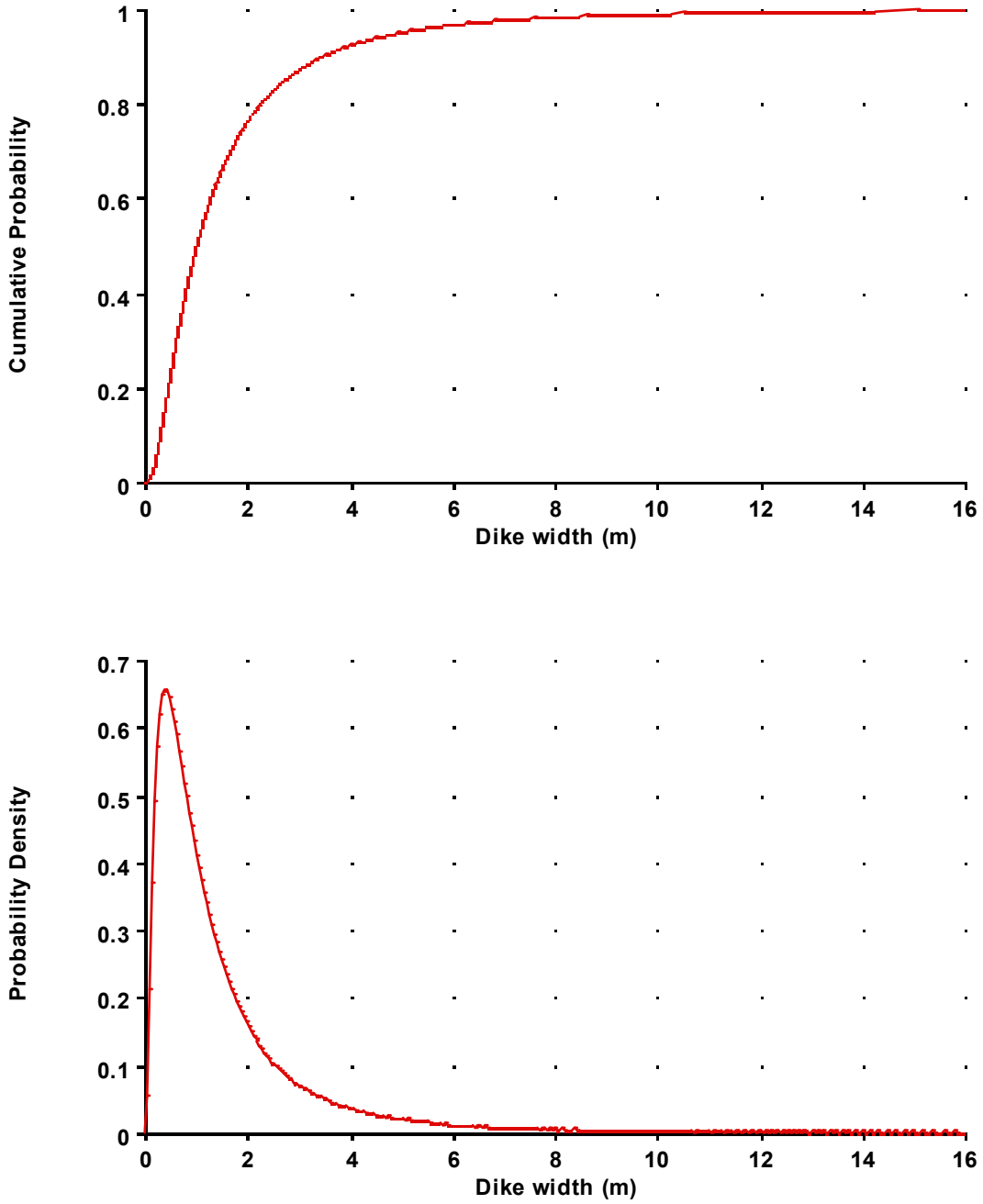

Figure D.7-5. Assessment of the Width of a Potential Dike at Repository Depth

Dike Azimuth. Both the present-day stress field and the distributions of fractures and faults in the YMR must be considered in assessing azimuths of potential future dikes.

The minimum-principal regional stress direction in the YMR is NNE. In an otherwise uniform homogeneous crust, dikes will tend to open perpendicular to this direction but propagate (strike) parallel to this direction. Azimuths of mapped faults and features (e.g., the alignment of Quaternary cones in Crater Flat) inform my estimate of dike azimuth at repository depth. At several locations where dikes can be seen—including the Solitario Canyon dikes and within the Pliocene southeast Crater Flat basalts—they are associated with faults. Most of those structural features trend N-S, and the faults that trend N-S are reported to have steep dips (Dickerson and Drake, 2004, as reported in Perry et al, 2006).

My assessment of dike azimuth weights local stress indicators most heavily. My preferred dike azimuth is N-S +/-30 degrees. My 90% confidence interval for dike azimuths ranges from N30°E to N30°W. This distribution is illustrated in Figure D.7-6.

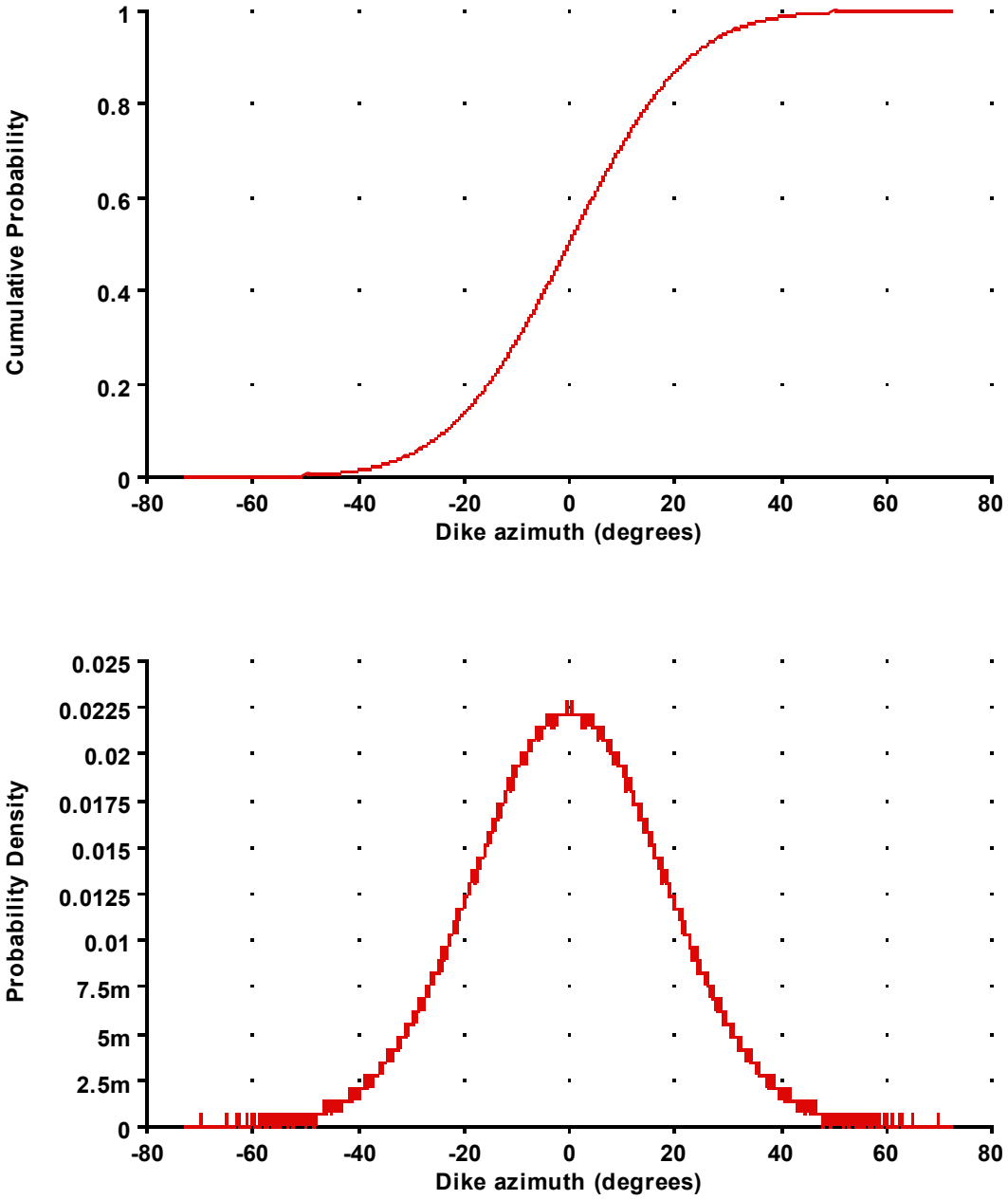

NOTE: Zero represents north. For values less than 0.01 on the y-axis, suffix notation is used (m = 10^{-3} and u = 10^{-6}, so 5m = 0.005).

Figure D.7-6. Assessment of Dike Azimuth at Repository Depth

Characteristics of Sills

Of potential vertically ascending dikes in the YMR, a very few could become sills at repository depth. I define the fraction of dikes that become sills by the term α. The "sill-from-dike" scenario is characterized by assuming that fraction α of dikes at 300 m give birth to a sill. Only one sill is associated with a dike. The presence of a sill, if one exists, does not affect conduit formation (discussed below).

The assessment of α is made considering Paiute Ridge, where sills are associated with lithologic changes that reflect contrasts in the mechanical properties of the wall rock. Such properties may not exist below Yucca Mountain. If they do, sills are more likely to occur.

At the regional scale, σ_3 is approximately horizontal (normal to the acceleration of gravity) and oriented roughly NNE. Given isotropic and homogeneous rock properties and a uniform stress field, α is small, between 0.01 and 0.05. This range is represented by a normal distribution having limits of 0.01 and 0.05, representing the 20th and 80th percentiles, respectively. This analysis assumes that a dike can be represented as an elliptical hole or a mathematical crack in a host rock that is homogeneous and isotropic. Dikes that experience any significant overpressure, $\delta p = p_m - \sigma_3$ (p_m is magma pressure, σ_3 the dike-normal compressive stress, and δp the overpressure), generate high tensile stresses at the dike tip and generally will not become arrested. An arrested dike is a necessary precondition for a sill to form. According to this model, for a dike tip to become arrested and a sill possibly to form (rather than the dike propagating to the surface), the crust must be heterogeneous and anisotropic. That is, there must be a transverse discontinuity or an abrupt change in Young's modulus.

The Tiva Canyon Tuff unit, which is exposed at the surface above the repository site, dips at shallow angles (5° to 10°) to the southeast. The tuffs that underlie the Tiva Canyon Tuff have roughly the same mechanical properties, although variations in Young's modulus could occur even within a single tuff unit. A sequence of bedded Plinian air-fall deposits intercalated with highly welded pyroclastic flow deposits of the same or different lithologic tuff units, for example, could create a stress barrier, variations in Young's modulus, and/or horizontal discontinuities that could act as planes of weakness and horizons where lateral magma injection could take place (that is, a sill could form). Although these factors have been studied elsewhere [for example Gudmundsson (2003) and references therein], I have not made a detailed application to the repository site. Inspection of the Yucca Mountain Project report, *Subsurface Geotechnical Parameters Report* (BSC 2007), however, suggests that variations in Young's modulus do not exceed a factor of 5. This finding suggests that dike arrest by heterogeneous properties might lead to a small α factor.

A final consideration for sill formation is rotation of the principal stress tensor at a depth of 300 m due to transient heating imposed by radioactive decay. Project literature suggests that the effect of heating is to rotate σ_3 and σ_1 such that σ_3 may not remain sub-horizontal (BSC 2004). That is, for example, if σ_1 was to be rotated from its current orientation and become sub-horizontal, σ_3 becomes sub-vertical, and other factors remain the same, sill formation would be enhanced. This effect would tend to increase α. The period of heating will be relatively short-lived, however, and likely would produce no effects within the 10-ky and 1-My periods of interest.

My final assessment of the likelihood of sill formation is as follows. Given a dike at 300 m, the probability of it giving rise to a sill is α, where α is drawn from the distribution illustrated in Figure D.7-7. The most likely (mode) value of the distribution is 0.05, and the 99th percentile value is 0.10.

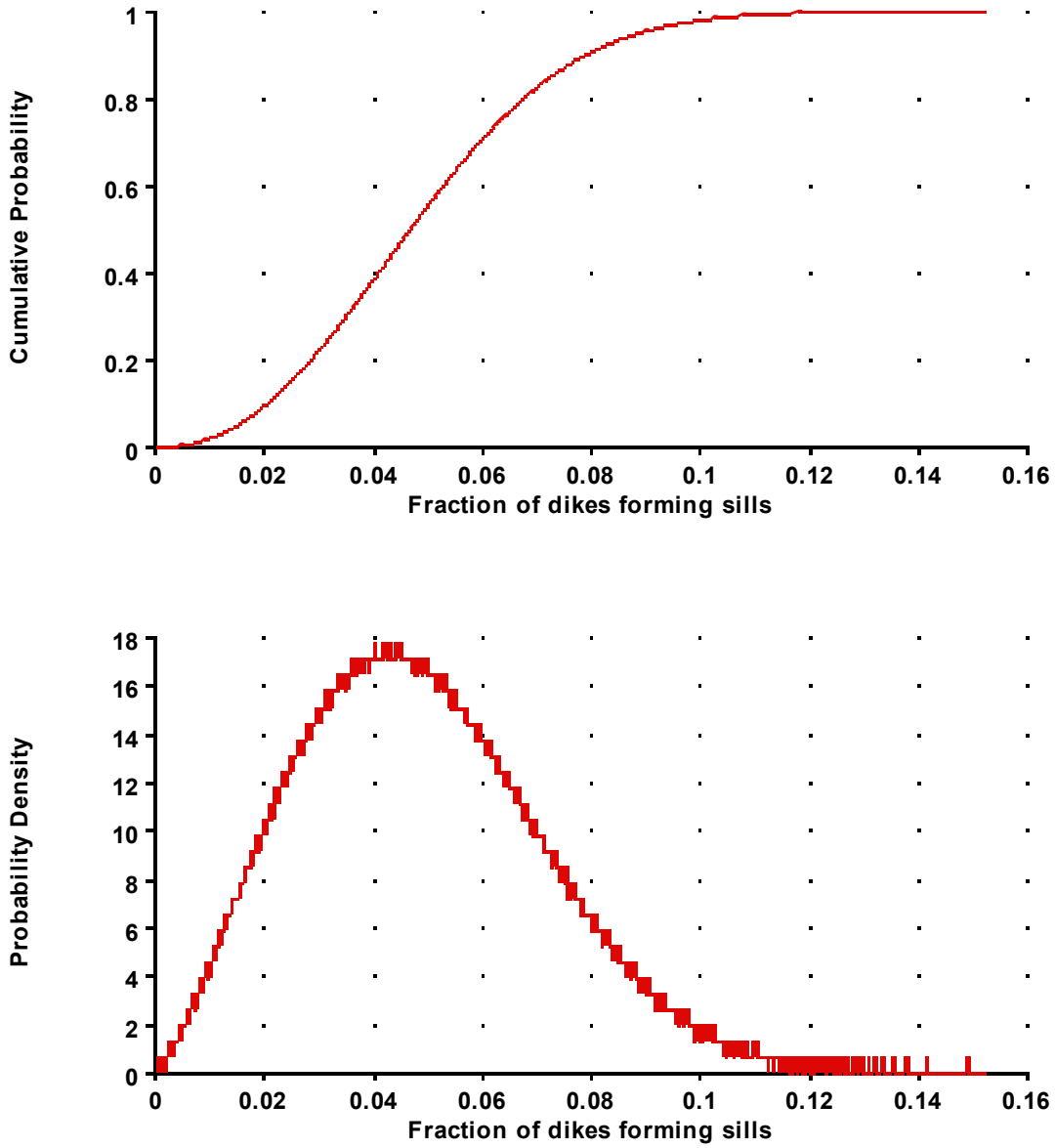

Figure D.7-7. Assessment of the Fraction of Dikes That Would Form Sills at Repository Depth

Sill Dimensions. The thickness of a potential sill would range from 10 m (10th percentile) to 50 m (95th percentile). The mode of this distribution is about 20 m. The full distribution for thickness is illustrated in Figure D.7-8.

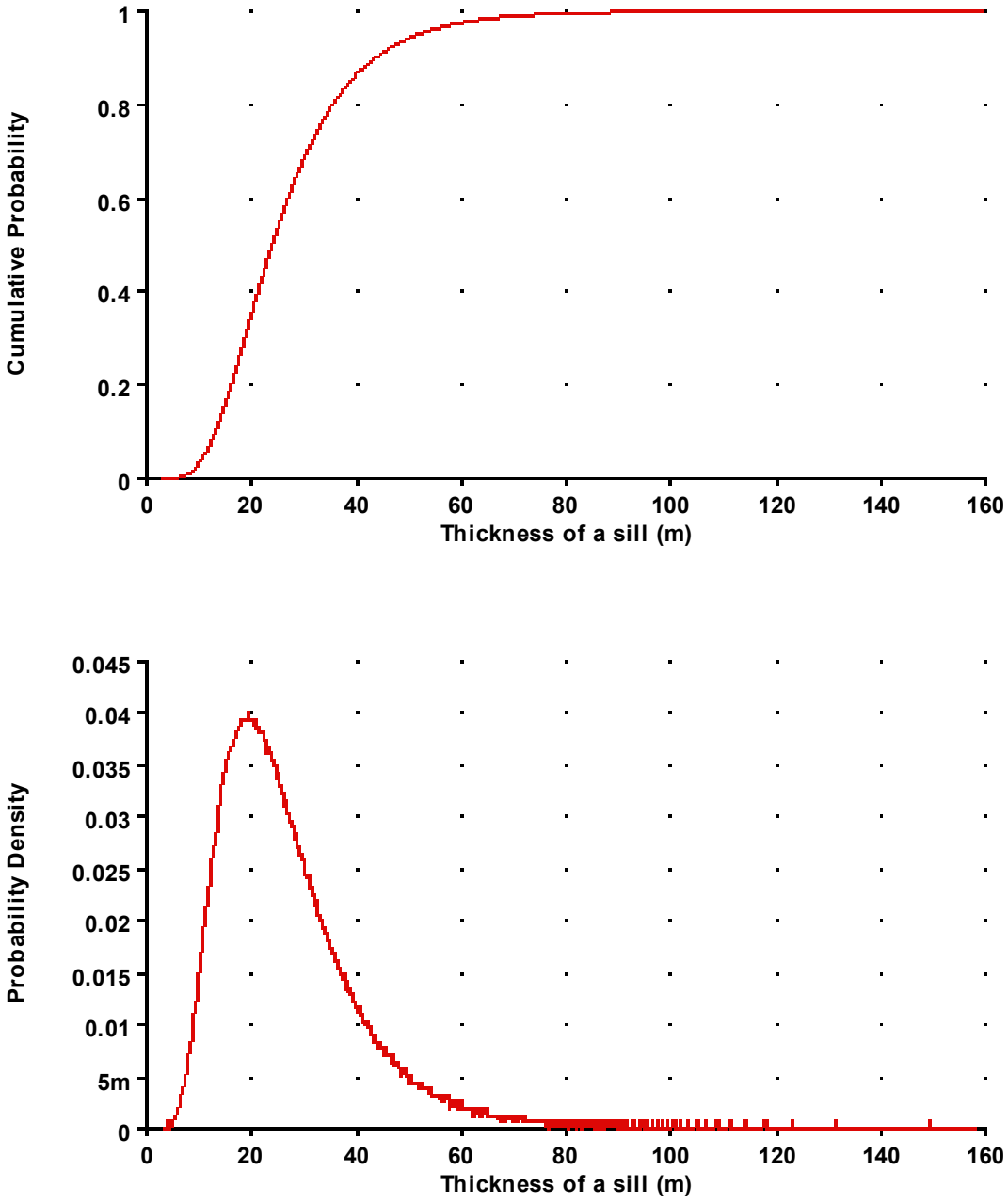

NOTE: For values less than 0.01 on the y-axis, suffix notation is used (m = 10^{-3} and u = 10^{-6}, so 5m = 0.005).

Figure D.7-8. Assessment of the Thickness of a Sill, Given That One Forms at Repository Depth

If a sill were to form, approximately 10 percent of the magma volume can be assumed to go into it. The remaining 90 percent would become potentially eruptive volume.

If sills are assumed to be roughly tabular, the length of a potential sill can be calculated from magma volume and sill thickness: l = square root (V_e/10*h), where l is the side of the square, V_e is magma volume, and h is sill thickness. If a sill were to occur, the midpoint of the sill would be located along the length of a dike following the same distribution described below in the section "Conduit Location."

Conduit Formation and Geometry

Conduit geometry is characterized by estimates of the numbers and locations of conduits on a dike and the conduit diameter at repository depth, as shown in Figure D.7-9.

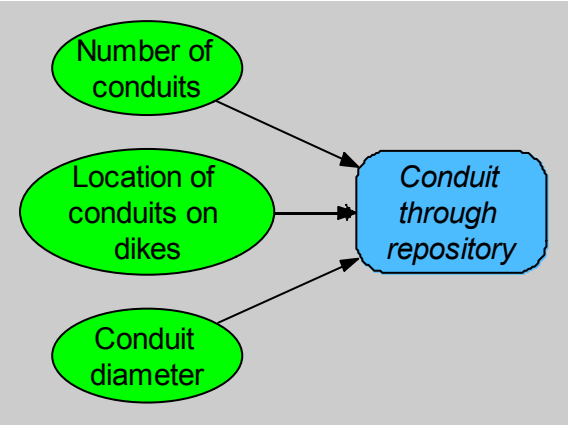

Figure D.7-9. Components of the Model for Conduit Geometry

Number of Conduits. Development of conduits is related to the volume of magma within a dike system. For an event of volume 0.05 km^3 or less, my assessment is that only one conduit is possible. For events of larger volumes, the number of conduits may vary. Table D.7-3 below shows my assessment of the probability distribution describing the number of conduits in an event given various volumes.

Table D.7-3. Number of Conduits as a Function of Magma Volume

Number of Conduits	Magma Volume (km^3)				
	0.05 or less	0.1	0.5	0.7	1
1	1	0.7	0.3	0.15	0.1
2	0	0.2	0.4	0.35	0.15
3	0	0.1	0.3	0.4	0.5
4	0	0	0	0.1	0.15
5	0	0	0	0	0.1

If a conduit is column producing, then ash will be generated and a cone will form. Most of the Quaternary Crater Flat events are known to have produced ash and hence eruptive columns; others were probably fissure eruptions (e.g., Makani Cone). Eruptive characteristics of the Pliocene events are less certain, but some events likely did not produce columns. Based on my field observations and published literature (Valentine and Keating, 2007; Valentine et al., 2006 and 2007), 80 percent of events occurring in the YMR during the past 1 Ma produced columns. Therefore, I expect that 80 percent of the conduits formed during any future events would be column producing.

My assessment is based on my assessment of the probability that a column formed during eruption of the following analog events.

- Red Cone: 1.0
- Black Cone: 1.0
- Makani Cone: 0.1
- Little Cones (2 conduits): 0.8, 0.8
- Lathrop Wells: 1.0
- Hidden Cone: 1.0
- Little Black Peak: 0.7

Conduit Location. The location of a conduit on a dike is represented by a symmetric distribution that places the highest probability in the center of the dike and allows a small probability (~10 percent) for the conduit to occur at either end of the dike. This distribution is shown in Figure D.7-10.

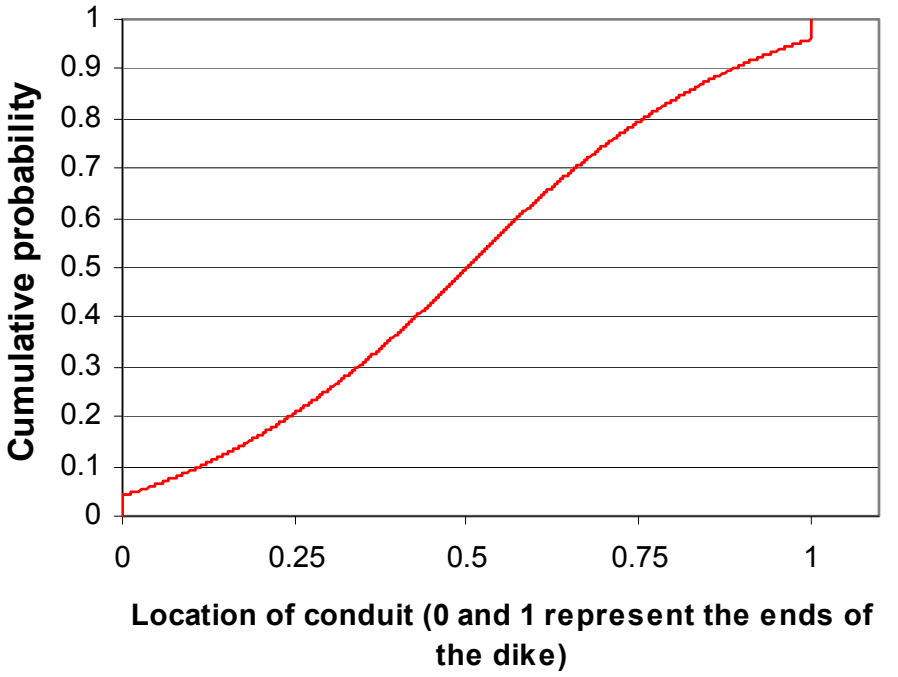

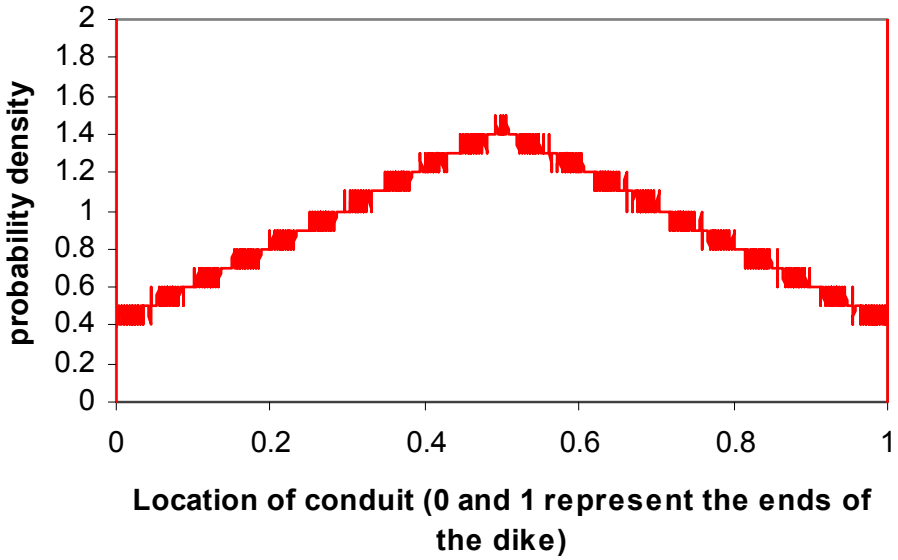

Figure D.7-10. Assessment of the Location of a Conduit along the Length of a Dike

If multiple conduits occur within an event, the distribution for conduit location should be used to place the first conduit on a random dike segment. The second, third, and subsequent conduits will be located on the longest remaining dike segments, utilizing the same distribution. The longest remaining segment may be a sub-parallel segment or a subsection of a dike that already contains a conduit. If multiple conduits occur on a single dike, they must be separated by a minimum distance of three conduit diameters. This assessment is based on the observations LANL scientists made regarding analog volcanoes in the western United States (data developed for the PVHA-U and published as Keating et al., 2008).

Conduit Diameter. Diameters of conduits that could form at repository depth are defined by the following cumulative probability distribution: dike width (lower bound), 25 m (10th percentile); 75 m (50th percentile); 150 m (90th percentile); and 250 m (99th percentile). Conduit diameters are based on volcanologic observations of ancient analog systems and on theoretical fluid dynamical models of magma transport of compressible (multiphase) magma flows. In simulating events, the maximum conduit diameter is constrained by the volume of the event. That is, the total volume of the conduit(s), calculated assuming a cylindrical conduit to repository depth, must not exceed the volume of the event. If the event were to include a sill, it is assumed that 10 percent of the magma volume would be retained in the sill. The total volume of conduits in the event, therefore, must not exceed 90 percent of the volume of the event. The assessment for conduit diameter is illustrated in Figure D.7-11.

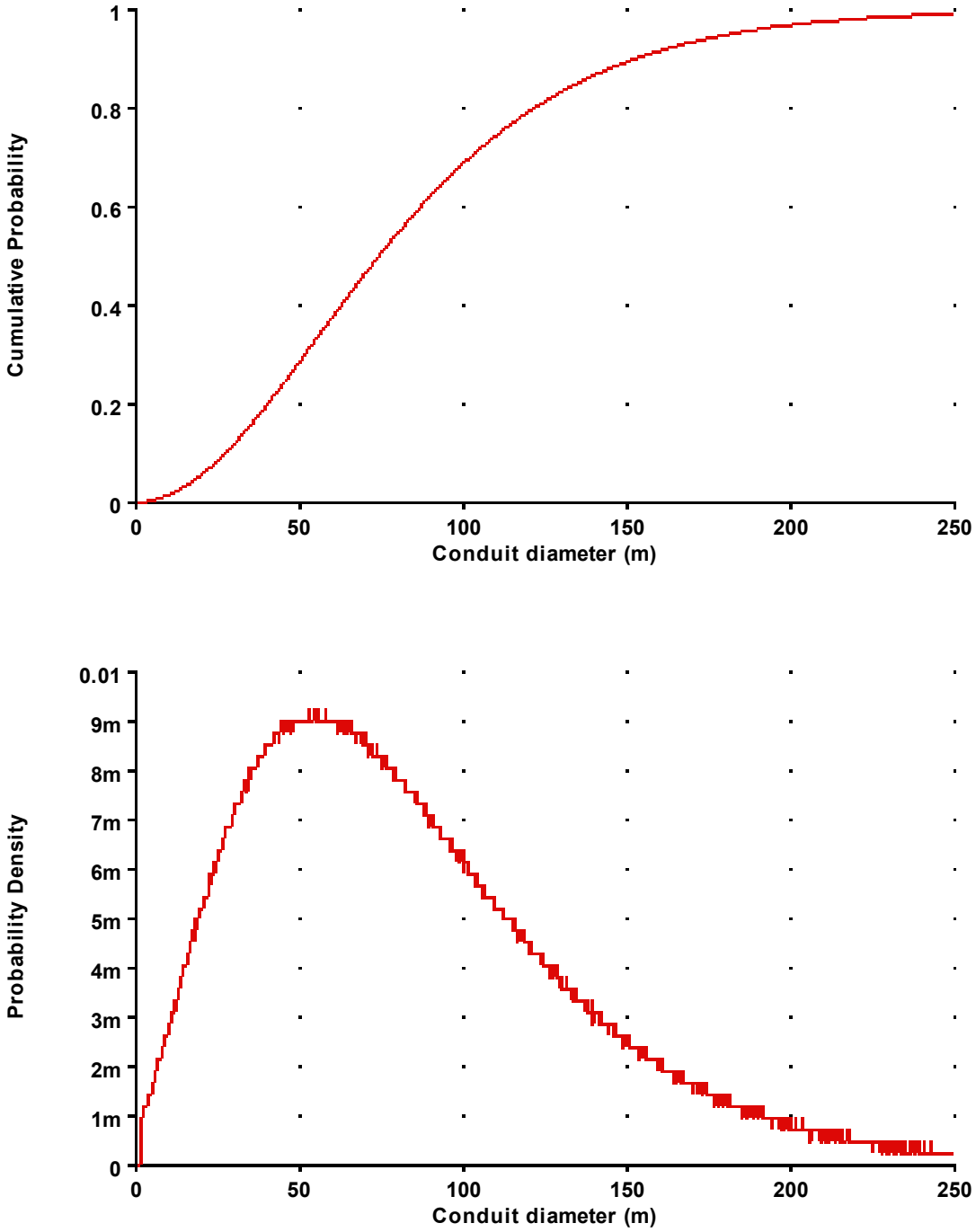

NOTE: Dike width defines the minimum diameter, and magma volume defines the maximum diameter. Figure illustrates assessment for a hypothetical dike that is 1 m wide and an event that involves a volume of 0.15 km^3. For values less than 0.01 on the y-axis, suffix notation is used (m = 10^{-3} and u = 10^{-6}, so 5m = 0.005).

Figure D.7-11. Assessment of the Diameter of a Conduit at Repository Depth

D.7.2 SPATIAL MODEL

My region of interest is shown in Figure D.7-12. The boundaries of this region are spatially defined by Buckboard Mesa to the northeast, Thirsty Mountain and Sleeping Buttes to the northwest, and Anomalies C and D to the south. Given the small number of volcanic events within the region, I believe the analysis should be kept simple; data that require a great amount of manipulation are inappropriate.

The primary data for spatial modeling are the ages of volcanic events in the YMR and the volumes of magma erupted. Other data, including those related to tomography, gravity, cumulative extension, or the spatial density of faults, have higher intrinsic uncertainties.

I consider two approaches to estimating the spatial distribution of potential future igneous events: (1) spatial smoothing, and (2) spatial smoothing combined with other geologic data.

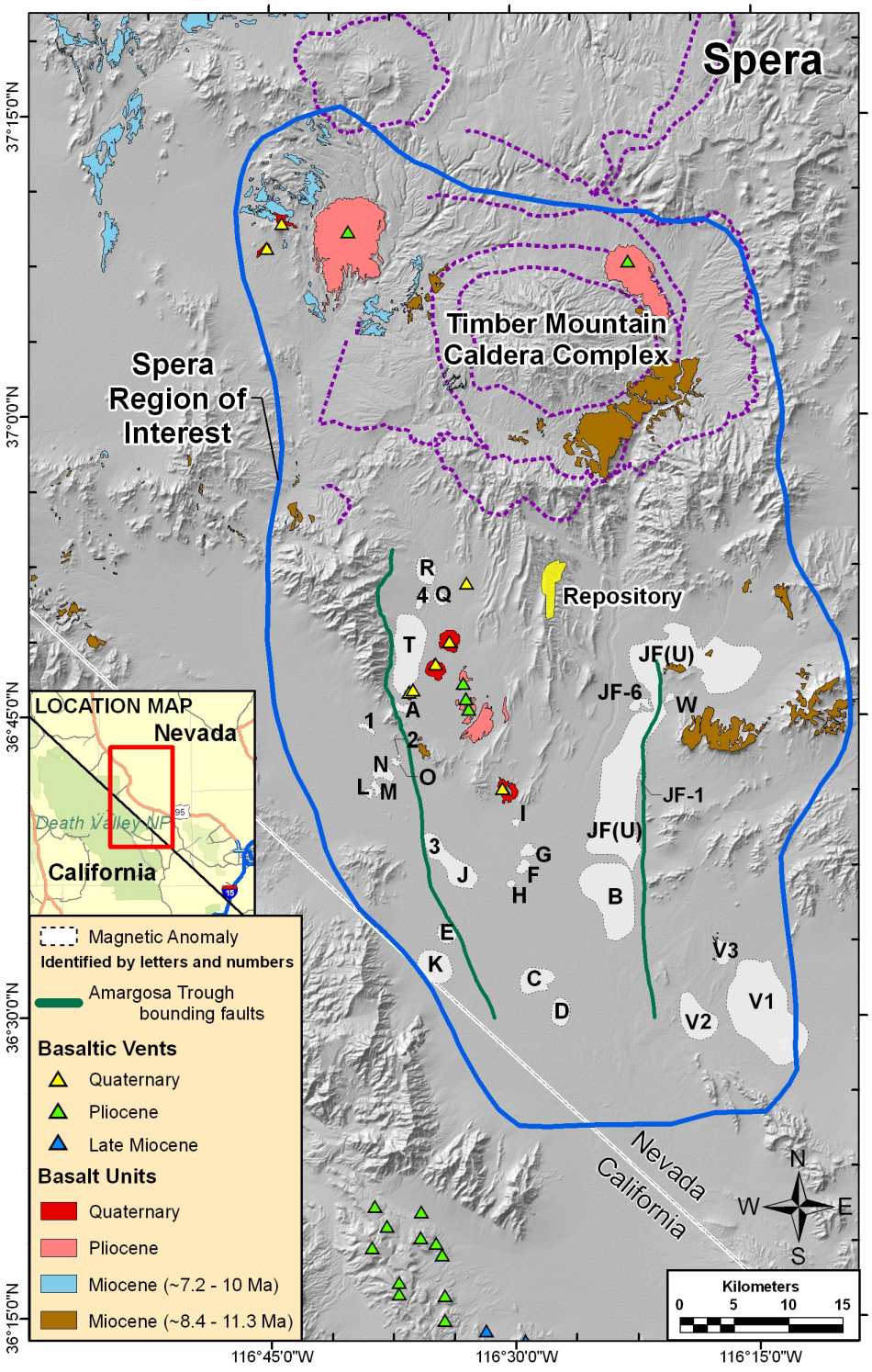

Figure D.7-12. Region of Interest

D.7.2.1 Spatial Smoothing

My basic spatial model uses Gaussian kernel estimation; alternative models for the smoothing distance, *h*; and weighting of events in Table D.7-1 based on both volumes and the inverse of event ages.

I use *h* values of 5 km (weight = 0.75) and 10 km (weight = 0.25). My assessment for the smoothing distance is based on potentially applicable distances between past events: about 11 km between the events in Quaternary Crater Flat; about 1 to 4 km between individual cones; the lengths of my so-called super–events (as described in Table D.7-1); and lengths of fissures in Miocene locations (which might provide a maximum).

I use two approaches to weight past events in the smoothing model to estimate the spatial distribution of future events: (1) smoothing based on the volumes of events (events having larger volumes receive higher weights), and (2) smoothing based on the ages of events (younger events receive higher weights). Both approaches have value. Volume is related to energy, which is an important factor, and proximity to the present can be important for estimating future activity. After exploring various combinations of weighting based on volumes and the inverse of ages, I concluded that both approaches are equally informative. Thus, both are included and assigned equal weight in my spatial smoothing model.

D.7.2.2 Incorporating Geologic Data Sets

For this approach, I start with the spatial intensity derived from spatial smoothing, then combine those maps with other geologic data. Geologic data that I consider include data on cumulative extension, lithostatic pressure, and tomography.

The available data on cumulative extension from Fridrich et al. (1999) are integrated over the past 12.7 Ma, which is significantly longer than the period of interest. Also, most of the extension probably occurred before the <5 Ma period of interest, based on the analysis of Fridrich et al. (1999). The data set covers only a small area of Crater Flat and extends only slightly into the Yucca Mountain block. Thus, many of the volcanic events of interest are outside the area characterized. All the volcanoes are confined to the area between the 50-percent and 100-percent extension contours, which is consistent with the model of volcanism for extended regions. Given the limitations of the data and their spatial extent, however, I do not use them directly in this analysis. Because the spatial density of faults also correlates with cumulative extension and likely is related to displacement on those faults in the Miocene, those data also are inappropriate for quantitative use within the <5-My period of interest. Qualitatively, it is important to keep these constraints in mind, however.

It is unclear whether data on lithostatic pressure are useful in modeling the location of potential future events, given the discrepancies in correlations between volcanic features and lithostatic pressure in various areas. In the Lunar Crater and Reveille volcanic fields, for example, cones and vents appear to be associated with areas having both high- and low-pressure contours. In the YMR, volcanic features are located only in low-pressure areas. Based on my examination, there appears to be a statistically meaningful difference between the distribution of lithostatic pressures at the locations of past events in my region of interest and the distribution of lithostatic

pressures at locations where no past events occurred. Therefore, I give some weight to a model that combines lithostatic pressure data with the spatial smoothing model.

Figure D.7-13 shows my assessment of the relationship between lithostatic pressure and future events. Specifically, the distribution shown in Figure D.7-13 represents my assessment of the likely pressure values at the location of a hypothetical future event. The figure shows both the empirical distribution of values at past events (red lines/bars) and my assessment of the value at a possible future event (blue lines/bars).

I also considered the tomographic data. The differences between the Biasi and Humphreys maps reflect different interpretations of the data. I weight the two interpretations equally. Figures D.7-14 and D.7-15 show contouring of the two interpretations developed by Dr. Chuck Connor to highlight regions of high, intermediate, and low seismic velocity. Tomographic data are used to help constrain eruption probabilities, because those data provide one of the few sources of information regarding the state of the Earth's mantle at the depths where magma is generated by partial melting of peridotite. The slowness of some seismic waves with respect to a radially symmetric Earth correlates with high temperature, high water content, the presence of small amounts of melt, and/or mineralogical constitution of the source. Some of these effects correlate with each other, and more than one effect may contribute to slow seismic waves. It is difficult to distinguish the underlying physical cause of slowness without additional data, although high temperature and a small amount of melt (which generally are correlated) seem to be the most important contributors. From my own thermochemical modeling of the phase equilibria of partial melting of peridotite, a depth of partial melting in the range 60 to 75 km, followed by shallower fractional crystallization, is the scenario most consistent with the composition of Lathrop Wells. The tomographic data depicted in Figures D.7-14 and D.7-15 correspond to seismic slowness at depths of about 70 km, consistent with models of the phase equilibria of partial melting. After reviewing the contours shown in Figures D.7-14 and D.7-15, I elect to use this characterization of the velocity in my models. After reviewing the distribution of seismic velocities at the locations of past events in my region of interest and the distribution of velocities at locations without events, I conclude that the tomographic data give meaningful information about the locations of events. If the extent of the high, intermediate, and low velocity areas are equal, my assessment is that the likelihood of the velocity being high, intermediate, or low at the location of a potential future event is 0.25, 0.35, and 0.40, respectively. That is, it is slightly more likely that the velocity at a future event would be slow or average rather than fast.

I believe the data on lithostatic pressure and tomography give relatively independent information on the locations of potential future events, and that both are equally informative. Accordingly, I weight the interpretation of lithostatic pressure data and the interpretation of tomographic data equally in my final model.

Finally, I consider the location, age, and volume of past events to be the most informative factors related to the locations of potential future events. Thus, my final model places higher weight on the volume- and inverse-age-weighted spatial smoothing approach than on the interpretation of the geologic datasets. I assign a weight of 0.75 to the smoothing model and 0.25 to the model modified by geologic data sets.

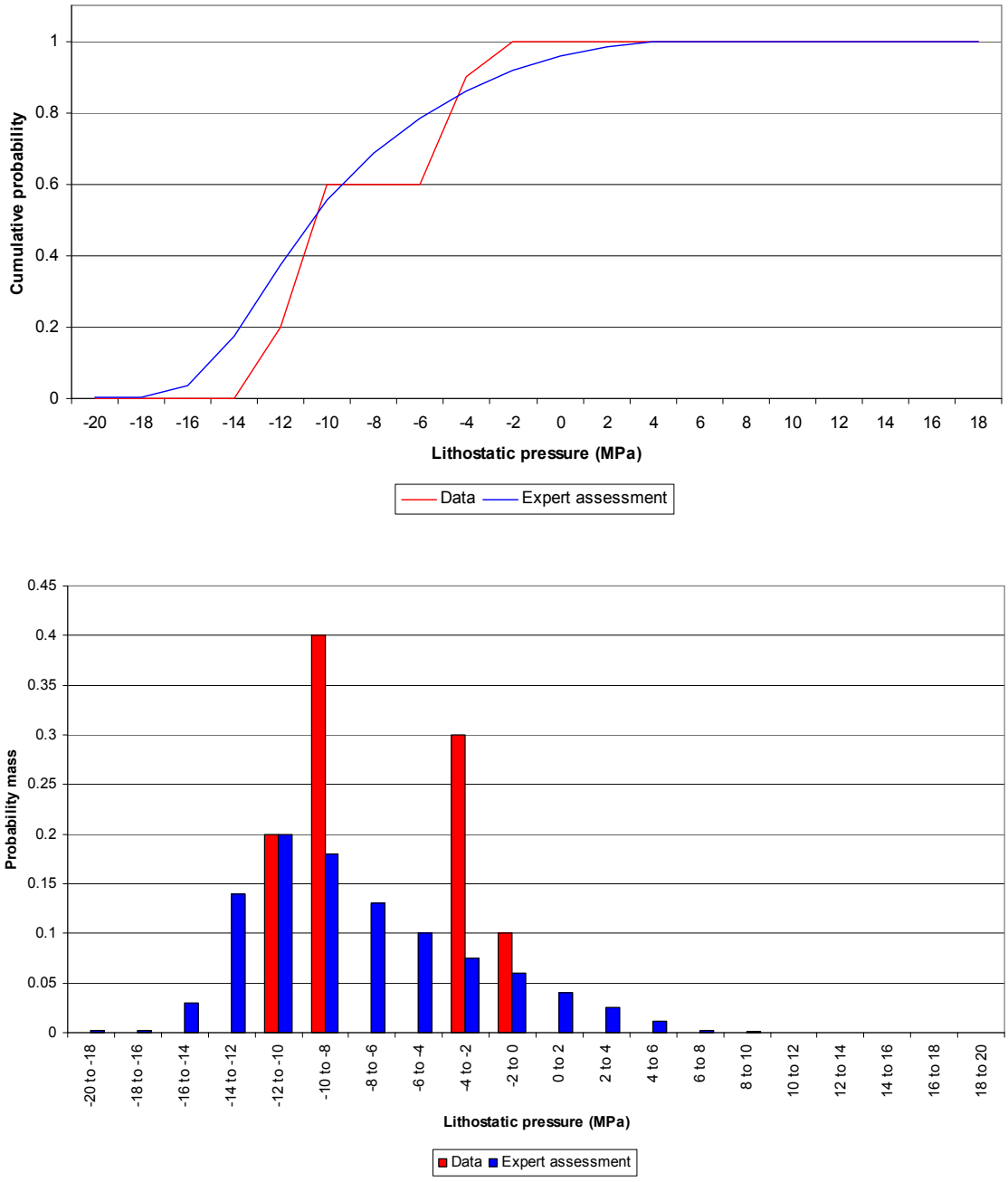

NOTE: Red lines/bar represent the value at past event in the region of interest; blue lines/bars represent the assessment of the value at a future event.

Figure D.7-13. Assessment of the Likely Value of Lithostatic Pressure at the Location of a Hypothetical Future Event

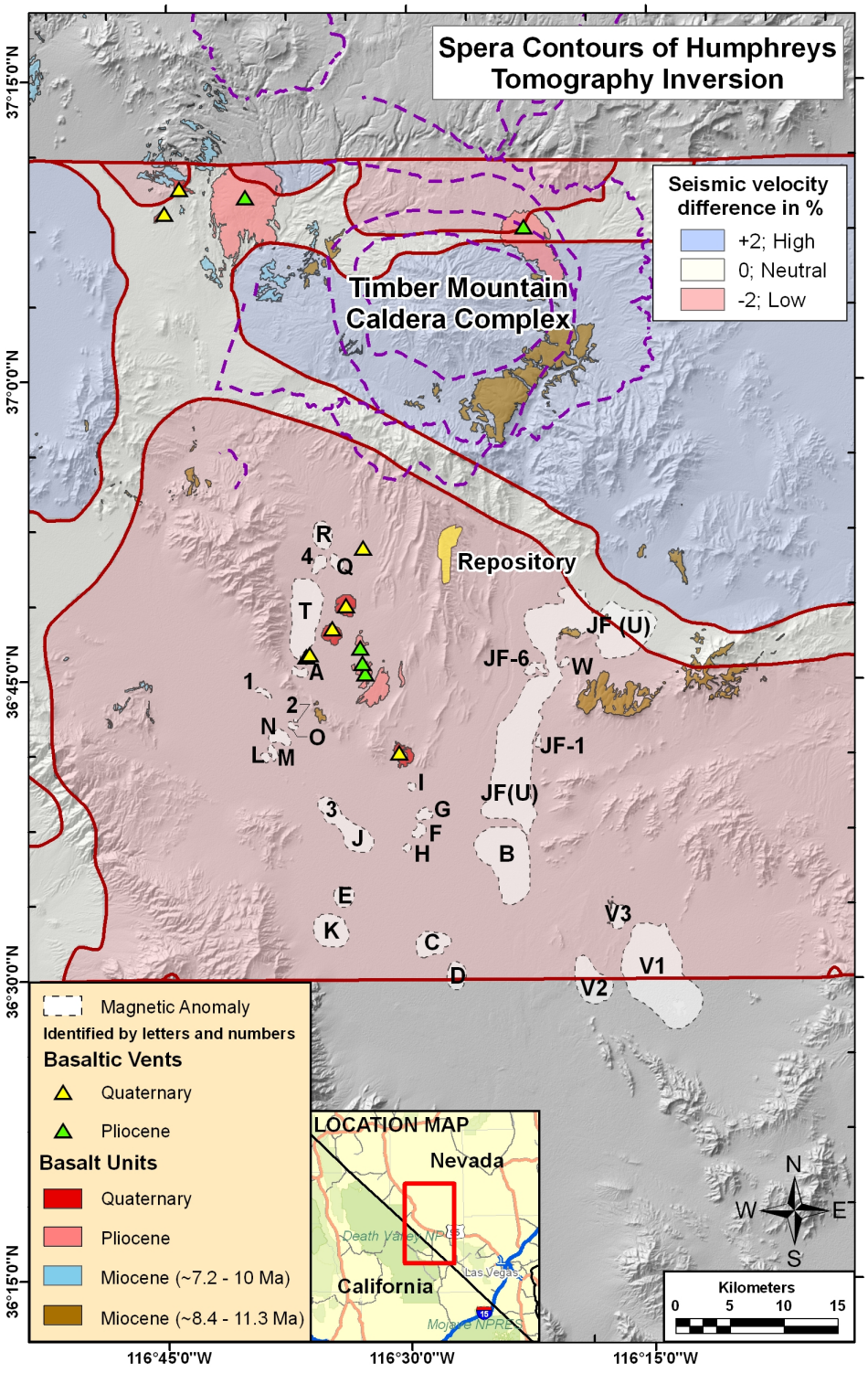

Figure D.7-14. Contours of Humphreys' Interpretation of Tomographic Data

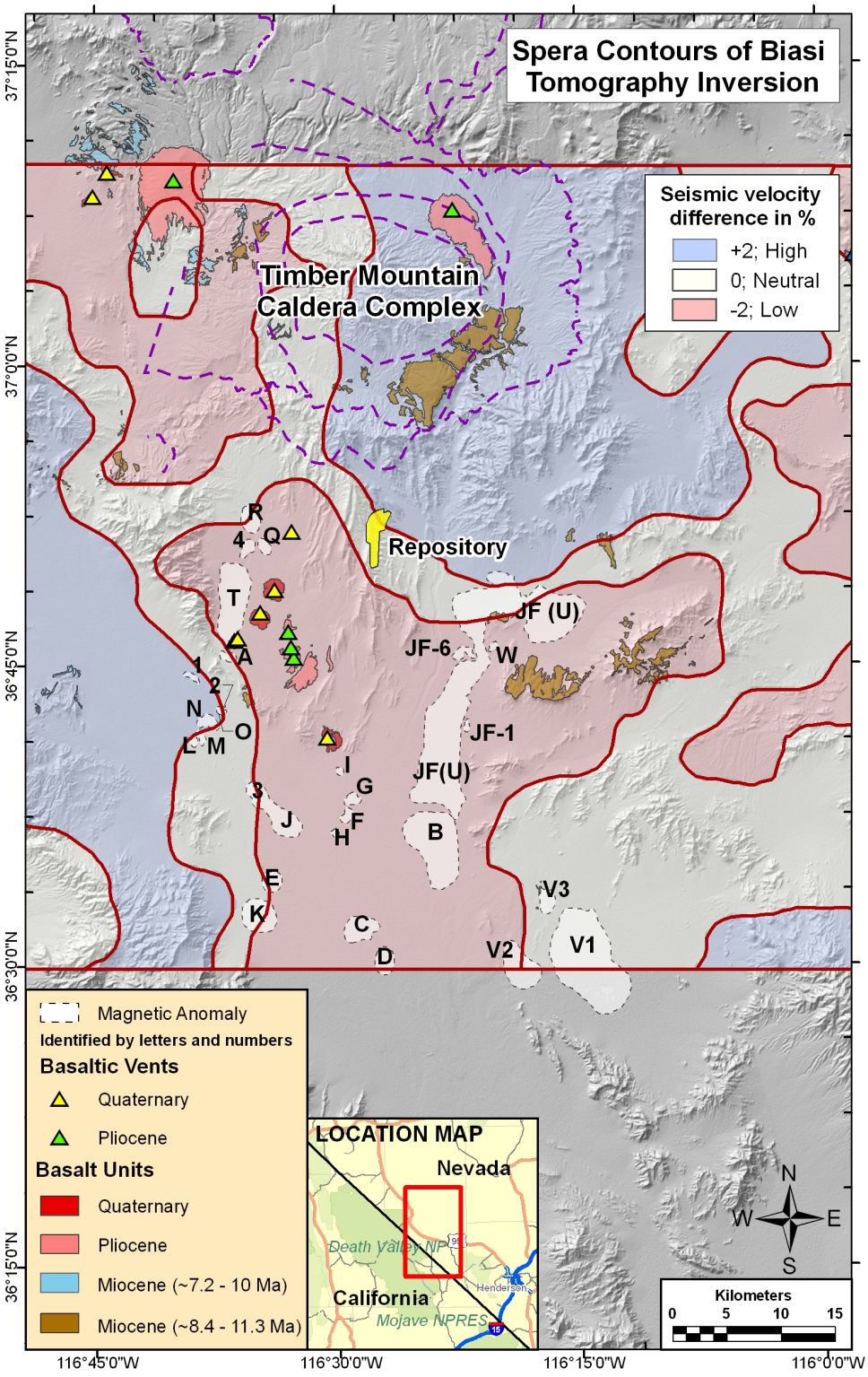

Figure D.7-15. Contours of Biasi's Interpretation of Tomographic Data

D.7.3 TEMPORAL MODEL

The period of interest for a temporal evaluation is post-5 Ma. Events in the YMR that are older than about 5 Ma reflect activity in the waning part of the silicic caldera cycle that occurred primarily north and northwest of Yucca Mountain. I believe that that volcanism is related only indirectly to the younger volcanism in and around Crater Flat. The caldera-related older magmas are volumetrically dominated by silicic ignimbrites. The basalts that do occur are geochemically distinct from the <5 Ma basaltic volcanics considered relevant to future possible activity at and near Yucca Mountain.

I use a time-volume model similar to the conceptual model presented by Dr. Richard Carlson (PVHA-U Workshop 2), because the thermal energy involved in an eruption scales directly with the volume of that eruption. Hence a time-volume model roughly captures the energetics of magmatism that represents, in my conceptualization, a first-order feature. An advantage of the time-volume model is that it rather directly uses an observable quantity. This model requires an estimate of the rate of magma production, estimated by the slope of the curve that describes cumulative volume over time, and an estimate of the volume per event.

Cumulative volumes versus time are calculated using the volume estimates in Table D.7-1. Figure D.7-16 shows the cumulative volume over time and three alternative models fit to those data: (a) cumulative volume as a linear function of the square root of time; (b) a linear fit to the cumulative volumes of Quaternary events only; and (c) a linear fit to 2.87-Ma and younger events (from the Buckboard Mesa event).

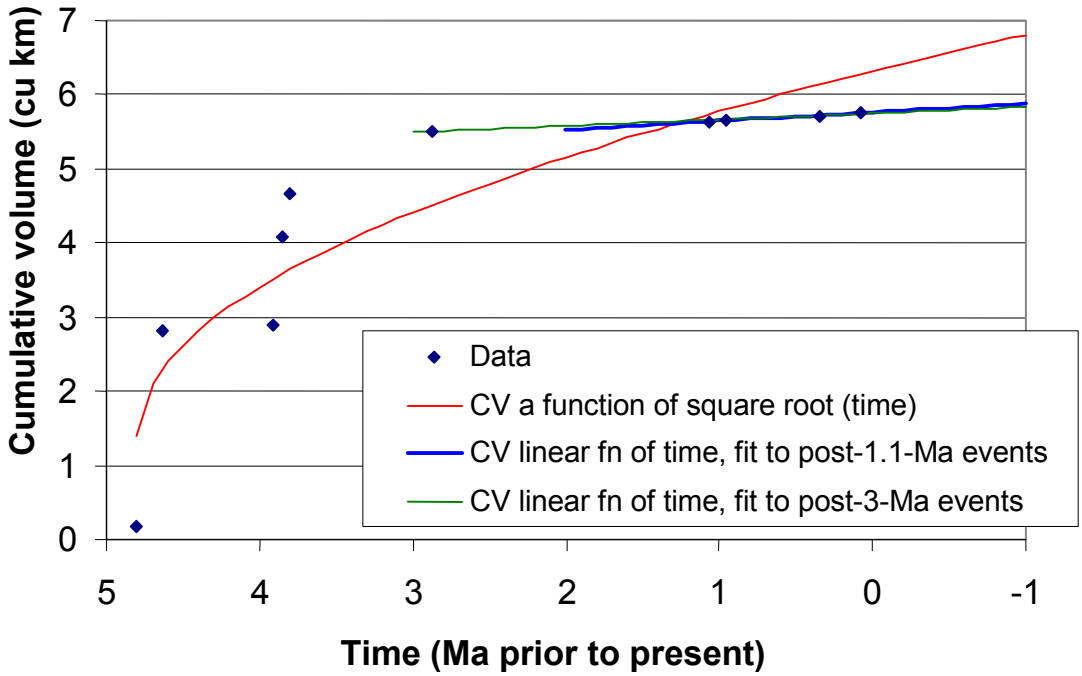

Figure D.7-16. Plot of Cumulative Volume (CV) over Time for Events in My Region of Interest (see Table D.7-1) and Alternative Models Fit to the Data

Although the $t^{1/2}$ time function used in the past by Dr. Richard Carlson has some very general basis in heat transfer theory, its applicability to the problem at hand is remote at best. There are far too many natural complexities involved in the real process to use a simple heat conduction model for the rate of magma production. I consider that linear fits are more representative of what I would expect in the near future. I prefer models based on more data, and the linear fit to post-3-Ma events is a better-fitting model than is the fit to post-1.1-Ma events only. I weight these two models 0.75 and 0.25, respectively.

To estimate the volume per event as a function of time, I weight two alternatives equally: (a) an assessment of the volume of future events (as described above in Section D.7.1.2), and (b) the event count and volumes of post-1.1-Ma events only. For method (a), which uses the full distribution of my assessment, the median recurrence rate and associated mean repose interval are $\sim 1.6 \times 10^{-6}$ yr^{-1} and 634 ka, respectively. Different statistics derive from using only the post-1.1-Ma volcanic volumes. For example, when Quaternary Crater Flat is assumed to represent four events, the median recurrence rate and repose interval are 2.9×10^{-6} yr^{-1} and 345 ka, respectively. Equal weighting was used because both methods have intrinsic merit. Method (b) uses the raw post-1.1-Ma data directly, whereas method (a) uses Monte Carlo simulations based on the full statistical distribution of the volume-per-event assessment outlined previously. By way of illustration, using just the median of my volume-per-event assessment of 0.05 km^3 per event produces the following values: 95% probability of finding a recurrence rate greater than 1.2×10^{-6} yr^{-1} (i.e., repose interval less than 840 ka); 50% probability of finding a recurrence rate greater than 1.8×10^{-6} yr^{-1} (repose interval less than 550 ka); and a 5% probability of a recurrence rate greater than 2.5×10^{-6} yr^{-1} (repose interval less than 398 ka).

D.7.3.1 One-Million-Year Assessment: Implications for Magnitude of Events

The increased uncertainty for the 1-My future period compared to the 10-ky period is related primarily to the interaction between local climate—specifically the hydrologic state of the shallow crust (i.e., the depth to the water table)—and possible phreatomagmatic activity. Farther north in the Lunar Crater volcanic field, for example, phreatomagmatic explosion craters or maars were created during an older, wetter climate (the North American pluvial period). I understand, however, that models of future climate for the Yucca Mountain area indicate that the groundwater table is expected to rise by at most 100 m.

The chances of an explosive phreatomagmatic eruption are enhanced when the water table is high (close to the surface), because the isothermal compressibility of water at low pressure is proportional (in fact nearly equal) to $1/p$, where p is the local lithostatic pressure (equal to 1/3 of the trace of the stress tensor: $_{1/3}\sum_{i}^{3}\sigma_i$). When magma contacts cold groundwater, the groundwater becomes heated and expands. The expansion, ΔV, is given by the relationship $\Delta V = \Re(T_{hot} - T_{cold})/p$, where ΔV is the expansion per kilogram of H_2O; $\Re$ is the gas constant for H_2O (462 J/kg K); p is the pressure (in Pascals, Pa); and the temperature difference is that between cold and heated groundwater. To illustrate the strong effect that depth to water table has on volumetric expansion, consider the following example. Assume that the depth at which rising magma encounters the water table is either 600 m (case A) or 200 m (case B) beneath the surface. Further assume that ΔT is 700° K. For case A, the volumetric expansion is 0.022 m^3/ kg of H_2O. For case B the volumetric expansion is 0.066 m^3/ kg of H_2O. At very shallow

depths, say 10 m, the expansion is equal to 1.32 m^3/kg of H_2O. Although the depth of the water table may have only a second-order effect on the probability of eruption, the style of eruption can change dramatically when phreatomagmatism comes into play. Our limited ability to make predictions regarding climate—especially the annual precipitation 1 My into the future at Yucca Mountain—constrains the ability of this volcanologist to forecast the probability of phreatomagmatic eruptions. If the water table rises a few tens of meters, the increased probability for phreatomagmatic activity may be marginal and within the limits of other uncertainties. Musgrove and Schrag (2006**)** provide an interesting critical discussion regarding climate change at Yucca Mountain. I do not have the expertise to forecast the climate 1 My into the future. The future climate will depend on myriad factors including what is perhaps most vexing – human behavior. That is, what will be the global human response to the issue of global warming and human-induced climate change?

Another source of uncertainty within the 0- to 1-My time frame is a possible change in regional tectonic conditions. At the global scale of plate tectonics, 1 My is not long. Even fast-moving tectonic plates (plates that move at rates of about 0.1 m/yr) move only 100 km in 1 My. Over a time scale on the order of 10 to 30 Ma, volcanism has waned in the southwest part of North America, and there is no reason to expect this trend to change in the next 1 My.

In summary, my assessments for the future interval 0 to 1 My are the same, proportionally, as those for the future interval 0 to 10 ky.

D.7.4 REFERENCES

Bechtel SAIC Company (BSC), 2007, Subsurface Geotechnical Parameters Report: Las Vegas, Nevada, Bechtel SAIC Company, ANL-SSD-GE-000001 REV 00.

BSC, 2004, Dike/Drift Interactions: Las Vegas, Nevada, Bechtel SAIC Company, MDL-MGR-GS-000005 REV 01.

Dickerson, R.P., and Drake, R.M., 2004, Geologic map of south-central Yucca Mountain, Nye County, Nevada, Pamphlet to accompany Miscellaneous Field Studies Map: U.S. Geological Survey, MF–2422, 26 p.

Fridrich, C.J., Whitney, J.W., Hudson, M.R., and Crowe, B.M.., 1999, Space-time patterns of late Cenozoic extension, vertical axis rotation, and volcanism in the Crater Flat basin, southwest Nevada, in Wright, L.A., and Troxel, B.W. (eds.), Cenozoic Basins of the Death Valley Region: Boulder, Colorado, Geological Society of America Special Paper 333.

Gudmundsson, A., 2003, Surface stresses associated with arrested dykes in rift zones: Bulletin of Volcanology, v. 65, p. 606-619.

Keating, G.N., Valentine, G.A., Krier, D.J., and Perry, F.V., 2008. Shallow plumbing systems for small-volume basaltic volcanoes: Bulletin of Volcanology, v. 70, pp. 563-582, DOI 10.1007/s00445-007-0154-1.

Los Alamos National Laboratory (LANL), 2007, Ar/Ar age determinations, volume, location and elevation of Plio/Pleistocene volcanoes in the Yucca Mountain region, Rev. 3: Excel spreadsheet titled, Volcano_volume_age_location_Rev03.xls.

Musgrove, M. and Schrag, D.P. (2006). Climate history at Yucca Mountain: Lessons learned from Earth History. In Uncertainty Underground: Yucca Mountain and the Nation's High-Level Waste, (eds.) Macfarlane, A. M. and Ewing, R.C. pp. 149-162.

Perry, F., Cogbill, A., Kelley, R., Lewis, C. Cline, M., Fleck, R., and Peterman, Z., 2006, Preliminary results and interpretations of a high-resolution aeromagnetic survey and drilling program to investigate buried volcanic features near Yucca Mountain: White Paper (Drill Hole Results Rev 5) provided to PVHA-U Expert Panel, dated June 30.

Valentine, G.A., and Keating, G.N., 2007, Eruptive styles and inferences about plumbing systems at Hidden Cone and Little Black Peak scoria cone volcanoes (Nevada, USA): Bulletin of Volcanology, DOI 10.1007/s00445-007-0123-8.

Valentine, G.A., Krier, D.J., Perry, F.V., and Heiken, G., 2007, Eruptive and geomorphic processes at the Lathrop Wells scoria cone volcano: Journal of Volcanology and Geothermal Research, v. 161, p. 57-80.

Valentine, G.A.., Perry, F.V., Krier, D., Keating, G.N., Kelley, R.E., and Cogbill, A.H., 2006, Small-volume basaltic volcanoes: eruptive products and processes, and post-eruptive geomorphic evolution in Crater Flat (Pleistocene), southern Nevada: Geological Society of America Bulletin 118, p.1313-1330, DOI 10.1120/B25956.1.

INTENTIONALLY LEFT BLANK

D.8 GEORGE THOMPSON'S ELICITATION SUMMARY FOR PVHA-U PROJECT

Two types of igneous events are identified as having the potential to disrupt the Yucca Mountain radioactive waste repository: an igneous intrusion into the repository, or a conduit passing through it. The probability that either type of event would disrupt the repository is a function of the spatial and temporal distribution of volcanism in the area and the physical geometry of each type of igneous event. These factors, and the relationships among them, are illustrated in Figure D.8-1. Models and assessments of the geometry of dikes, dike systems, and conduits are summarized in Section D.8.1, followed by models and assessments of the spatial and temporal distributions of igneous events.

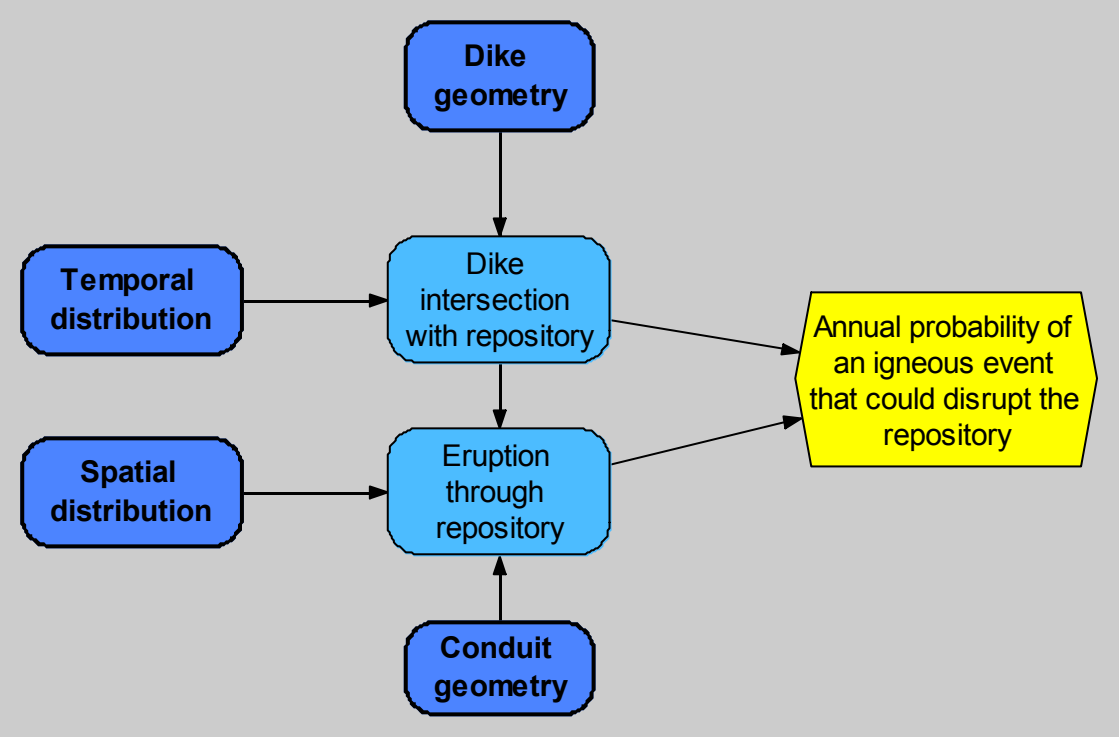

NOTE: The yellow hexagon represents the final result of the assessment. Dark blue rounded rectangles represent sub-models; light blue nodes represent values calculated from other inputs; and arrows indicate influences of one variable on one or more others.

Figure D.8-1. Overall Structure of Model

D.8.1 EVENT DEFINITION

The small volumes of post-silicic igneous activity in the Yucca Mountain region (YMR, defined as the region within a radius of about 50 km centered on Yucca Mountain) are related to pockets of melt or incipient melt in the mantle. Viscoelastic propagation of stresses, possibly due to earthquakes and associated extension (for example, faulting coeval with the Lathrop Wells eruption), may trigger these pockets of melt to ascend to the surface.

I define a (significant) event as a temporally distinct batch of magma that reaches to within 0.5 km of the ground surface. The duration of an event may be as long as 100 to 10,000 years.

Each new dike or dike swarm that forms as a result of accumulated elastic strain is considered a separate event. The time required to accumulate elastic strain to produce a new event (dike injection) is an order of magnitude longer (100,000 years). There is no reason for a new dike to follow the trace of an old dike.

Given that vesiculation, which tends to occur within about 1 km of the ground surface, may begin before a dike would reach the repository horizon, an eruption would become likely for any dike that reached the depth of the repository. I estimate that nearly all dikes that reach repository depth would reach the surface.

All of the following assessments pertain to possible future events in the vicinity of Yucca Mountain, and all characteristics given are appropriate for repository depths.

D.8.1.1 Characterization of Past Events

The events that have occurred in the Crater Flat-Amargosa Desert area and that have occurred within the period of interest (the past 4 Ma) are identified in Table D.8-1. My period of interest is based on the oldest Pliocene events in Crater Flat and the northern Amargosa Desert (3.9 Ma).

We cannot use rock chemistry alone to constrain the relationship between the Quaternary Crater Flat cones. Given that I assess the duration of an event to be as long as 10,000 years, it is most likely that the alignment of Red Cone, Black Cone, Makani Cone, and Little Cones in Crater Flat represent a single event, although I allow for the possibility that they represent up to four separate events, as shown in Table D.8-1. The close proximity of the two Little Cones indicates to me that they should be considered a single event (or part of a larger event). Similarly, Anomalies F, G, and H most likely were a single event, but I allow for the possibility that they represent separate events. The alignment of those cones, taken as indicators of stress alignment, is strikingly prominent within the Basin and Range Province, reflecting a deeper alignment in the crust.

Table D.8-1. Relevant Volcanic Events in the Region of Interest

Event Name/Location	Number of Events	Age* (Ma)	Volume* (km^3)
Anomalies F, G, and H in Amargosa Desert	1 event or 3 separate events (probabilities = 0.95, 0.05)	3.9	Anomaly G: 0.028 Anomaly F: 0.029 Anomaly H: 0.006
Anomaly B (Basalt of Drill Holes FF25-1 and FF5-1 in Amargosa Desert)	1	3.85	1.227
Basalt of Southeast Crater Flat	1	3.8	0.585
Quaternary Crater Flat Cones	1, 2, 3, or 4 events (probabilities = 0.95, 0.03, 0.01, and 0.01) If 2 events: Red Cone, Black Cone, and Makani Cones are one event; Little Cones are one event. If 3 events: Red Cone and Black Cone are one event; Makani Cone is one event; and Little Cones are one event. If 4 events: Red Cone, Black Cone, and Makani Cone are each separate events; Little Cones are one event	1.07	Red Cone: 0.055 Black Cone: 0.06 Makani Cone: 0.002 Little Cones: 0.034
Lathrop Wells Cone	1	0.077	0.048

* Age and volume estimates are based on consideration of Los Alamos National Laboratory (LANL) (2007).

It is possible that the source of the 3.8-Ma basalts in southeast Crater Flat and Amargosa Desert (Anomalies B, F, G, and H) was a single deep pocket of magma about 70 km deep (in which case they could all be considered a single event). But it is highly unlikely they were a single event given the lack of physical proximity and differing geochemistry of the various basalts. My assessment is that they represent multiple events.

D.8.1.2 Event Characteristics and Geometry

The characterization of potential future events in the YMR includes the event geometry, which is defined by several variables, as shown on Figure D.8-2: the length of a dike system, the number, spacing, and orientation of dikes in a dike system; and the number, location, and geometry of conduits within an event. Assessments were made for each variable.

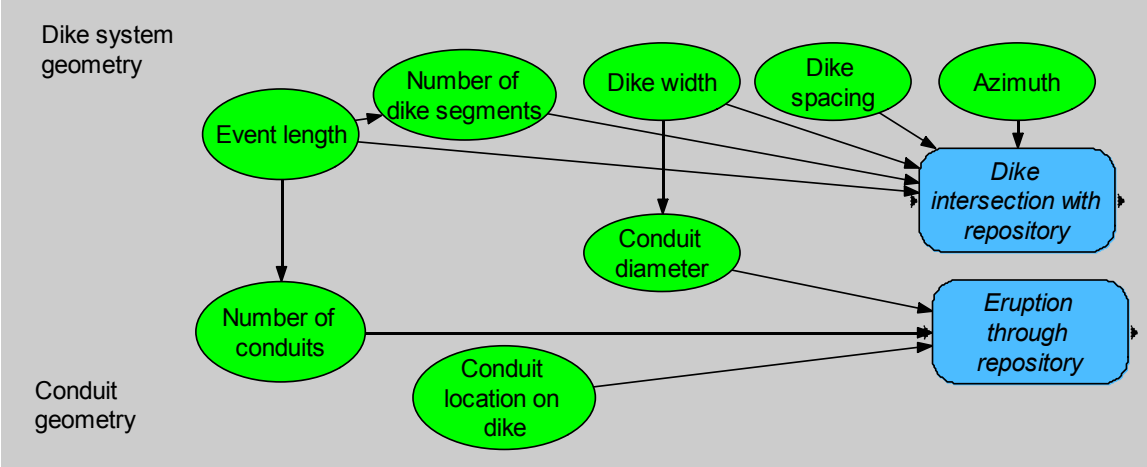

Figure D.8-2. Components of the Model of Dike System and Conduit Geometry

Dike System and Sill Geometry

An event consists of one or more dike segments and one or more conduits. If an event includes more than one dike segment, those segments will tend to occur in a right-stepping en echelon pattern, described in more detail below.

Dike System Length. I define the length of an event as the total length of all dike segments in the event. Event length is related to the volume and effusion rate of magmatic activity. Dikes hundreds of kilometers long can be observed throughout the world, generally in association with flood basalts. The dikes associated with small basaltic cones such as those in the YMR, however, are short and narrow. For the Quaternary cinder cones in the YMR, both geologic and geophysical evidence points to short dike segments within a few hundred meters of the ground surface (Valentine and Perry, 2006). For individual cinder cones such as Lathrop Wells, the associated dike probably is not much longer than the eruption fissure. Dike lengths in the shallow subsurface may be related to depth of erosion and/or curvature of the dike front, so there is much uncertainty in measured dike lengths.

The upper kilometer or two of the crust comprises a zone of low elasticity, as evidenced by low seismic velocity. Below this depth the regional stress regime exerts a controlling effect on structural deformation and the geometry of dike systems. A cross section of the upper few kilometers of the crust, as shown diagrammatically in a paper by Delaney and Pollard (1982), illustrates that dikes may transition upward into an en echelon array. Tuff fill in Crater Flat extends to a depth of about 3 km. Below this depth one would expect continuous, less segmented dikes that are controlled by regional stress.

To develop an assessment of the total lengths of potential future events/dike systems, I consider the vent and cone alignments observed in the YMR. The estimated total event length can be slightly longer than the length of cone alignments, allowing for the total length of all dike segments that may extend beyond the observed cones. The Quaternary Crater Flat alignment of cones indicates that total event length can be as great as 15 km. The 3.8-Ma southeast Crater Flat events may be associated with an event about 3 to 4 km long, whereas the Lathrop Wells

cone may represent an event involving a single dike that is only about 1 km long. My estimate of total potential event length, based on these observations, is illustrated in Figure D.8-3. This distribution is based on the following assessments: 15 km represents about the 99th percentile of possible event lengths; 1 km represents about the 1st percentile; it is most likely that the event length will be between 3 and 5 km; and the overall distribution has a lognormal shape.

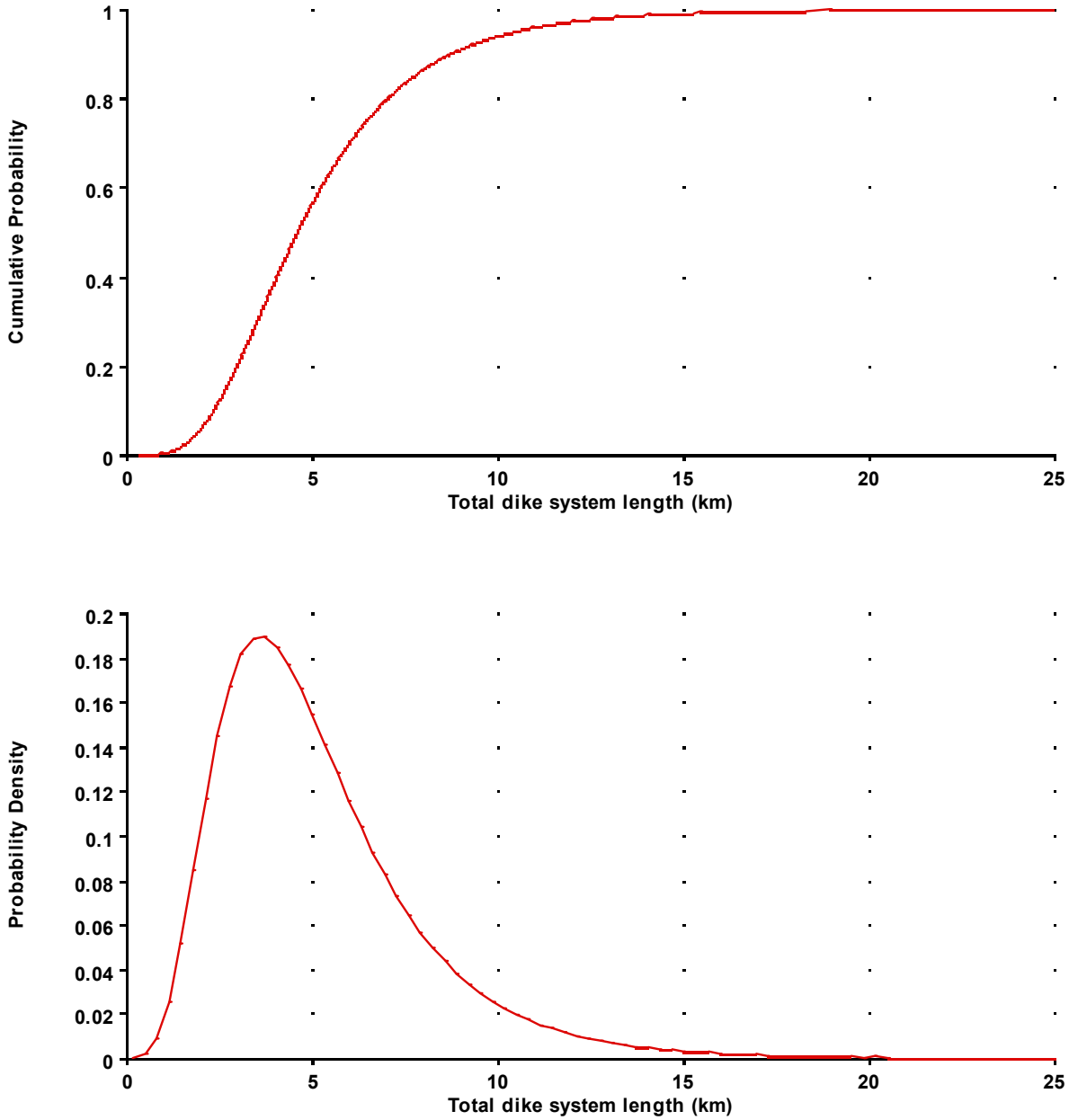

NOTE: Top graph is a cumulative distribution function; bottom graph is a probability density function.

Figure D.8-3. Assessment of the Total Length of an Event, or Total Length of Dikes in a Dike System

Number of Dike Segments. Consideration of the number of dike segments associated with an individual event must include the expected volumes of potential future eruptions. Both the total length of the dike system and the number of dike segments are a function of event volume; that is, long dike systems comprising multiple dike segments typically require a large volume of magma.

There is evidence for possibly three or four dike segments associated with the Quaternary Crater Flat cones. Lathrop Wells likely represents one segment. Because volcanic events in the YMR have involved decreasing magma volumes through time, a future event is more likely to have a small volume than a large volume.

The Solitario Canyon dike may provide some indication that it is possible for as many as three dike segments to form given a total event length of 1 km. For a total event length of 1 km, my assessment is that there can be one, two, or three dike segments (probabilities of 0.95, 0.04, and 0.01, respectively).

The number of dike segments increases as the total event length increases. The minimum number of dike segments is always one, and my assessment is that the maximum possible number can be estimated as approximately one per every half-kilometer of event length. This assessment is based on the possibility that the separation between the Little Cones (about 400 m) could provide evidence of the shortest potential dike segments (0.5 km). In general, I think fewer dike segments are more likely than a large number, and the overall shape of the distribution for the number of dikes should have a lognormal shape.

For a total event length of 1 km, the most likely number of dike segments is one (but there can be from one to three); for a total event length of 4 km, the most likely number of dike segments is two (but there can be from one to eight); for a total event length of 15 km, the most likely number of dike segments is five (but there can be from one to 30).

My assessments of the number of dike segments for event lengths of 1, 4, and 15 km are shown in Figure D.8-4.

The lengths of individual dike segments should be derived from my assessments of the total event length and the number of dike segments per event. The minimum length of a dike segment should be about 400 m, based on the separation between the Little Cones.

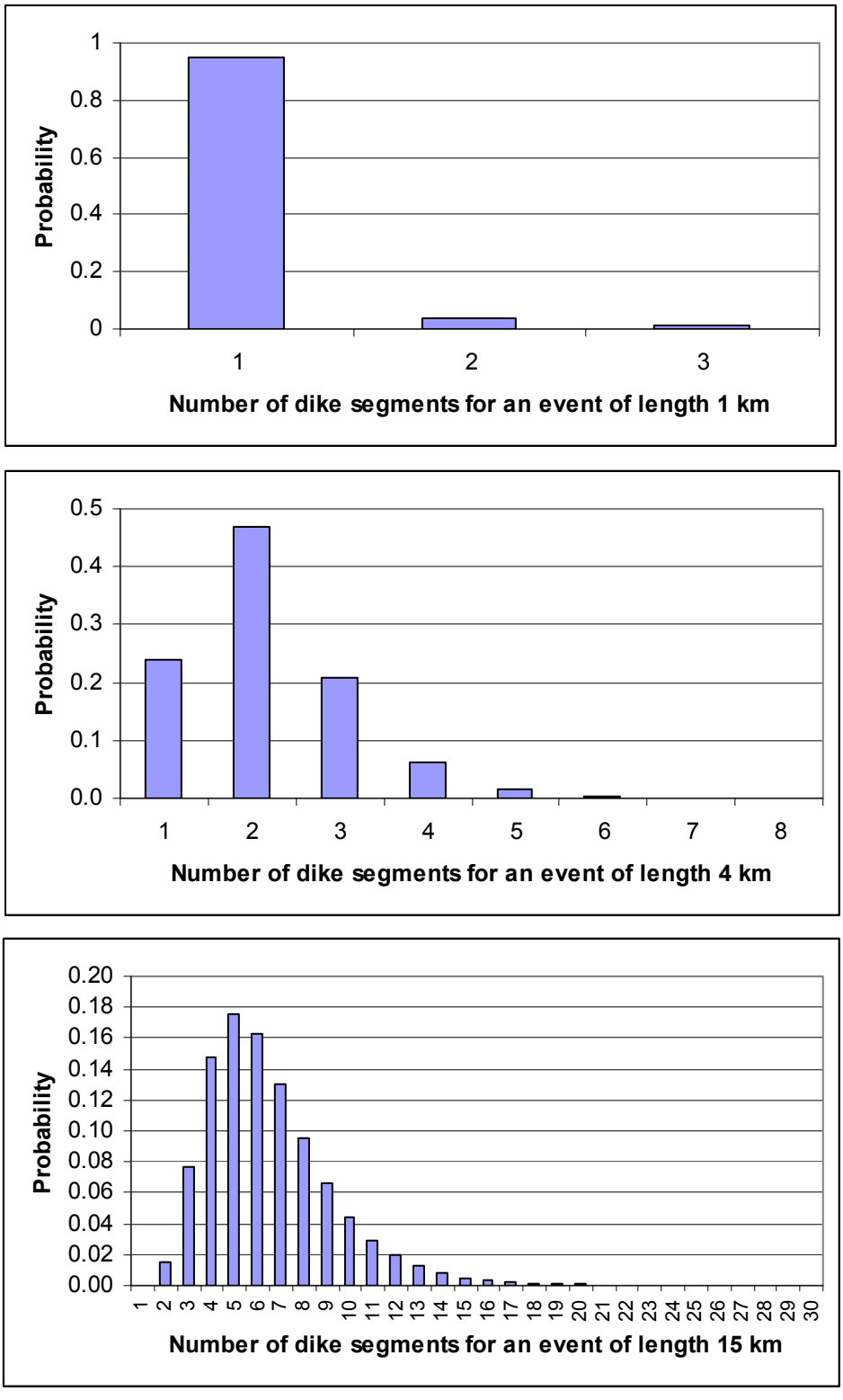

Figure D.8-4. Assessment of the Number of Dike Segments Given Events of Three Different Lengths

Location/Spacing of Dike Segments. Extensional strain rates are sufficiently low in the YMR that any future igneous event is not expected to produce multiple sub-parallel dikes. Multiple sub-parallel dikes typically form from high magma volumes and pressures, conditions that are unlikely in the YMR. Based on geologic patterns (such as fault orientations) in the YMR, if an event were to involve multiple dike segments, they likely would be arranged as N-S segments that step to the right in an en echelon manner, with very little overlap along strike. Right-stepping en echelon dikes appear to form the alignment of Quaternary Crater Flat cones. Dikes tend to step over at the tips because of the rigidity of rocks; overlap occurs at the points where dikes taper. Dike segments arranged in an en echelon pattern will have overlaps ranging from zero to 10 percent of the segment length.

The distance between Little Cones and Makani Cone in the E-W direction is about half that in the N-S distance. This configuration represents a wide event (i.e., large step-over distances between dike segments) relative to dike step-over in the well-studied San Rafael swell area. An event width of about half the event length represents a maximum separation between dikes for the YMR. I expect step-over distances and total event width generally would be smaller rather than larger. Figure D.8-5 shows my assessment of event width as a function of event length.

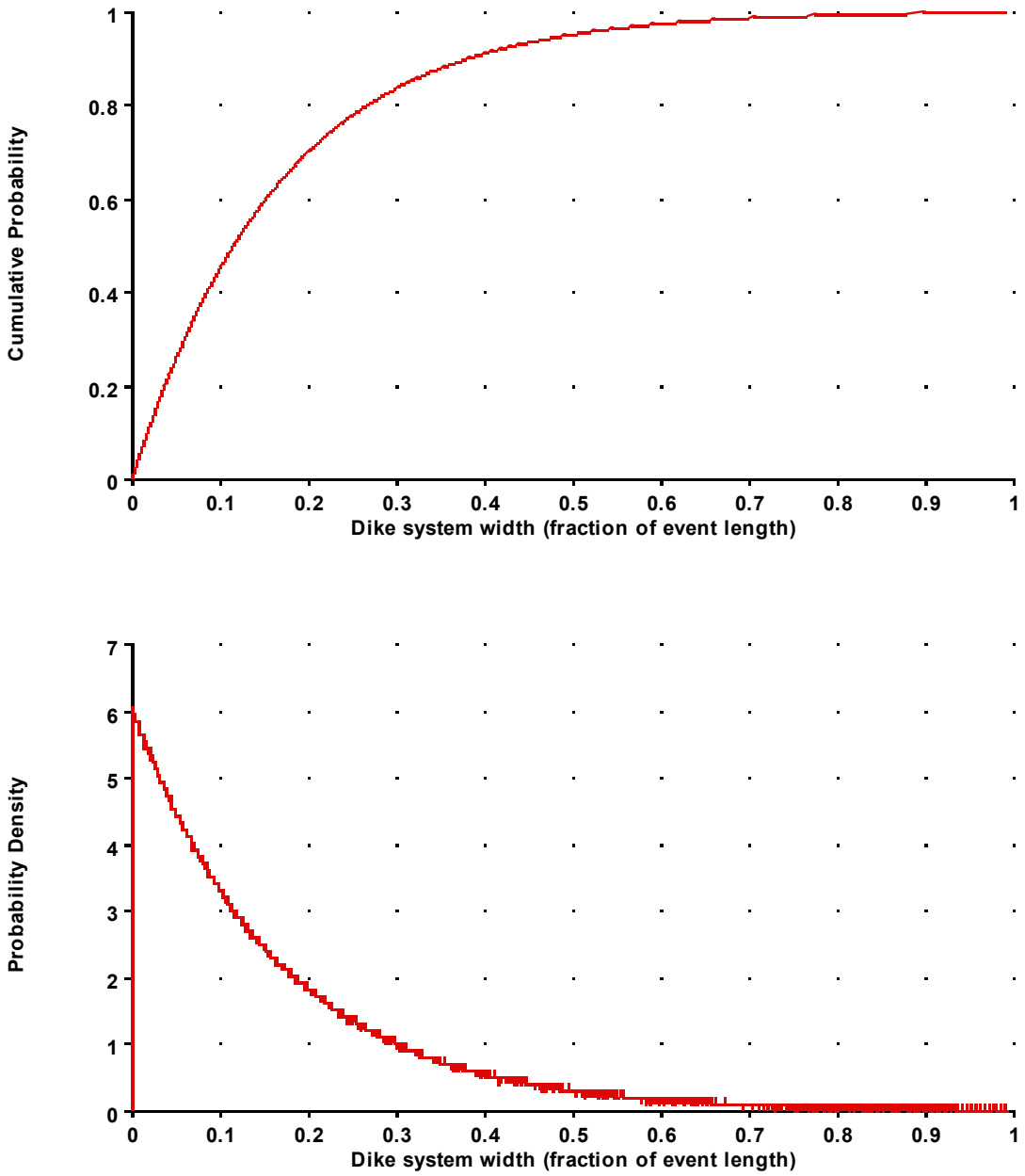

Figure D.8-5. Assessment of the Total Width of a Dike System as a Fraction of the Total Event Length

Dike Azimuth. The various geologic and geophysical data sets for the YMR and worldwide support the interpretation that dikes are intruded perpendicular to the direction of least principal regional stress. Tom Parsons and I (Parsons et al., 2006) modeled Lathrop Wells by examining the stresses on a 20-km-long plane perpendicular to the direction of least principal regional stress. The stresses produced by documented coeval fault movements to the north indicate a favorable location for dike injection at Lathrop Wells.

In the present stress regime of the YMR, dikes at depth should be emplaced preferentially in a NNE direction. As dikes rise from a homogeneous stressed region of deep crust and approach the shallow subsurface, their orientations are influenced by pre-existing faults. Fault capture of dikes occurs especially in the upper few hundred meters of the subsurface. For example, I have observed evidence of dike capture at about 500 m below ground surface on the Comstock fault near Virginia City, Nevada. Faults generally are more crooked than are dikes. Fault trends in the YMR are inherited from an older period of roughly E-W extension. Predominantly normal faults have developed a strike-slip component to accommodate the change in direction of regional stress. In addition, the local stress regime is likely to change near a fault. Cohesion or tensile strength in rocks is significant at shallow depths; with increased depth, cohesion quickly becomes negligible compared to shear resistance. Dikes that have been eroded to a few hundred meters below original ground surface are almost always observed to have been intruded vertically.

A major N-S regional structural trend is indicated by the Bare Mountain fault and the Pliocene Crater Flat dikes. Accordingly, the preferred azimuth for potential future dikes in the upper few hundred meters of the subsurface is N-S. The faults mapped from geologic and aeromagnetic data, which range from N15°W to N30°E, indicate the uncertainty in azimuth. The range N15°W to N30°E also incorporates directions of regional stress through time; incorporates earthquake focal mechanisms; and fits the alignment of Anomalies F, G, and H and the orientation of (8-Ma) dikes at Paiute Ridge. The direction of stress has changed from the mid-Miocene to present throughout a wide region of the Basin and Range Province from about N15°W to about N30°E. Moreover, the southern part of Yucca Mountain has been rotated clockwise, as shown by paleomagnetic data. I assess the azimuth of potential future dikes in the YMR to be between N15°W and N30°E, with a low probability of values outside this range, as illustrated in Figure D.8-6.

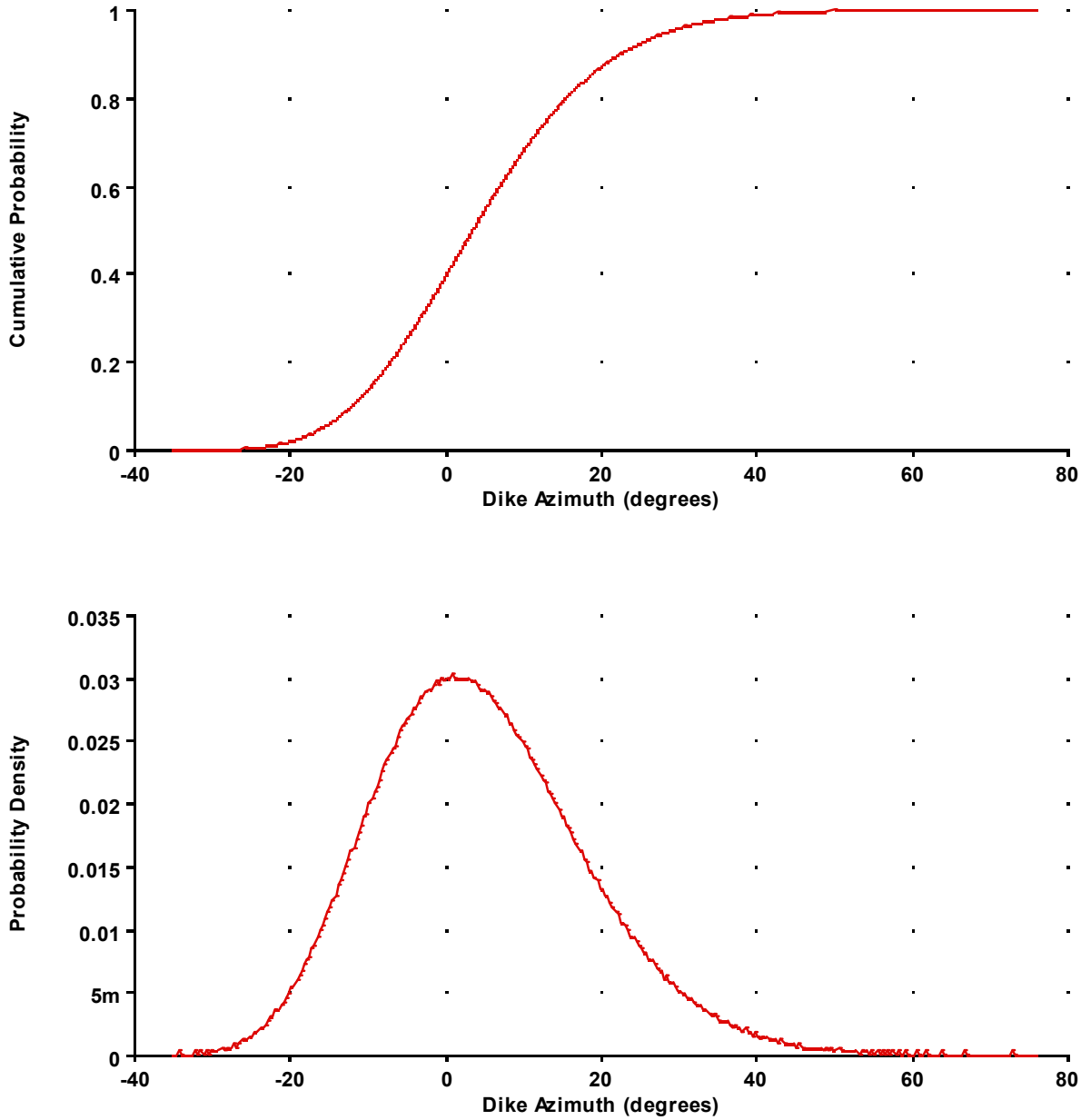

NOTE: Zero represents north.

Figure D.8-6. Assessment of Dike Azimuth

Dike Width. Many dikes associated with individual events, such as the mid-ocean ridge dikes observed in Oman, are 1 to 2 m wide. Dikes such as those associated with flood basalts can be tens of meters wide, although indistinguishable separate events may have contributed to that total width. A dike width of 1 to 3 m is approximately equivalent to the elastic-rebound extension associated with a large normal-faulting earthquake in the Basin and Range tectonic province. Dikes that are much narrower than 1 m tend to be quenched before they can propagate far.

Dike widths observed in the YMR provide the primary basis for my assessment of uncertainty in the width of potential future dikes. Based on observations at Paiute Ridge, a large volume of magma injected at a high rate may produce wider dikes than commonly seen in the YMR. My assessment is that dike widths for the low volumes characteristic of Pliocene-Quaternary events in the YMR should range from 0.5 to 2 m (representing about a 90% confidence interval), with a very low probability of dikes narrower or wider. The mode is a width of about 1 m. This assessment is illustrated in Figure D.8-7.

Sills. Magma must have a high volume and pressure in order to form sills, conditions that are not expected in the YMR. Sills form when the least principal stress direction is vertical (less than the two horizontal stress directions). This condition occurs only if there is a strong enough burst of magmatic activity to inflate dikes to the point of overcoming the least principal stress in the horizontal direction. At that point, the vertical stress becomes the least principal stress direction. This condition occurred at Paiute Mesa (8 Ma), where voluminous dikes are associated with sills. Because small-volume eruptions involving low rates of magma injection are expected in the YMR, sills are unlikely to form. Anomaly A (possibly representing a sill), which is 10 Ma, was formed in a different stress regime and therefore is not an appropriate analog. I conclude that sills are about as unlikely as a silicic eruption in the YMR and can be eliminated from further consideration.

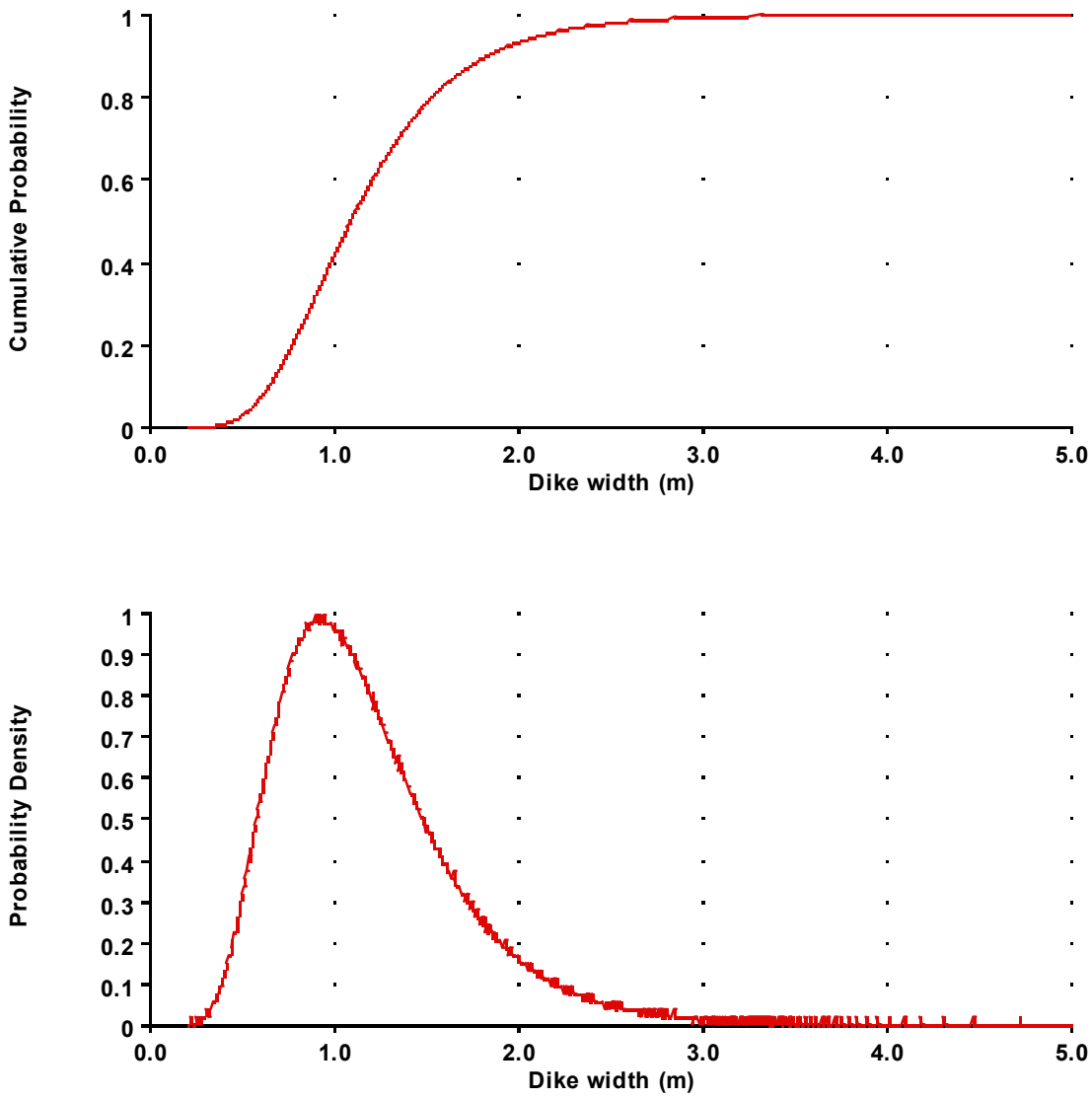

Figure D.8-7. Assessment of Dike Width

Conduit Formation and Geometry

Conduit geometry is defined by the number and locations of conduits on dikes in an event and the conduit diameter at repository depth (see Figure D.8-2). In places such as Iceland or Hawaii, which experience a high rate of eruption, continuous eruptions can occur along fissures and then focus into a few conduits. If a dike erupts at a single location, heat supply and wall rock erosion are concentrated and the dike will widen, forming a conduit at that location. Rock is eroded where the first breakthrough occurs. Breakthrough lowers the magma pressure in other areas along the dike. My assessment is that if a dike segment were to reach repository depth, a conduit likely would form. This judgment relies on evidence that fragmentation depths are ≥1 km, based on estimates of water and volatile content for magmas in the YMR. Therefore, all events would produce at least one conduit. Because of the low magma volumes, however, there would be only one conduit per dike segment, and not every dike segment associated with an event necessarily would have a conduit.

My assessment of the probable number of conduits per future event for various event lengths is shown below in Table D.8-2, subject to the constraint that there would be at most one conduit per dike segment.

Table D.8-2. Number of Conduits as a Function of Event Length

Number of Conduits	Probability		
	1 km	4 km	15 km
1	0.95	0.375	0.03
2	0.05	0.375	0.07
3		0.2	0.1
4		0.05	0.2
5			0.4
6			0.1
7			0.07
8			0.03

Conduits tend to occur near the center of a dike; there is a lower probability of occurrence on the ends of the dike. This assessment is based on the analogy of dike-fed conduits in ocean ridges. The distribution for conduit location tapers at each end and is rounded in the middle, as illustrated in Figure D.8-8.

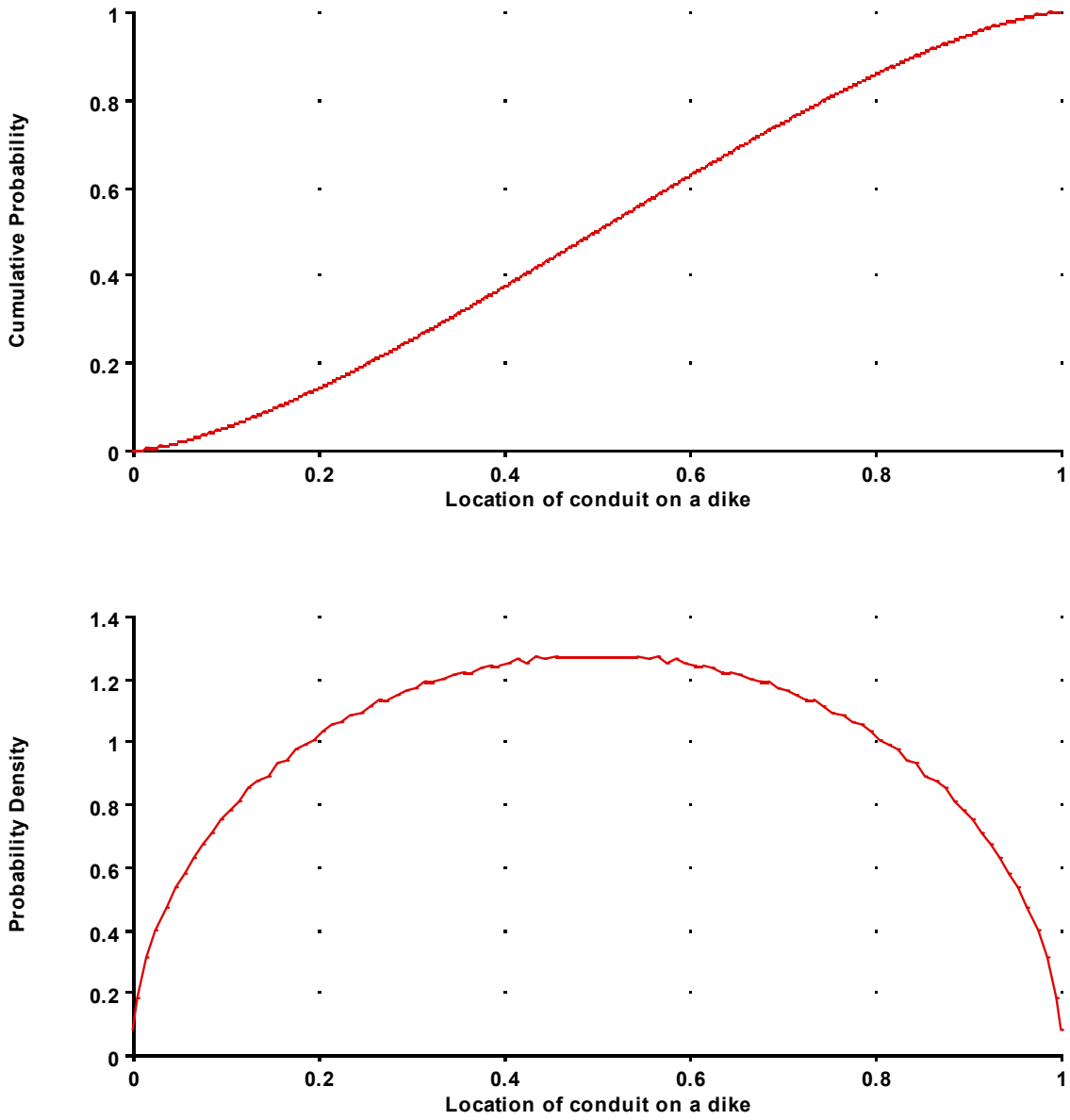

NOTE: Zero and 1 represent the endpoints of the dike.

Figure D.8-8. Assessment of the Location of a Conduit on a Dike

Conduit Diameter. My estimates of the dimensions of potential future conduits at repository depth are based on analogs in the YMR (Basalt Ridge and southeast Crater Flat). Paiute Ridge probably is not a good analog because of its higher volumes of magma. Conduit diameter can be expressed as a function of dike width, although I have observed near-surface, funnel-shaped conduits sloped at approximately the angle of repose. The most likely width of a conduit is three to four times the width of the dike. There is an 80% likelihood that conduit diameter would be 10 times dike width or less. The maximum conduit diameter I can envision, given the probable

magnitude of future events, is about 30 times dike width. There is a 99% chance the diameter would be smaller than that. This probability distribution is shown in Figure D.8-9.

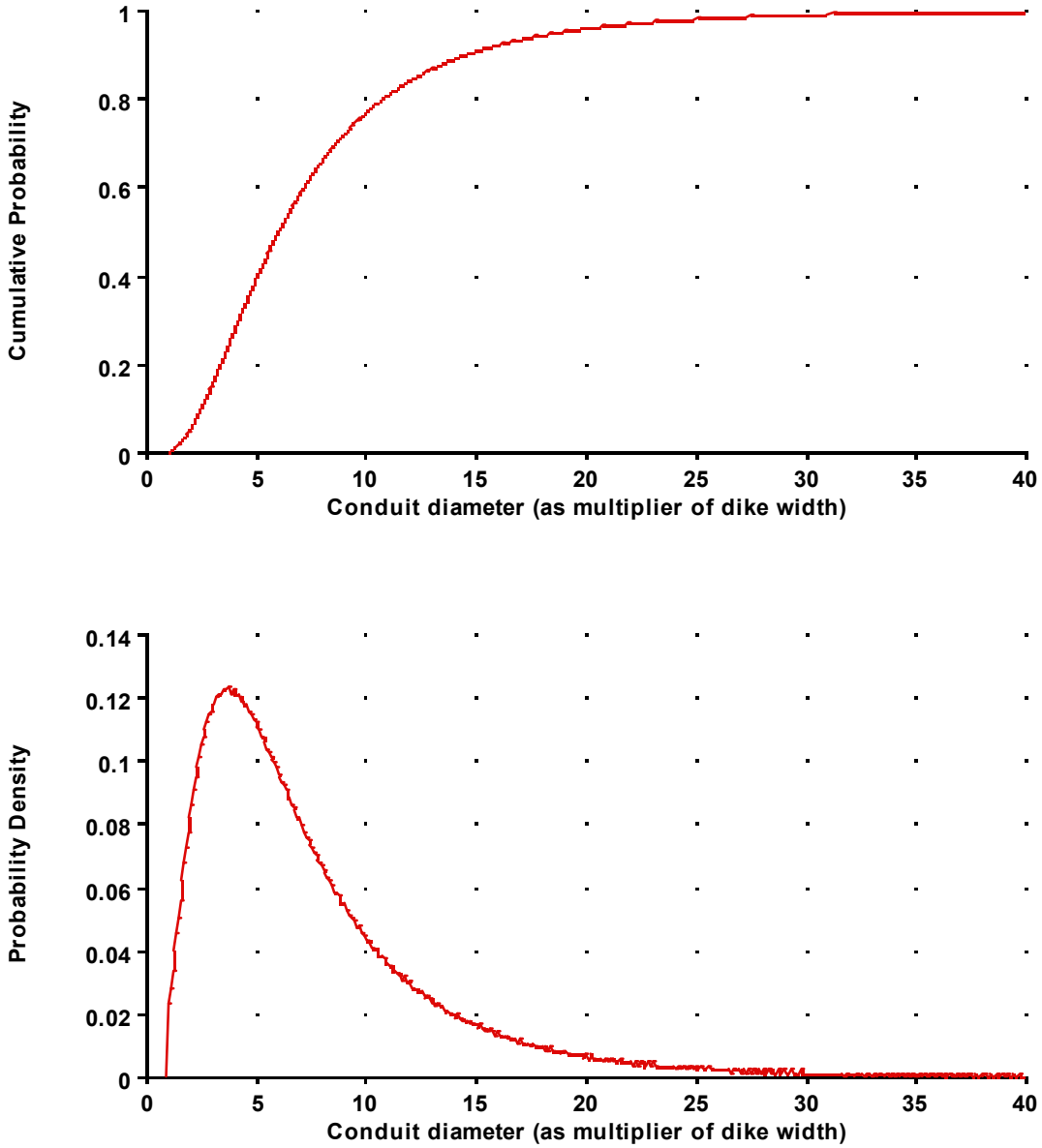

Figure D.8-9. Assessment of the Diameter of a Conduit as a Multiplier of Dike Width

Column-Producing Conduits. I think that all conduits that I identify in my assessment would be associated with eruptions that produce columns. I expect future magmas in the YMR to be very gaseous. Studies of eruptive facies have shown that at least one cone in Crater Flat (Makani Cone) apparently was associated with fissure eruptions and was not column-producing, but it is highly likely that the others produced columns.

D.8.2 SPATIAL MODEL

Each areal domain responds differently to tectonic extension, as reflected in the region's topography [see Parsons and Thompson (1991) for examples worldwide]. Extension accommodated by dikes typically produces low topographic relief, as reflected in Crater Flat and Amargosa Desert to the south. In contrast, the high-relief Yucca Mountain block is characterized by faulting that occurred during the past 10 Ma. This difference in response occurs because dike injection relieves elastic strain without normal faulting. In the absence of magmatism, normal faulting, with its accompanying topographic relief, relieves elastic extension. Geophysical data indicate that Crater Flat basin narrows with increasing depth, so that the subsurface width of the basin is smaller than what is observed at the ground surface. Based on Brocher et al. (1998, Figure 6), the center of Crater Flat at depth is the focus for extension, and the magnitude of extension is about 8 km. Where normal faults converge below Crater Flat, dikes probably accommodate at least part of this significant extension. This inference is consistent with Crater Flat being a locus of magmatism at the surface. Dikes can penetrate the elastico-viscous (ductile) lower crust from their source in the mantle, because they are injected rapidly compared to the relaxation time in these materials. That is, a component of elastic strain is expected in the lower crust and upper mantle. In the near-surface crust beneath Crater Flat, where differences in tectonic stress are necessarily small because of low rock strength, dikes have leaked into (been captured by) normal faults.

The lower topographic elevation and lower free-air gravity in Crater Flat compared to Yucca Mountain are correlated with magmatism in Crater Flat and lack of magmatism in Yucca Mountain. This correlation can be explained by contrasting stress regimes. Dikes in the elastic crust (below the uppermost weak zone that cannot support much accumulated stress) propagate perpendicular to the least horizontal stress. In Yucca Mountain, the maximum principal stress is vertical and the least horizontal stress, measured by hydraulic fracturing in boreholes, is oriented WNW-ESE (Stock et al., 1985). Hydrofractures, analogous to incipient dike injections, are vertical and oriented NNE-SSW. The difference between the maximum principal stress, estimated by the vertical load at any given depth, and the least principal stress, measured by hydraulic fracturing pressure, increases approximately linearly with depth. The least principal stress is maintained throughout the depth of investigation at about one-half the maximum (vertical) principal stress (Stock et al., 1985). Significantly, this difference in stresses is closely enveloped by the frictional shear resistance (strength) of the rocks. Thus, the rocks are close to failing by normal faulting. In contrast, anywhere that magma is supplied at a pressure that exceeds the least principal stress, magma injection forms dikes perpendicular to that stress. The buoyant pressure of magma need not exceed the lithostatic load, as commonly claimed, but must only exceed the least principal stress (Parsons and Thompson, 1991). As a consequence of these relations, dike injection and inflation may inhibit normal faulting and consequent topographic relief by decreasing the accumulated stress difference.

Why, one might ask, is the free-air gravity anomaly superior to topographic elevation alone in indicating that an area is less or more favorable to dike injection? The free-air anomaly senses total mass below the topographic surface, thereby accounting for variations in density (Parsons et al., 2006). As outlined in the preceding paragraph, the difference between the vertical load and the least horizontal stress increases linearly with depth in the Yucca Mountain area (and commonly in other actively extending regions). At any given depth, therefore, the least

horizontal stress is greater where the free-air anomaly is greater and vise versa. For a dike to be injected, magma pressure must overcome this least horizontal stress. In the YMR, because magma volumes and fluxes generally have been small during the past 5 Ma, stress should be an important or controlling factor in the locations of injection. Conversely, in a region of high magma volume and flux, where tectonic extension is slow compared to magna supply, the stress state and therefore the free-air gravity anomaly would be less important. Empirical observation reveals no volcanism in the Yucca Mountain block in the past 10 Ma. Free-air anomaly data show a strong contrast between Crater Flat and the Yucca Mountain block.

Topographic relief in the YMR is a result of normal faulting. Three faults in the area (Solitario Canyon, Crater Flat, and Windy Wash) contain ash associated with the 80-ka Lathrop Wells eruption, suggesting that faulting likely occurred within weeks or months of the Lathrop Wells eruption. By releasing stress near the faults and increasing stress near Lathrop Wells, this faulting probably produced conditions favorable for injection of a dike below Lathrop Wells. Or, the eruption of Lathrop Wells produced conditions favorable for faulting [see Parsons et al. (2006) for background references and modeling].

D.8.2.1 Region of Interest and Zone Boundaries

My general region of interest for this assessment is shown in Figure D.8-10. Because post-4-Ma volcanic events are most relevant to assessing future volcanism, my region of interest includes the 4-Ma and younger basalts of Crater Flat and the Amargosa Desert. Features related to the Amargosa Trough and to the calderas that surround Yucca Mountain are included. Only the extensional region within the Basin and Range Province is included. The region to the west, which is characterized by a strike-slip regime, is excluded.

I define two zones: (1) the post-4-Ma volcanic domain in the Crater Flat-Amargosa Desert (CF-AD), and (2) the Yucca Mountain fault domain. Although their ages are unknown, Anomalies C and D are included in my definition of the CF-AD zone. The boundaries of the zones are defined by fundamental differences in geologic structure that control the locus of volcanism, as discussed in the following section. Figure D.8-10 illustrates these zones.

Past events that are not part of the CF-AD volcanic domain are Buckboard Mesa, Thirsty Mountain, Little Black Peak, and Hidden Cone. These features are, however, relevant to our understanding of the regional cooling history and the apparent decrease in eruptive volume through time.

The boundary between the CF-AD volcanic zone and the Yucca Mountain fault domain zone is defined by: (1) the uncertainty in the location of the boundary, and (2) the change in volcanic rate across the boundary. The change in volcanic rate between zones is gradual, not abrupt, and the ramp, or transition distance for the rate change, differs along the boundary. The uncertainty boundaries shown in Figure D.8-10, which represent a combination of uncertainties in the location of the zone boundary and in the transition distance, represent about a 90% confidence interval. The transition distance is roughly half the total distance between the minimum and maximum boundaries for the CF-AD volcanic domain shown in Figure D.8-10.

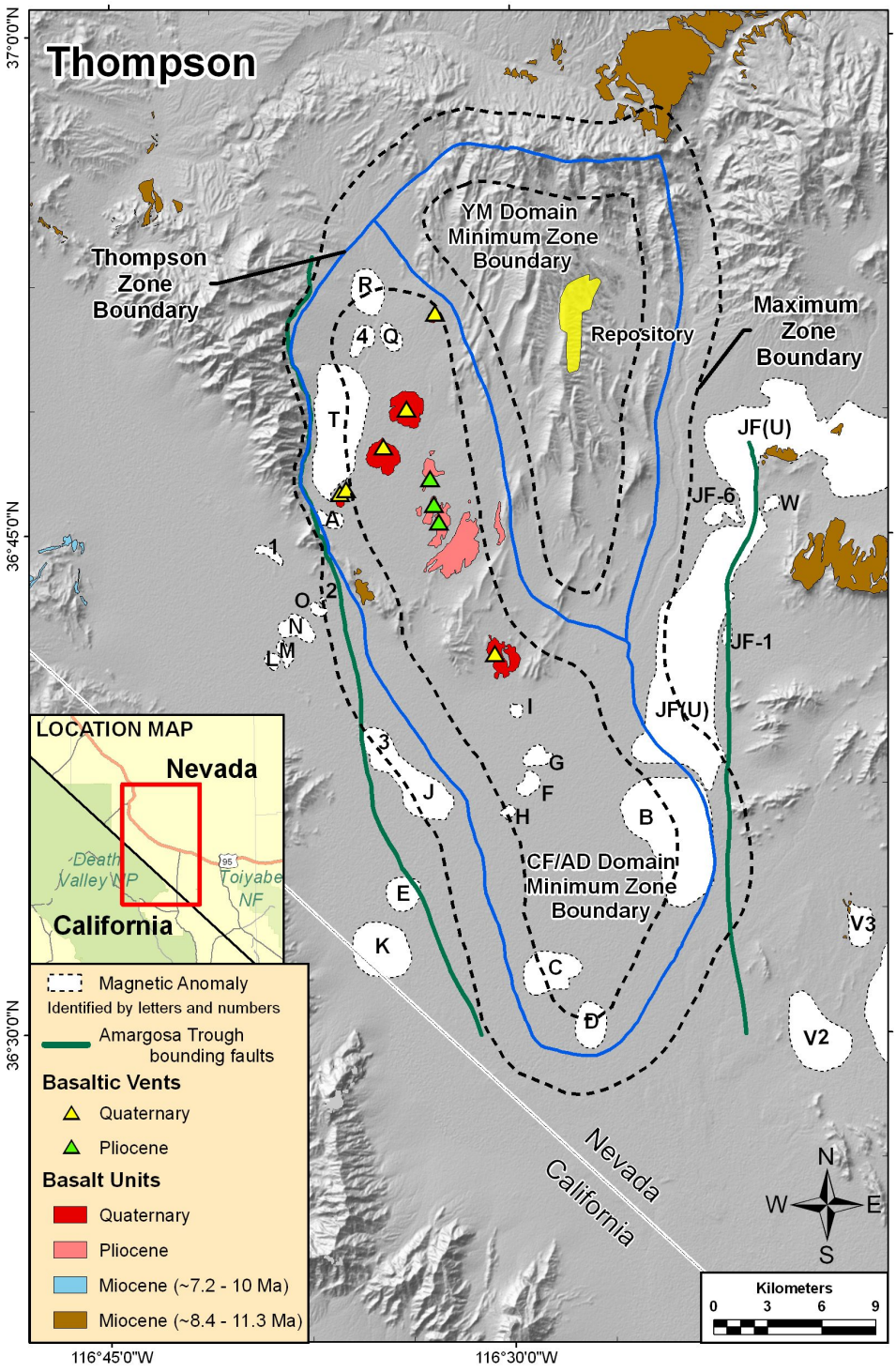

NOTE: Blue line shows my best estimate of the zone boundaries, representing the 50th percentile of the distribution on boundary location. Dashed lines represent the minimum and maximum extents of the zone boundaries.

Figure D.8-10. General Region of Interest Showing My Defined Zones and Associated Uncertainty

Physically, the boundary represents the current zone of stress change indicated by the free-air gravity anomaly. Uncertainty in the location of the boundary represents uncertainty in the stress and in the distance over which it changes. For example, I expect that dikes would die out to the northeast within the zone boundary between Crater Flat and Yucca Mountain and within the Bare Mountain boundary zone to the southwest, but dikes easily might penetrate the southwest boundary zone toward the Amargosa Desert. The boundary also represents a change in the way extension is accommodated, as reflected by the change in the throw of faults across the boundary. The boundary also separates structural domains.

Extension in Crater Flat Basin and Boundary with Yucca Mountain Fault Domain

The CF-AD volcanic zone is located within an asymmetrical structural depression, or graben, bounded by the Bare Mountain master fault to the west and many smaller faults near and within Yucca Mountain to the east. The faults to the east typically dip west toward the Bare Mountain fault and converge southwest toward the Bare Mountain fault, where they die out. None of the eastern faults is known to cut the Bare Mountain fault (Fridrich et al., 1999, Figure 1; Brocher et al., 1998). The width of the graben on the Brocher et al. (1998) seismic section measures roughly 20 km, from the Bare Mountain fault to the unnamed fault just east of the summit of Yucca Mountain. The Crater Flat volcanic cones are located above the structurally deepest part of the graben, which is only about 10 km wide.

The principal eastern faults (including the Solitario Canyon fault and the unnamed fault directly east of it) converge on the Bare Mountain fault beneath Crater Flat at a depth of 10 to 20 km, which coincides roughly with the base of the seismogenic zone (the brittle-ductile transition). The tectonic extension that produced a graben at the surface is focused in a narrow zone at depth beneath Crater Flat. Below the brittle-ductile transition, tectonic extension presumably is accommodated by a combination of magma emplacement and ductile spreading. Using the analogy of spreading centers in ocean crust, central grabens usually are underlain in the mid-crust by composite (sheeted) dikes. Moreover, at the continental Ethiopian rift system, seismic evidence indicates the presence of an underlying axial dike system (Keranen et al., 2004). Clearly, extension by dike injection can be complementary to tectonic extension by normal faulting, a tradeoff that likely operates in Crater Flat.

Because the eastern set of faults converges southwestward toward Crater Flat and the Bare Mountain master fault, but does not cross the Bare Mountain fault, I infer that fault displacements must decrease or terminate in that direction and that dikes rather than faults accommodate some of the extension at depth. This conclusion may conflict with the interpretation of Fridrich et al. (1999) that extension on the eastern set of faults increases to the southwest. Fridrich et al. assign “infinite” extension to the Bare Mountain fault, which of course would be true of each fault discontinuity. Fridrich et al. (1999), however, also compute and contour an average percent extension based on a model of fault blocks uniformly tilted on parallel planar faults in domino fashion. If conditions are right, a calculation (Thompson, 1960; Nur et al., 1989) enables extension to be determined based on only the initial dip of faults (angle between originally horizontal strata and fault planes) and dip of the strata. With simplified assumptions, Fridrich et al. (1999) contour the percent extension based simply on the dip of the strata, overlooking the geometrical requirement that both ends of a section must be at the same structural elevation for the calculation to be accurate. To illustrate the problem, consider a

half-graben bounded by a master normal fault on one side and a downwarp that includes few or no faults on the other side. Stratal dips on the downwarp would have no relation to extension.

I estimate total extension across the Crater Flat basin directly from the Brocher et al. (1998) section. I estimate this extension to be 8 km (roughly 60 to 100 percent of the original width), of which 4 km is associated solely with the Bare Mountain fault. No comparable section is available farther south, but as noted previously the convergence in strike and dip of the eastern set of faults toward the Bare Mountain fault suggests a decrease in total extension. Moreover, gravity data do not show an increase in depth to pre-Tertiary rocks toward the south.

Perhaps the much slower Quaternary extension rate is of more direct importance to the locations of potential future volcanism than is total extension. Fridrich et al. (1999, Figure 6) summarize the late Quaternary data from their fault trenching. The extension rate in three transects from north to south increases from 0.008 mm/yr to 0.030 mm/yr and then to 0.059 mm/yr. It should be emphasized, however, that the southernmost part of Crater Flat basin was not included in any of the analyses of extension because of the alluvial cover (Fridrich et al., 1999, p. 202). This basin is precisely the area of youngest volcanism.

It is important to note that the northerly striking Bare Mountain master fault originated when regional extension was WSW-ENE. The fault maintained that strike when extension changed to WNW-ESE. The eastern set of faults, especially the southern parts that were tectonically rotated, were subjected to the later direction of extension. The alignments of both this set of faults and the Quaternary Crater Flat cones reflect the younger stress state.

I conclude that the fault domain that includes the set of faults on the eastern side of Crater Flat near Yucca Mountain transitions southwestward into the Crater Flat volcanic domain, where extension has been accommodated partly by dike injection.

The uncertainty in location of the boundary of the zones is generally greater in the southwest part of the CF-AD zone than in the northeast, because topographic and free-air gravity gradients are higher and better defined to the northeast and correspond to the limit of volcanism in this part of the zone. To the southwest, the Yucca Mountain faults converge in both strike and dip toward the Bare Mountain master fault and must die out or terminate against it. In this location, I visualize a physical transition between extension by normal faulting and extension by dike formation at depth beneath Crater Flat.

Rate Variation within Zones

We must consider the variation in rate of volcanism that might be expected to occur within the CF-AD zone. For post-4-Ma basalts in Crater Flat, the erupted volume of magma is significantly larger along the axis of the zone than at the edges, as evidenced by the voluminous magma associated with Red Cone and Black Cone, Lathrop Wells, and the 3.8-Ma southern Crater Flat basalts. This difference in volume is consistent with a fault zone that narrows at depth in the center of the basin, as imaged on the seismic reflection profile that runs from east of Yucca Mountain to Bare Mountain. Because the axis of the larger-volume centers reflects a continuous underlying structure, it is appropriate to assume that the future rate of volcanism will be approximately uniform along the axis, and higher along that axis than at the edges of the zone.

After examining conditional spatial intensity maps based on my zone boundaries and the transition distance I define above, I believe that the variation in rate of volcanism within the CF-AD zone is captured appropriately by the assumption of a homogenous rate within each zone and a gradual transition in rate between zones.

Within the Yucca Mountain fault domain, one might expect a higher probability of volcanism to the south, with little expected difference between the central and northern areas. No significance is given to the Solitario Canyon dike in this regard because of its age. Perhaps variations in the slip rate of faults within the domain would provide a basis for assessing the variation in rates of volcanism, although the use of short-term (late Quaternary) slip rates likely would not be precise enough to be useful. In the absence of compelling evidence to the contrary, I assume there is no variation in rate of volcanism within the Yucca Mountain zone.

Other Geologic Data

I considered two geologic databases as potentially appropriate for combination with the rate intensities derived from the zone-based spatial models described above: cumulative extension data and gravity data. Geologic data pertaining to Late Cenozoic cumulative extension in the Crater Flat basin are available from Fridrich et al. (1999). These data, however, are not useful for the present analysis. It is inappropriate to use the post-12.7-Ma extension contours, because that period is extremely long compared to the 4-Ma period of interest for the spatial model and also because tectonic rates have decreased markedly (see also the above discussion under "Extension in Crater Flat Basin and Boundary with Yucca Mountain Fault Domain.")

Free-air gravity data reflect lateral variations in mass, including topographic masses and density, most of which occur within 3 km of the surface. Free-air gravity data for the region of interest indicate clear boundaries. Tom Parsons, Allen Cogbill, and I used gravity data as a proxy for lithostatic pressure and least-principal stress, because in extensional areas worldwide the least principal stress is close to one-half the lithostatic pressure (Parsons et al., 2006). Lithostatic pressure data have a strong correlation with volcanism in the Yucca Mountain area—these data can be used as a basis for separating the Crater Flat and Yucca Mountain blocks. The data also support the concept that the highest potential for volcanism is along the structural axis of the Crater Flat basin. Because the spatial zone models described previously already account for this information, however, I see no need to combine the gravity/lithostatic pressure data directly with the spatial intensities derived from the zone models.

D.8.3 TEMPORAL MODEL

I use two approaches to estimate the recurrence rate within each of the two zones in the region of interest: a homogenous Poisson model, and a model based on eruptive volumes through time.

D.8.3.1 Homogenous Poisson Model

The first approach assumes a homogenous Poisson process, whereby the recurrence rate is estimated based on the number of past events within each zone during the period of interest. The period of interest is defined as post-4-Ma volcanism. The events in the CF-AD zone are given in Table D.8-1 and discussed above in Section D.8.1.1. The events in Table D.8-1 are used to define a recurrence rate for the CF-AD zone.

Within the Yucca Mountain fault domain, no events have occurred in the post-4-Ma time frame. To assess the rate in this fault domain, then, an average normalized rate (per km^2) is assessed based on the number of events in a larger background zone. To calculate this background rate, I use the post-4-Ma events in the relatively large background region shown in Figure D.8-11.

The region shown in Figure D.8-11 is based on isotopic data from Livaccari and Perry (1993, Figure 1). I like the logic behind the Amargosa Valley Isotopic Province of G. Yogodinski, reviewed in PVHA-96 (CRWMS M&O, 1996), because it shows similar lithosphere beneath Plio-Quaternary cones within the zone, but not beneath the Cima, Lunar, or Reveille volcanic fields. The background rate should be calculated based on Quaternary and Pliocene events (post-4 Ma) in this zone, excluding those events that lie within the CF-AD zone. There are four known relevant events in the background zone: Buckboard Mesa, the two Sleeping Butte cones, and the Clayton Valley cone. The volcanic events in this background zone are given in Table D.8-3.

Table D.8-3. Relevant Events in the Background Zone

Event Name/Location	Number of Events	Age (Ma)
Buckboard Mesa	1	2.9*
Hidden Cone	1	0.35*
Little Black Peak	1	0.35*
Clayton Valley Cone	1	0.39**

* Age based on consideration of LANL (2007).
**Age based on Wood and Kienle, 1990.

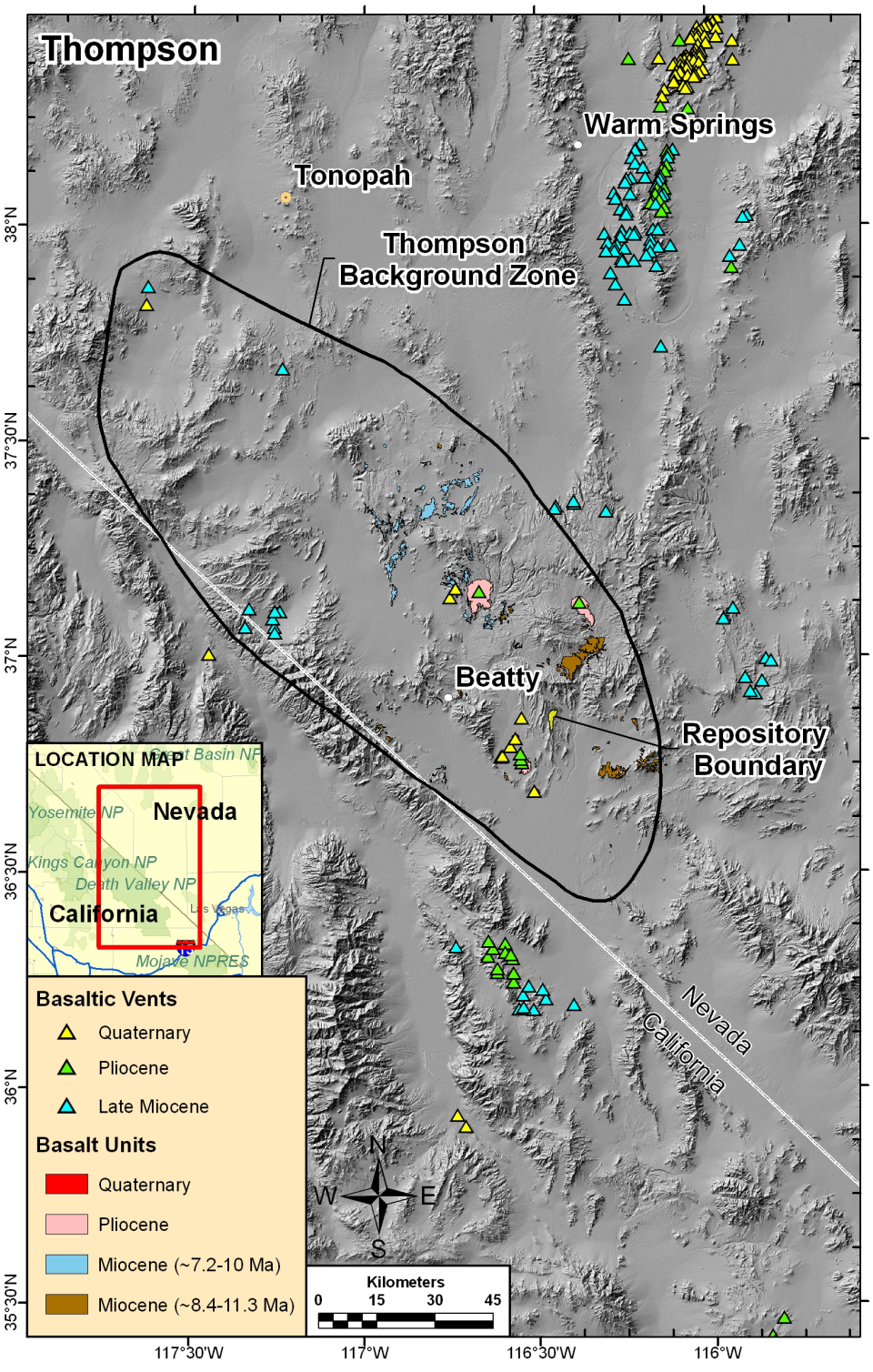

NOTE: Post-4 Ma events are a subset of the green (Pliocene) and yellow (Quaternary) triangles.

Figure D.8-11. Background Zone

D.8.3.2 Time-Volume Model

The second temporal model is a time-volume model that uses the rates of volume change (both cumulative volume and volume per event) to estimate a recurrence rate for the CF-AD zone. Volcanism in the Yucca Mountain region has been waning during the past 11 Ma, as indicated by a decrease in the volume of erupted magma. I use this decrease, shown graphically in Valentine and Perry (2006) and other publications, to develop inputs for the time-volume model. Those inputs are estimates of the rate of magma production and the volume per event.

The rate of magma production can be estimated as the slope of a curve showing the change in cumulative volume over time. In considering the change in cumulative volume over time, the conceptual model of conductive heat loss discussed by Richard Carlson (in PVHA-U Workshop 2) seems appropriate. A model of cumulative volume as a function of time should be fit to the events identified in Table D.8-1. Volume per event does not appear to be predictable as a function of time. My assessment of the volumes of potential future events is based on the mean and variance of the volume of events in the CF-AD volcanic domain in the past 2 Ma (as shown in Table D.8-1).

I prefer the time-volume model because it takes into account the clear change in volumes that has occurred in the YMR during the past several million years. The two alternative temporal models for the recurrence rate within the CF-AD volcanic domain are assigned the following weights: homogeneous Poisson (0.25), and time-volume (0.75).

Implications for One-Million-Year Time Frame

It is possible that the current extensional tectonic regime will be overtaken by a strike-slip regime. That is, the influence of Walker Lane could increase. I do not expect such a change to occur in a time frame that would affect my estimates significantly.

Based on the steady-state history and declining magmatism/tectonism of this part of the Basin and Range throughout the past several million years, a change in style of volcanism (from basaltic cones to silicic calderas) is extremely unlikely in the YMR. Tectonic changes, even a change from an extensional to a strike-slip regime, occur over periods on the order of one million years or longer. Silicic eruptions in the YMR can therefore be eliminated from further consideration.

D.8.4 REFERENCES

Brocher, T.M., Hunter, W.C., and Langenheim, V.C., 1998, Implications of seismic reflection and potential field geophysical data on the structural framework of the Yucca Mountain-Crater Flat region, Nevada: Geological Society of America Bulletin 110, p. 947-971.

CRWMS M&O, 1996, Probabilistic volcanic hazard analysis for Yucca Mountain, Nevada. Las Vegas, Nevada: prepared for the U.S. Department of Energy. BA0000000-01717-2200-00082 Rev 0.

Delaney, P.D., and Pollard, D.D., 1982, Solidification of basaltic magma during flow in a dike: American Journal of Science, vol. 282, p. 856-885, June.

Fridrich, C.J., Whitney, J.W., Hudson, M.R., and Crowe, B.M., 1999, Space-time patterns of late Cenozoic extension, vertical axis rotation, and volcanism in the Crater Flat basin, southwestern Nevada, in Wright, L.A., and Troxel, B.W. (eds.), Cenozoic Basins of the Death Valley Region: Boulder, Colorado, Geological Society of America Special Paper 333, p. 197-212.

Keranen, K., Klemperer, S., Gloaguen, R., and the EAGLE Working Group, 2004, Three-dimensional seismic imaging of a proto-ridge axis in the main Ethiopian rift: Geology, vol. 32, p. 949-952.

Los Alamos National Laboratory (LANL), 2007, Ar/Ar age determinations, volume, location and elevation of Plio/Pleistocene volcanoes in the Yucca Mountain region, Rev. 3: Excel spreadsheet titled, Volcano_volume_age_location_Rev03.xls.

Livaccari, R.F., and Perry, F.V., 1993, Isotopic evidence for preservation of Cordilleran lithospheric mantle during the Sevier-Laramide orogeny, Western United States: Geology, v. 21, p. 719-722, August.

Nur, A., Ron, H., and Scotti, O., 1989, Mechanics of distributed fault and block rotation, in Kissel, C., and Laj, C. (eds.), Paleomagnetic Rotations and Continental Deformation: Boston, Kluwer Academic Publishers, p. 209-228.

Parsons, T., and Thompson, G.A., 1991, The role of magma overpressure in suppressing earthquakes and topography—worldwide examples: Science, v. 253, p. 1399-1402.

Parsons, T., Thompson, G.A., and Cogbill, A.H., 2006, Earthquake and volcano clustering via stress transfer at Yucca Mountain, Nevada: Geology, v. 34, no. 9, p. 785-788, September.

Stock, J. M., Healy, J.H., Hickman, S.H., and Zoback, M.D., 1985, Hydraulic fracturing stress measurements at Yucca Mountain, Nevada, and relationship to regional stress fields: Journal of Geophysical Research, v. 90, p. 8691-8706.

Thompson, G.A., 1960, Problem of late Cenozoic structure of the Basin Ranges: Report of the International Geological Congress, XXI Session, Part XVIII, p. 62-68, Norden.

Valentine, G.A., and Perry, F.V., 2006, Decreasing magmatic footprints of individual volcanoes in a waning basaltic field: Geophysical Research Letters, vol. 33, L14305, DOI: 10.10292006GL026743.

Wood, C.A., and Kienle, J., 1990, Volcanoes of North America: United States and Canada: Cambridge University Press, Cambridge.

APPENDIX E

DETAILS OF HAZARD FORMULATION AND CALCULATIONS

This appendix presents additional details on the mathematical formulations used to compute the volcanic hazard, provides some notes on the specific calculations for individual experts, as appropriate, and describes the calculation of the aggregate hazard. The mathematical formulations and calculations described below were implemented in and conducted using three software codes: RateDens (STN: 11246-1.0-00), EventSim (STN: 11247-1.0-01), and LTree (STN: 11245-1.0-01). Much of the mathematical formulation described below is also included in the Design Documents associated with each code (U.S. Department of Energy, 2008a, 2008b, 2008c).

E.1 MATHEMATICAL FORMULATIONS OF THE HAZARD CALCULATIONS

The measure of volcanic disruption hazard is the annual frequency of intersection of the repository footprint, v_I, by a volcanic feature (e.g., dike, sill, an eruption column-producing conduit, or a non-column-producing vent). The basic formulation for calculating v_I is given by the equation:

$$\nu_I(t) = \iint_R \lambda(x,y,t) \times P_I(x,y)\, dx\, dy \qquad \text{(Eq. E-1)}$$

where $v_I(t)$ indicates that v_I is a function of time; $\lambda(x,y,t)$ is the rate density (frequency of volcanic events per unit time per unit area) at location (x, y) in the region of interest, R, at time t; and $P_I(x,y)$ is the conditional probability that a volcanic event centered at location (x,y) will intersect the repository.

The calculation is performed by discretizing the region of interest, R, on a grid with spacing Δx and Δy and replacing the integral Equation E-1 by the equivalent summation:

$$\nu_I(t) = \sum_{i=1}^{N_x} \sum_{j=1}^{N_y} \lambda(x_i, y_j, t) \times P_I(x_i, y_j) \Delta x \Delta y \qquad \text{(Eq. E-2)}$$

The rate density can be defined as the product of a rate parameter, $\lambda(t)$, and a conditional spatial mass density, $f(x,y)$. When this approach is used, Equation E-2 is replaced by:

$$\nu_I(t) = \sum_{i=1}^{N_x} \sum_{j=1}^{N_y} \lambda(t) \times f(x_i, y_j) \times P_I(x_i, y_j) \Delta x \Delta y \qquad \text{(Eq. E-3)}$$

A variety of models can be used to calculate each of these three components of the calculation: the temporal rate model, the conditional spatial mass density, and the conditional probability of intersection.

E.2 TEMPORAL MODELS

Three rate models are used to represent the rate of volcanic events (the $\lambda(t)$ of Equation E-3): a homogenous Poisson model, a Poisson model with a time-dependent rate estimate based on estimates of the rate of change of magma volume over time, and a temporal clustering model.

E.2.1 Homogenous Poisson model

The underlying probabilistic model used here is the assumption that the occurrence of volcanic events conforms to a Poisson process with homogenous rate. Homogenous Poisson models are commonly used to represent the hazard from rare events. The Poisson model forms the basis of the probabilistic seismic hazard methodology developed by Cornell (1968, 1971).

The homogenous Poisson process specifies that the probability distribution for the number of events, *n*, occurring in time period *t* is given by:

$$P(n) = \frac{(\lambda t)^n e^{-\lambda t}}{n!} \qquad \text{(Eq. E-4)}$$

where λ is the mean rate of occurrence of events per unit time.

The rate parameter λ can be estimated directly or derived from information on past events.

For experts who chose to derive a rate based on past events, the estimate of the rate parameter is based on two inputs: the number of events *N* in time period T, where T is defined as the time between the oldest of the *N* events and the present.

Following Solow (2001), we take a Bayesian approach to estimating a distribution for the rate parameter λ. As shown there, if the prior distribution on the rate, $\pi(\lambda)$, is assumed to be Gamma (α,β), the distribution for the rate parameter for a homogenous Poisson model also follows a Gamma distribution with parameters $\alpha+N-1$ and $\beta+T$.[1] We assume a Jeffreys' prior[2] for $\pi(\lambda)$, which is proportional to $1/\lambda$, equivalent to setting $\alpha = 0$ and $\beta = 0$. So the resulting distribution on the rate parameter, λ, is Gamma (*N-1*, *T*).

Given a unique set of inputs, uncertainty in the true rate of volcanic events given those inputs is estimated directly from the Gamma distribution: the mean rate, λ, is given by the mean of the Gamma (*N-1, T*) distribution as: $\frac{N-1}{T}$, and confidence intervals for the rate estimate are given directly by the appropriate percentiles of the Gamma (*N-1, T*) distribution.

The uncertainty in λ is represented by a discrete approximation of the continuous Gamma distribution in the logic tree formulation. The specific discrete approximation used for the various expert models differs. As discussed in Section 3.1, a commonly used three-point approximation (the extended Pearson-Tukey approximation) for a continuous distribution is to

[1] Our parameters differ slightly from those in the study by Solow (2001). In that paper, the likelihood function is estimated based on *n* events in an arbitrary observation period *t*; in our formulation the likelihood function is based on N events in a time period T that is defined by the age of the oldest event, effectively reducing the degrees of freedom in the likelihood function by one.

[2] In Bayesian analysis, a Jeffreys' prior is often used as a "noninformative" prior distribution. It is selected to be invariant to transformations of the parameter, and is defined as being proportional to the square root of the Fisher information. Jeffreys' prior may be an "improper prior," meaning that it is not a true density function. The Jeffreys' prior for the Poisson distribution is improper. Defintion and calculation of Jeffreys' prior for a variety of distributions can be found in Gelman et al. (1995, Section 2.9).

use the 5th, 50th, and 95th percentiles and weight them 18.5%, 63%, and 18.5%, respectively. In the logic trees of Section 3.2, the nodes representing the rate for a homogenous Poisson model are illustrated as three-point approximations, and in almost all cases are modeled with the extended Pearson-Tukey approximation. For the background rate in the models for GT and AM, and for the rate in the region of interest but outside the Crater Flat zone for MK, however, we chose to model the uncertainty in the rate with additional branches in the approximation. The purpose of this increased discretization was only to create a "smoother" appearing frequency of intersection distribution. The mean frequency is insensitive to the number of points used to represent the rate distribution, as long as the approximation is moment-preserving (which the approximations used here are). A 9-point approximation based on Miller and Rice's moment-matching approach (1983) was used. For this approximation, the fractiles of the distribution used are as the branches on the logic tree node: (0.01209, 0.07266, 0.1821, 0.3302, 0.5, 0.6698, 0.8179, 0.9273, 0.9879) and each branch is assigned the following probability: (0.03448, 0.08599, 0.13081, 0.16202, 0.1734, 0.16202, 0.13081, 0.08599, 0.03448).

E.2.2 Poisson Model with a Time-Varying Rate (the time-volume rate model)

Crowe et al. (1995) present estimates of the rate of volcanic events based on the model:

$$\lambda(t) = \frac{dV_M(t)/dt}{V_E(t)} \qquad \text{(Eq. E-5)}$$

where $dV_M(t)/dt$ is the instantaneous rate of magma production and $V_E(t)$ is the time varying magma volume per volcanic event at time t.

Estimating the magma production rate using this model requires estimates of both $dV_M(t)/dt$ and $V_E(t)$. Experts using this model identified relevant past events, and provided estimates of the age and volume of each event, and specified a functional form for each relationship. The parameters for $V_M(t)$ and $V_E(t)$ are then found by regression analysis using the specified data and functional form.

Uncertainty in $\lambda(t)$ is modeled by developing three point representations of the uncertainty in either or both of $V_M(t)$ and $V_E(t)$ from regression analyses and then using the resulting combinations assuming the two parameters are independent.

Three functional forms were used by various experts to estimate $V_M(t)$ (referred to below as cumulative volume or $CV(t)$) : a linear model, a square-root of time model, and a log-time model. The three models are illustrated through the example below.

Table E-1 lists the post-4 Ma events for MK's model (his most likely event set). Figure E-1 illustrates the best fit (by linear regression) of each of the three approaches used to model CV.

Table E-1. Events Used to Fit a Cumulative Volume Model for Mel Kuntz

Event	Age (Ma)	Volume (km^3)
Anomalies FGH	3.9	0.063
Anomaly B	3.8	1.227
Pliocene basalt of Crater Flat	3.8	0.585
Buckboard Mesa	2.87	0.838
Red Cone, Black Cone, Makani Cone	1.07	0.117
Little Cones	1.07	0.034
Hidden Cone	0.35	0.032
Little Black Peak	0.35	0.014
Lathrop Wells	0.08	0.048

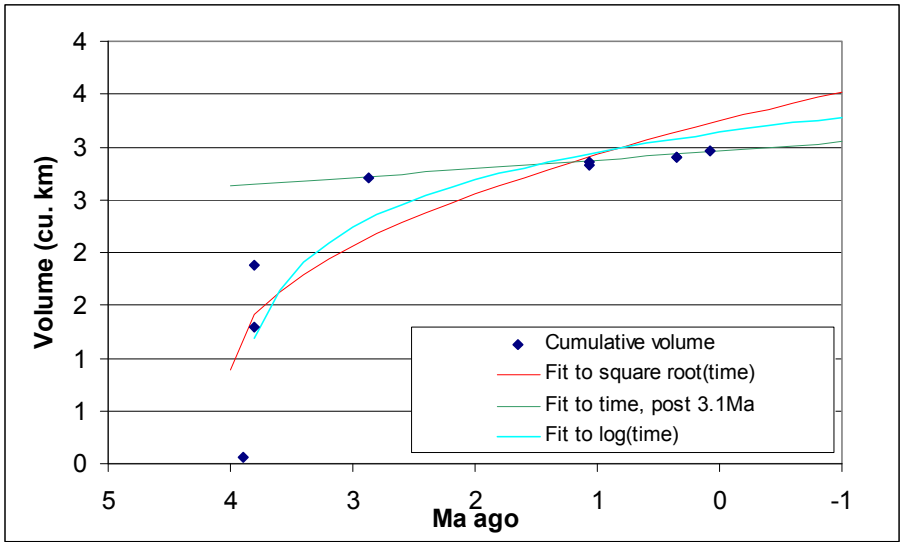

Figure E-1. Illustration of the Best Fit of Three Alternative Models of Cumulative Volume to Past Events

The linear model has the form:

$$CV(t) = c_1 + c_2 \text{ x } (t_{0+}t) \qquad \text{(Eq. E-6)}$$

Where t_0 represents the start of the expert-defined time period of interest (in this example, 4 Ma) and t is the time relative to the present ($t = -3$ means 3 Ma prior to the present day, $t = 1$ would mean 1 My in the future). The constants c_1 and c_2 are found by linear regression using the data for that expert. The rate of change (dCV/dt) for this model is c_2. For this example, the best fit linear regression is:

$$CV(t) = 2.63 + 0.084 \text{ x } (3.9+t)$$

And the regression fit is significant (F = 200, significance = 0.009). Uncertainty in dCV/dt is modeled using the 90% confidence interval for c_2 (0.067 to 0.101). In the logic tree formulation,

the best fit for c_2 is interpreted as the 50th percentile, the 90% confidence bounds are interpreted as the 5th and 95th percentiles, and the three-point extended Pearson-Tukey approximation is used (that is, the 5th, 50th, and 95th percentiles are weighted 18.5%, 63%, and 18.5%, respectively).

The square-root of time model has the form:

$$CV(t) = c_1 + c_2 \times \sqrt{t_0 + t}$$

and (Eq. E-7)

$$\frac{dCV}{dt} = \frac{c_2}{2 \times \sqrt{t_0 + t}}$$

where t_0 represents an arbitrary time at least as old as the first event in the linear fit (t_0 can be specified or found as part of the linear regression). Again, the constants c_1 and c_2 (and, potentially, t_0) are found by linear regression using the data for that expert. For this example, the best fit linear regression is:

$$CV(t) = 0.88 + 1.18 \times \sqrt{(3.9 + t)}$$

The regression fit is significant (F = 12.7, significance = 0.02). Uncertainty in dCV/dt is modeled using the 90% confidence interval for c_2 (0.47 to 1.89). In the logic tree formulation, the best fit for c_2 is interpreted as the 50th percentile, the 90% confidence bounds are interpreted as the 5th and 95th percentiles, and the three-point extended Pearson-Tukey approximation is used.

The log-time model has the form:

$$CV(t) = c_1 + c_2 \times \ln(t_0 + t)$$

and (Eq. E-8)

$$\frac{dCV}{dt} = \frac{c_2}{t_0 + t}$$

where t_0 and t are interpreted as before. Again, the constants c_1 and c_2 (and, potentially, t_0) are found by linear regression using the data for that expert. For this example, the best fit linear regression is:

$$CV(t) = 2.24 + 0.65 \times \ln(4 + t)$$

The regression fit is significant (F = 18.5, significance = 0.013). Uncertainty in dCV/dt is modeled using the 90% confidence interval for c_2 (0.33 to 0.97). The logic tree formulation is as described above.

The linear model was used by MK and FS, the square-root model was used by MK, and the log-time model was used by WH, AM, MK, and GT. The best fit regression for each of these models is summarized in that expert's subsection of Section 3.2.

Two approaches were used to model $V_E(t)$: a lognormal distribution on volume fit to the volume of specified past events identified by the experts (generally the Quaternary events), and, for one expert, an expert-specified $V_E(t)$ function. For those experts modeling the volume per event based on the volume of specified past events, the mean and variance of the volumes of those specified past events were used to define a lognormal distribution representing uncertainty in the volume per event. The 5th, 50th, and 95th percentiles of that lognormal distribution were then used to represent uncertainty in the volume per event in the logic tree formulation.

The same discretization approach was used for the expert-specified distribution on $V_E(t)$. In some cases we chose to model the uncertainty in the volume per event with additional branches in the approximation. The purpose of this increased discretization was only to create a "smoother" appearing frequency of intersection distribution, and we used the same 9-pt approximation described above in Section E.2.1.

E.2.3 Temporal Clustering

The temporal clustering model is based on an assumption that volcanic events tend to occur in "clusters" of activity with finite duration, followed by periods of quiescence between clusters. The model is implemented as a combination of two Poisson models: clusters are assumed to occur according to a Poisson process with an arrival rate λ_c, and *within* a cluster events are assumed to occur according to a Poisson process with a different arrival rate, λ_w. At any point in time, the rate depends on whether that time is within a cluster or between clusters:

$$\lambda(t) = \begin{cases} \lambda_w & \text{with probability } \mathrm{P}_W(t) \\ \lambda_c & \text{with probability } 1 - \mathrm{P}_W(t) \end{cases} \qquad \text{(Eq. E-9)}$$

where $P_W(t)$ represents the probability that time t is within a cluster. Uncertainty about whether time t is within a cluster or between clusters is modeled explicitly in a logic tree for the hazard calculation.

The cluster recurrence rate λ_c can be estimated exactly as for the homogenous Poisson model described above with N equal to the number of past clusters and T calculated as the time from initiation of the first cluster to the present.

Event recurrence within clusters λ_w can be estimated as described above where N is the total number of events and T is the total duration of previous clusters, including, if applicable, the time of the "current" cluster. The estimate of the total duration of previous clusters requires an estimate of the duration of a cluster, d.

The probability of any arbitrary time t falling within a cluster is calculated as the sum of two estimates: the probability that t falls within a cluster with a known initiation date (e.g., the "current cluster"), $\mathrm{P_{Wc}}(t)$, and the average probability of being in a cluster at any point in time, $\mathrm{P_A}(t)$.

$$P_W(t) = P_{Wc}(t) + (1 - P_{Wc}(t))^* P_A(t) \quad \text{(Eq. E-10)}$$

An estimate of $P_{Wc}(t)$ requires an estimate of the duration of a cluster, $\boldsymbol{d}$, and an assessment of the probability that the present time is within the current cluster, $P_{Wc}(0)$.

$$P_{Wc}(t) = P_{Wc}(0) + F_{\mathbf{d}}(t + t_{ci}) \quad \text{(Eq. E-11)}$$

where $F_{\mathbf{d}}(x)$ is the cumulative distribution function for the assessment of cluster duration, evaluated at x, and t_{ci} represents the time of initiation of the "current cluster."

The average probability of being in a cluster at any point in time, p_{at}, is equal to the average of the cluster duration divided by the average time between clusters.

The details of the assessments for the one expert (MS) who used the temporal clustering model are discussed in his elicitation summary in Appendix D. Applying the discussion above to MS's assessments for the temporal clustering model:

- Cluster duration is zero (a single event) with probability 0.2; if not zero, cluster duration is defined by a normal (170, 70) distribution (in thousands of years), truncated at 0 and 300. The mean cluster duration is 133,000 years (including the 20% chance of a cluster being of zero duration)

- Four past clusters were identified with the oldest cluster initiating at 4.8 Ma, giving a mean estimated annual cluster recurrence rate of 6.25e-7.

- The average probability of being in a cluster is 0.083.

- There is uncertainty in the within-cluster rate that derives both from uncertainty about the length of past clusters and the uncertainty about whether the present time is within the "current cluster." If the event at Lathrop Wells was a one-event cluster, the mean within-cluster annual recurrence rate is 2.54e-5; if the event at Lathrop Wells represents the initiation of a cluster than is not yet over, the mean within-cluster annual recurrence rate is 2.16e-6.

E.3 SPATIAL MODELS

Several alternative approaches were used to model the conditional spatial mass density of events (the $f(x_i,y_j)$ across the region of interest R from Equation E-3). This calculation gives the conditional probability density (probability per unit time) of an event at each point within the gridded region of interest, assuming that one event occurs within that region.

E.1.2.1 Locally Homogenous Zones

In the locally homogenous zone spatial modeling approach, the underlying model is the assumption that the relative probability of occurrence of volcanic events within a locally homogenous zone is everywhere the same. The rate within a zone may be temporally homogenous or temporally varying, defined by any of the temporal models described above, but at any point in time the rate is uniform across the zone.

The locally homogenous spatial model is implemented by dividing the region of interest into a number of non-overlapping zones, Z_k, k = 1 to n, each with area A_k, and each with a unique rate estimate. In this modeling approach, we skip the separation of the rate model from the conditional spatial density, and instead go directly to the rate density estimate ($\lambda(x, y, t)$) of Equation E-2.

Given the assumption of a uniform spatial density, the density parameter in each zone is equal to the inverse of the zone area, [$f(x,y) = 1/A_k$]. If the rate of occurrence in the zone is $\lambda_k(t)$, then the rate density of events at any point in that zone is given by:

$$\lambda(x_i, y_j, t_k) = \lambda_k(t) \times \frac{1}{A_k}(t) \qquad \text{(Eq. E-12)}$$

The boundary between two zones represents a change in the rate density. This change in rate density may be considered either a step-change at the boundary, or a change that occurs over some transition distance between a defined zone and a background zone. In the latter case, an estimate must be provided for the transition distance. The rate transition is implemented by assuming that the rate density within zone k decays linearly to zero with distance from the zone boundary over a specified distance, h. This distance may differ for different portions of the zone boundary.

With the assumption that $f(x,y)$ decreases linearly from $1/A_k$ at the zone boundary to zero over a distance h, the spatial density at any point x, y within the transition zone, Z, is given by:

$$f_Z(x, y) = \frac{(h - d)/h}{A_T} \qquad \text{(Eq. E-13)}$$

where d is the distance of the point from the zone boundary and A_T is the area of the transition zone.

However, the effective area of each zone has now expanded by A_T. Thus, the sum of the conditional spatial density over the effective area of the zone, $A + A_T$ will exceed unity, requiring renormalization to produce a proper density function. The renormalization factor is the summation of $f(x,y)$ over the entire effective region of the zone and is approximately equal to the area within the zone plus one-half of the area within the transition region. Thus, the spatial density becomes:

$$f(x, y) = \frac{1}{A + A_T/2} \text{ for (x,y) within } A \qquad \text{(Eq. E-14)}$$

$$f(x, y) = \frac{(h - d)/h}{A + A_T/2} \text{ for (x,y) within } A_T$$

The method used to compute the volcanic hazard directly calculates the normalization factor by summing the spatial density over the zone and transition areas and then renormalizes the spatial density function to unity.

E.3.2 Parametric Spatial Density Function

Nonhomogenous spatial models provide a means of specifying a smooth variation of the spatial density of volcanic events, $f(x,y)$, within the region of interest. Sheridan (1992) has developed a model for volcanic fields in which the spatial density of events is represented by a bivariate Gaussian distribution. The resulting volcanic field has an elliptical shape defined by five parameters, the coordinates of the center of the field, the length of the major and minor axes, and the orientation of the major axis. The spatial density of future events associated with the field is given by the expression:

$$f(x,y) = \frac{e^{-[\mathbf{x}-\mu_{\mathbf{x}}]^T \Sigma_{\mathbf{x}}^{-1} [\mathbf{x}-\mu_{\mathbf{x}}]/2}}{2\pi \left|\Sigma_{\mathbf{x}}\right|^{1/2}} \qquad \text{(Eq. E-15)}$$

where $\boldsymbol{x}$ is the location of point (x,y), $\boldsymbol{\mu}$ is the location of the center of the field, and $\boldsymbol{\Sigma_x}$ is the covariance matrix of $\boldsymbol{x}$, defining the size and shape of the field. The exponent T and -1 in the equation above indicate the transpose and inverse, respectively, of the matrix, and $|\boldsymbol{\Sigma}_{\mathbf{x}}|$ indicates the determinant of the covariance matrix.

The specification of the Gaussian field parameters can be through reference to better developed fields considered analogous or they can be estimated from the local data. The expert who specified the bivariate Gaussian model in this analysis chose to estimate the parameters of Gaussian volcanic fields from the local data. In this approach, the expert identifies a set of volcanic events that constitute a field and the five parameters of a bivariate Gaussian distribution are estimated directly from the x and y locations of those events using standard maximum likelihood estimators of the mean of x and y and the covariance matrix of x and y. The five parameters of the field are the mean of the x and y locations, μ_x and μ_y, and the covariances of the x and y locations, σ^2_x, σ^2_y, and σ^2_{xy}.

Given n observed events, the maximum likelihood estimators for the field parameters are (Johnson and Wichern 1992):

$$\mu = \frac{1}{n}\sum_{i=1}^{n} x_i$$

$$\boldsymbol{\Sigma}_{\mathbf{x}} = \frac{1}{n}\sum_{i=1}^{n} (x_i - \mu_x)^{\mathrm{T}} (x_i - \mu_x) \qquad \text{(Eq. E-16)}$$

where $\boldsymbol{x_i}$ is the location of the i^{th} event in the field.

E.3.2.1 Uncertainty in Spatial Density Estimates from a Parametric Spatial Function

There is uncertainty in estimating the field parameters because of the limited size of the data set. This uncertainty is incorporated into the spatial density estimate by defining a joint distribution for the five field parameters, estimating the asymptotic standard errors for each, and then varying each by ± one standard error. This generates 3^5 (243) possible sets of field parameters. These

243 possible sets of field parameters are treated as branches on a logic tree node in the overall hazard calculation.

The asymptotic covariance of the estimated field midpoint $\boldsymbol{\mu}$ is equal to $\boldsymbol{\Sigma_x}/n$.

To ensure that the covariance matrix for each possible parameter set is positive definite and to preserve the orientation of the field shape as the σ^2_x and σ^2_y components of the covariance matrix are varied, the standard errors for the eigenvalues and the eigenvector of the covariance matrix are calculated, rather then the standard error for the components themselves. The eigenvalues λ of the covariance matrix are calculated from the characteristic equation for the matrix with *I* defined as the identity matrix (Strang 1980, p. 182):

$$\left|\Sigma - \lambda I\right| = 0$$

which, solving for the values of the eigenvalues λ_1 and λ_2, gives

$$\lambda_1, \lambda_2 = \frac{Tr(\Sigma) \pm \sqrt{Tr(\Sigma) - 4\left|\Sigma\right|}}{2}$$

where *Tr(Σ)* = the Trace of covariance matrix = $\sigma_x^2 + \sigma_y^2$ and $|\Sigma|$ = the determinant of $\Sigma = \sigma_x^2\sigma_y^2 - (\sigma_{xy}^2)^2$.

Because the eigenvalue form of the covariance matrix results in uncorrelated variates, the asymptotic standard errors for the eigenvalues are given by:

$$\sigma_\lambda = \lambda\sqrt{\frac{2}{n}} \qquad \text{(Eq. E-17)}$$

The unit eigenvector of the covariance matrix is obtained by solving the set of equations defined by:

$$(\Sigma - \lambda I)[c_1, s_1]^T = 0 \text{, subject to } c_1^2 + s_1^2 = 1$$

which yields the following expressions for c_1 and s_1:

$$c_1 = \frac{-\sigma_{xy}^2}{\sqrt{(\sigma_{xy}^2)^2 + \left(\sigma_x^2 - \lambda_1\right)^2}}$$

$$s_1 = \frac{\sigma_x^2 - \lambda_1}{\sqrt{(\sigma_{xy}^2)^2 + \left(\sigma_x^2 - \lambda_1\right)^2}}$$

To calculate the standard error for c_1, it is first rewritten as follows:

$$c_1 = \frac{-\sigma_{xy}^2}{\sqrt{(\sigma_{xy}^2)^2 + \left(\sigma_x^2 - \lambda_1\right)^2}} = -r\sqrt{\frac{\sigma_x^2\sigma_y^2}{(\sigma_{xy}^2)^2 + \left(\sigma_x^2 - \lambda_1\right)^2}} =, \text{where}$$

$$r = \frac{-\sigma_{xy}^2}{\sqrt{(\sigma_x^2\sigma_y^2)}}$$

Using the approximation for the variance of a function of a variable (Benjamin and Cornell 1970, p. 180) with the equation above gives the following expression for the standard error for c_1:

$$\sigma_{c_1} = \sqrt{Var(z)\left(\frac{\partial c_1}{\partial r}\cdot\frac{\partial r}{\partial z}\right)^2} \approx \frac{|\Sigma|}{\sqrt{n\sigma_x^2\sigma_y^2\left[\left(\sigma_{xy}^2\right)^2 + \left(\sigma_x^2 - \lambda_1\right)^2\right]}} \qquad \text{(Eq. E-18)}$$

where $z = \frac{1}{2}\ln\left(\frac{1+r}{1-r}\right)$ is the Fisher z-transformation of r (Fisher 1925).

To define probabilities for the 243 alternative parameter sets, the relative likelihood of each parameter set producing the observed field data is used. The relative likelihood of a particular set of field parameters, $\boldsymbol{\mu}^j$ and $\boldsymbol{\Sigma}^j$, being the "correct" model that generated the observed set of events was computed by (Johnson and Wichern 1992):

$$L(\mu^j, \Sigma^j) = \frac{\exp\left(-\sum_{i=1}^{n}(x_i - \mu^j)^T(\Sigma^j)^{-1}(x_i - \mu^j)/2\right)}{(2\pi)^n\left|\Sigma^j\right|^{n/2}} \qquad \text{(Eq. E-19)}$$

This equation was used to compute the likelihood that each of the 243 alternative parameter sets would produce the events originally used to fit the field. The resulting values are normalized to sum to unity to define a discrete probability distribution across the alternative parameter sets.

The bivariate Gaussian volcanic field model defines the spatial density of future events associated with a field. It is also possible to consider the volcanic field to be superimposed on a larger spatially homogenous background zone representing the hazard from random volcanic events not associated with an identifiable field. In this case, the rate density at any point is considered to be the maximum of the background rate or the field rate at that point.

E.3.3 Kernel Density Estimation

Kernel density estimation is a nonparametric approach to estimating spatial densities based on the locations of past events and an expert-defined "kernel" function. The kernel function is combined with the locations of past events, and the resulting density surface is renormalized over the region of interest to obtain a conditional spatial density function.

In PVHA-U, experts utilizing this modeling approach specified a Gaussian kernel function. In the basic formulation, the Gaussian kernel has the form of a two-dimensional Gaussian density function:

$$K^G(d_i, h) = \frac{e^{-d_i^T d_i / 2h^2}}{2\pi h^2} \quad \text{(Eq. E-20)}$$

where $\boldsymbol{d_i}^T\boldsymbol{d_i}$ is the distance between point *(x,y)* and event *i* ($\boldsymbol{d_i}$ is the vector of relative coordinates), and *h* is the smoothing parameter or bandwidth. The parameter *h* in the Gaussian kernel is specified by the expert and represents one standard deviation of a normal distribution.

The spatial density of volcanic events in the region is given by:

$$f(x, y) = \frac{1}{N}\sum_{i=1}^{N} K^G(d_i, h) \quad \text{(Eq. E-21)}$$

N is the normalizing constant: the number of events being used to fit the kernel density estimator.

Several modifications to this approach are possible and were used by various experts in this analysis, including limiting the kernel density estimate by zone boundaries, differential weighting of events, and use of an anisotropic kernel function.

Kernel density estimation within a defined zone. If the kernel density function is to be limited to the boundaries of a specific zone, *Z*, the normalizing constant *N* from (Equation E-21) is replaced by the sum of the un-normalized spatial density over the zone and Equation E-19 becomes:

$$f(x, y) = \frac{1}{\sum_{Z} K(d_i, h)} \sum_{i=1}^{N)} K^G(d_i, h) \quad \text{(Eq. E-22)}$$

Differential weighting of past events. The equations above fit a kernel density estimator to past events with all events weighted equally: it is possible to weight past events based on a variety of expert-defined parameters. To implement differential weighting of past events based on an expert-specified set of weights w_i for each past event *i*, the kernel functions are scaled by the appropriate weighting factor prior to summing and normalizing. Equation E-21 becomes:

$$f(x, y) = \frac{1}{\sum_{i} w_i} \sum_{i=1}^{N} w_i K^G(d_i, h) \quad \text{(Eq. E-23)}$$

Anisotropic kernel function. Equation E-18 defines a Gaussian kernel function that is symmetric around a center point. Anisotropic kernel functions can be used instead to introduce a preferred orientation for smoothing (Silverman 1986). In this approach, the bandwidth *h* is replaced with a covariance matrix describing the shape of the kernel density function, and the kernel function of Equation E-18 is replaced by a more general form:

$$K^G(d_i') = \frac{\exp(-d_i'^T \Sigma_k^{-1} d_i' / 2)}{2\pi |\Sigma_k|^{-1/2}} \quad \text{(Eq. E-24)}$$

The vector $\boldsymbol{d_i'}$ defines the relative coordinates between point *(x,y)* and event *i,* and $\boldsymbol{\Sigma_k}$ is a covariance matrix of the kernel given by

$$\Sigma_k = \begin{bmatrix} h_x^2 & \varphi \\ \varphi & h_y^2 \end{bmatrix} \quad \text{(Eq. E-25)}$$

Where h_x and h_y define the smoothing distances in the x and y directions, and φ defines the rotation of the kernel function. The covariance matrix is specified by the expert.

E.3.3.1 Uncertainty in Spatial Density Estimates Based on Kernel Density Estimate: Bootstrapping

Like the parametric density estimate described above, kernel density estimation aims to approximate the spatial distribution of future events based in part on the locations of past events. With a small number of past events, there is uncertainty in how well a model fit to those events will approximate the "true" spatial distribution for future events.

Following a suggestion by Connor (presentations at Workshop 2 and Connor and Connor (in press)), uncertainty in the fit of the kernel density estimator to the event locations is modeled using a statistical simulation approach known as the "bootstrap" (Efron 1981; Efron and Tibshirani 1993). Conceptually, the bootstrap method addresses uncertainty by treating the past events as one observation of an infinite variety of event sets that could be produced by some underlying spatial density. The underlying spatial density is approximated, and then that approximation is treated as a sampling distribution for simulation. For each iteration of the bootstrap simulation, *N* events (where *N* = the number of events in the past event set) are sampled from the sampling distribution, and a new kernel density estimate is fit to those points. The new kernel density estimate uses the same parameters (the same kernel function, bandwidth, and weighting function for past events) as used in the original kernel density estimate. Each iteration of the bootstrap, then, generates a new spatial density estimate. Each of these density estimates is treated as an equally likely representation of the conditional spatial density in the logic tree.

In these PVHA-U analyses, two approaches are taken for developing the sampling distribution for bootstrap simulation (the bootstrap procedure under the two approaches is otherwise identical). The first approach follows the traditional description of the bootstrap: the original data set (the number, locations, and relative weights of identified past events) is used directly as the sampling distribution. If the expert's data set includes *N* events, then *N* events are sampled with replacement from this empirical distribution. A new kernel density estimate is fit to those sampled points, using the same kernel function, bandwidth estimate, and event weighting used in the original specified model. This approach provides the most straightforward way to maintain differential weighting of past events through the generation of alternative spatial densities.

In the second approach, known as the "smoothed bootstrap," the best fit of the kernel density estimate to the set of identified past events is used as the sampling distribution (it is "smoothed" in that the bootstrap samples are taken from this continuous approximation distribution rather than from the discrete empirical distribution). For each iteration of the bootstrap, *N* events are sampled from the approximating distribution, and a new kernel density estimate is fit to those events. The smoothed approach has the conceptually appealing feature of allowing simulated events for the bootstrap to occur anywhere within the region of interest, but it is difficult to incorporate differential weighting of past events in this approach.

For every model that used a kernel density estimate, an uncertainty was added to the logic tree structure to represent uncertainty in the spatial density estimate, with the branches of that node representing iterations of the bootstrap for that model. For computational reasons, the number of iterations of the bootstrap was limited to 100.

Some testing was done to explore the effect of the number of bootstrap iterations on an early version of a model that uses kernel density estimation as well as the geology-informed estimation approach described below. The appropriate number of iterations in any Monte Carlo simulation is a matter of technical judgment, and depends on the number of iterations required to yield a stable estimate of the value of interest to the decision-makers or analysts. The end result we care about in PVHA-U is the frequency of intersection, so the appropriate number of iterations was evaluated in light of the stability of some statistics of the ultimate frequency of intersection distribution: the mean, the signal-to-noise ratio (the mean divided by the standard deviation), and the 5th, 50th, and 95th fractiles.

Table E-2 shows the results of calculating the frequency of intersection with 15 different runs of the bootstrap: 10 runs at 100 iterations, and 5 runs at 400 iterations. As shown, the signal-to-noise ratio changes little across all runs, indicating that the estimate is relatively stable even at 100 iterations. The mean and the median estimates appear similarly stable, and the differences in the stability of the 5th and 95th percentiles for 100 versus 400 iterations are small. Based on this analysis, and computational constraints, 100 iterations of the bootstrap were run for all experts' final models.

Table E-2. Results of Testing the Number of Bootstrap Iterations Required to Yield a Stable Estimate of the Frequency of Intersection

Run #	1	2	3	4	5	
# Iterations	**100**	**100**	**100**	**100**	**100**	
Mean	1.654E-08	1.671E-08	1.692E-08	1.697E-08	1.684E-08	
SD	2.762E-08	2.775E-08	2.814E-08	2.868E-08	2.800E-08	
Mean/SD	**0.599**	**0.602**	**0.601**	**0.592**	**0.601**	
5th	1.960E-10	1.933E-10	2.205E-10	2.019E-10	2.116E-10	
50th	6.643E-09	6.540E-09	6.750E-09	6.581E-09	6.670E-09	
95th	9.775E-08	9.536E-08	9.784E-08	9.915E-08	9.738E-08	
Run #	**6**	**7**	**8**	**9**	**10**	
# Iterations	**100**	**100**	**100**	**100**	**100**	**SD of the Statistics (for 100 iterations)**
Mean	1.654E-08	1.671E-08	1.692E-08	1.697E-08	1.684E-08	1.74E-10
SD	2.762E-08	2.775E-08	2.814E-08	2.868E-08	2.800E-08	4.13E-10
Mean/SD	**0.599**	**0.602**	**0.601**	**0.592**	**0.601**	**4.31E-03**
5th	1.960E-10	1.933E-10	2.205E-10	2.019E-10	2.116E-10	1.13E-11
50th	6.643E-09	6.540E-09	6.750E-09	6.581E-09	6.670E-09	8.13E-11
95th	9.775E-08	9.536E-08	9.784E-08	9.915E-08	9.738E-08	1.37E-09
Run #	**11**	**12**	**13**	**14**	**15**	
# Iterations	**400**	**400**	**400**	**400**	**400**	**SD of the Statistics (for 400 iterations)**
Mean	1.695E-08	1.679E-08	1.662E-08	1.687E-08	1.682E-08	1.22E-10
SD	2.837E-08	2.815E-08	2.767E-08	2.815E-08	2.829E-08	2.72E-10
Mean/SD	**0.597**	**0.596**	**0.601**	**0.599**	**0.595**	**2.38E-03**
5th	2.021E-10	1.995E-10	1.981E-10	2.031E-10	2.069E-10	3.42E-12
50th	6.669E-09	6.672E-09	6.642E-09	6.668E-09	6.672E-09	1.28E-11
95th	9.809E-08	9.871E-08	9.683E-08	9.759E-08	9.886E-08	8.35E-10

NOTE: SD = standard deviation.

E.3.4 Geology Data in Spatial Models

Geology data can be included directly in spatial models by combining expert interpretation of the data's relevance to future event locations with the spatial distribution of those data over their region of interest. In practice, this geology-derived spatial distribution is always combined with the spatial distribution estimated using one or more of the methods described above to define a new "data-informed" spatial density estimate.

Two approaches were used for combining geology data with other spatial intensity maps.

The first approach for incorporating geology data involves developing spatial intensity maps based on interpretations of the data, and then combining those using an additive weighting approach with spatial intensity maps developed through other means. To develop the spatial intensities based on the geology data, a Bayesian updating approach is used. In these cases, experts provide a probability function of the relative likelihood of observing different values for geology data given that a future volcano occurs or does not occur at a location. Starting with an

assumption of a homogenous spatial density, this assessment of the quality of the new information is used to update the spatial density using Bayes' Theorem:

$$P(e_{x,y}|A) = \frac{P(A|e) \times P(e_{x,y})}{P(A)} \quad \text{(Eq. E-26)}$$

where $P(e_{x,y}|A)$ is the conditional (or *posterior*) probability of an event given a specific geology data value, A, $P(A|e)$ is the probability of observing the geology value, A, given that a future event occurs, $P(e_{x,y})$ is the *prior* probability of an event, and $P(A)$ is the probability of observing the given geology data value.

After applying Bayes' rule to each point in (x,y), the spatial intensities must be normalized so that they sum to one across the grid. Equation E-23 becomes:

$$f_G(x,y) = \frac{\frac{P(A|e) \times P(e_{x,y})}{P(A)}}{\sum_R \frac{P(A|e) \times P(e_{x,y})}{P(A)}} \quad \text{(Eq. E-27)}$$

Experts provided weights for combining the geologically derived spatial intensities with those derived from other approaches, and the resulting "geology-informed" conditional spatial density estimate is given by.

$$f(x,y) = w_G \times f_G(x,y) + w_E \times f_E(x,y) \quad \text{(Eq. E-28)}$$

where the subscript G refers to geologic weights or spatial intensities and the subscript E refers to weights or spatial intensities derived from the primary spatial modeling approach used by the expert.

One expert (CC) defined an alternative approach for combining his interpretation of geologic data with the spatial density estimated using other approaches. In this case, he defined a weighting function for crustal density data that is used to scale the spatial density at each point in the region of interest. The appropriate weight corresponding to the crustal density value at each grid point is multiplied by the spatial intensity derived from kernel density estimation at that point, and the resulting grid is then normalized so that the sum of spatial intensities over the grid equals one:

$$f(x,y) = \frac{w(\rho,x,y) \times f_K(x,y)}{\sum_R w(\rho,x,y) \times f_K(x,y)} \quad \text{(Eq. E-29)}$$

where $w(\rho,x,y)$ is the weight for the given value of crustal density at point (x,y) and $f_K(x,y)$ is the spatial intensity derived from kernel density estimation.

E.4 CONDITIONAL PROBABILITY OF INTERSECTION

The conditional probability of intersection at any point (the $P_I(x,y)$ of Equation E-3) is defined as the probability that an event located at (x, y) would intersect the repository footprint. To

determine $P_I(x,y)$, we simulate events at every (x, y), and then test every feature within an event for intersection with a polygon that represents the repository footprint.

E.4.1 Event Simulation

The characteristics of potential future volcanic events in the area around Yucca Mountain are specified by each expert both in terms of the types of igneous features that would comprise an "event" (dikes, sills, eruption column-producing conduits, and non-column-producing vents), and the geometries and relative placement of those features. Each expert developed a unique definition of an igneous event. Those definitions included estimates, with uncertainty, of the number and size/geometry of each type of feature, and how those features would be located relative to each other. The uncertainties in the number, size, and placement of igneous features in an event mean an infinite number of different individual "events" are possible under each expert's event definition. To model alternative events for each expert, a computational approach known as Monte Carlo simulation is used (e.g., Robert and Casella 2005). In a simulation approach, each of the relevant characteristics is defined by a probability distribution, then one sample is drawn from each distribution defining each of the characteristics of an event, and together those samples define a single event. This process is repeated thousands (or tens or hundreds of thousands) of times, and the resulting set of simulated events represents the range of possible events. The nature of simulation is such that over many iterations, events occur in proportion to their relative probabilities.

As discussed above, the appropriate number of iterations in any Monte Carlo simulation is a matter of technical judgment, and depends on the number of iterations required to yield a stable estimate of the value of interest to the decision-makers or analysts. The end result we care about in PVHA-U is the frequency of intersection, so the appropriate number of iterations was evaluated in light of the stability of some statistics of the frequency of intersection distribution: the mean, the signal-to-noise ratio (the mean divided by the standard deviation), and the 5th, 50th, and 95th fractiles.

Table E-3 shows the results of calculating the frequency of intersection for one expert using 10 different runs of the event simulator: 5 runs of 100,000 iterations (changing the seed value for the random number generator each time), and 5 runs of 500,000 iterations (also changing the seed value for the random number generator each time). In this model, simple Monte Carlo sampling is used. As shown, there is very little difference in the signal-to-noise ratio between any of the runs, and the difference between those values for runs 1 to 5 (with 100,000 iterations) is very close to the difference between those values for runs 6 to 10 (with 500,000 iterations). Similarly, the standard deviations across the calculated percentile values for runs 1 to 5 are small and very close to the same values for runs 6 to 10. In addition, informal tests were conducted with two experts, with the results of 1,000,000 iterations of their event simulator compared to the results with 100,000 iterations. Differences in the calculate frequency of intersection, were less than the precision of the results presented in this report.

Based on this assessment, 100,000 runs of the event simulator was deemed sufficient, and all the results presented in Section 4 are based on 100,000 iterations of each expert's individual event simulator.

Table E-3. Results of Testing the Number of Iterations of the Event Simulator Required to Yield a Stable Estimate of the Frequency of Intersection

Run #	1	2	3	4	5	
# of Iterations	**100,000**	**100,000**	**100,000**	**100,000**	**100,000**	**SD of the Estimates**
Mean	2.06E-08	2.06E-08	2.07E-08	2.06E-08	2.06E-08	1.5.E-11
SD	5.74E-08	5.74E-08	5.74E-08	5.74E-08	5.73E-08	4.3.E-11
5th	8.14E-10	8.14E-10	8.15E-10	8.14E-10	8.13E-10	6.1.E-13
50th	9.04E-09	9.04E-09	9.06E-09	9.05E-09	9.04E-09	6.7.E-12
95th	5.77E-08	5.77E-08	5.78E-08	5.77E-08	5.76E-08	4.2.E-11
Mean/SD	0.36	0.36	0.36	0.36	0.36	3.9.E-05
Run #	**6**	**7**	**8**	**9**	**10**	
# of Iterations	**500,000**	**500,000**	**500,000**	**500,000**	**500,000**	**SD of the Estimates**
Mean	2.06E-08	2.07E-08	2.06E-08	2.06E-08	2.06E-08	4.5.E-12
SD	5.74E-08	5.74E-08	5.74E-08	5.74E-08	5.74E-08	1.1.E-11
5th	8.14E-10	8.14E-10	8.14E-10	8.14E-10	8.14E-10	1.7.E-13
50th	9.05E-09	9.05E-09	9.05E-09	9.05E-09	9.05E-09	1.6.E-12
95th	5.77E-08	5.77E-08	5.77E-08	5.77E-08	5.77E-08	8.4.E-12
Mean/SD	0.36	0.36	0.36	0.36	0.36	5.9.E-05

NOTE: SD = standard deviation.

The event simulator for each expert is unique, designed around their unique definition of events. The assessments for each expert are summarized and illustrated in Section 3.2, and described in detail in Appendix D. In implementing the event simulator, these parameters are modeled using a variety of approaches and distributions. Table E-4 lists the specific representations of the event parameters used in the event simulator, for each expert. Two experts provided multiple event definitions. Connor's two event definitions differ only in the number of centers per event, as discussed in Section 3.2.1. All other parameters are defined by the same distributions, summarized in Table E-4. Crowe provided three unique event definitions, each associated with one or more of his defined rate models. The parameters and representations shown in Table E-41 correspond to those specified for the steady-state and increasing rate models (which are the most highly weighted models). For details of the implementation of the alternative event definitions, and additional details on the implementation of the event simulator for all experts, see the Design Document for EventSim v. 1.0 (DOE 2008a).

Table E-4. Summary of Event Model Parameters and Representations for Each Expert's Event Simulator

Expert	Parameter	Representation
Connor (for events associated with the YMR dataset)	Center length	normal(0.6, 2) km, truncated at 0.6 km
	Center width	normal(0.1, 1) km, truncated at 0.1 and restricted to be less than center length
	Number of dikes	normal(1, 5), truncated at 1 and rounded to nearest integer value
	Number of vents	discrete uniform (0, 6)
	Number of sills	exponential(1/6), rounded to nearest integer value
Crowe (for events associated with the steady state and increasing rate models)	Number of conduits	discrete: {(1,3,3,4);(0.454, 0.182, 0.273, 0.091)}
	Event azimuth	Mixture of 5 uniform distributions: (–25,–15) degrees with probability 0.137 (–15,–5) degrees with probability 0.182 (–5,5) degrees with probability 0.227 (5,15) degrees with probability 0.227 (15,30) degrees with probability 0.227
	Event length	Conditional on number of conduits in the event: if 1 conduit: triangular(2.7, 3.4, 5) km if 2 conduits: uniform(2.7, 6.5) km if 3 conduits: uniform(6.5, 12) km if 4 conduits: uniform(10, 15) km
	Event width	Conditional on number of conduits in the event: if 1 conduit: triangular(0.2, 0.3, 0.7) km if 2 conduits: uniform(0.2, 0.6) km if 3 conduits: uniform(1, 1.5) km if 4 conduits: uniform(1,1.5) km
	Conduit diameter	triangular(10, 35, 80) m
	Number of dikes	Conditional on number of conduits in the event: if 1 conduit: 1 or 2, with probability 1/3, 2/3 if 2 conduits: 2 or 3, equally likely if 3 conduits: 3 or 4, equally likely if 4 conduits: 4 or 5, equally likely
	Dike azimuth	Mixture of 5 uniform distributions: (–25,–15) degrees with probability 0.015 (–15,–5) degrees with probability 0.091 (–5,5) degrees with probability 0.636 (5,15) degrees with probability 0.182 (15,30) degrees with probability 0.076
	Dike length	Conditional on number of conduits in the event: if 1 conduit: triangular(0.6, 3.1, 5) km if 2 conduits: uniform(0.7, 3.3) km if 3 conduits: triangular(0.7, 3.3, 5) km if 4 conduits: triangular(0.5, 3.1, 5) km

Table E-4. Summary of Event Model Parameters and Representations for Each Expert's Event Simulator (Continued)

Expert	Parameter	Representation
Crowe (for events associated with the steady state and increasing rate models) (continued)	Dike width	triangular(1,5, 3, 6.5) m
	Dike spacing	triangular(0.1 0.4, 1) km off the conduit-bearing dike
	Vent spacing	normal(0.4, 0.2) km, truncated at 0.1 and 1 km
	Vent diameter	triangular(dike width, 10, 20) m
Hackett	Dike system length	lognormal(mean = 2.38, st. dev. = 1.52) km, truncated at 13 km
	Dike system width multiplier	normal(10, 4). Truncated at 5 and 10
	Ratio of longest dike to shortest dike	normal(1, 1.1), truncated at 1 and 3
	Dike azimuth	Mixture of truncated normal distributions: normal(–5, 5) degrees, truncated at –90 and 90, with probability 2/3 normal(25, 10) degrees, truncated at –90 and 90, with probability 1/3
	Dike width	lognormal(mean = 1.65,st. dev = 1.30) m
	Number of conduits	discrete: {(0, 1, 2, 3); (0.1, 0.72, 0.135, 0.045)}
	Conduit diameter	lognormal(mean = 20.34, st. dev. = 15.95) m
	Conduit location on a dike	triangular (0, 0.5, 1) where 0 and 1 represent the dike ends
	Sill formation probability	lognormal(mean = 0.001,st. dev. = 0.0014), truncated at 0.01
	Sill location along a dike	triangular (0, 0.5, 1) where 0 and 1 represent the dike ends
	Sill length	triangular(100, 300, 500) m
Kuntz	Number of dikes	discrete: {(1, 2, 3, 4, 5, 6); (0.4, 0.25, 0.15, 0.1, 0.05, 0.05)}
	Dike length	lognormal(mean = 3.13, st. dev. = 3.54) km, truncated at 0.2 and 15 km
	Dike azimuth	Mixture of truncated normal distributions: normal(–5, 7.5) degrees, truncated at –90 and 90, with probability 2/3 normal(30, 7.5) degrees, truncated at –90 and 90, with probability 1/3
	Dike width	beta(0.66, 2.8) m, min of 0.5, max of 10.5
	Dike spacing	gamma(shape = 1.49, scale = 0.735) km, shifted by 0.5 km
	Conduit diameter	beta (2, 3) m, min = dike width, max = 100m
	Probability of sill formation	triangular (0.04, 0.1, 0.5)
	Sill thickness	triangular(5, 50, 200) m
	Sill depth	triangular(100, 175, 400) m
	Sill location along a dike	beta(1.5,1.5), where 0 and 1 represent the dike ends
	Sill length	triangular(20, 500, 1000) m
	Aspect ratio of sill	uniform(1, 3)

Table E-4. Summary of Event Model Parameters and Representations for Each Expert's Event Simulator (Continued)

Expert	Parameter	Representation
McBirney	Number of dikes	geometric(0.5), max = 10
	Dike system length	gamma(shape =1.8, scale = 1.15) km
	Dike width	triangular(0.1, 0.5, 2) m
	Dike azimuth	beta(12, 12) degrees, min= −90, max = 90
	Dike spacing	lognormal(mean = 0.212, st. dev. = 0.209), shifted −0.01 and truncated at 0.01
	Conduit diameter	gamma(shape = 3.7, scale = 1.5) m, truncated a minimum value of dike width
	Sill probability	uniform(0, 0.1)
	Sill length	triangular(0, 500, 1000) m
Sheridan	Number of conduits	discrete: {(1, 2, 3);(0.75, 0.2, 0.05)}
	Dike system length	gamma(shape = 1.16, scale = 2.43) km, truncation at 0.1km
	Dike azimuth	mixture of truncated normals (truncation at −90 and 90 degrees): normal(0, 30), with probability 1/3 normal(−15, 20), with probability 1/3 normal(30, 20), with probability 1/3
	Dike width	normal(1.9, 0.9) m, truncated at 0.1
	Dike spacing	lognormal(mean = 1.06, st. dev. = 0.368) km, shifted −0.5, truncated at a minimum of 0
	Conduit diameter	beta, with parameters a complex combination of other simulated variables
	Sill length	lognormal(mean = 294, st. dev = 128) m, shifted −50
	Sill aspect ratio	uniform(1, 2)
Spera	Magna volume per event based on Quaternary	exponential(15) km^3
	Dike system length	gamma(shape = 2.5, scale = 1) km
	Dike width	lognormal(mean = 1.596, st. dev. = 1.971) m
	Dike azimuth	normal (0, 18) degrees, truncated at −90 and 90 degrees
	Event ellipse aspect ratio	uniform(4, 12)
	Conduit diameter	gamma(shape = 3.14, scale = 29) m, shifted −7.4 m
	Conduit location on a dike	triangular(−0.2, 0,5, 1), truncated at 0 and 1, where 0 and 1 represent the ends of the dike
	Probability of sill formation	weibull(shape = 2.3, scale = 0.055)
	Sill location along a dike	triangular(−0.2, 0,5, 1), truncated at 0 and 1, where 0 and 1 represent the ends of the dike
Thompson	Dike system length	lognormal(mean = 5.58, st. dev. = 2.78) km, shifted −0.4 km
	Dike system width	exponential(6) multiplied by the dike system length
	Dike width	lognormal(mean = 1.185, st. dev. = 0.5) m
	Dike azimuth	gamma(shape = 18, scale = 3.2) degrees, shifted −53 degrees
	Conduit diameter	lognormal(mean = 7.644, st. dev. = 6.048) m, truncated at a minimum of 1 m
	Conduit location on a dike	beta(1.5, 1.5), where 0 and 1 represent the ends of the dike

E.4.2 Calculating the Conditional Probability of Intersection

The simulated events are characterized in terms of the locations of igneous features on a local *x,y* grid. To calculate the conditional probability of intersection at each point in the region of interest, each simulated event is "placed" at random within 1 km^2 of the specified point. This randomization minimizes the effect of the choice of grid spacing, which otherwise would have the potential to affect the probability of intersection calculation, particularly for small events. Every feature in the event is then tested to determine whether it (a) intersects or (b) lies within a polygon representing the repository footprint (both are referred to as "intersections" throughout this analysis). If the event contains a feature that intersects the repository footprint, it is called an intersecting event and the specific features which intersect are tallied.

This calculation is repeated for every simulated event, and the proportion of events that intersect is treated as the conditional probability of intersection of an event at that point (e.g., if 10,000 of 100,000 simulated events intersects, the conditional probability of intersection at that point is 0.1). Similarly, the same set of calculations is repeated for every grid point in the region of interest, resulting in a conditional probability of intersection for every *x, y* point in the region of interest.

E.4.2.1 Testing for Intersection

Each simulated event is characterized by the locations of all igneous features within that event on a local *x, y* grid. When the event is placed at a location in the region of interest, those locations are translated into the locations of all the features within the region of interest. All features are represented by points and lines. Dikes are represented by their endpoints and the line between them; conduits and vents are represented by their midpoints and by four lines through each midpoint representing four diameters (at 0, 45, 90, and 135 degrees); sills are represented by their midpoints and four lines through each midpoint to points on the circumference similarly located at 0, 45, 90, and 135 degrees. One expert provided points defining the circumference of conduits, vents, and sills, and for that expert those points and the lines between them are used directly.

Intersection testing is conducted as follows:

- Each point representing the location of an igneous feature (dike endpoints, conduit, vent, and sill centers) is tested to see if it lies within a polygon representing the repository footprint. If so, that feature intersects the footprint.

- For each line segment (e.g., between dike endpoints, between points on the circumference of a conduit), the line is tested to see if it crosses any one of the line segments representing the repository footprint polygon. If so, that line segment intersects the footprint.

E.4.2.2 Repository Footprint

The repository footprint is defined for the purposes of PVHA-U as the region including and surrounding the repository emplacement drifts where the presence of an igneous feature such as a dike, conduit, vent, or sill could disrupt the waste in the repository.

This region is defined as extending approximately six and half meters beyond the edges of the outermost drifts (including perimeter and access drifts) and ventilation shafts, because any igneous event that occurred within that distance of a drift that is connected to the emplacement drifts would have potential to disrupt waste packages.[3]

Figure E-2 illustrates the repository footprint based on the locations of the drifts and ventilation shafts, and the 75 points used to represent that footprint as a polygon (DTN: MO0806REPFTPBB.000) in the computer codes used to calculate frequency of intersection. Differences between the two are virtually impossible to see: the polygon created by connecting the points with line segments encompasses 99.952% of the area of the actual footprint.

[3] The 6.5 m "buffer" is based on analyses in SNL 2007, Sections 6.3.1 and 6.4.1.

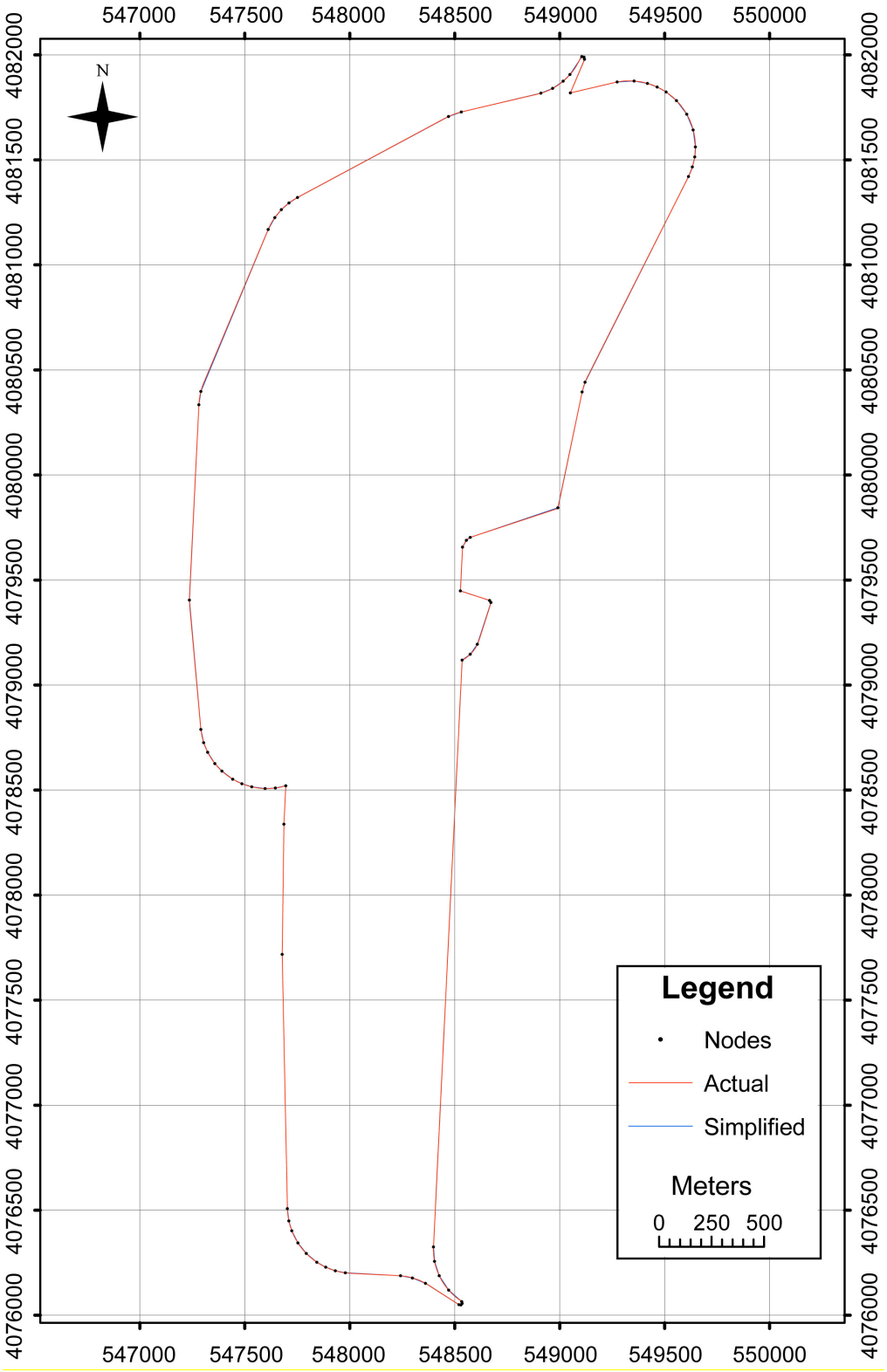

NOTE: The red line represents the footprint of the repository, as described in the text. The black dots and the blue lines connecting illustrate the representation of this footprint in the computer codes used to calculate the conditional probability of intersection.

Figure E-2. The Repository Footprint

E.5 DISTRIBUTION ON THE FREQUENCY OF INTERSECTION AND MEAN FREQUENCY OF INTERSECTION

The sections above describe the mathematical formulations used to calculate all the components of Equation E-3, the frequency of intersection. Section 3.1 describes the logic tree methodology used to model uncertainty in the frequency of intersection: logic tree nodes are defined for every uncertainty identified by an expert as relevant to the rate of future events and their spatial distribution, with branches for every specified alternative used to represent that uncertainty. In addition, the sections above describe how additional uncertainty in the spatial density from models fit to specified past events is modeled and incorporated in the logic tree approach. The result is a set of pairs: a probability and a frequency of intersection for each path through the logic tree for each expert, which defines a probability mass function (pmf) for the frequency of intersection. The mean of that distribution, $\bar{v}_I(t)$, is calculated by multiplying each frequency by its associated probability and summing:

$$\bar{v}_I(t) = \sum_{j \in M} p_j \times v_I(j,t) \qquad \text{(Eq. E-30)}$$

where M represents the set of all alterative parameter sets, p_j represents the probability associated with parameter set j, and $v_I(j,t)$ represents the frequency of intersection calculated for parameter set j at time t.

That PMF is summed across its range to generate a cumulative distribution function (CDF).

The final step in calculating the frequency of intersection for PVHA-U (the aggregate hazard) is to combine the frequency of intersection distributions from the 8 experts into a single probability distribution. The procedure is straightforward: the probabilities on each expert's logic tree are divided by 8, so that the sum of the probabilities of all the branches for all 8 logic trees is unity. This results in an aggregate pmf that represents equal weighting of all experts. The mean and the CDF for the aggregate distribution is calculated as described above.

INTENTIONALLY LEFT BLANK